Improving salt weathering resistance of hydraulic mortars with an encapsulated crystallisation inhibitor

Kamat, Ameya

DOI
10.4233/uuid:409423fa-70a3-43d9-b4df-c5e8567660ca

Publication date
2024

Document Version
Final published version

Citation (APA)
Kamat, A. (2024). *Improving salt weathering resistance of hydraulic mortars with an encapsulated crystallisation inhibitor*. [Dissertation (TU Delft), Delft University of Technology]. https://doi.org/10.4233/uuid:409423fa-70a3-43d9-b4df-c5e8567660ca

Improving salt weathering resistance of hydraulic mortars with an encapsulated crystallisation inhibitor

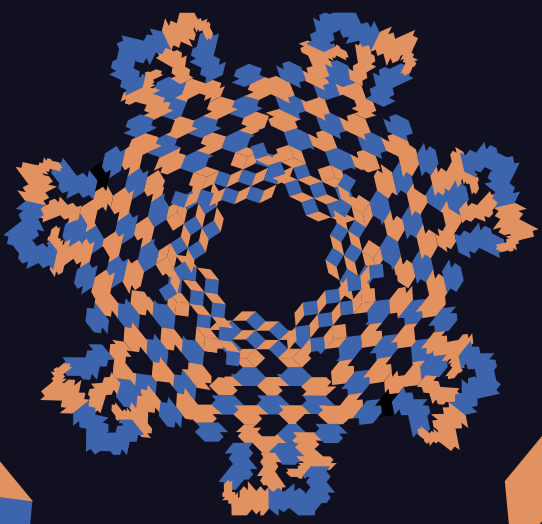

Ameya Kamat

Improving salt weathering resistance of hydraulic mortars with an encapsulated crystallisation inhibitor

Improving salt weathering resistance of hydraulic mortars with an encapsulated crystallisation inhibitor

Dissertation

for the purpose of obtaining the degree of doctor
at Delft University of Technology,
by the authority of the Rector Magnificus, Prof. dr. ir. T.H.J.J. van der Hagen,
chair of the Board for Doctorates,
to be defended publicly on
Friday 25 October 2024 at 10:00 o'clock

by

Ameya Anand KAMAT

Master of Science in Civil Engineering,
Delft University of Technology, the Netherlands
born in Mumbai, India.

This dissertation has been approved by the promotors.

Composition of the doctoral committee:

Rector Magnificus	chairperson
Prof. dr. ir. E. Schlangen	Delft University of Technology, promotor
Dr. B. Lubelli	Delft University of Technology, promotor
Independent members:	
Prof. dr. M. Steiger	University of Hamburg, Germany
Prof. dr. C. M. Rodríguez Navarro	University of Granada, Spain
Prof. dr. ir. M. T. Kreutzer	Delft University of Technology
Prof. dr. S. J. Picken	Delft University of Technology
Dr. O. Çopuroğlu	Delft University of Technology, reserve member

Dr. D. Palin (University of Cambridge, England) has contributed greatly to the realisation of this dissertation

This work is part of the research programme 'MORtars with mixed-in Inhibitors for mitigation of SAlt damage (MORISAL)' with project number 17636, which is financed by the Netherlands Organisation for Scientific Research (NWO).

Keywords: Salt weathering; sodium chloride; crystallisation inhibitor; hydraulic mortars; chitosan-alginate hydrogels; controlled-release

Printed by: Ipskamp printing, Enschede

Cover design: Ameya kamat and Mi Lin (Emeline), inspired by Escher's Metamorphose

Comic strip: Ameya Kamat (@delftsmauw)

ISBN 978-94-6366-936-8

An electronic version of this dissertation is available at
http://repository.tudelft.nl/.

To you future researcher,
I hope you reach for the stars

Contents

1

Introduction

1


THE MICROSCOPIC WORLD OF MORTAR
THE PORE REPUBLIC OF MORTAR
Calcite; $CaCO_3$
Alite; C_3S
Belite; C_2S
THE MORISAL PROJECT
NWO AND TU DELFT
STARRING
Na^+
Cl^-
FREE FLOWING, FREE SPIRITED HARMLESS ON THEIR OWN
NaCl
"THE HALITE ALLIANCE"
POWERFUL AND VIOLENT, THE MAIN VILLAINS OF OUR STORY
FeCN
CN^-
Fe^{II}
FERROCYANIDE, a.k.a. FeCN, KINGDOM OF INHIBITORS, HERO OF OUR STORY
WATER
SUPPORTS LIFE ON EARTH, INCITES CONFLICTS HERE.
SO CALLED "INDEPENDENT RESEARCHER" YOUR NARRATOR.

1.1. Problem definition

Soluble salts, ubiquitous in nature, are powerful weathering agents and are responsible for various geological formations in the universe. Unfortunately, salt-induced weathering poses a threat to buildings, sculptures and art objects (e.g. murals and frescoes) made of porous materials [1]. Salt induced weathering, also referred to as salt damage, follows a two step process. In the first step, soluble salts (e.g. containing chlorides, sulfates and nitrates) originating from various sources, such as ground water, sea salt-spray, de-icing salts permeate in porous building materials through capillary pores and are transported in the material along with moisture. In the second step, crystallisation of salts within the pore network impose stresses on the pore-walls and cause damage [2]. The damage is manifested in the form of a progressive material loss and, if left untreated, can lead to severe decay (see Figure 1.1 for examples).

Mortar, a common building material often used as bedding or pointing in masonry or as plaster and render in buildings, is highly susceptible to salt damage. Mortars composed of weaker binders, such as hydrated and hydraulic lime, are especially vulnerable, due to their relatively low mechanical properties. However, even cement-based mortars, despite their high strength, are likely to deteriorate under repeated action of salts [3]. Plasters and renders, which lie on the evaporative surfaces of the buildings, are in particular at risk, due to high salt accumulation and a constant exposure to a changing environment (temperature and humidity). As a result, the service life of plasters and renders is usually compromised and these materials need to be replaced regularly, with high maintenance costs for the owner. The stakes are even higher in the built cultural heritage, when valuable historic buildings and objects are at risk.

Despite few centuries of research on salt crystallisation, effective solutions to prevent salt damage remain elusive. In the building industry, traditional approaches, such as increasing mechanical properties of building materials (using cement binders) or suppressing moisture transport (and thus salt transport) using water repellent additives, have often exhibited low compatibility with existing materials [4]. Other solutions, such as desalination treatments and controlling indoor climate, are not always feasible [5]. In the last two decades, the use of crystallisation inhibitors has been proposed as an alternative to the traditional solutions and has shown promising results [6]. Crystallisation inhibitors are chemicals that can delay crystal nucleation and suppress crystal growth of salts, and in doing so, mitigate salt damage.

In recent years, incorporating crystallisation inhibitors during mortar production has been shown to significantly improve the resistance of air-lime mortar against salt-induced weathering, in both laboratory setting and in field applications [7]. However, two issues still need to be resolved before this technology can be developed commercially.

The first issue concerns the possibility of mixing inhibitors in hydraulic mortars to prevent salt damage. Until now, the effect of inhibitor on salt crystallisation has been studied only in air-lime mortars. This mortar constitutes only a small fraction of today's mortar production, and it is mainly used in the restoration of

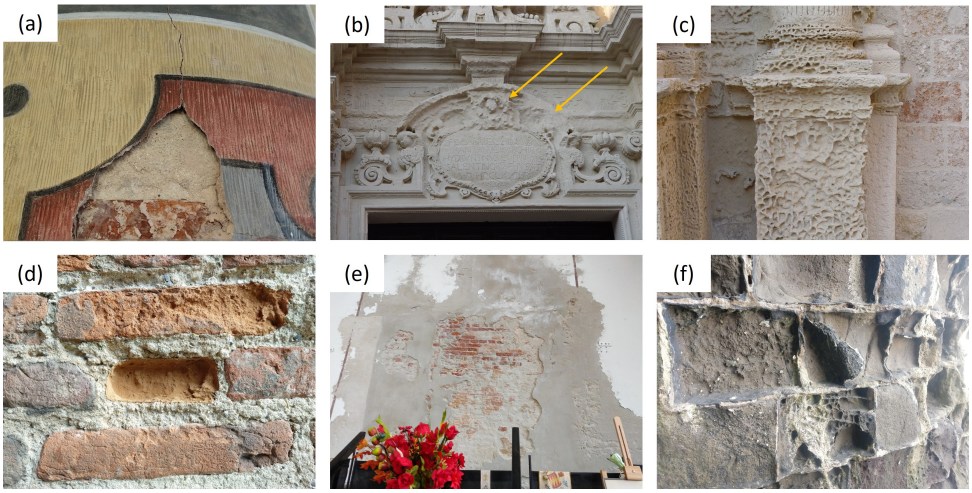

Figure 1.1: Examples of salt damage in different parts of the world (a) Lime mortar fresco, The Netherlands (b) Ornamental Limestone (Lecce) lintel, Italy. Picture by Barbara Lubelli (c) Limestone (Lecce) column, Italy. Picture by Barbara Lubelli. (d) Bricks, The Netherlands.(e) Plaster, The Netherlands. (f) Basalt (Deccan), India

built cultural heritage. Whereas, hydraulic binders which are more widely used in renovations and new constructions, are also susceptible to salt damage. Since, hydraulic mortars and air lime-based mortars have a different chemical composition and hardening behaviour, the presence of inhibitor might affect hydraulic mortars differently than air lime. Hence, the interaction between the inhibitor and hydraulic binders requires investigation.

The second issue which needs further investigation concerns the inhibitor's susceptibility to leaching out of the mortar [8]. Rapid leaching of the inhibitor would deplete its concentration in the mortar and, over time, reduce its effectiveness to mitigate salt damage. Assessing the leaching of the inhibitor from mortar is therefore crucial. Subsequently, if needed, a solution needs to be devised to minimise leaching of the inhibitor, so that the service life of the mortars can be prolonged.

1.2. Objectives and research questions

The main objective of this research is to develop hydraulic mortars with crystallisation inhibitors for a better salt-weathering resistance and a longer service life than currently existing solutions. The mortar prototype to be developed is targeted but not limited to repair/ renovation mortars for plastering and rendering of old and new buildings. To achieve this research objective, the two main issues (i) possible interaction between the inhibitor and hydraulic binders and (ii) leaching of the inhibitor out of mortar need to be addressed. To tackle these issues, following research questions, as identified based on the knowledge gaps from the literature review (Chapter 2) need to be answered:

1. What is the effect of the inhibitor on the properties of hydraulic mortars?
2. How severe is the leaching of the inhibitor from mortar and how can it be quantified?
3. What is the feasibility of encapsulating the inhibitor and tuning its release from capsules?
4. How effective is encapsulation in slowing down leaching of the inhibitor from mortar?
5. How are the properties of hydraulic mortars affected due to capsule incorporation?
6. What is the durability of hydraulic mortars with encapsulated and/or mixed-in inhibitor with respect to salt damage?

1.3. Scope of the research

The research scope is defined to make this study feasible within a four year period. Therefore, the scope is narrowed down to one salt, sodium chloride and its well-known crystallisation inhibitor, sodium ferrocyanide. The effect of salt mixtures is not considered in this research. Among the hydraulic binders, natural hydraulic lime and ordinary Portland cement are considered.

1.4. Research plan

The research consists of a series of experiments designed to answer the research questions and address the two main issues related to the inhibitor-binder interaction and leaching of the inhibitor. The overall research plan is shown in Figure 1.2. The plan consists of five phases (I) hypothesis formulation (II) exploratory study (III) prototype development (IV) prototype testing (V) Conclusions.

In phase I (hypothesis formulation), the relevant literature is reviewed to identify knowledge gaps, formulate research questions and propose hypotheses for addressing them. The scope of the literature, when needed, is expanded beyond the field of building materials, to borrow inspiration from various disciplines, such as polymer chemistry and bio-medicine.

In phase II (exploratory study), the research branches in two parallel exploratory studies. One study focuses on the interaction between the inhibitor and the hydraulic binder (marked in blue, Figure 1.2) and another on assessing the leaching of the inhibitor (marked in orange, Figure 1.2). The conclusions from this phase informs the design of phase III.

In phase III (prototype development), a proof-of-concept involving encapsulation of the inhibitor is proposed, as a mean to reduce leaching of the inhibitor from the mortar. First, based on the literature review, capsule materials with a suitable release mechanism are selected. Next, the feasibility of encapsulating the inhibitor is determined experimentally and relevant capsule properties, such as release response and encapsulation efficiency, are characterised. Based on the results of

these tests, the most suitable capsules are selected to be incorporated in the prototype mortar and the leaching of the encapsulated inhibitor from the mortar is assessed.

In phase IV (prototype testing), prototype mortar specimens are prepared and the effect of capsules on the properties of mortar is investigated. To conclude the research, the durability of prototype mortars, containing the inhibitor in encapsulated and mixed-in form, is assessed using an accelerated salt weathering test in the laboratory.

In phase V (conclusions), conclusions are drawn by analysing and correlating the findings from the different research phases and an outlook is provided for further research.

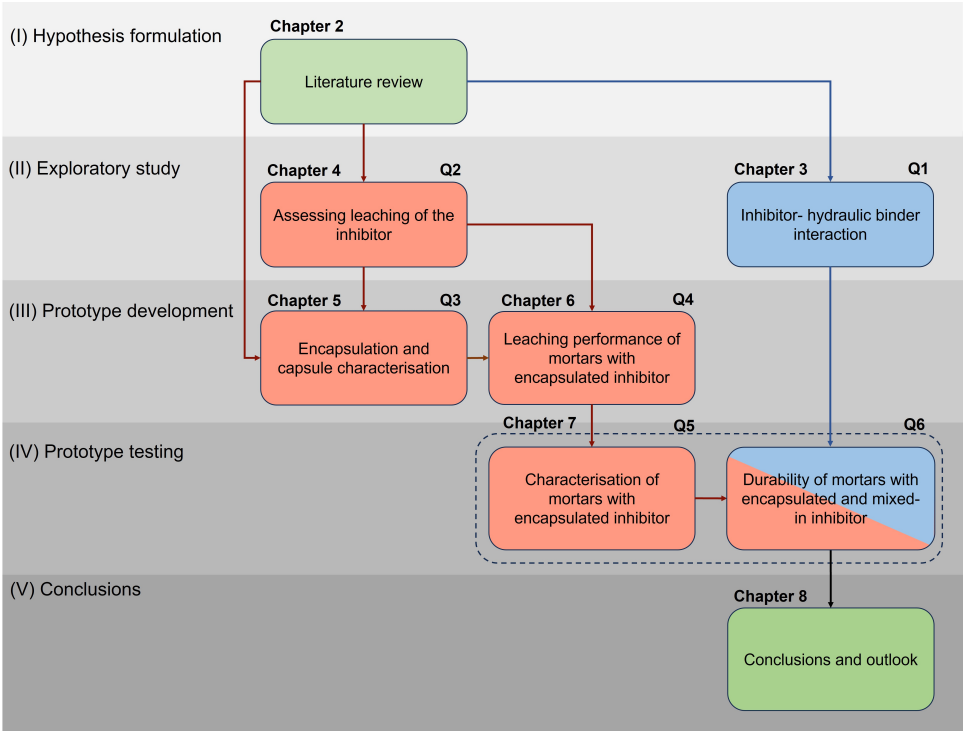

Figure 1.2: A flowchart showing the research plan with its different phases. The research flow of the two main issues is marked in blue and orange. The research questions are shown with a prefix Q and reference of each phase to the chapters in this thesis is also provided. The arrows show the connection between different phases.

1.5. Outline of the thesis

The thesis consists of 8 chapters and follows a paper-based format. Chapter 3 to Chapter 7 are based on peer-reviewed articles. The connections between chapters, research questions and different research phases are shown in Figure 1.2.

Chapter 1 (This chapter) introduces the reader to the problem definition, the research objectives, the research scope and the structure of this thesis.

Chapter 2 is a literature review, subdivided in three parts. The first part provides the theoretical background on the mechanisms of salt damage and transport. The second part reviews the state of the art in the field of crystallisation inhibitors and their applications to porous building materials. The third part reviews pros, cons and limitations of different encapsulation strategies, and speculates on the choice of capsule materials suitable to the scope. The research gaps are highlighted and the research questions are formulated keeping in mind the final research objective.

Chapter 3 studies the effect of the crystallisation inhibitor on the properties of mortar and binder paste made using (i) natural hydraulic lime (ii) ordinary portland cement. Experimental characterisation techniques are used to study fresh and hardened properties of mortars with the mixed-in inhibitor in different concentrations. Various properties such as workability, hydration, mechanical and transport properties are measured.

In **Chapter 4**, a test protocol for assessing the leaching behaviour of the inhibitor from mortar is proposed. The protocol is tested experimentally on mortars prepared with the mixed-in inhibitor under two transport mechanisms:- diffusion and advection. Analytical techniques are used to quantify the leached inhibitor.

Chapter 5 reports the preliminary results on the preparation of capsules containing the inhibitor. The capsule composition is varied, and the release of the inhibitor from the capsules is tested in bulk solutions having a pH range from 7 to 13.

In **Chapter 6**, capsules, based on the results of Chapter 5, are further characterised and the release of the inhibitor from capsules is measured in a synthetic pore solution. Subsequently, select capsules containing the inhibitor are added to the mortar and the leaching of the inhibitor the from mortar is measured, as per the methodology developed in Chapter 4. The leaching rate of the inhibitor from mortars with encapsulated inhibitor is compared to that measured in mortars with mixed-in inhibitor.

Chapter 7 involves assessing the effect of the capsules on the properties of mortar and testing the durability of the mortar prototypes against salt damage. The physical and chemical properties of the mortar prototypes are assessed using complementary characterisation techniques. Hydraulic mortar specimens with encapsulated inhibitor, mixed-in inhibitor and reference mortar (without inhibitor) are subjected to an accelerated salt weathering test. Two types of mortar systems are tested: (i) a single layer natural hydraulic lime mortar; (ii) a commercial two-layer cement based salt accumulating plaster system. The results of mortars with encapsulated and mixed-in inhibitor are compared to their respective reference mortars.

Chapter 8 summarises the main findings of the research and provides an outlook

for future work.

Appendix A and **Appendix B** provide supporting data to **Chapter 6** and **Chapter 7** respectively, while **Appendix C** provides data on additional experiments carried out during this PhD thesis that can be valuable for future research.

References

[1] A. Goudie and H. Viles, *Salt weathering hazards* (John Wiley & Sons Ltd, Chichester, 1997) p. 256.

[2] G. W. Scherer, *Stress from crystallization of salt,* Cement and Concrete Research **34**, 1613 (2004).

[3] H. Haynes, R. O'Neill, M. Neff, and P. Kumar Mehta, *Salt Weathering of Concrete by Sodium Carbonate and Sodium Chloride,* ACI Materials Journal **107**, 258 (2010).

[4] C. Groot, R. van Hees, and T. Wijffels, *Selection of plasters and renders for salt laden masonry substrates,* Construction and Building Materials **23**, 1743 (2009).

[5] E. Franzoni, *Rising damp removal from historical masonries: A still open challenge,* Construction and Building Materials **54**, 123 (2014).

[6] M. P. Bracciale, S. Sammut, J. Cassar, M. L. Santarelli, and A. Marrocchi, *Molecular Crystallization Inhibitors for Salt Damage Control in Porous Materials : An Overview,* Molecules **25**, 1873 (2020).

[7] S. Granneman, *Mitigating salt damage in lime-based mortars by built-in crystallization modifiers*, Ph.D. thesis, Delft University of Technology (2019).

[8] S. J. Granneman, B. Lubelli, and R. P. van Hees, *Effect of mixed in crystallization modifiers on the resistance of lime mortar against NaCl and Na2SO4 crystallization,* Construction and Building Materials **194**, 62 (2019).

2

Literature Review

This chapter presents the reader with background information on the general concepts of salt damage, the state-of the art on the use of crystallisation inhibitors to mitigate salt damage and reviews potential capsule materials to slow down leaching of the inhibitor in mortar. At the end of the chapter, the research gaps are identified, and hypotheses are formulated to set the stage for the experimental campaign.

2

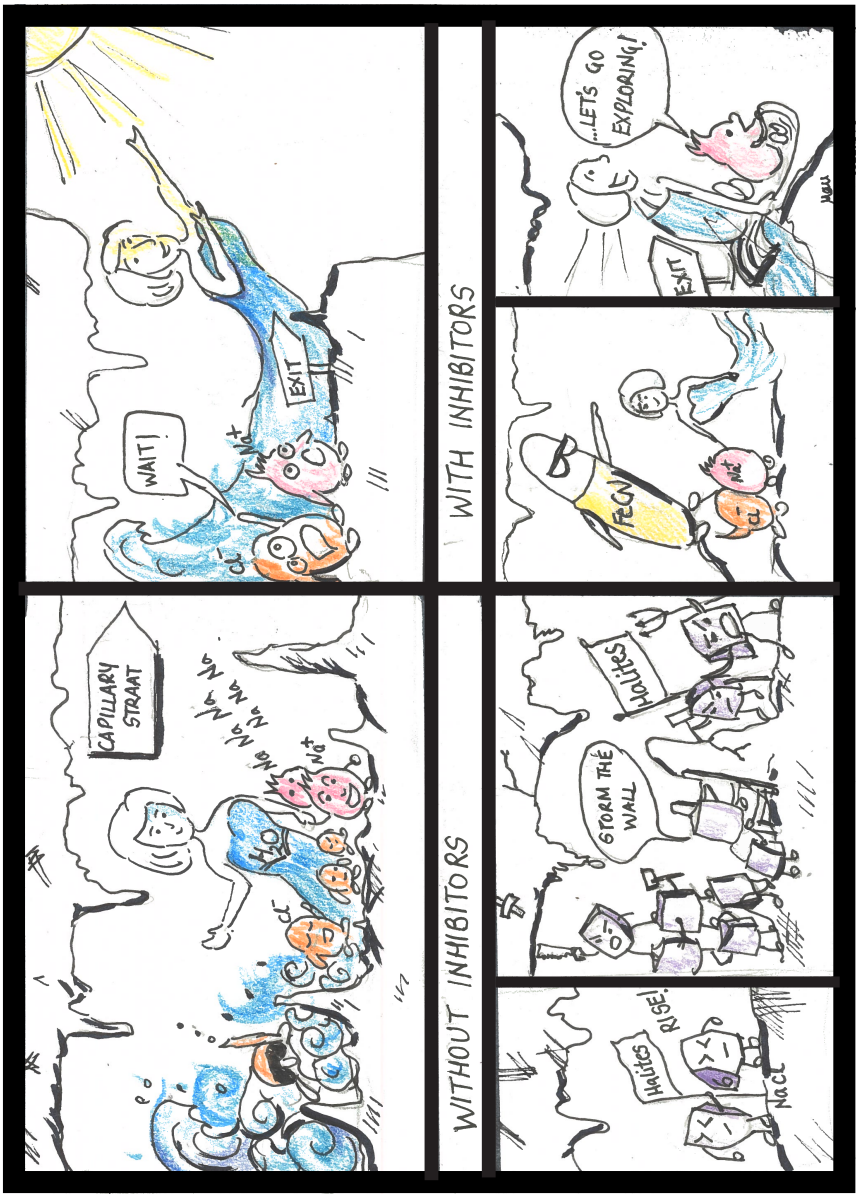
CAPILLARY STRAAT
WAIT!
EXIT
WITHOUT INHIBITORS
WITH INHIBITORS
STORM THE WALL
HALITES
RISE!
NaCl
...LET'S GO EXPLORING!
EXIT
FECN

2.1. Introduction

The main objective of this research is to improve the service life of hydraulic mortars against salt weathering. The research explores the use of a crystallisation inhibitor to mitigate salt (NaCl) crystallisation-induced damage. In this regard, a literature review is carried out with the aim to understand the state of the art on the applications of the crystallisation inhibitor in building materials and identify the underlying challenges and bottlenecks. The literature review is structured in three parts:

In the first part (Section 2.2 and Section 2.3), the reader is introduced to the general concept of salt crystallisation damage in porous building materials and its underlying mechanism. This part provides the reader with background information necessary to understand the problem and the reasoning behind various concepts that will emerge in the subsequent chapters of this thesis.

In the second part (Section 2.4), the state of the art on the use of the crystallisation inhibitor in porous building materials is critically reviewed with a focus on mortars with mixed-in inhibitors. The advantages, limitations and bottlenecks of mortars with mixed-in inhibitors are identified and discussed. One of the key identified challenges pertains to the susceptibility of the inhibitor to leach out of mortar. To address this challenge, a third part is added to this chapter.

In the third part, (Section 2.5), encapsulation of the inhibitor is explored as a potential solution to slow down leaching of the inhibitor out of mortar. Various materials for designing capsules are reviewed based on the capsule's release mechanism. Due to a lack of available options within the field of building materials, the review is extended to other fields, such as medicine, pharmacy and polymer chemistry. Potential capsule materials from these fields are identified to address the problem. However, applying these materials to mortar lead to new challenges and knowledge gaps. These are also identified and discussed.

Finally, the research gaps are pointed out that lead to the formulation of the research questions reported in Section 1.2.

2.2. Mechanism of salt damage

Soluble salts exist everywhere in nature and can enter building materials in a variety of ways. Ground water is a primary source of salts containing chlorides, nitrates sulfates [1]. Salts can permeate in the porous building materials that are in contact with the groundwater through capillarity. Salts can also originate from other sources e.g. deicing salts, salt spray (marine environment) and can be already present in the building materials [2].

Salt damage mechanism is governed by two processes: Salt transport and development of crystallisation pressure within the porous building materials.

- Salt crystals precipitate when solutions become supersaturated. Transport processes such as moisture evaporation and ionic mass transport greatly influence salt concentrations and supersaturation. Salts crystallising within the pores may lead to severe damage and is referred to as subflorescence [4]. Salts that crystallise/ precipitate on the surface, referred to as efflorescence,

Figure 2.1: Example of salt damage to a lime-based render, garden wall of Stolzenfels Castle [3]. The left panel shows spalling of the render caused due to subflorescence (in-pore salt crystallisation). The right panel shows presence of salt efflorescence (minor aesthetic issue)

are relatively harmless and do not cause damage (also evident in Figure 2.1). Salt transport can lead to localised accumulation of salts in porous media and can affect the severity of damage. (See Section 2.2.2)

- Crystallisation of salts (from supersaturated solutions) within the pores cause stresses on the pore walls. Generation of stresses has been attributed to various mechanisms e.g. development of crystallisation pressure, hydration pressure and differential thermal expansion [5]. Damage occurs when these stresses exceed the material strength [6]. So far, there is no unanimous consensus on the relevance of each damage mechanism. However, for anhydrous salts such as sodium chloride, hydration pressure is not valid as NaCl does not have any hydrated phases above 0°C [7] while differential thermal expansion would need high temperatures (greater than 54°C) to develop stresses from NaCl crystals that are uncommon in the built environment [8]. Development of crystallisation pressure is thus the most relevant mechanism to explain NaCl induced damage. (See Section 2.2.1).

To fully understand the salt damage mechanism , it is essential to understand

both the above aspects. In the next sections, the main concepts about the crystallisation pressure theory and dominant salt transport mechanisms are summarised.

2.2.1. Development of crystallisation pressure

In 1905, Becker and Day were the first to observe pressure exerted by a crystal growing in between two glass plates [9]. The experiment measured the displacement of the glass plates as a consequence of a growing alum crystal exerting pressure on them. The setup of Becker and Day worked only under certain conditions. One of the conditions required for the development of crystallisation pressure was the presence of a thin liquid film between the surface of the crystal and the surface of the constraint [10]. Further, the thin film postulated to be of order 1-2 nm (δ in Figure 2.2) had to be supersaturated [6]. As per Flatt, the thin film acts as a diffusive layer that transports ions along the confined side which are necessary for the crystal growth [11].

Correns and Steinborn were the first to propose a mathematical model for the crystallisation pressure based on supersaturation [12, 13] as shown in Equation 2.1:

$$P_c = \frac{RT}{V_m} ln\left(\frac{c}{c_s}\right) \tag{2.1}$$

Where, P_c is the crystallisation pressure, R is the universal gas constant, T is the temperature, V_m is the molar volume of the crystal and the ratio $\frac{c}{c_s}$ is expressed as supersaturation. The supersaturation ratio corresponds to the concentration of the salts in a solution to its concentration at saturation. As per the model, the crystallisation pressure is directly proportional to the supersaturation. However, the equation of Correns does not take into account the hydrated phases of salt crystals and non-ideality of aqueous phases, leading to erroneous results [14].

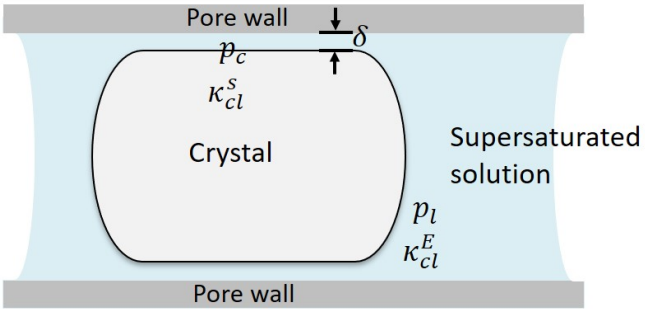

Figure 2.2: Schematic of a crystal going in a cylindrical confined pore and in contact with a supersaturated solution. the pore walls are separated by a thin film of super-saturated solution.

An alternative to the Correns model, the equation proposed by Everett has been also widely used in the literature [15]. The model is based on the curvature of the crystal-liquid interface (Equation 2.2) and relates crystallisation pressure to the pore radius.

$$P_c = \gamma_{cl}\left(\frac{dA}{dV}\right) \tag{2.2}$$

Where, γ_{cl} is the inter-facial energy of the crystal-liquid interface. The curvature dA/dV is proportional to $1/r$ with r being the pore radius. This approach has been preferred by some researchers to the Correns approach as pressure can be related to a measurable parameter i.e. pore radius [16]. Applying this equation, a pore radius in the range of nano-metres would be required to develop pressures that exceed the tensile strength of most rocks or mortar [11]. However, salt damage is also observed in materials with larger pores than nanometer scale and that cannot be directly explained by this model.

In 2005, a model combining both supersaturation and pore geometry was proposed by Steiger [16, 17] and can calculate crystallisation pressure (based on thermodynamic equilibrium) for small as well as large crystals (Equation 2.3).

$$\Delta p_i = \frac{\nu RT}{V_m}\left(ln\frac{m}{m_0} + ln\frac{\gamma_{\pm}}{\gamma_{\pm,0}} + \frac{\nu_0}{\nu}ln\frac{a_w}{a_{w,0}}\right) - \gamma_{cl,i}\frac{dA_i}{dV} \tag{2.3}$$

where, $\frac{m}{m_0}$ corresponds to the supersaturation expressed as molality and similar to the one in Corren's equation described earlier (Equation 2.1). $\gamma_{\pm}$ is the mean ionic coefficient introduced to take into account the non-ideal behaviour of the solution. ν corresponds to the number of ions on complete dissociation of the salt where as, ν_0 refers to the number of water molecules in a salt hydrate. a_w refers to the water activity. These additional model parameters overcome the discrepancies of the Corren's model and can be generalised to salts with hydrated phases. The second part of the equation is similar to the model proposed by Everett [15] and becomes only relevant for crystallisation in small pores. The main advantage of this model is that it can explain development of crystallisation pressure for hydrated as well anhydrous phases and in small as well as large pores.

Despite Steiger's generalised approach, experimental validation of crystallisation pressure still remains challenging. Studies in drying of salt contaminated porous media have shown that changes in solubility (and therefore supersaturation) can be observed using nuclear magnetic resonance (NMR) and may be related to the crystallisation pressure [18]. So far, only a few macroscopic experiments have been able to measure the force due to growing crystals between glass plates (confinement) [19, 20]. Both these studies recorded pressure below the thermodynamic limit proposed by Steiger's model. Accurate measurement of the contact area of the growing crystals was cited to be a bottleneck in the measurement of crystallisation pressure [20]. Recently, a controlled crystallisation experiment [21] with an accurate measurement of crystal's load bearing contact area also measured pressure below the thermodynamic limit, similar to [19]. The authors concluded that the equilibrium conditions assumed in Steiger's model (Equation 2.3) may not be sufficient to explain the experimental findings and the maximum pressure limit maybe be governed by the disjoining pressure instead of the thermodynamics limit. Factors like nature of surface roughness, surface charge and fluid composition would thus

need to be considered to explain the mechanism more accurately. Furthermore, the equilibrium conditions (the basis for the crystallisation pressure model) from a drying porous medium seldom exist. Thus, the crystallisation pressure model may not perfectly represent field conditions.

2.2.2. Transport of moisture and salts in porous materials

Transport of moisture and soluble salts play a key role in development of the crystallisation pressure. The salts can be introduced or transported in porous materials only as dissolved ions (aqueous state). The ionic transport of the salts is therefore directly coupled to the moisture transport. The moisture transport in porous materials is driven by two processes, capillary transport and evaporation (drying). The salt transport is driven by two processes, namely, advection and diffusion. The combination of all these processes lead to phase transition from salt ions to crystals and determine the location of crystallisation within porous materials. These mechanisms are discussed in the following sub-sections.

2.2.2.1. Capillary transport and evaporation of moisture

When porous materials come in contact with water (e.g. ground water), the water is drawn and transported in the porous materials due to differences in capillary pressure. The capillary pressure depends on the pore size distribution and the wetting properties of the water-material interface, such as the interfacial tension and the contact angle. The transport flux J, due to capillary pressure in a porous material follows Darcy's law (Equation 2.4) [22]:

$$J = -\frac{k}{n}\nabla p \tag{2.4}$$

where, k is the permeability of the porous material, n is the viscosity of the liquid (water) and ∇p is the pressure gradient.

Evaporation is a moisture transport mechanism that results in the drying of porous materials. During evaporation, the moisture transport takes place as the liquid phase transforms into a gaseous phase by overcoming the vapour pressure. Evaporation is driven by the temperature and the relative humidity.

In porous materials, when coupled with capillary transport, the drying of a saturated porous material is characterised by two stages. In the first stage, the outgoing moisture at the surface, due to evaporation, is less than the incoming moisture due to capillary transport [23]. As a result, a continuous liquid flow is maintained in the porous medium as seen in Figure 2.3a. During this stage, the moisture transport within a porous material takes place completely through a liquid phase, meaning the dissolved salt ions, if present, are also transported.

In the second stage of drying, the rate of incoming moisture via capillaries is lower than the rate of evaporation. This results in the loss of uniform moisture flow and causes formation of isolated liquid pockets [23] as shown in Figure 2.3b. Air invades the pores and a receding drying front is formed. Moisture transport cannot take place through a liquid phase and is now dominated by the vapour phase. In specimens that are contaminated with salts, the salts can no longer be transported

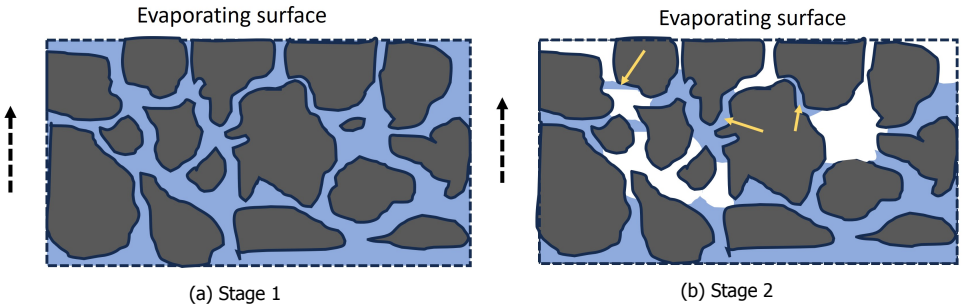

Figure 2.3: Drying of porous media is characterised by two stages. (a) through a continuous liquid film (b) Receding drying front and formation of isolated liquid pockets (yellow arrows)

to the surface and precipitate when the solution becomes supersaturated. Depending on the location of the drying front, salts may crystallise as subflorescence causing severe damage.

2.2.2.2. Advection of salt ions

Advection is defined as the transport of mass (salt ions) due to the bulk motion of the solution. The bulk motion of the solution in a porous material is driven by the capillary transport and evaporation. The resulting velocity of the solution, transports the ions (solute). The advection equation is shown in Equation 2.5. v_l is the bulk velocity of the solution and c is the concentration of the salt ions.

$$\frac{\partial c}{\partial t} + \nabla(c \cdot v_l) = 0 \tag{2.5}$$

The direction of the salt ions is the same as the direction of the liquid transport, i.e. towards the drying surface. As water evaporates, the ions precipitate from a supersaturated solution as salt crystals.

2.2.2.3. Diffusion of salt ions

Diffusion is a transport mechanism driven by a concentration gradient. In the case of salt ions in a solution, they flow from a higher to a lower concentration. The process of diffusion continues until a levelling of concentration is achieved. Diffusion equation as described by the Fick's law is shown in Equation 2.6.

$$\frac{\partial c}{\partial t} - D_{eff}\nabla^2 c = 0 \tag{2.6}$$

Where, c is the concentration of ions and D_{eff}, the effective diffusion coefficient for a porous material, is a function of the porosity, the tortuosity (degree of interconnectivity of pores) as well as the diffusion coefficient of ions in a bulk solution.

2.2.2.4. Advection-diffusion and Péclet's number

Advection and diffusion occur simultaneously with one mechanism usually dominating the other. The competition between advection and diffusion is mathematically

expressed as a dimensionless ratio called Péclet's number (Pe). Experimentally for a uni-directional flow, Pe can be approximately calculated using Equation 2.7 [24]:

$$Pe = \frac{|u|L}{D\varepsilon} \tag{2.7}$$

Where, u is the first approximation of the drying rate (velocity of the liquid) during the first stage of drying. L corresponds to the characteristic length scale and can be approximated to the length of the specimen. D_{eff} is the effective diffusion coefficient as a function of tortuosity, and ε is the maximum porosity that can be saturated with the fluid. The numerator represents the rate of advective transport and the denominator is related to the rate of diffusive transport. Thus, a high value of Pe (Pe»1) is an indication of a dominant advective transport and a Pe<1 is dominated by diffusive transport.

As an example, a high Pe (Pe>1) is usually observed during the first drying stage, where most of the salts are transported near the evaporative surface. During the second stage, the Pe drops below 1 as the continuous liquid transport is broken and bulk velocity of the solution decreases. Lower Pe coincides with a diffusion dominated transport where levelling of concentration takes place [25, 26]. Additionally, factors like pore clogging due to salt crystallisation have shown to also make salt transport diffusion-controlled [27]. In summary, the distribution of salts is localised at the evaporation surface during advection dominated transport and is more uniformly distributed during diffusion driven transport. Higher advection thus encourages salt efflorescence, while diffusion may lead to a more in depth crystallisation (subflorescence).

2.3. Crystallisation of sodium chloride

Sodium chloride (NaCl) is the most commonly occurring salt in the environment [1]. Ground water and salt-spray along coastal regions are common sources of NaCl. In low lying areas like the Netherlands, sea flooding is also a source of NaCl loading in buildings [28]. NaCl is often responsible for damage which can be observed in materials and structures.

The solubility limit of sodium chloride (6.1 mol kg^{-1}) is independent of the temperature and the sodium chloride crystals do not contain any hydrated phases above 0°C (Figure 2.4a) [7]. Thus, the crystallisation of sodium chloride is generally an evaporation driven process. Being a very soluble salt, NaCl is also hygroscopic, i.e. it can exchange moisture with the environment. As per Figure 2.4b, equilibrium of moisture exchange is achieved at a relative humidity (RH) of 0.75. The RH of equilibrium does not change much depending on the temperature. NaCl crystals when exposed to a RH above 0.75, adsorb moisture from the surroundings until an equilibrium is reached. In the process, the crystal undergoes dissolution (deliquescence) if the salt concentration drops below the solubility limit. On the contrary, when a salt solution is exposed to a RH less than 0.75, the crystals precipitate from the solution as the water evaporates and the solution becomes supersaturated.

NaCl crystals (halite), have a different macroscopic crystal morphology depending on various environmental conditions. The evolution of the crystal morphology

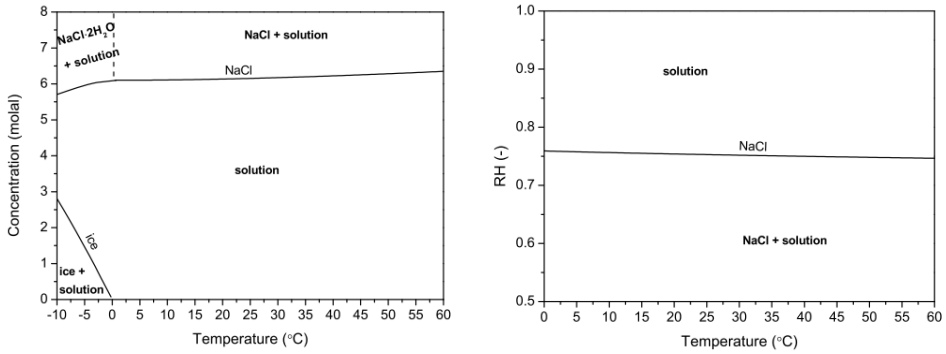

(a) Solubility of NaCl

(b) Equilibrium RH of NaCl

Figure 2.4: Sodium chloride solubility and phase diagram adapted from [7]. Solubility and equilibrium RH, and thus the crystallisation of NaCl is only slightly dependent on temperature changes.

is dependent on crystal's contact area with the saturated solution [29]. A NaCl crystal growing from a completely immersed saturated solution, tends to develop face-centered cubic crystals {100}, typically observed in large pores of building materials. Differently, a NaCl crystal growing from a thin film of a saturated solution on a substrate, develops whisker-like forms reminiscent of the efflorescence [29]. This change of morphology is strongly related to the degree of supersaturation and growth kinetics. When the supersaturation is low, NaCl crystals show a spiral growth forming from the centre to the outward edges of the cube resembling a pyramid on each cubic face [30]. After crossing a critical supersaturation, $S \approx 1.45$, the crystal cannot grow as a cube, due to a limited surface area and needs to form new surfaces. This results in the formation of interconnected cubes (hopper crystals) along one direction [31] and is followed by an increase in the crystal growth rate. At even higher supersaturation, the hopper crystal needs to form newer surfaces, resulting in a rougher, branched crystal morphology resembling dendrites or whiskers [32]. Besides, the presence of surface impurities has a role in the evolution of the crystal morphology. For instance, NaCl crystals growing from a saturated solution with no impurities, nucleates homogeneously i.e. spherical nucleation in a bulk solution. The result is also a cubic habit (equilibrium form) (Figure 2.5a). Whereas, the crystals precipitating for instance on a mortar surface cause heterogeneous nucleation i.e. nucleation on an available surface or an impurity like a dust particle [33]. The resulting crystal habit is not perfectly cubic (Figure 2.5b).

Damage due to NaCl crystallisation reported in the field is often seen in the form of flaking, sanding and powdering of building materials [4, 36]. Various case studies report severe progressive damage due to NaCl crystallisation [1, 37, 38]. Despite the aggressive damage observed in the field, laboratory experiments have had less success in replicating the damage. Studies involving partial or continuous immersion of porous specimens in salt solutions i.e. wetting the specimens with a salt solution from one side and drying from the other side have failed to induce damage, leading only to efflorescence formation [39, 40]. Especially, in case of

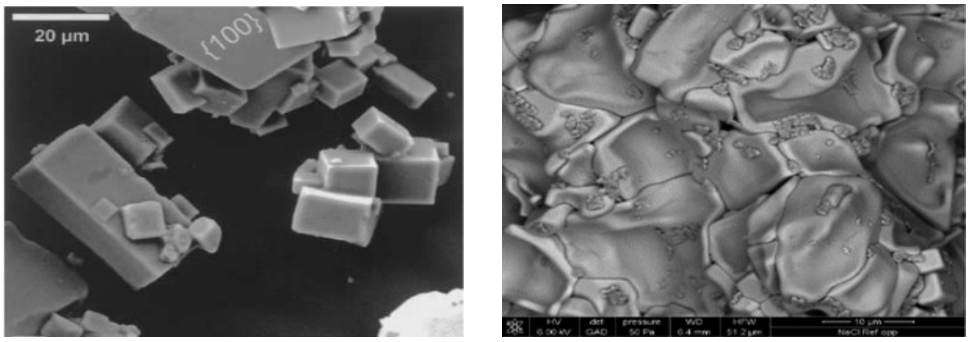

(a) (b)

Figure 2.5: (a): Example of a homogeneous nucleation; SEM image showing cubic crystals of NaCl from a droplet of a supersaturated salt solution [34]. (b): Example of a heterogeneous nucleation: SEM image showing crystals of halite precipitated on a mortar substrate likely to contain impurities. The habit of NaCl is not perfectly cubic. [35]. Reproduced with permission

.

continuous immersion, a receding drying front is prevented enhancing the advection of salt ions to the surface as efflorescence, with Na ions measuring $Pe >> 1$ [26]. As per Gentillini et al. the high tendency of NaCl to form efflorescence instead of subflorescence can also be attributed to the small size of chloride ions, giving them high mobility in porous media [41]. Alternatively, subjecting NaCl contaminated substrates to crystallisation-deliquescence cycling under humidity changes has been more effective in inducing salt crystallisation damage [42–44] as observed in Figure 2.6. Repeated deliquescence-crystallisation cycles on a drop of saturated NaCl solution have shown to reduce nucleation density and increase the crystal size [45, 46]. Perhaps, formation of larger crystals lead to higher pore clogging and higher crystallisation pressures causing more damage to porous substrates. Recently published RILEM accelerated test recommendations [47] based on deliquescence-crystallisation cycles has shown promising results [48]. Experience from the laboratory suggests that recurrent in-pore crystallisation cycles are necessary to induce damage.

2.4. Reducing salt damage using crystallisation modifiers

Various strategies exist to address salt damage in building materials. In mortar, traditionally, strategies focused on increasing the mechanical strength of materials e.g. using high strength cement-based mortars or preventing salt ingress in building materials by using water-repellent additives in mortar. Both these repair strategies have shown negative outcomes in the long term, especially in historic buildings due to low compatibility with low-strength existing materials [50]. Other strategies such as using desalination poultices [51, 52], efflorescence removal by brushing [23] and controlling relative humidity to prevent dissolution cycles are not always

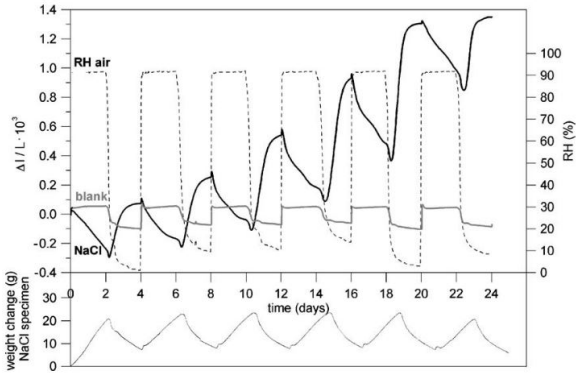

Figure 2.6: Successive humidity cycles cause higher irreversible strains in NaCl contaminated lime-mortar specimens. Blank specimens (without NaCl) show negligible and reversible strains [49]. Image reproduced with permission.

feasible [53]. This has led to research alternative solutions to tackle salt damage such as polymeric surface treatments to prevent disjoining pressure [54] and use of consolidants to improve mechanical properties [55]. In the last decades, use of crystallisation modifiers has shown promising results in mitigating salt damage [33, 56]. In the next sub-section, keeping in mind the main aim of this research, a background on the use of crystallisation modifiers, and in particular inhibitors, is provided.

2.4.1. Crystallisation modifiers

Crystallisation modifiers are chemicals that alter the process of salt crystallisation. Based on their mechanism, crystallisation modifiers are further classified [33] as (a) crystallisation promotors: chemicals that promote crystal nucleation at a lower supersaturation, therefore inducing lower crystallisation pressures; (b) crystallisation inhibitors: chemicals that inhibit/ delay crystallisation. allowing salt ions to remain longer in the solution, facilitating their transport outside the porous medium; (c) crystal habit modifiers: chemicals that alter crystal morphology by adsorbing preferentially on specific crystal faces and blocking crystal growth on those faces.

Crystallisation modifiers are selective to specific salts/ compounds [57]. For instance, modifiers made of polyphosphonates [58, 59] that have shown to be effective on modifying sodium sulphate (Na_2SO_4) crystallisation are not effective in modifying other types of salt crystals e.g. NaCl [60].

2.4.2. Alkali-ferrocyanides and NaCl crystallisation

Several crystallisation modifiers of NaCl exist (e.g. alkali ferrocyanides, nitrilotriacetamide, cadmium chloride, sodium metaphosphate and Iron(III) meso-tartaric acid) [61]. Among these, alkali (i.e. Na and K) ferrocyanides are the most effective inhibitors of NaCl crystallisation [62]. The effect of alkali ferrocyanides (i.e. tetrasodium (or potassium) hexacyanoferrate(II), hereafter referred to as FeCN) as

a crystallisation inhibitor [63] and a crystal growth modifier of NaCl [64] has been known for a long time. FeCN is extensively used as an anti-caking agent in preventing agglomeration of NaCl crystals in the production of table salt [65]. The active part of the inhibitor is the hexacyanoferrate(II) ($[Fe(CN)_6]^{4-}$) ion composed of a central iron (II) coordinating atom, complexed by six cyanide ligands having a net negative charge as shown in Figure 2.7.

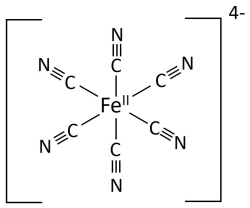

Figure 2.7: Hexacyanoferrate (II) anion with a net negative charge, the active component of the inhibitor

The working mechanism of FeCN on crystal growth of sodium chloride has been explained in the last decade [65]. During nucleation, the $[Fe(CN)_6]^{4-}$ anions are sorbed onto {100} faces of NaCl crystals replacing $[NaCl_5]^{4-}$ cluster. The $[Fe(CN)_6]^{4-}$ cluster fits perfectly in the NaCl lattice but a charge mismatch blocks crystal growth, resulting in crystal growing along the <111>direction and the formation of dendritic rather than cubic {100} crystals [34]. The blocking of crystal growth on specific crystal surfaces lowers the surface energy and increases supersaturation [66]. The interaction between FeCN and NaCl in bulk solutions has been studied by various researchers. High supersaturation values (1.6 to 3 (C/C_0)) [63, 67] and a delayed onset of crystal nucleation [34, 62], combined with dendritic crystal growth have been reported (Figure 2.8). Moreover, FeCN has been shown to remain stable in an alkaline pH range, similar to that of mortars [68]. All the above effects of FeCN on NaCl crystallisation have sparked interest in exploring the possibility of using FeCN as an additive to prevent salt damage in porous materials.

2.4.3. Use of inhibitor in porous building materials

In 2002, Selwitz and Doehne were the first to study the effect of FeCN on NaCl crystallisation in limestone specimens [70]. Specimens were contaminated with NaCl solution via capillary absorption. In some specimens, FeCN was added to the NaCl solution during the contamination phase. Specimens containing FeCN exhibited higher NaCl efflorescence (Figure 2.9) and no visible damage when compared to NaCl contaminated specimens without FeCN. The efflorescent crystals were not adherent to the surface and could be easily brushed off. In a follow up experiment, Rodriguez-Navarro et al. reported a delay in NaCl crystal nucleation in presence of FeCN, even at concentrations as low as 10^{-4} mol L^{-1} [34]. This delay in nucleation allows Na^+ and Cl^- ions to remain in solution for a longer time, aiding them to be easily transported to the drying surface. Lubelli et al. showed that FeCN in salt contaminated porous materials enhanced the drying rate of specimens and favoured

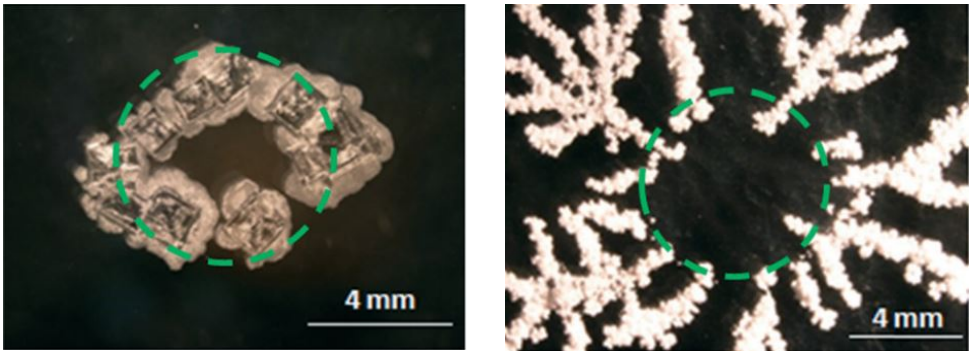

(a) (b)

Figure 2.8: NaCl crystallisation from a drop of saturated brine (Original droplet boundaries are also indicated) (a) Regular cubic halite precipitation and limited creeping observed in the absence of FeCN. (b) Dendrtitic crystals and creeping of crystals away from the original drop boundary observed in the presence of FeCN. [69] Reproduced with permission.

efflorescence [59]. Gupta et al. investigated transport of NaCl in presence of FeCN in fired-clay bricks also reported higher transport of salt ions to the surface. They attributed this behaviour to the formation of dendritic crystal habits with a high surface area, inducing faster evaporation with advection governing the ionic transport of salts [67]. Dendritic crystal growth also promotes creeping of salts and aids advection of salts to the evaporating surface (see Figure 2.8). Subsequent studies have demonstrated that FeCN when present in solution along side NaCl, supports effective desalination of various porous materials such as stones, bricks, mortar and brine rich-soil by delaying nucleation and favouring efflorescence. [71–74].

A study on NaCl contaminated lime-cement mortars under crystallisation and deliquescence cycles showed irreversible dilation. Such dilation was not observed on specimens which were contaminated with NaCl solution containing FeCN [42]. SEM images of mortar pores showed that the NaCl crystals in presence of FeCN were localised and not adhering to the porewalls, thereby possibly not transferring stresses from the crystals to the pore walls. Gupta et al. showed that NaCl crystals in presence of FeCN tended to be smaller and irregular [67]. As per the observations of Granneman et al.[35], FeCN increases nucleation density of NaCl crystallisation i.e. produces higher number of nucleating sites resulting in smaller crystals instead of an agglomerated large crystal (Figure 2.10). Small crystals may lead to less pore clogging and these factors may contribute towards mitigating salt damage by lowering the crystallisation pressure. However, this hypothesis is not yet investigated experimentally [35].

In the studies cited so far, FeCN was introduced along with NaCl solution through capillary absorption. However, it has been shown that FeCN is only effective in delaying nucleation of Na^{+}_{aq} and Cl^{-}_{aq} ions and does not alter the crystal morphology or solubility of already precipitated crystals [34]. Introducing FeCN solution (e.g. with a spray), as a means to desalinate salt contaminated porous materials has shown

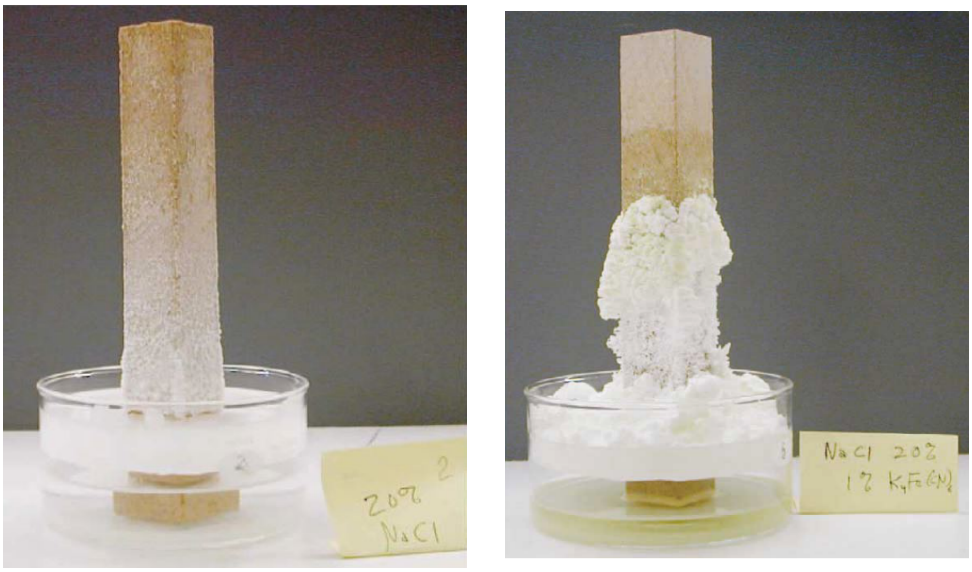

(a) without FeCN

(b) with FeCN

Figure 2.9: Effect of FeCN on NaCl crystallisation in porous limestone [70]. (a) Crystallisation of NaCl on porous limestone forming an adherent layer. (b) Enhanced efflorescence and higher salt desalination observed on porous limestones in presence of FeCN. Salt crust appears fluffy and non-adherent to the limestone substrate. Reproduced with permission.

limited success. Simply spraying FeCN solution on an already salt contaminated limestone surface, did not lead to increased efflorescence in limestone specimens [75]. As per Rivas et al. spraying FeCN on salt contaminated granite surface led to desalination, limited to a depth of first 1.5 mm from the surface i.e. only in the region where moisture could penetrate and dissolve the existing NaCl crystals [71]. Gupta et. al showed that spraying FeCN solution on contaminated specimens works by taking measures to prevent moisture evaporation and allowing enough time for the salts to dissolve and FeCN anions to diffuse in the specimen depths [76]. These measures are difficult to implement on a building site.

2.4.4. Development of mortars with mixed-in inhibitors

As discussed in the previous section, in order to maximise the effectiveness of FeCN in limiting salt damage, it is necessary that FeCN is present in the porous materials prior to salt crystallisation. In mortars, one way to achieve this is by incorporating FeCN during the mortar production process. In a pilot study dating back to 2010, FeCN was incorporated in lime-cement mortar specimens during mixing stage of mortar preparation [78]. As a result, FeCN was available in the substrate before the salt ingress. The specimens were contaminated with NaCl solution and subjected to a salt weathering test. Mortars with mixed-in inhibitors showed 100 times less material loss compared to control specimens; the inhibitor favoured NaCl efflorescence and dendritic crystal growth. The study concluded that FeCN remains

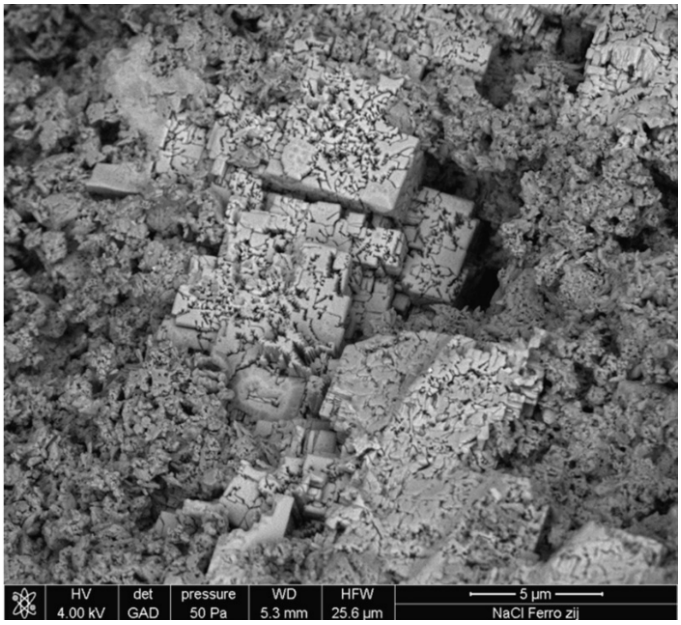

Figure 2.10: Electron microscope image of the changed crystal habit of NaCl in presence of FeCN on a mortar substrate. High nucleation density (high number of nucleation sites with smaller crystals) of altered NaCl crystals is visible alongside cubic NaCl crystals [77]. Reproduced with permission.

effective when mixed directly in mortar during production. Since then, these positive results have also been reported in other experimental studies in air lime-based mortars [77, 79, 80]. Experimental research also showed that addition of FeCN does not affect fresh and/or hardened properties of air lime mortars [81]. A field application of lime plaster containing FeCN on a NaCl contaminated wall showed no damage after four years of application. Differently, the lime plaster without the inhibitor showed severe damage in the form of powdering [82]. All these results make mortars with mixed-in FeCN a promising strategy to address salt damage in repairs, renovations and new constructions. However, these studies also revealed some challenges that still need to be investigated. These are discussed in the following sub-section.

2.4.4.1. Potential challenges for mortars with mixed-in inhibitor

Until now, the research on mortars with mixed-inhibitors has been carried out on air-lime mortars. Air-lime mortars constitute only a small fraction of the mortars used in the building industry today [83]. Hydraulic binders, such as natural hydraulic lime (NHL) and ordinary portland cement (OPC), are more commonly used in restoration/renovation works and new constructions respectively and are also susceptible to salt damage [84, 85]. Therefore, the resistance of hydraulic mortars against salt crystallisation could be possibly improved by incorporating FeCN during mortar preparation. One of the first steps in this direction would be to understand

any possible interaction between FeCN and hydraulic binders that could negatively affect the mortar properties. Past research has shown that some additives can have negative effects on fresh and hardened properties of various cementitious materials. For instance, the addition of plasticisers containing polycarboxylate ethers (PCE) for improving concrete workability have an unintentional effect in retarding cement hydration [86] or addition of hydrophobic agents have a negative effect on concrete's compressive strength [87]. Even though FeCN did not affect properties of air-lime mortar negatively [81], this does not guarantee the same effect on hydraulic mortars, as these binders differ in chemical compositions.

One of the major differences between hydraulic and air-lime mortars is their primary mechanism of strength development and hardening behaviour. Air-lime binders rely solely on the process of carbonation i.e. the reaction of calcium hydroxide ($Ca(OH)_2$) with with carbon dioxide (CO_2) from the atmosphere to form different phases of calcium carbonate ($CaCO_3$) [88]. Whereas, hydraulic mortars contain additional reactive phases such as monocalcium silicate (CS), dicalcium silicate (C_2S), and tricalciumsilicate (C_3S) (this last only occurring in OPC) and minor phases such as calcium (ferro) aluminate (C_3A, C_4AF). [89]. The calcium silicate phases react with water (hydration reaction) to form calcium-silicate hydrate (CSH) phases that are primarily responsible for the development of the micro-structure and the mechanical properties of hydraulic mortars. Carbonation plays only a secondary role in the micro-structure development of hydraulic mortars. FeCN ions might interfere with the hydration of these reactive phases by forming different hydrates. This interaction needs to be investigated to establish the feasibility in extending the application of mixed-in inhibitors to mortars based on hydraulic binders.

Another important challenge in the development of mortars with mixed-in inhibitors emerged during the study by Granneman et al. [77]. Mortar specimens containing FeCN subjected to a test consisting of several wetting and drying cycles showed negligible amount of FeCN inside the specimens at the end of the test. The loss in FeCN was attributed to leaching of FeCN out of the substrate. In fact, the high solubility of NaFeCN (17g/100 mL at 25°C) [90] in water makes FeCN vulnerable to leaching. When in solution, $[Fe(CN)_6]^{4-}$ ions can be easily transported to the evaporation surface, both by advection and diffusion. Excessive transport of FeCN will lead to depletion of FeCN in the depths of the mortar and might diminish its positive effect on salt crystallisation damage in the long term. Despite being crucial for durability of mortars with mixed-in inhibitors, the leaching behaviour of FeCN is still unexplored. Difficulties pertain to a lack of methodology in quantifying FeCN leaching from mortar. Several standard tests exist for assessing leaching of soluble species from mortar but they would need to be adapted to replicate the FeCN transport observed in the field and to accurately measure FeCN concentrations. Thus, a systematic leaching test needs to be designed; able to take into account FeCN leaching under both diffusion and advection driven transport. Implications of such a study may provide insights in controlling leaching and assessing the effectiveness of these strategies. Some strategies to control leaching are discussed in detail in the Section 2.5.

A third issue with using FeCN in porous materials pertains to a chromatic alter-

ation that may limit the application of FeCN. Blue stains have been reported when FeCN was used in desalination of granite [71] and on a lime plastered wall panel [82]. Blue colour is a result of a reaction between Fe(III) and $[Fe(CN)_6]^{4-}$ ions forming 'Prussian blue' (Ferric ferrocyanide), a common inorganic pigment [91]. Prussian blue can be even formed without any need of solvent (moisture) as long as Fe and FeCN come in mechanical contact with each other [92]. Fe is usually present as trace elements in various mineral aggregates and bricks. Even in the absence of Fe in the building materials, Prussian blue can be formed from a partial photolytic degradation of FeCN to Fe(III) ions [93]. Thus, preventing or controlling the formation of blue is challenging. More research is needed in this direction to address this bottleneck.

2.5. Encapsulation and release of the inhibitor

In the previous section, rapid leaching of the inhibitor has been identified as one of the primary challenges in the development of (hydraulic) mortars with mixed-in inhibitor. Slowing down leaching of the inhibitor from the mortar can prolong its effectiveness over an extended period and thus, improve the service life of the mortar. Encapsulation of the inhibitor may offer a solution to this issue.

Encapsulation, i.e. a technique to enclose active ingredients inside relatively stable shells called capsules, has been prevalent since the 19th century in the pharmaceutical field, as a way to protect and deliver medicines [94]. Today, capsules are used in a wide range of fields, including medicine [95, 96], food and agriculture [97], fragrance and cosmetics [98] as well as construction [99]. There is an extensive literature available on encapsulation techniques, capsule materials [100] and capsule release mechanisms [101]. In this review, capsule materials potentially suitable for application in mortar are classified based on the release mechanisms of their cargo (diffusion, rupture and dissolution/disintegration) as shown in Figure 2.11, [102], and discussed in the following subsections.

2.5.1. Rupture-based release

The encapsulated chemicals (cargo) can be released from the capsules by inducing rupture/ fracturing in the capsule shells. This is an active form of release, where the capsules protect the cargo until rupture of the capsule shell. Rupture-based release is one of the most commonly used mechanisms in self-healing materials [103]. The rupture of the capsules is induced by mechanical loads that propagate cracks in the material and the cracks are then repaired by the healing agent released from the capsules. The rupture-based capsules can be optimised to crack under specific loads by tuning the thickness, diameter and the stiffness of the capsule shells [104].

In the research on self-healing cementitious materials, various materials for making rupture-based capsules have been tested such as glass, ceramics [105, 106] and an array of synthetic polymers, including polystyrene [107, 108], methacrylate [109], phenolformaldehdye [110] and polyurea [111–113]. Brittle capsule materials such as glass, have shown low survivability during concrete mixing process and consequently, a premature release of the cargo [104, 114]. On the other hand,

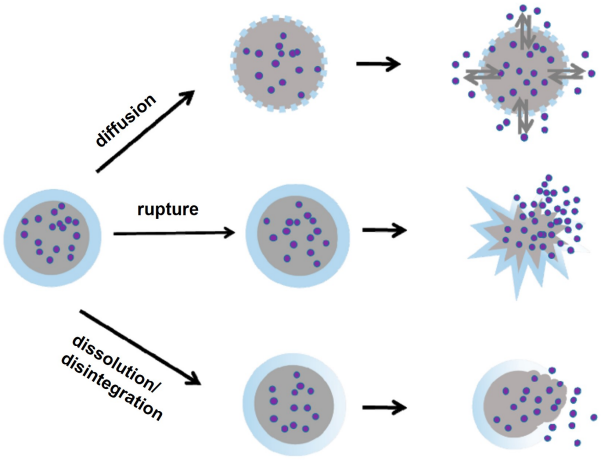

Figure 2.11: Different types of release mechanisms in capsule based systems. Image adapted from [102].

flexible materials like polylactic acid are able to survive the concrete mixing process but face the risk of erosion and disintegration in alkaline conditions, present in cementitious materials. Other polymers such as polyurethane and polystyrene face difficulties in getting ruptured under mechanical loads, preventing the release of the cargo [110]. It seems that a good compromise between survivability during mixing and rupture during service life can be obtained by using capsules made of preheated thermoplastics, such as polystyrene and polymethyl methacrylate [108]. These capsules transition from a flexible state during mixing to a brittle state after concrete hardening.

The major advantage of rupture-based of release is that the cargo is released only when needed i.e. when rupture is initiated (e.g. when material is damaged). However, application of rupture-based capsules leads to an instantaneous (burst) release of the complete cargo and the process is irreversible i.e. the capsules once triggered, cannot be reused.

2.5.2. Dissolution/disintegration-based release

The release of the cargo from capsule shells can be triggered by dissolution or disintegration of the capsule shell. This is an active form of release which relies on chemical reactions that induce dissolution or disintegration of the capsule shells. For example, a chemical reaction can be induced that can remove the cross-linker or depolymerise the capsule shells [101]. Xiong et al. designed silver alginate capsules based on chloride ion trigger [115]: the presence of chloride ions remove the cross-linking silver ions from the silver alginate network, leading to disintegration of the capsule shell and release of the cargo. In other cases, pH changes have been used to trigger the release of the cargo [116, 117]. In this research, the release of the cargo was delayed/ tuned by controlling the thickness of the capsule shell

[116, 117]. Other triggers used to depolymerise the capsule structure to release the cargo include near-infrared radiation [118], NaCl concentration [118], hydrolysis [101], and acids [119, 120].

The dissolution-based capsules can be used in cases where mechanical rupture of capsules is not desired or possible. In contrast to rupture-based capsules, dissolution-based capsule shells can be designed to obtain a delayed release by taking into account the specific chemical trigger and the rate of reaction. However, the major disadvantage of dissolution-based capsules is an irreversible change to the capsule structure, meaning, the capsules once triggered, cannot be reused.

2.5.3. Diffusion-based release

Release of the cargo from the capsules via diffusion is driven by the concentration gradient between the cargo inside and outside the capsules through a permeable membrane. This is a passive form of release, where a triggering event is not necessary to release the cargo. The permeability, porosity and the thickness of the capsule control the rate of transport of the cargo from the capsules. Additionally, the molecular weight and the bulk diffusion coefficient of the cargo affect the rate of release from the capsules.

Diffusion as a release mechanism from capsules has been thoroughly investigated in the pharmaceutical industry to obtain controlled-release of drugs. One of the classic examples is the delivery of aspirin using capsules. Introduction of high doses of aspirin directly leads to peptic ulcers. However, when introduced through semipermeable ethyl cellulose [121] or pentaestergum-coated capsules [122], aspirin is released slower and health hazards are minimised. Early studies have shown that polymeric membranes, such as polyvinyl-alcohol (PVA) and ethylene-vinyl acetate (EVA), can be engineered to obtain a sustained release of proteins and macromolecules through diffusive shells [123]. Koole et al. demonstrated that the rate of release can be adjusted by changing the porosity and the size of capsules [124]. Mun et al. managed to obtain a controlled release of the cargo from alginate-polycaprolactone capsules by controlling its amount in the capsule. Higher the amount of cargo in the capsules, higher the rate of release, due to a larger concentration gradient [125].

Diffusion-based capsules have been shown to be effective in obtaining controlled release of macromolecules (molecular weight > 1000 $g\,mol^{-1}$), such as proteins and enzymes, which have diameters comparable to capsule pores [126]. However, controlling the release of small molecules such as glucose, ethanol and NaFeCN (molecular weight: 484.06 $g\,mol^{-1}$) using just diffusion-based release is challenging, due to small size of the molecules. Triggers such as pH changes, heat, light, etc. have shown to be able to modify capsule permeability, by inducing swelling or constriction of the capsule pores, thereby supplementing diffusion-based release and allowing for a better control of release of small-molecule cargo [101].

For example, Zheludkevic et al. designed capsules [99] for aluminium surface coatings to deliver corrosion inhibitors (molecular weight 119 $g\,mol^{-1}$) by tuning the capsule permeability in response to pH changes. In this research, Zheludkevic et al. showed that the corrosion activity of aluminium lead to pH changes and that in

turn increase the capsule permeability, facilitating the release of the encapsulated corrosion inhibitor. As the pH is recovered by the corrosion inhibitor, the capsule permeability decreases again, preventing further release of the corrosion inhibitor. A similar strategy was also adopted using methyl methacrylate acid (MMA) as shell material to control release of corrosion inhibitors in highly alkaline and highly acidic environments [127]. Hofmeister et al. used polymeric nanocapsules to encapsulate 'fragrance-imparting volatile liquids' for a controlled release of the fragrance [98]. The authors created a high diffusion barrier, sensitive to pH and temperature changes, and showed that the release kinetics can be tailored by changing the polymer shell thickness.

In construction materials, within the field of bacteria-induced self-healing concrete, porous capsules have been used both to protect bacteria from harsh environments [128] and to provide reservoirs for storing and delivering nutrients for bacterial growth [129]. In another study within building materials, diffusion-based insoluble acrlyate capsules have been used to obtain a controlled-release of superplasticisers in bulk solutions of different pH [130]. The authors showed that the release rate of the superplasticisers was dependent on the swelling behaviour of the capsules driven by pH changes.

Diffusion-based capsules have several advantages over capsules based on other release mechanisms. Firstly, the release of cargo from the capsules does not affect the integrity of the capsules structure. Secondly, external stimuli e.g. pH can be used to design smart tunable release from capsules. A possible disadvantage of diffusion-based release capsules is the difficulty in controlling the release of small molecule cargo. Additionally, since diffusion-based release is a passive form of release, release of the cargo might still occur when not necessary, and thus lead to a wastage of the cargo.

2.5.4. Suitability of capsules based on the release mechanism

In the context of this PhD research, the main aim is to design capsules that can slowly release the crystallisation inhibitor to prevent the occurrence of salt-induced damage, and thereby extend the service life of the mortars. Considering this aim, rupture-based and dissolution-based capsules do not seem appropriate. In both cases, the complete cargo is released instantaneously at the first triggering event. The capsules undergo irreversible changes and the cargo cannot be released again, meaning this cannot be a long-term solution. Moreover, rupture based capsules require a triggering event, like fracture, to release the cargo; such capsules would thus only work at the moment damage induced by salt damage has already occurred and thus would not be effective to prevent salt damage.

Differently, capsules with a diffusion-based release may be designed to slow down the release of the inhibitor from the capsules and reduce its leaching from mortar. In mortar, pH changes over its service life are expected due to carbonation. Thus, diffusion-based capsules supplemented with a response to a pH-stimulus can be useful to design smart capsules. Additionally, considering the low molecular weight of the inhibitor, controlling its release just under diffusion could be challenging and relying on an additional pH-stimulus could provide a better control

over the inhibitor release.

Among materials which can be used for diffusion-based release, bio-based polymer hydrogels might offer a suitable option for application in this research, i.e. encapsulation and controlled release of the inhibitor. Bio-based polymer hydrogels belong to a class of capsules that also rely on external stimulus such as pH changes.The properties of hydrogels, with focus on their pros and cons for potential application in this research for encapsulation of the inhibitor, are presented in the next subsections.

2.5.5. Bio-based polymer hydrogels

Hydrogels are three-dimensional hydrophilic polymer networks capable of changing their pore-size by swelling or shrinking and therefore; this property make hydrogels a suitable candidate for the preparation of capsules with a diffusion-based release mechanism [131]. In recent years, there is a growing interest in using hydrogels composed of naturally occurring (bio-based) polysaccharides and proteins as delivery systems in a wide range of fields [132]. The interest stems from the presence of rich functional groups on these polymers that can be exploited to tune reversible swelling and release response [133]. Besides, polysaccharides-based hydrogels (e.g. alginates, agarose, chitosan and cellulose) or protein-based hydrogels (e.g. gelatin, pectin and collagen) are abundant in nature, low cost and commercially available [134]. Furthermore, they are non-toxic and bio-degradable and thus more sustainable than synthetic polymers [132]. They are also relatively easy to be produced; simple techniques such as extrusion dripping can be used to prepare capsules.

Among bio-based hydrogels, alginate and chitosan have been extensively researched in controlled-release systems in the field of medicine. Moreover, in cementitious materials, these hydrogels have been shown to be suitable as an additive to aid curing and improve frost resistance [135]. Although not particularly researched for controlled-release applications in the building industry, some of the properties of alginate and chitosan can make them a possible candidate for the encapsulation and release of FeCN in mortars. Therefore, the relevant properties of alginate and chitosan, their potential in controlled-release applications across different fields and their suitability to mortar-based applications are discussed in the following sub-sections.

2.5.5.1. Alginate

Alginate (salt of alginic acid) is an anionic polysaccharide derived from brown algae [136]. It is composed of linear alternating chain blocks of α-1,4-L-guluronic acid (G block) and β-1,4-D-manuronic acid (M block), both containing carboxyl groups (-COOH) [137]. In presence of divalent cations, like Ca^{2+}, Sr^{2+} or Ba^{2+}, alginate strands ionically cross-link to form a 3D polymer network [138, 139] (Figure 2.12). In the production of alginate capsules, a soluble calcium source (e.g. $CaCl_2$) is usually preferred as a cross-linking agent over other divalent metals [138] due to its low toxicity. The production of alginate capsules is relatively simple. They can be synthesised using simple extrusion dripping technique and in mild gelation

conditions (e.g. in aqueous solutions, at room temperature and neutral pH) [140].

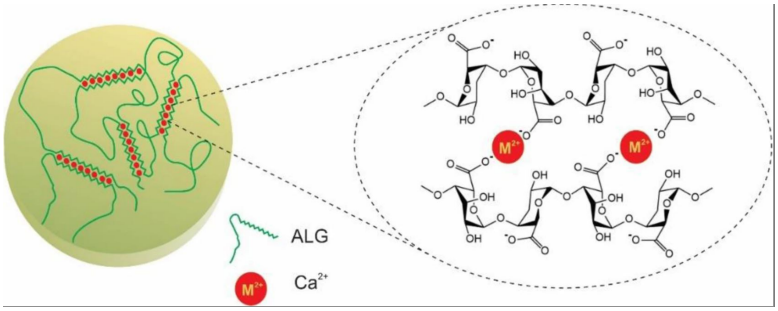

Figure 2.12: Crosslinking of alginate (ALG) with divalent metal ions (M^{2+}) to form the 3D structures with an intrinsic porosity. [141].

Alginate capsules show a pH-responsive swelling and shrinking behaviour. When in aqueous solutions with pH above its acid dissociation constant value (pKa), the carboxyl group ($-COOH$) on alginate chains de-protonates (loses H^+) and becomes negatively charged ($-COO^-$). For alginates this occurs above a pH of 4-4.5 [126]. The negative charge on adjacent alginate strands leads to inter-molecular repulsion between the strands and consequent swelling of the 3D network [137]. As the pH increases, the repulsion increases leading to higher swelling and to an increased capsule permeability. Conversely, under acidic conditions, alginates shrink and reduce their permeability, thereby preventing the release of the cargo. The swelling behaviour of alginate capsules has been exploited to tune controlled-release of cargo in response to pH changes [95] (Figure 2.13). In physiological conditions, alginate hydrogels have been used towards targeted delivery of drugs in alkaline intestinal fluid by-passing the acidic gastric environment [142].

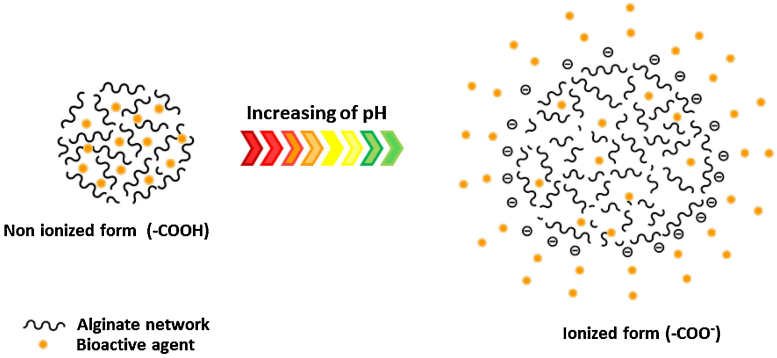

Figure 2.13: pH response of alginate capsules. As the pH increases, alginate chains become negatively charged repelling each other. The repulsion causes the alginate chains to move away from each other, swelling the capsules and releasing the cargo. [137]. The net charge on alginates range from neutral in low pH to negative in high pH. Reproduced with permission.

Within construction materials, alginate capsules have found applications as suit-

able superabsorbent polymers to improve internal curing and frost resistance of concrete [135]. In self-healing asphalt, calcium alginate capsules have been used to introduce ashpalt rejuventors [143, 144]. The above studies have shown that alginate capsules do not interact chemically with these building materials and have been shown to survive the mixing process. However, alginate capsules have not been explored in construction/building materials for controlled-release applications.

Main advantages of alginate capsules are easy production methods and chemical inertness in cementitious materials. One of the main disadvantage of alginate capsules for application in this research can be its high swelling or disintegration in alkaline conditions [145], conditions prevalent in mortar. These conditions could result in a faster release of the cargo. A second possible disadvantage of alginate capsules is the loss of cargo due to leakage during production, that can lead to a wastage of the cargo [146].

2.5.5.2. Chitosan

Chitosan (D-glucosamine) is a cationic polysaccharide obtained from deacetylation of chitin (i.e. exoskeleton of shrimps, crabs and other crustaceans) and is the second most abundant natural polymer after cellulose [147, 148]. Chitosan is commonly used for targeted drug delivery and wound dressing, thanks to its bio-compatibility and non-toxic nature. Chitosan is pH responsive and its swelling behaviour is opposite to that of alginates [149]. Amine groups ($-NH_2$) on chitosan are positively charged ($-NH_3^+$) in acidic conditions with pH <6.5 and deprotonate to $-NH_2$ in alkaline conditions [150] (see Figure 2.14). Thus, in alkaline conditions, chitosan capsules shrink forming a low permeability network, retaining higher amount of cargo. This behaviour has been demonstrated and exploited in drug-delivery applications, where chitosan has been shown to better retain the cargo at high pH and to release it faster at low pH [151].

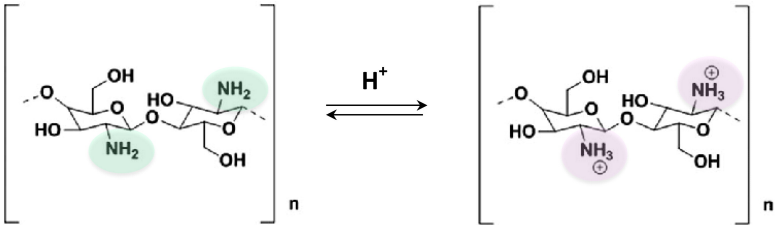

Figure 2.14: Protonation and deprotonation of amine groups NH_2 of chitosan in low and high pH respectively. The net charge on chitosan ranges from positive in low pH and neutral in high pH [148]

Compared to alginate, chitosan capsules have lower permeability and have thus a greater control on the release of small molecules [152]. Chitosan being mainly used for controlled-release of medicines, its response to pH changes is well known up to 7.4, as this is relevant in the physiological conditions [133, 147, 153, 154]. However, there are only few studies available on chitosan's behaviour at higher pH, a condition which is relevant to cementitious materials.

In cementitious materials, Wang et al. explored pH-response of chitosan modified with methacrylic anhydride for application in immobilisation of bacteria in self-healing concrete [155]. The authors reported that chitosan capsules shrank in the concrete environment (pH>12) and did not disintegrate.

Summarising, the main advantage of chitosan is its pH-driven swelling/shrinking behaviour; at high pH, chitosan will shrink and release the cargo slower. This property of chitosan can be exploited to slow down release of the inhibitor in mortar. A possible limitation of chitosan for the specific application foreseen in this PhD work, could be an electrostatic interaction between the negatively charged $[Fe(CN)_6]^{4-}$ ions and positively charged amine groups on chitosan [156]. This might interfere in the encapsulation process of the inhibitor.

2.5.5.3. Chitosan-alginate polyelectrolyte complex

Alginate and chitosan can be combined together to form a polyelectrolyte complex (PEC) through a process called complex coacervation. In this process, the negatively charged carboxyl group on the alginate chains (COO^-) forms ionic bonds with the positively charged amine groups (NH_3^+) on the chitosan chains [157] . Presence of calcium ions alongside complex coacervation is also necessary to improve the mechanical strength and the stability of the PEC capsules (Figure 2.15). The resulting chitosan-calcium alginate PEC is more robust than just chitosan-alginate PEC (without calcium) [158].

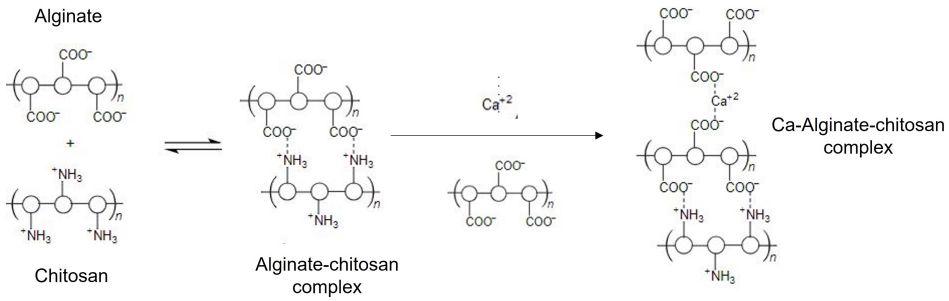

Figure 2.15: Formation of a chitosan-alginate complex due to interaction between two oppositely charged polymers. Addition of calcium to the polymer further reinforces the complex with additional cross-links and improves stability. Modified from [157] and reproduced with permission.

Due to the presence of both, carboxyl and amine groups, the PEC has different properties than individual alginate or chitosan [159]. Some of the limitations of alginate, such as swelling in high pH, can be overcome by incorporating chitosan in the alginate matrix, thanks to an opposite pH response (See Figure 2.16). As per George et al., for the PEC, "The easy solubility of chitosan in low pH is prevented by the alginate network and the possible dissolution of alginate at higher pH is prevented by chitosan which remains stable at high pH" [145]. Incorporation of chitosan in alginate networks counteracts the swelling of alginate networks [149] and decreases the permeability of alginate networks for slowing down the release of the cargo [160, 161].

Various studies have demonstrated the superiority and tunability of the PEC over individual alginate and chitosan. Pasparakis et al. showed that chitosan-alginate PEC retarded release of an encapsulated drug (Verapamil) by 30% as compared to alginate-only capsules [162]. One of the reasons for the slower release is the reduction of permeability via chitosan-alginate bonding [160]. Moreover, the presence of a multi-layered structure due to chitosan-alginate cross-links has been shown to reduce the diffusivity of the encapsulated cargo, slowing down its release [163]. The PEC exhibits a higher stability and integrity of the hydrogel network under high pH conditions. This higher stability is attributed to the presence of chitosan that resists erosion of the alginate networks [164]. Encapsulation in chitosan-alginate PEC has been successfully used in vitro for the controlled-release of various chemicals, including small molecules, up to a pH of 7.4 (physiological conditions) [161, 165–168]

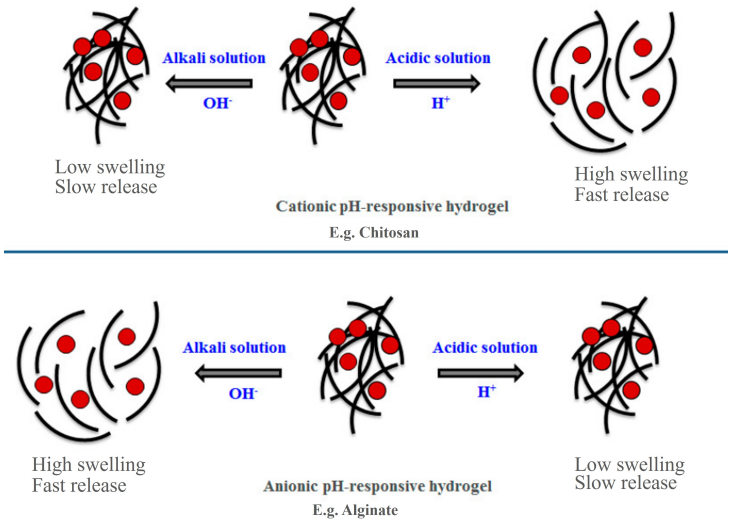

Figure 2.16: Opposite pH response of chitosan (cationic) and alginate (anionic) polymers. The image is adapted from [169]. Combination of both the polymers in a polyelectrolyte complex and varying their proportions can be used to tune a specific swelling response

Research on application of chitosan-alginate PEC in construction materials is very limited. In the only study of PEC application in concrete, chitosan-alginate capsules were studied as a medium to encapsulate and protect bacteria for self-healing applications [170]. The authors investigated the swelling of the different hydrogels (calcium alginate and PEC) under a pH range of 6-12 and concluded that above pH 12, chitosan-calcium alginate PEC capsules shrink, while calcium alginate capsules (without chitosan) swell. These results suggest that chitosan-alginate PEC capsules might be suitable for encapsulation and controlled release of inhibitor in mortar.

The main advantage of the PEC is that the swelling of the capsules and therefore, the release of the cargo at a certain pH, can be tuned by altering the individual alginate and chitosan concentrations. A possible limitation could be a more complicated capsule production process and possibly, high production costs.

2.5.6. Possible effects of capsules on the properties of mortar

Some studies have shown that incorporating capsules in concrete has a negative effect on the mechanical properties of the concrete, such as compressive and flexural strength [170, 171]. Low mechanical properties have been associated with the introduction of weak capsule-mortar interfaces and higher defects in the concrete matrix [172]. Another drawback might lie in the hydophilicity of the hydrogels. Hydrogels, such as alginates and chitosan, added during concrete/ mortar production have shown to adsorb large amount of mixing water, negatively affecting the workability/ slump of the fresh concrete/ mortar [135]. Aditionally, adsorption of water by hydrogel capsules may also affect the process of hydration and micro-structure formation in mortars.

2.6. Identified research gaps

Based on the literature review, it is clear that incorporating sodium ferrocyanide in air-lime mortars has positive effects in preventing NaCl induced damage. However, the application of crystallisation inhibitors is still in its early stage of development and several knowledge gaps have been identified:

- The crystallisation inhibitor may interact with hydraulic mortars and affect their properties, such as workability, setting-time, hydration and carbonation, mechanical and physical properties. Until now, the effect of crystallisation inhibitor on properties of hydraulic binders is still unexplored.

- The long-term effectiveness of the inhibitor in mortars can be compromised due to inhibitor's susceptibility to leach out of mortar. Quantifying the rate of leaching of the inhibitor from mortar is therefore crucial for assessing its long term effectiveness. Despite the practical relevance, there is a lack of data and test methods on assessing the leaching behaviour of the inhibitor from mortar.

- If necessary, encapsulation and controlled-release of inhibitors may provide a solution to reduce the leaching rate of the inhibitor and prolong the service life of mortars. Hydrogels, such as chitosan, alginate or their combination have been identified as potential materials for encapsulation and diffusion-based release of the inhibitor. Despite their applications for controlled-release in several fields, such as medicine, agriculture and cosmetics, their behaviour in building materials is still unknown.

- The effectiveness of hydraulic mortars with mixed-in inhibitor against salt damage is still unknown. Similarly, the effect of the encapsulated inhibitor

on the properties, durability and service life of mortar against salt damage still miss experimental validation.

References

[1] A. E. Charola, *Salts in the Deterioration of Porous Materials : An Overview,* Journal of the American institute for conservation **39**, 327 (2000).

[2] A. E. Charola and C. Bläuer, *Salts in Masonry: An Overview of the Problem,* Restoration of Buildings and Monuments **21**, 119–135 (2015).

[3] M. Auras, *Poultices and mortars for salt contaminated masonry and stone sculptures,* in *International conference on Salt Weathering of buildings and stone sculptures*, edited by L. Ottosen, I. Rori-Dalgaard, P. Larsen, I. Brajer, P. Bollingsoft, M. Marcianik, and M. Svane (Technical University of Denmark, Copenhagen, Denmark, 2008) pp. 197–217.

[4] ICOMOS, *ICOMOS-ISCS: Illustrated glossary on stone deterioration patterns*, Tech. Rep. (Champigny/Marne, 2008).

[5] C. T. Oguchi and S. Yu, *A review of theoretical salt weathering studies for stone heritage,* Progress in Earth and Planetary Science **8**, 32 (2021).

[6] G. W. Scherer, *Crystallization in pores,* Cement and Concrete Research **29**, 1347 (1999).

[7] H. Derluyn, *Salt transport and crystallization in porous limestone: neutron-X-ray imaging and poromechanical modeling*, Ph.D. thesis, ETH Zurich (2012).

[8] R. U. Cooke and I. J. Smalley, *Salt Weathering in Deserts,* Nature **220**, 1226 (1968).

[9] G. Becker and A. Day, *The Linear Force of Growing Crystals and an Interesting Pseudo-Solid,* in *Proceedings of Washington Academy of Sciences vol (VII)* (1905) pp. 251–300.

[10] S. Taber, *The growth of crystals under external pressure,* American Journal of Science **41**, 532 (1916).

[11] R. J. Flatt, *Salt damage in porous materials: how high supersaturations are generated,* Journal of Crystal Growth **242**, 435 (2002).

[12] C. W. Correns and W. Steinborn, *Experimente zur Messung und Erklarung der sogenannten Kristallisationskraft,* Zeitschrift Fur Kristallographie, Mineralogie und Petrografie **101**, 117 (1939).

[13] C. W. Correns, *Growth and dissolution of crystals under linear pressure,* Discussions of the Faraday Society , 267 (1949).

[14] R. Flatt, M. Steiger, and G. Scherer, *A commented translation of the paper by C.W. Correns and W. Steinborn on crystallization pressure,* Environmental Geology **52**, 187 (2007).

[15] D. H. Everett, *The thermodynamics of frost damage to porous solids,* Transactions of the Faraday Society **57**, 1541 (1961).

[16] M. Steiger, *Crystal growth in porous materials - I: The crystallization pressure of large crystals,* Journal of Crystal Growth **282**, 455 (2005).

[17] M. Steiger, *Crystal growth in porous materials - II: Influence of crystal size on the crystallization pressure,* Journal of Crystal Growth **282**, 470 (2005).

[18] L. A. Rijniers, H. P. Huinink, L. Pel, and K. Kopinga, *Experimental Evidence of Crystallization Pressure inside Porous Media,* Physical Review Letters **94**, 075503 (2005).

[19] J. Desarnaud, D. Bonn, and N. Shahidzadeh, *The Pressure induced by salt crystallization in confinement,* Scientific Reports **6**, 23 (2016).

[20] V. Koudelková, B. Wolf, V. Hrbek, and T. Vítů, *Experimental measurement of disjoining force at the glass–salt interface: A direct evidence of salt degradation potential caused by crystallization pressure,* Journal of Cultural Heritage **42**, 1 (2020).

[21] L. Li, F. Kohler, J. Dziadkowiec, A. Røyne, R. M. Espinosa Marzal, F. Bresme, E. Jettestuen, and D. K. Dysthe, *Limits to Crystallization Pressure,* Langmuir **38**, 11265 (2022).

[22] G. W. Scherer, *Stress from crystallization of salt,* Cement and Concrete Research **34**, 1613 (2004).

[23] A. M. Sawdy-Heritage, A. Heritage, and L. Pel, *A review of salt transport in porous media, assessment methods and salt reduction treatments,* in *Salt weathering of buildings and stone sculptures (SWBSS)* (Copenhagen, Denmark, 2008).

[24] H. P. Huinink, L. Pel, and M. A. J. Michels, *How ions distribute in a drying porous medium: A simple model,* Physics of Fluids **14**, 1389 (2002).

[25] L. Pel, H. Huinink, and K. Kopinga, *Salt transport and crystallization in porous building materials,* Magnetic Resonance Imaging **21**, 317 (2003).

[26] L. Pel, H. Huinink, and K. Kopinga, *Ion transport and crystallization in inorganic building materials as studied by nuclear magnetic resonance,* Applied Physics Letters **81**, 2893 (2002).

[27] S. Gupta, H. P. Huinink, M. Prat, L. Pel, and K. Kopinga, *Paradoxical drying of a fired-clay brick due to salt crystallization,* Chemical Engineering Science **109**, 204 (2014).

[28] B. Lubelli, R. van Hees, and C. Groot, *The performance of restoration plaster in the field: investigation and monitoring of two case studies,* in *International RILEM Workshop on Repair Mortars for Historic Masonry* (RILEM ublication proceedings, 2004) pp. 231–241.

[29] K. Zehnder and A. Arnold, *Crystal growth in salt efflorescence,* Journal of Crystal Growth **97**, 513 (1989).

[30] I. Sunagawa and K. Tsukamoto, *Growth spirals on NaCl and KCl crystals grown from solution phase,* Journal of Crystal Growth **15**, 73 (1972).

[31] J. Desarnaud, H. Derluyn, J. Carmeliet, D. Bonn, and N. Shahidzadeh, *Hopper Growth of Salt Crystals,* The Journal of Physical Chemistry Letters **9**, 2961 (2018).

[32] K. Sangwal, *Growth kinetics and surface morphology of crystals grown from solutions: Recent observations and their interpretations,* Progress in Crystal Growth and Characterization of Materials **36**, 163 (1998).

[33] S. J. Granneman, B. Lubelli, and R. P. van Hees, *Mitigating salt damage in building materials by the use of crystallization modifiers – a review and outlook,* Journal of Cultural Heritage **40**, 183 (2019).

[34] C. Rodriguez-Navarro, L. Linares-Fernandez, E. Doehne, and E. Sebastian, *Effects of ferrocyanide ions on NaCl crystallization in porous stone,* Journal of Crystal Growth **243**, 503 (2002).

[35] S. Granneman, *Mitigating salt damage in lime-based mortars by built-in crystallization modifiers*, Ph.D. thesis, Delft University of Technology (2019).

[36] *Monument Diagnosis and Conservation System,* .

[37] A. Goudie and H. Viles, *Salt weathering hazards* (John Wiley & Sons Ltd, Chichester, 1997) p. 256.

[38] H. A. Viles and A. S. Goudie, *Rapid salt weathering in the coastal Namib desert: Implications for landscape development,* Geomorphology **85**, 49 (2007).

[39] D. Benavente, M. A. García Del Cura, A. Bernabéu, and S. Ordóñez, *Quantification of salt weathering in porous stones using an experimental continous partial immersion method,* Engineering Geology (2001), 10.1016/S0013-7952(01)00020-5.

[40] C. Rodriguez-Navarro and E. Doehne, *Salt Weathering : Influence of Evaporation Rate , Supersaturation and Crystallization Pattern,* Earth Surface Processes and Landforms **24**, 191 (1999).

[41] C. Gentilini, E. Franzoni, S. Bandini, and L. Nobile, *Effect of salt crystallisation on the shear behaviour of masonry walls: An experimental study,* Construction and Building Materials **37**, 181 (2012).

[42] B. Lubelli, R. P. J. Van Hees, H. P. Huinink, and C. J. W. P. Groot, *Irreversible dilation of NaCl contaminated lime-cement mortar due to crystallization cycles,* Cement and Concrete Research **36**, 678 (2006).

[43] B. Lubelli, R. P. van Hees, and C. J. Groot, *The effect of environmental conditions on sodium chloride damage: A step in the development of an effective weathering test,* Studies in Conservation **51**, 41 (2006).

[44] T. D. Gonçalves, L. Pel, and J. D. Rodrigues, *Influence of paints on drying and salt distribution processes in porous building materials,* Construction and Building Materials **23**, 1751 (2009).

[45] J. Desarnaud and N. Shahidzadeh-Bonn, *Salt crystal purification by deliquescence/crystallization cycling,* EPL (Europhysics Letters) **95**, 48002 (2011).

[46] S. Gupta, L. Pel, and K. Kopinga, *Crystallization behavior of NaCl droplet during repeated crystallization and dissolution cycles: An NMR study,* Journal of Crystal Growth **391**, 64 (2014).

[47] B. Lubelli, I. Rörig-Daalgard, A. M. Aguilar, M. Aškrabić, K. Beck, C. Bläuer, V. Cnudde, A. M. D'Altri, H. Derluyn, J. Desarnaud, T. Diaz Gonçalves, R. Flatt, E. Franzoni, S. Godts, D. Gulotta, R. van Hees, I. Ioannou, A. Kamat, T. De Kock, B. Menendez, S. de Miranda, C. Nunes, E. Sassoni, N. Shahidzadeh, H. Siedel, Z. Slížková, M. Stefanidou, M. Theodoridou, R. Veiga, and V. Vergès-Belmin, *Recommendation of RILEM TC 271-ASC: New accelerated test procedure for the assessment of resistance of natural stone and fired-clay brick units against salt crystallization,* Materials and Structures **56**, 101 (2023).

[48] B. Lubelli, A. M. Aguilar, K. Beck, T. De Kock, J. Desarnaud, E. Franzoni, D. Gulotta, I. Ioannou, A. Kamat, B. Menendez, I. Rörig-Dalgaard, and E. Sassoni, *A new accelerated salt weathering test by RILEM TC 271-ASC: preliminary round robin validation,* Materials and Structures **55**, 238 (2022).

[49] B. Lubelli, R. P. Van Hees, H. P. Huinink, and C. J. Groot, *Irreversible dilation of NaCl contaminated lime-cement mortar due to crystallization cycles,* Cement and Concrete Research **36**, 678 (2006).

[50] C. Groot, R. van Hees, and T. Wijffels, *Selection of plasters and renders for salt laden masonry substrates,* Construction and Building Materials **23**, 1743 (2009).

[51] L. Pel, A. Sawdy, and V. Voronina, *Physical principles and efficiency of salt extraction by poulticing,* Journal of Cultural Heritage **11**, 59 (2010).

[52] L. Randazzo, G. Montana, A. Castiglia, and M. F. La Russa, *Salt extraction from lime-based mortars: An experimental study using different poultice formulations,* Construction and Building Materials **255**, 119391 (2020).

[53] E. Franzoni, *Rising damp removal from historical masonries: A still open challenge,* Construction and Building Materials **54**, 123 (2014).

[54] S. Andreotti, E. Franzoni, E. Ruiz-Agudo, G. W. Scherer, P. Fabbri, E. Sassoni, and C. Rodriguez-Navarro, *New polymer-based treatments for the prevention of damage by salt crystallization in stone,* Materials and Structures **52**, 17 (2019).

[55] M. Bassi, E. Sassoni, and E. Franzoni, *Experimental Study on an Innovative Biopolymeric Treatment Against Salt Deterioration of Materials in Cultural Heritage,* Frontiers in Materials **8**, 1 (2021).

[56] M. P. Bracciale, S. Sammut, J. Cassar, M. L. Santarelli, and A. Marrocchi, *Molecular Crystallization Inhibitors for Salt Damage Control in Porous Materials : An Overview,* Molecules **25**, 1873 (2020).

[57] C. Rodriguez-Navarro and L. G. Benning, *Control of crystal nucleation and growth by additives,* Elements **9**, 203 (2013).

[58] E. Ruiz-Agudo, C. Rodriguez-Navarro, and E. Sebastián-Pardo, *Sodium Sulfate Crystallization in the Presence of Phosphonates: Implications in Ornamental Stone Conservation,* Crystal Growth & Design **6**, 1575 (2006).

[59] B. Lubelli and R. P. van Hees, *Effectiveness of crystallization inhibitors in preventing salt damage in building materials,* Journal of Cultural Heritage **8**, 223 (2007).

[60] M. M. Saleh, S. S. Darwish, and M. Elzoghby, *The effectiveness of some crystallization inhibitors in preventing salt damage to limestone,* Journal of Crystal Growth **585**, 126606 (2022).

[61] A. A. Bode, V. Vonk, F. J. Van Den Bruele, D. J. Kok, A. M. Kerkenaar, M. F. Mantilla, S. Jiang, J. A. Meijer, W. J. Van Enckevort, and E. Vlieg, *Anticaking activity of ferrocyanide on sodium chloride explained by charge mismatch,* Crystal Growth and Design **12**, 1919 (2012).

[62] M. A. R. Blijlevens, E. R. Townsend, P. Tinnemans, W. J. P. van Enckevort, and E. Vlieg, *Effect of the Anticaking Agent FeCN on the Creeping Properties of Alkali Halide Crystals,* Crystal Growth & Design **22**, 6575 (2022).

[63] A. Glasner and M. Zidon, *The crystallization of NaCl in the presence of [Fe(CN)6]4- ions,* Journal of Crystal Growth **21**, 294 (1974).

[64] E. C. H. Davies, *Growth of salt flowers on coal and other solids,* Journal of Chemical Education **11**, 409 (1934).

[65] A. A. Bode, S. Jiang, J. A. Meijer, W. J. Van Enckevort, and E. Vlieg, *Growth inhibition of sodium chloride crystals by anticaking agents: In situ observation of step pinning,* Crystal Growth and Design **12**, 5889 (2012).

[66] E. R. Townsend, W. J. Van Enckevort, J. A. Meijer, and E. Vlieg, *Additive Enhanced Creeping of Sodium Chloride Crystals,* Crystal Growth and Design **17**, 3107 (2017).

[67] S. Gupta, K. Terheiden, L. Pel, and A. Sawdy, *Influence of Ferrocyanide Inhibitors on the Transport and Crystallization Processes of Sodium Chloride in Porous Building Materials,* Crystal Growth & Design **12**, 3888 (2012).

[68] T. Páez, A. Martínez-Cuezva, J. Palma, and E. Ventosa, *Revisiting the cycling stability of ferrocyanide in alkaline media for redox flow batteries,* Journal of Power Sources **471**, 228453 (2020).

[69] E. R. Townsend, F. Swennenhuis, W. J. Van Enckevort, J. A. Meijer, and E. Vlieg, *Creeping: An efficient way to determine the anticaking ability of additives for sodium chloride,* CrystEngComm **18**, 6176 (2016).

[70] C. Selwitz and E. Doehne, *The evaluation of crystallization modifiers for controlling salt damage to limestone,* Journal of Cultural Heritage **3**, 205 (2002).

[71] T. Rivas, E. Alvarez, M. J. Mosquera, L. Alejano, and J. Taboada, *Crystallization modifiers applied in granite desalination: The role of the stone pore structure,* Construction and Building Materials **24**, 766 (2010).

[72] T. Rivas, J. Feijoo, I. de Rosario, and J. Taboada, *Use of Ferrocyanides on Granite Desalination by Immersion and Poultice-Based Methods,* International Journal of Architectural Heritage **11**, 588 (2017).

[73] J. Cassar, A. Marrocchi, M. Santarelli, and M. Muscat, *Controlling crystallization damage by the use of salt inhibitors on Malta's limestone | Control de los da?os por cristalizaci?n en la caliza de Malta mediante inhibidores de sales,* Materiales de Construccion **58**, 281 (2008).

[74] K. L. Platt, D. M. Di Toro, R. F. Carbonaro, N. A. Bugher, T. F. Parkerton, L. J. Eastcott, and P. T. Imhoff, *Ferrocyanide enhanced evaporative flux to remediate soils contaminated with produced water brine,* Journal of Hazardous Materials **442**, 130028 (2023).

[75] E. Doehne, *Salt weathering: a selective review,* Geological Society, London, Special Publications **205**, 51 (2002).

[76] S. Gupta, *Sodium chloride crystallization in drying porous media: influence of inhibitor*, Ph.D. thesis, TU Eindhoven (2013).

[77] S. J. Granneman, B. Lubelli, and R. P. van Hees, *Effect of mixed in crystallization modifiers on the resistance of lime mortar against NaCl and Na2SO4 crystallization,* Construction and Building Materials **194**, 62 (2019).

[78] B. Lubelli, T. G. Nijland, R. P. Van Hees, and A. Hacquebord, *Effect of mixed in crystallization inhibitor on resistance of lime-cement mortar against NaCl crystallization,* Construction and Building Materials **24**, 2466 (2010).

[79] D. Ergenç, J. Feijoo, R. Fort, and M. Alvarez de Buergo, *Effects of potassium ferrocyanide used for desalination on lime composite performances in different curing regimes,* Construction and Building Materials **259**, 120409 (2020).

[80] J. Feijoo, D. Ergenç, R. Fort, and M. A. de Buergo, *Addition of ferrocyanide-based compounds to repairing joint lime mortars as a protective method for porous building materials against sodium chloride damage,* Materials and Structures **54**, 14 (2021).

[81] S. J. Granneman, B. Lubelli, and R. P. Van Hees, *Characterization of lime mortar additivated with crystallization modifiers,* International Journal of Architectural Heritage **12**, 849 (2018).

[82] B. Lubelli, E. d. Bouvrie, T. G. Nijland, and A. Kamat, *Plasters with mixed-in crystallization inhibitors: Results of a 4-year monitoring of on-site application,* Journal of Cultural Heritage **59**, 10 (2023).

[83] B. A. Silva, A. P. Ferreira Pinto, and A. Gomes, *Natural hydraulic lime versus cement for blended lime mortars for restoration works,* Construction and Building Materials **94**, 346 (2015).

[84] A. Moropoulou, K. Polikreti, A. Bakolas, and P. Michailidis, *Correlation of physicochemical and mechanical properties of historical mortars and classification by multivariate statistics,* Cement and Concrete Research **33**, 891 (2003).

[85] H. Haynes, R. O'Neill, M. Neff, and P. Kumar Mehta, *Salt Weathering of Concrete by Sodium Carbonate and Sodium Chloride,* ACI Materials Journal **107**, 258 (2010).

[86] D. Marchon and R. J. Flatt, *Science and Technology of Concrete Admixtures* (Elsevier Ltd, 2016) pp. 279–304.

[87] H. Kang, S. Kang, and B. Lee, *Strength and water-repelling properties of cement mortar mixed with water repellents,* Materials **14** (2021), 10.3390/ma14185407.

[88] K. Van Balen, *Carbonation reaction of lime, kinetics at ambient temperature,* Cement and Concrete Research **35**, 647 (2005).

[89] A. H.-W. U. Foster, *Scottish Lime Centre Trust*, Tech. Rep. December (Ediburgh, 2004).

[90] J. A. N. Friend, J. E. Townley, and R. H. Vallance, *CCCIII.—The solubility of sodium ferrocyanide in water between 0° and 104°,* J. Chem. Soc. , 2326 (1929).

[91] M. Ware, *Prussian blue: Artists' pigment and chemists' sponge,* Journal of Chemical Education **85** (2008), 10.1021/ed085p612.

[92] A. Kraft, *The Preparation of Prussian Blue in a Mortar: An Example to Teach Sustainable Chemistry with Mechanochemical Reactions,* Sustainable Chemistry **4**, 54 (2023).

[93] D. D. Kuhn and T. C. Young, *Photolytic degradation of hexacyanoferrate (II) in aqueous media: The determination of the degradation kinetics,* Chemosphere **60**, 1222 (2005).

[94] F. Podczeck and B. Jones, *Pharmaceutical capsules*, 2nd ed. (Pharmaceutical Press, London, 2004) p. 272.

[95] J. Li and D. J. Mooney, *Designing hydrogels for controlled drug delivery,* Nature Reviews Materials **1**, 1 (2016).

[96] M. R. Marques, E. Cole, D. Kruep, V. Gray, D. Murachanian, W. E. Brown, and G. I. Giancaspro, *Liquid-filled gelatin capsules,* Pharmacopeial Forum **35**, 1029 (2009).

[97] S. P. Friedman and Y. Mualem, *Diffusion of fertilizers from controlled-release sources uniformly distributed in soil,* Fertilizer Research **39**, 19 (1994).

[98] I. Hofmeister, K. Landfester, and A. Taden, *PH-Sensitive nanocapsules with barrier properties: Fragrance encapsulation and controlled release,* Macromolecules **47**, 5768 (2014).

[99] M. L. Zheludkevich, D. G. Shchukin, K. A. Yasakau, H. Möhwald, and M. G. Ferreira, *Anticorrosion coatings with self-healing effect based on nanocontainers impregnated with corrosion inhibitor,* Chemistry of Materials **19**, 402 (2007).

[100] N. Venkata Naga Jyothi, P. Muthu Prasanna, S. Narayan Sakarkar, K. Surya Prabha, P. Seetha Ramaiah, and . G. Srawan, *Microencapsulation techniques, factors influencing encapsulation efficiency,* Journal of Microencapsulation **27**, 187 (2010).

[101] A. P. Esser-Kahn, S. A. Odom, N. R. Sottos, S. R. White, and J. S. Moore, *Triggered release from polymer capsules,* (2011).

[102] M. Hu, J. Guo, Y. Yu, L. Cao, and Y. Xu, *Research advances of microencapsulation and its prospects in the petroleum industry,* Materials **10**, 369 (2017).

[103] S. R. White, N. R. Sottos, P. H. Geubelle, J. S. Moore, M. R. Kessler, S. R. Sriram, E. N. Brown, and S. Viswanathan, *Autonomic Healing of Polymer Composites,* Nature **409**, 794 (2001).

[104] C. Xue, W. Li, J. Li, V. W. Tam, and G. Ye, *A review study on encapsulation-based self-healing for cementitious materials,* Structural Concrete **20**, 198 (2019).

[105] V. C. Li, Y. M. Lim, and Y. W. Chan, *Feasibility study of a passive smart self-healing cementitious composite,* Composites Part B: Engineering **29**, 819 (1998).

[106] K. Van Tittelboom, N. De Belie, D. Van Loo, and P. Jacobs, *Self-healing efficiency of cementitious materials containing tubular capsules filled with healing agent,* Cement and Concrete Composites **33**, 497 (2011).

[107] B. Van Belleghem, R. Montoya, J. Dewanckele, N. Van Den Steen, I. De Graeve, J. Deconinck, V. Cnudde, K. Van Tittelboom, and N. De Belie, *Capillary water absorption in cracked and uncracked mortar - A comparison between experimental study and finite element analysis,* Construction and Building Materials **110**, 154 (2016).

[108] B. Hilloulin, K. Van Tittelboom, E. Gruyaert, N. De Belie, and A. Loukili, *Design of polymeric capsules for self-healing concrete,* Cement and Concrete Composites **55**, 298 (2015).

[109] D. Y. Wu, S. Meure, and D. Solomon, *Self-healing polymeric materials: A review of recent developments,* (2008).

[110] L. Lv, Z. Yang, G. Chen, G. Zhu, N. Han, E. Schlangen, and F. Xing, *Synthesis and characterization of a new polymeric microcapsule and feasibility investigation in self-healing cementitious materials,* Construction and Building Materials **105**, 487 (2016).

[111] P. Giannaros, A. Kanellopoulos, and A. Al-Tabbaa, *Sealing of cracks in cement using microencapsulated sodium silicate,* Smart Materials and Structures **25** (2016), 10.1088/0964-1726/25/8/084005.

[112] A. Kanellopoulos, P. Giannaros, and A. Al-Tabbaa, *The effect of varying volume fraction of microcapsules on fresh, mechanical and self-healing properties of mortars,* Construction and Building Materials **122**, 577 (2016).

[113] A. Al-Tabbaa, C. Litina, P. Giannaros, A. Kanellopoulos, and L. Souza, *First UK field application and performance of microcapsule-based self-healing concrete,* Construction and Building Materials **208**, 669 (2019).

[114] K. Van Tittelboom and N. De Belie, *Self-Healing in Cementitious Materials—A Review,* Materials **6**, 2182 (2013).

[115] W. Xiong, J. Tang, G. Zhu, N. Han, E. Schlangen, B. Dong, X. Wang, and F. Xing, *A novel capsule-based self-recovery system with a chloride ion trigger,* Scientific Reports **5**, 1 (2015).

[116] B. Dong, Y. Wang, G. Fang, N. Han, F. Xing, and Y. Lu, *Smart releasing behavior of a chemical self-healing microcapsule in the stimulated concrete pore solution,* Cement and Concrete Composites **56**, 46 (2015).

[117] Y. Wang, G. Fang, W. Ding, N. Han, F. Xing, and B. Dong, *Self-immunity microcapsules for corrosion protection of steel bar in reinforced concrete,* Scientific Reports **5** (2015), 10.1038/srep18484.

[118] Y. Zhang, G. Zhu, B. Dong, J. Tang, J. Li, G. Yang, S. Hong, and F. Xing, *One-Step Generation of Multistimuli-Responsive Microcapsules via the Multilevel Interfacial Assembly of Polymeric Complexes,* ACS Applied Materials & Interfaces **11**, 43741 (2019).

[119] A. P. Esser-Kahn, N. R. Sottos, S. R. White, and J. S. Moore, *Programmable Microcapsules from Self-Immolative Polymers,* Journal of the American Chemical Society **132**, 10266 (2010).

[120] S. T. Phillips and A. M. Dilauro, *Continuous head-to-tail depolymerization: An emerging concept for imparting amplified responses to stimuli-responsive materials,* ACS Macro Letters **3**, 298 (2014).

[121] R. C.-C. T. C.-Y. Yang, S.-Y. Tsay, *Encapsulating aspirin into a surfactant-free ethyl cellulose microsphere using non-toxic solvents by emulsion solvent-evaporation technique,* Journal of Microencapsulation **18**, 223 (2001).

[122] Y. V. Pathak, M. Shingatgiri, and A. K. Dorle, *In vivo performance of pentaestergum-coated aspirin microcapsules,* Journal of Microencapsulation **4**, 107 (1987).

[123] R. LANGER and J. FOLKMAN, *Polymers for the sustained release of proteins and other macromolecules,* Nature **263**, 797 (1976).

[124] L. H. Koole, M.-A. B. Kruft, Y. B. Aldenhoff, N. E. van 't Oost, M. J. van Kroonenburgh, and F. H. van der Veen, *Sustained local drug delivery from a radiopaque implanted reservoir,* Nature Biotechnology **16**, 172 (1998).

[125] A. Mun, H. Simaan Yameen, G. Edelbaum, and D. Seliktar, *Alginate hydrogel beads embedded with drug-bearing polycaprolactone microspheres for sustained release of paclobutrazol,* Scientific Reports **11**, 1 (2021).

[126] W. R. Gombotz and S. F. Wee, *Protein release from alginate matrices,* Advanced Drug Delivery Reviews **31**, 267 (1998).

[127] H. Choi, Y. K. Song, K. Y. Kim, and J. M. Park, *Encapsulation of triethanolamine as organic corrosion inhibitor into nanoparticles and its active corrosion protection for steel sheets,* Surface and Coatings Technology **206**, 2354 (2012).

[128] D. Palin, V. Wiktor, and H. M. Jonkers, *A bacteria-based bead for possible self-healing marine concrete applications,* Smart Materials and Structures **25**, 084008 (2016).

[129] V. Wiktor and H. M. Jonkers, *Quantification of crack-healing in novel bacteria-based self-healing concrete,* Cement and Concrete Composites **33**, 763 (2011).

[130] T. Ballweg, H. von Daake, D. Hanselmann, D. Stephan, K. Mandel, and G. Sextl, *Versatile triggered substance release systems via a highly flexible high throughput encapsulation technique,* Applied Materials Today **11**, 231 (2018).

[131] A. H. Karoyo and L. D. Wilson, *A review on the design and hydration properties of natural polymer-based hydrogels,* Materials **14**, 1 (2021).

[132] N. Behabtu and S. Kralj, *Enzymatic Polymerization Routes to Synthetic-Natural Materials: A Review,* ACS Sustainable Chemistry and Engineering **8**, 9947 (2020).

[133] G. Deen and X. Loh, *Stimuli-Responsive Cationic Hydrogels in Drug Delivery Applications,* Gels **4**, 13 (2018).

[134] F. Ofridam, M. Tarhini, N. Lebaz, E. Gagniere, D. Mangin, and A. Elaissari, *pH-sensitive polymers: Classification and some fine potential applications,* Polymers for Advanced Technologies **32**, 1455 (2021).

[135] C. Schröfl, K. A. Erk, W. Siriwatwechakul, M. Wyrzykowski, and D. Snoeck, *Recent progress in superabsorbent polymers for concrete,* Cement and Concrete Research **151**, 106648 (2022).

[136] H. H. Tønnesen and J. Karlsen, *Alginate in drug delivery systems,* Drug Development and Industrial Pharmacy **28**, 621 (2002).

[137] L. Agüero, D. Zaldivar-Silva, L. Peña, and M. Dias, *Alginate microparticles as oral colon drug delivery device: A review,* Carbohydrate Polymers **168**, 32 (2017).

[138] R. Russo, M. Malinconico, and G. Santagata, *Effect of cross-linking with calcium ions on the physical properties of alginate films,* Biomacromolecules **8**, 3193 (2007).

[139] Y. A. Mørch, I. Donati, B. L. Strand, and G. Skjåk-Bræk, *Effect of Ca 2+ , Ba 2+ , and Sr 2+ on Alginate Microbeads,* Biomacromolecules **7**, 1471 (2006).

[140] E.-S. Chan, B.-B. Lee, P. Ravindra, and D. Poncelet, *Prediction models for shape and size of ca-alginate macrobeads produced through extrusion–dripping method,* Journal of Colloid and Interface Science **338**, 63 (2009).

[141] F. Abasalizadeh, S. V. Moghaddam, E. Alizadeh, E. Akbari, E. Kashani, S. M. B. Fazljou, M. Torbati, and A. Akbarzadeh, *Alginate-based hydrogels as drug delivery vehicles in cancer treatment and their applications in wound dressing and 3D bioprinting,* Journal of Biological Engineering **14**, 17 (2020).

[142] A. Shilpa, S. S. Agrawal, and A. R. Ray, *Controlled Delivery of Drugs from Alginate Matrix,* Journal of Macromolecular Science, Part C: Polymer Reviews **43**, 187 (2003).

[143] A. Tabaković, W. Post, D. Cantero, O. Copuroglu, S. J. Garcia, and E. Schlangen, *The reinforcement and healing of asphalt mastic mixtures by rejuvenator encapsulation in alginate compartmented fibres,* Smart Materials and Structures **25**, 084003 (2016).

[144] S. Xu, A. Tabaković, X. Liu, and E. Schlangen, *Calcium alginate capsules encapsulating rejuvenator as healing system for asphalt mastic,* Construction and Building Materials **169**, 379 (2018).

[145] M. George and T. E. Abraham, *Polyionic hydrocolloids for the intestinal delivery of protein drugs: Alginate and chitosan - a review,* Journal of Controlled Release **114**, 1 (2006).

[146] M. L. Torre, P. Giunchedi, L. Maggi, R. Stefli, E. O. Machiste, and U. Conte, *Formulation and characterization of calcium alginate beads containing ampicillin,* Pharmaceutical Development and Technology **3**, 193 (1998).

[147] B. Qu and Y. Luo, *Chitosan-based hydrogel beads: Preparations, modifications and applications in food and agriculture sectors – A review,* International Journal of Biological Macromolecules **152**, 437 (2020).

[148] Z. Yaneva, D. Ivanova, N. Nikolova, and M. Tzanova, *The 21st century revival of chitosan in service to bio-organic chemistry,* Biotechnology & Biotechnological Equipment **34**, 221 (2020).

[149] T. W. Wong, *Alginate graft copolymers and alginate-co-excipient physical mixture in oral drug delivery,* Journal of Pharmacy and Pharmacology **63**, 1497 (2011).

[150] M. Rinaudc, G. Pavlov, and J. Desbrières, *Solubilization of Chitosan in Strong Acid Medium,* International Journal of Polymer Analysis and Characterization **5**, 267 (1999).

[151] N. Bhattarai, J. Gunn, and M. Zhang, *Chitosan-based hydrogels for controlled, localized drug delivery,* Advanced Drug Delivery Reviews **62**, 83 (2010).

[152] W. Song, G. Zhao, H. Zheng, G. He, J. Li, J. Zhang, Y. Chen, and Y. Wang, *Chitosan capsules with hydrogel core for encapsulation and controlled-release of small molecule materials,* Materials Letters **278**, 7 (2020).

[153] F. Croisier and C. Jérôme, *Chitosan-based biomaterials for tissue engineering,* European Polymer Journal **49**, 780 (2013).

[154] H. Xu and S. Matysiak, *Effect of pH on chitosan hydrogel polymer network structure,* Chemical Communications **53**, 7373 (2017).

[155] J. Wang, A. Mignon, G. Trenson, S. Van Vlierberghe, N. Boon, and N. De Belie, *A chitosan based pH-responsive hydrogel for encapsulation of bacteria for self-sealing concrete,* Cement and Concrete Composites **93**, 309 (2018).

[156] C. A. Rodrigues, E. Stadler, M. C. M. Laranjeira, and V. Drago, *The preparation and characterization of the hexacyanides immobilized in chitosan,* Journal of the Brazilian Chemical Society **8**, 7 (1997).

[157] A. C. Friedli, I. R. Schlager, and S. W. Wright, *Demonstrating encapsulation and release: A new take on alginate complexation and the nylon rope trick,* Journal of Chemical Education **82**, 1017 (2005).

[158] M. M. Daly and D. Knorr, *Chitosan□Alginate Complex Coacervate Capsules: Effects of Calcium Chloride, Plasticizers, and Polyelectrolytes on Mechanical Stability,* Biotechnology Progress **4**, 76 (1988).

[159] E. Taqieddin and M. Amiji, *Enzyme immobilization in novel alginate-chitosan core-shell microcapsules,* Biomaterials **25**, 1937 (2004).

[160] M. A. Santos and M. T. Machado, *Coated alginate–chitosan particles to improve the stability of probiotic yeast,* International Journal of Food Science and Technology **56**, 2122 (2021).

[161] A. D. Sezer and J. . Akbuga, *Release characteristics of chitosan treated alginate beads: I. Sustained release of a macromolecular drug from chitosan treated alginate beads,* Journal of Microencapsulation **16**, 195 (1999).

[162] G. Pasparakis and N. Bouropoulos, *Swelling studies and in vitro release of verapamil from calcium alginate and calcium alginate-chitosan beads,* International Journal of Pharmaceutics **323**, 34 (2006).

[163] A. K. Anal and W. F. Stevens, *Chitosan-alginate multilayer beads for controlled release of ampicillin,* International Journal of Pharmaceutics **290**, 45 (2005).

[164] Y. Murata, T. Maeda, E. Miyamoto, and S. Kawashima, *Preparation of chitosan-reinforced alginate gel beads - effects of chitosan on gel matrix erosion,* International Journal of Pharmaceutics **96**, 139 (1993).

[165] I. Hassan and A. Gani, *Alginate-Based pH-Sensitive Hydrogels Encoated with Chitosan as a Bioactive Cargo Carrier with Caffeic Acid as a Model Biomolecule,* ACS Food Science and Technology **2**, 667 (2022).

[166] J. A. A. D. Sezer, *Release characteristics of chitosan treated alginate beads: II. Sustained release of a low molecular drug from chitosan treated alginate beads,* Journal of Microencapsulation **16**, 687 (1999).

[167] M. L. Huguet and E. Dellacherie, *Calcium alginate beads coated with chitosan: Effect of the structure of encapsulated materials on their release,* Process Biochemistry **31**, 745 (1996).

[168] T. Wu, S. Yu, D. Lin, Z. Wu, J. Xu, J. Zhang, Z. Ding, Y. Miao, T. Liu, T. Chen, and X. Cai, *Preparation, Characterization, and Release Behavior of Doxorubicin hydrochloride from Dual Cross-Linked Chitosan/Alginate Hydrogel Beads,* ACS Applied Bio Materials **3**, 3057 (2020).

[169] S. Chatterjee and P. Chi-leung HUI, *Review of Stimuli-Responsive Polymers in Drug Delivery and Textile Application,* Molecules **24**, 2547 (2019).

[170] M. Gao, J. Guo, H. Cao, H. Wang, X. Xiong, R. Krastev, K. Nie, H. Xu, and L. Liu, *Immobilized bacteria with pH-response hydrogel for self-healing of concrete,* Journal of Environmental Management **261**, 110225 (2020).

[171] J. Y. Wang, H. Soens, W. Verstraete, and N. De Belie, *Self-healing concrete by use of microencapsulated bacterial spores,* Cement and Concrete Research **56**, 139 (2014).

[172] G. Souradeep and H. W. Kua, *Encapsulation Technology and Techniques in Self-Healing Concrete,* Journal of Materials in Civil Engineering **28**, 04016165 (2016).

3

Effect of a mixed-in crystallisation inhibitor on the properties of hydraulic mortars

In this chapter, the possibility to develop hydraulic mortars with mixed-in inhibitor is explored. As an essential first step, the influence of the inhibitor addition on the properties of hydraulic mortars is investigated. Two common types of hydraulic binders, natural hydraulic lime (NHL) and ordinary Portland cement (CEM I), are studied; the inhibitor is added in different concentrations during mortar (and binder paste) preparation. Relevant properties of mortar and binder paste, in fresh (hydration, workability, setting time) and hardened (mechanical strength, elastic modulus, pore size distribution, water absorption) state, are assessed using several complementary methods and techniques.

This chapter is based on the article published in AIMS Materials Science **9**, 4 (2022).

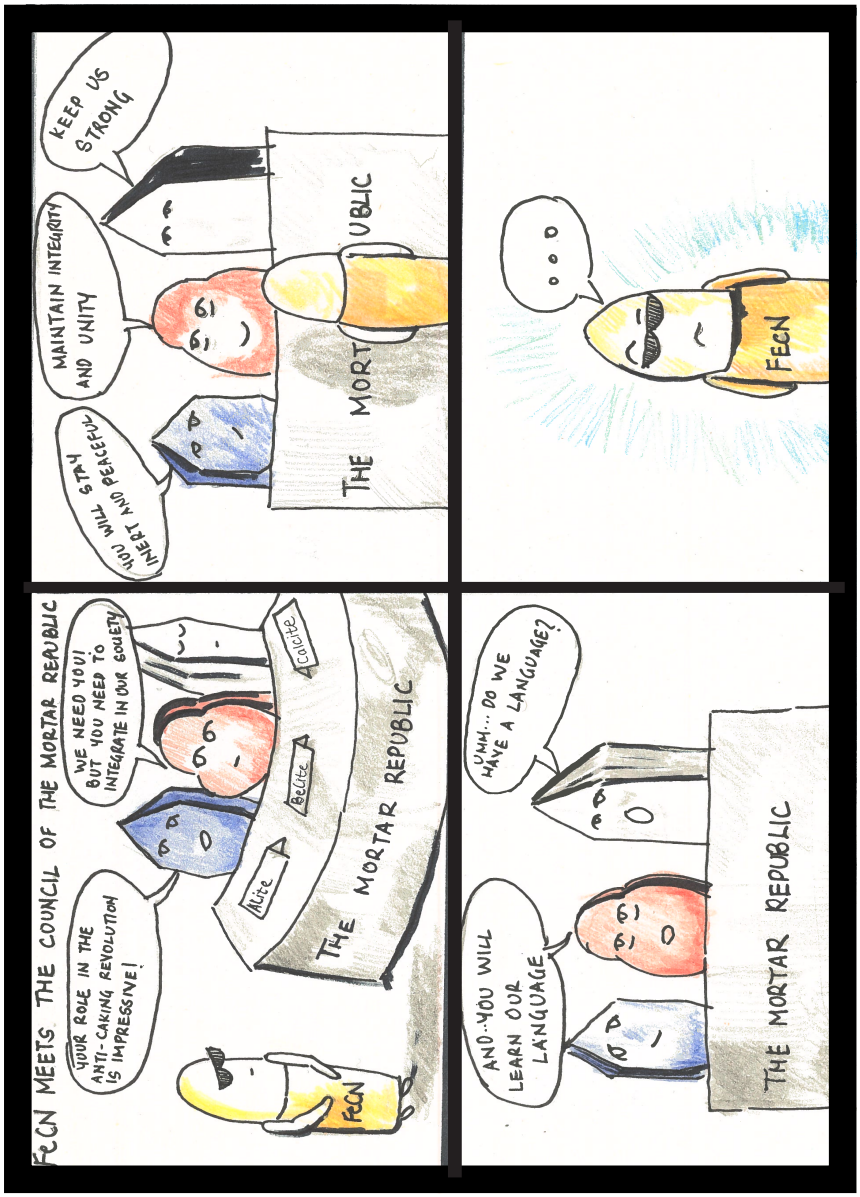
FCN MEETS THE COUNCIL OF THE MORTAR REPUBLIC
YOUR ROLE IN THE ANTI-CAKING REVOLUTION IS IMPRESSIVE!
WE NEED YOU! BUT YOU NEED TO INTEGRATE IN OUR SOCIETY
FCN
Alite
Belite
Calcite
THE MORTAR REPUBLIC
AND YOU WILL LEARN OUR LANGUAGE
UMM... DO WE HAVE A LANGUAGE?
THE MORTAR REPUBLIC
AND YOU WILL STAY INERT AND PEACEFUL
MAINTAIN INTEGRITY AND UNITY
KEEP US STRONG
THE MORTAR REPUBLIC
FCN

3.1. Introduction

Salt crystallisation in porous building materials (e.g. bricks and mortar) induces stresses [1] and is a recurrent/main cause of damage in buildings. Salt damage is particularly evident in plasters and renders making them vulnerable to salt decay, owing to various reasons. Due to their proximity to the outer, evaporative surface of the walls, plasters and renders are the location where salts tend to accumulate and undergo dissolution and crystallisation cycles in response to changing environment (RH and temperature changes, rain etc.).

Plaster and renders show therefore often a limited durability in the presence of moisture and salts. Different solutions have been proposed to improve the service life of these materials, such as the use of water repellent additives mixed in the mass (the so-called salt accumulating plasters) [2]). However, the durability of such solutions is limited and their compatibility with existing (historic) buildings is low, especially in the presence of high moisture content in the underlying masonry. Alternative solutions have been therefore sought to improve the durability of plaster and render mortars against salt decay. In the past years, the use of crystallisation inhibitors has been considered as a potentially durable solution against salt decay.

crystallisation inhibitors are molecules that alter the process of crystallisation by delaying nucleation and/or by modifying the crystal habit [3]. Alkali ferrocyanides (FeCN) have been shown to be effective in inhibiting NaCl growth and are commonly used as anti-caking agents [4]. In studies performed on bulk solutions, the presence of FeCN has shown to alter sodium chloride crystal morphology from a cubic habit to a dendritic pattern having a higher surface area [5]; this habit modification has shown to increase the rate of evaporation [6]. In early studies, the inhibitor was introduced in the building materials with salt solutions through capillary absorption. Researchers observed a larger amount of efflorescence in materials contaminated with an aqueous solution of NaCl and FeCN with respect to materials contaminated with NaCl solution, suggesting increased salt transport outside the porous substrate [6–8]. This was been attributed to both the inhibition of crystal nucleation, leading to a higher advection of salt ions to the surface, and to the faster evaporation rate, induced by the large evaporation surface of the branched crystals [9]. As per Granneman et al. [3], FeCN in porous materials leads to an increase in NaCl nucleation density due to high supersaturation and consequently smaller crystals. This is also thought to reduce pore clogging and lower crystallisation pressure in the pores.

A study revealed that FeCN was effective only if added prior to crystallisation (when Na and Cl are present as ions) whereas, its effect on modifying salt crystals and/or favouring their dissolution was not evident [6, 10]. Thus, for the inhibitor to be effective, it must be present in the building materials before salt crystallisation takes place. In mortars, a way to obtain these conditions is to add the inhibitor during mortar preparation. This approach was tested for the first time with promising results in air-hardening, (hydrated) lime-based mortars, to which sodium FeCN was added [11]. The lime mortar with mixed-in inhibitor showed an increased resistance to salt decay, in comparison to mortar without the inhibitor under an accelerated salt weathering test [12, 13], while showing a negligible effect on rele-

vant physical/chemical properties of mortar [14]. Hydrated lime-based mortars are often used in restoration works owing to good compatibility with historic materials. However, in renovation works and new constructions, hydrated lime mortars have been replaced with hydraulic mortars, on account of higher mechanical strength and faster setting. Even in the field of restoration, natural hydraulic lime as well as blended cement-lime mortars are seen to be potential alternatives to overcome limitations of traditional lime mortars [15–19]. Nonetheless, hydraulic mortars remain vulnerable to salt decay and the use of crystallisation inhibitors can be beneficial in improving their durability in those cases where moisture and salts are present.

Until now, the potential for the use of crystallisation inhibitors in hydraulic mortars has not been yet explored, which is limiting its application. The different mechanism of strength gain and setting between hydrated lime mortars and hydraulic mortars, may invalidate the positive results observed in the case of hydrated lime mortars with FeCN. In fact, whereas in hydrated lime mortars, carbonation is solely responsible for microstructure development, in hydraulic mortars hydration (i.e exothermic reaction between water and the binder) plays a primary role. In order to extend the concept of mixed in crystallisation inhibitors to hydraulic mortars, therefore, a first essential step towards the developments of hydraulic mortar with mixed-in inhibitor, consists in assessing if any interaction occurs between the inhibitor and the hydraulic binders (e.g. NHL or Portland Cement) that could negatively affect the mortar properties and/or performance.

This paper investigates the effect of sodium ferrocyanide on the properties of hydraulic mortars prepared with NHL and CEMI binders, by means of tests and experiments carried out in laboratory.

3.2. Materials

3.2.1. Building materials

Two types of hydraulic binders were tested, natural hydraulic lime (NHL) with a strength class of 3.5 and ordinary Portland cement (CEM I) with a strength class of 42.5. Standard river sand, as per EN 196-1 with a particle size distribution of 0.08-2 mm was used to prepare mortar specimens [20]. Sodium ferrocyanide decahydrate ($Na_4Fe(CN)_6 \cdot 10\,H_2O$) (Sigma Aldrich) was used as the crystallisation inhibitor.

3.2.2. Specimen preparation and storage conditions

Two types of specimens were prepared for performing various tests, namely, binder-paste specimens and mortar specimens. An overview of different types of specimens used in different tests can be found in Table 3.1.

3.2.2.1. Binder paste specimens

Control specimens (without inhibitor) were prepared by mixing binder and demineralised water to form a paste. The water-binder ratio (w/b) was maintained at 1 and 0.5 by weight for NHL and CEM I respectively.

To prepare specimens with mixed in inhibitor, sodium ferrocyanide decahydrate (FeCN) was first dissolved in demineralised water and subsequently added to the

binder to form a paste. Specimens with different inhibitor concentrations were prepared: 0.01%, 0.1% and 1% (weight of the inhibitor is expressed as a percentage of the binder weight). The concentrations were selected based on previous research [6, 12]. Paste specimens were immediately tested (heat of hydration and setting time) in their fresh state.

3.2.2.2. Mortar specimens

Mortar specimens were prepared according to the European standards, EN 459-2 [21] for NHL and EN 196-1 [20] for CEM I. Binder and sand were weighed in a 1:3 ratio. This ratio was chosen as per the standards to test the binder strength and was used for all the other tests to make meaningful comparisons. FeCN specimens were prepared with concentrations of 0.1% and 1% by weight of the binder. FeCN was first dissolved in the water used for the preparation of the mortar. The water-binder ratio (w/b) was fixed at 0.5 for CEM I and 0.6 for NHL. Additionally, control specimens (without inhibitor) were prepared as a reference. Mortar specimens were cast as prisms as well as slabs. Prisms were used for assessing the mechanical properties and the slabs were used to study transport related properties. Prisms were cast in polystyrene molds with dimension 160x40x40 mm and were compacted using a vibrating table as per EN 196-1 [20]. Mortar slabs were cast on a fired-clay brick and compacted by hand to obtain field comparable mortar which is more representative for studying moisture transport [22, 23]. A paper towel was placed on top of the brick before casting the mortar, to facilitate demoulding of the mortar slabs. The slabs had a size of 200x100 mm with a thickness of 20 mm.

After casting, all mortar specimens were covered in plastic and stored at lab conditions for the first 24 hours. CEM I specimens were demoulded/ detached from the brick substrate after 24 hours and transferred to the curing room. NHL specimens were transferred to the curing room after 24 hours with the moulds and demoulded/detached on day 5, in order to prevent damage during demoulding on account of slower hydration. The conditions in the curing room were maintained at 20°C / > 95% RH. Specimens were stored in the curing room until tested, to minimise carbonation.

3.3. Test methods

Various tests were performed on the paste and mortar specimens to assess the effect of the inhibitor on early age (fresh) properties and hardened properties of the mortars. A summary of the test methods, specimen number and size are presented in Table 3.1.

3.3.1. Characterisation of early age/fresh properties

3.3.1.1. Measurement of heat of hydration

The primary mechanism for the development of microstructure in hydraulic mortar takes place through hydration (reaction between binder and water). Since, the reaction is exothermic, monitoring the heat released during hydration provides indirect information on the microstructure development and the reaction products.

Table 3.1: Overview of test methods and specimens

Measured properties	Test method	Specimen type	Binder type	Inhibitor (%)[1]	Replicates	Size/ weight
Heat of hydration	Isothermal Calorimetry	Binder paste	NHL3.5, CEM I	0, 0.01, 0.1, 1	2	~7.5 g
Setting time	Vicat penetration	Binder paste	NHL3.5, CEM I	0, 1	2	-
Workability	Flow table test	Fresh mortar	NHL3.5, CEM I	0, 0.1, 1	2	-
Compressive and flexural strength	Compression/ 3-point bending	Mortar prisms	NHL3.5, CEM I	0, 0.1, 1	3	160×40×40 mm
E-modulus	Compression test	Mortar prisms	NHL3.5, CEM I	0, 0.1, 1	3	160×40×40 mm
Open porosity and Pore size distribution	MIP/N2	Mortar slabs	NHL3.5, CEM I	0, 0.1, 1	2	~4/1 g
Moisture transport	Capillary absorption and drying	Mortar slabs	NHL3.5, CEM I	0, 0.1, 1	4	50×20×20 mm

[1] Percentage of binder weight

The possible effects of binder-inhibitor interaction on early age reaction products can be thus captured.

The heat flow and the cumulative heat of hydration was measured on fresh binder paste specimens using an 8 channel thermometric isothermal calorimeter (TAM-Air). The test procedure is based on EN-196-11 [24]. Paste was prepared in the glass ampoule directly and placed in the calorimeter immediately. Quartz specimens with a known specific heat were used as a reference to eliminate background noise. The temperature of the calorimeter was set to 20±0.2 °C and the heat evolution was monitored continuously for 168 hours (7 days).

3.3.1.2. Setting time

Setting time is defined as the time required for the binder to completely lose its plasticity and attain a certain resistance to external pressure. The setting time of binder paste specimens, with and without the addition of the inhibitor, was measured using an automated Vicat Penetration test. The test was carried out according to EN 196-3 [25]. The depth of needle penetration was recorded automatically at fixed time intervals until the paste was completely set. The penetration curve was obtained as a function of time.

3.3.1.3. Workability

Workability refers to the measurement of consistency and in turn the ease of compaction/application during construction. A good workability is necessary for easy application of a mortar in practice. The workability was measured using a flow table

test as per EN-1015-3 [26]. Freshly mixed mortar was placed on a standard flow table in a cone in two steps. The table was jolted 15 times at a rate of 1 jolt/s. Two diametric readings of the flow were recorded and the mean value reported.

3.3.2. Characterisation of hardened properties

3.3.2.1. Measurement of compressive strength, flexural strength and elastic modulus

Compressive and flexural strength are indicative of load bearing capacities and to an extent durability of mortars. Whereas, elastic modulus provides information about stiffness of mortar and its ability to accommodate movements. Compression and flexural strength was measured on mortar prisms following EN 1015-11 norm [27]. The loading rate was maintained at 2.4 kN/s and 0.1 kN/s for compression and flexural test for CEM I specimens. In case of NHL specimens, the loading rate was reduced to 0.1 kN/s and 5 N/s for compression and flexural strength respectively. The test was performed at 28 days and at 90 days, to capture the short term and the long term mechanical effects.

Elastic modulus was measured on mortar prisms using an Instron universal testing machine. 4 Linear Variable Differential Transformer (LVDT) were glued to the specimen on the 4 sides to record the deformation (Figure 3.1(a)). The specimens were subjected to three compressive loading and unloading cycles (Figure 3.1(b)). The maximum force that the specimens were subjected to was limited to 9.5kN (5.9 MPa) for CEM I and 3kN (1.87 MPa) for NHL, in order to stay within the elastic limits. The elastic modulus was calculated as the ratio of the applied stress to the measured strain. The test was carried out on 28th day after casting.

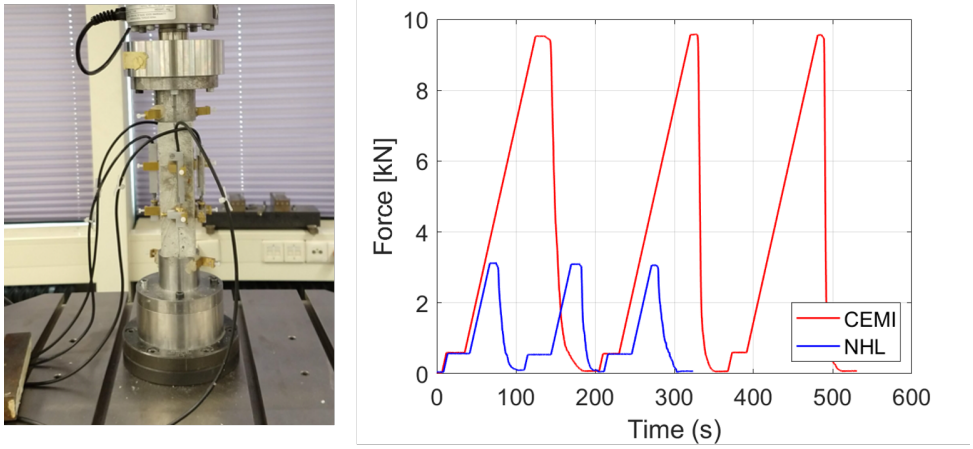

(a) (b)

Figure 3.1: (a) Experimental setup for measuring Young's modulus. Displacement measured using LVDT (b) Applied loading-unloading cycles for E-modulus measurements

3.3.2.2. Porosity and pore size distribution

Mercury intrusion porosity (MIP) was used to measure open porosity and the pore size distribution of the mortar specimens. The test was performed in Autopore IV series machine from Micromeritics. Solid samples were collected from the middle of the mortar slabs after 28 days of curing and were dried in a freeze drier to a constant weight. This was done to remove the moisture as well as prevent further hydration. Approximately, 4 g of sample was used on 2 replicates. The samples were subjected to a maximum intrusion pressure of 210 MPa and the contact angle between the mercury and the samples was assumed to be 141°. These conditions facilitated pore throat measurements between 400 µm and 0.01 µm.

In addition to MIP, N_2 adsorption method was used to obtain the pore size distribution of pores smaller than 0.01 µm. Micromeritics Gemini VII machine was used for the test. The test was performed on 1 g of freeze dried specimens. The size of the fragments that were tested were between 2-4 mm.

3.3.2.3. Measurement of water absorption and drying rate

The moisture transport properties of the mortars with the inhibitor and without the inhibitor were assessed through capillary absorption followed by drying. EN 1925 [28] was used as a guideline for capillary absorption. 50x50x20mm specimens were cut using a saw from the mortar slabs after 28 days of curing. 4 specimens from 4 different slabs were used as replicates, in order to keep the sampling representative. The specimens were first dried in an oven at 40°C until a constant weight was obtained. The lateral sides of the specimens were sealed using paraffin film to have a uni-directional moisture flow. The base of the specimens was in immersed in water to facilitate capillary absorption. The immersion level of the water was kept constant. Samples were weighed at prescribed time intervals with a precision of 0.01 g. For NHL, the time intervals as per the high absorbing substrate guidelines were used whereas, for CEM I, the time intervals as per the low absorbing substrate guidelines were used [28]. Two stages of water absorption with distinct slopes were recorded. The water absorption coefficient (WAC) calculated from Equation (3.1).

$$WAC = \frac{W_i - W_0}{A \cdot (\sqrt{t_i} - \sqrt{t_0})} \tag{3.1}$$

Where, W_0 is the dry weight of the specimen at time t_0. W_i is the weight of the specimen at time t_i which is the time at which transition between two absorption stages occur. A is the surface of the specimen in contact with water. Following capillary absorption, the specimens were dried in the oven at 40°C. The weight of the specimens was recorded regularly to obtain a drying curve. The measurements were performed until the specimens reached a constant weight.

3.4. Results and discussion

3.4.1. Effect of ferrocyanides on early age/ fresh properties

The results obtained from the heat of hydration measured using isothermal calorimeter are presented in Figure 3.2. The results are normalised to the weight of the

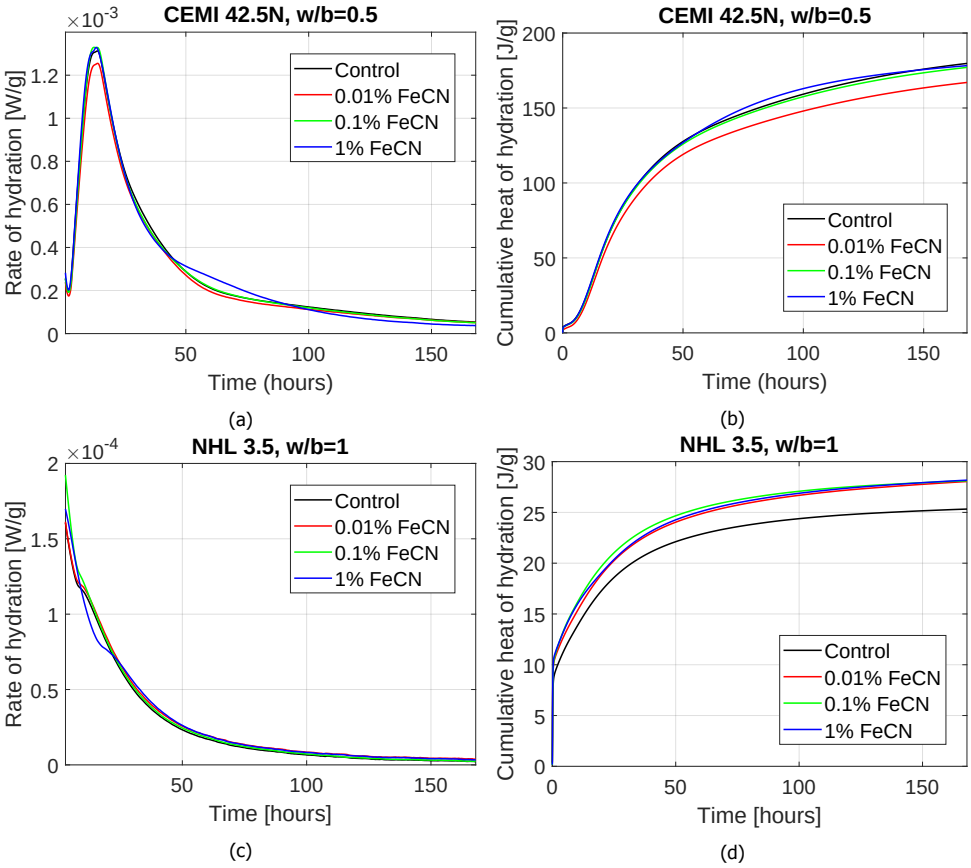

Figure 3.2: (a) Rate of hydration for CEMI (b) Cumulative heat of hydration for CEM I (c) Rate of hydration for NHL (d) Cumulative heat of hydration for NHL

specimen for comparative purposes. The hydration behaviour in CEM I is different to that of NHL due to different proportions of hydraulic phases (e.g. Alite (C_3S) and Belite (C_2S) phases) [29]. A higher heat was generated in CEM I than in NHL: this is due to the presence of higher amount of C_3S in CEM I; differently in NHL specimens C_2S is the dominant hydraulic phase. However, irrespective of the binder and their hydraulic components, the difference in the cumulative heat evolution between specimens with and without inhibitor negligible. The presence of FeCN ions in the pore solution do not seem to interact or form products with different hydraulic phases in CEM I or NHL.

The results of the Vicat penetration test (Figure 3.3) show that the penetration curve obtained in time is unaffected by the addition of inhibitor for both CEM I and NHL. The initial and final setting times for specimens with the inhibitor and without the inhibitor are comparable to each other.

The results of the workability measurements (Table 3.2 and Table 3.3), show

a minor increase in flow for CEM I specimens in which the inhibitor was added. On the other hand, a slight decrease in flow for NHL specimens. Considering the variation observed in the data, a correlation between addition of the inhibitor and the flow test cannot be clearly established; in any case the impact of the inhibitor on the workability of the mortar is minor.

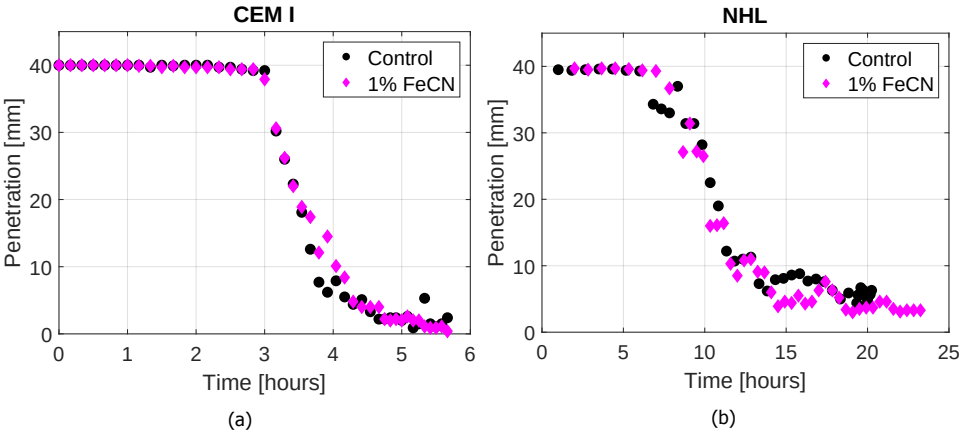

Figure 3.3: Vicat penetration test for (a) CEM I paste (b) NHL paste

3.4.2. Effect of ferrocyanides on hardened properties of mortar

The mechanical properties measured on mortar prisms are reported in Table 3.2 for CEM I and Table 3.3 for NHL. The results obtained for specimens with and without the inhibitor, at both 28 days and 90 days, show minor differences. The compressive (fc) and flexural strength (fb) observed at 90 days is higher than that at 28 days, as expected due to continued hydration.

Table 3.2: Comparison of CEMI mortar properties with different inhibitor content

Measured property	Control μ ± σ	0.1% FeCN μ ± σ	1% FeCN μ ± σ
Flow [mm]	151.7 ± 5.7	164 ± 4.6	165.7 ± 6.3
$fc_{28\ days}$ [MPa]	38.87 ± 1.69	37.29 ± 1.3	36.83 ± 2.8
$fc_{90\ days}$ [MPa]	41.02 ± 4.08	39.61 ± 2.88	37.82 ± 2.55
$fb_{28\ days}$ [MPa]	7.12 ± 0.8	8.14 ± 0.61	8.23 ± 0.29
$fb_{90\ days}$ [MPa]	8.13 ± 0.75	8.06 ± 0.07	7.56 ± 0.4
$E\text{-modulus}_{28\ days}$ [MPa]	35529 ± 1511	37105 ± 2514	35900 ± 2590
WAC [$g/m^2s^{0.5}$]	13.16	13.95	14.53
Open Porosity [%]	11.75	10.98	11.41

μ= mean, σ= standard deviation

In case of NHL specimens, the 28th day elastic modulus shows some scatter, but the values are not necessarily in the proportion of the added FeCN. The large scatter observed in NHL mortars is attributed to possible micro-cracking during cyclic loading. The applied maximum load of 1.87 MPa (50% of compressive strength) in combination with NHL's low mechanical strength probably induced inelastic behaviour in some specimens.

The pore size distribution for CEM I and NHL mortars, as measured by MIP (pore diameter between 100 µm and 0.01 µm) and N2 adsorption (pore diameter less than 0.01 µm) is presented in Figure 3.4. The average mean pore diameter of around 0.05 µm and 0.15 um was obtained for CEM I and NHL respectively, irrespective of the amount of inhibitor. The cumulative intrusion obtained for mortar specimens with and without FeCN is almost identical. The open porosity, as measured by MIP for CEM I (11.3 %) and NHL (23%), does not change significantly with the addition of the inhibitor. The pore size distribution for pores smaller than 0.01 µm is also unaffected (Figure 3.4b and 3.4d). Based on these results, it can be concluded that FeCN does not alter the pore structure in the studied hydraulic mortars.

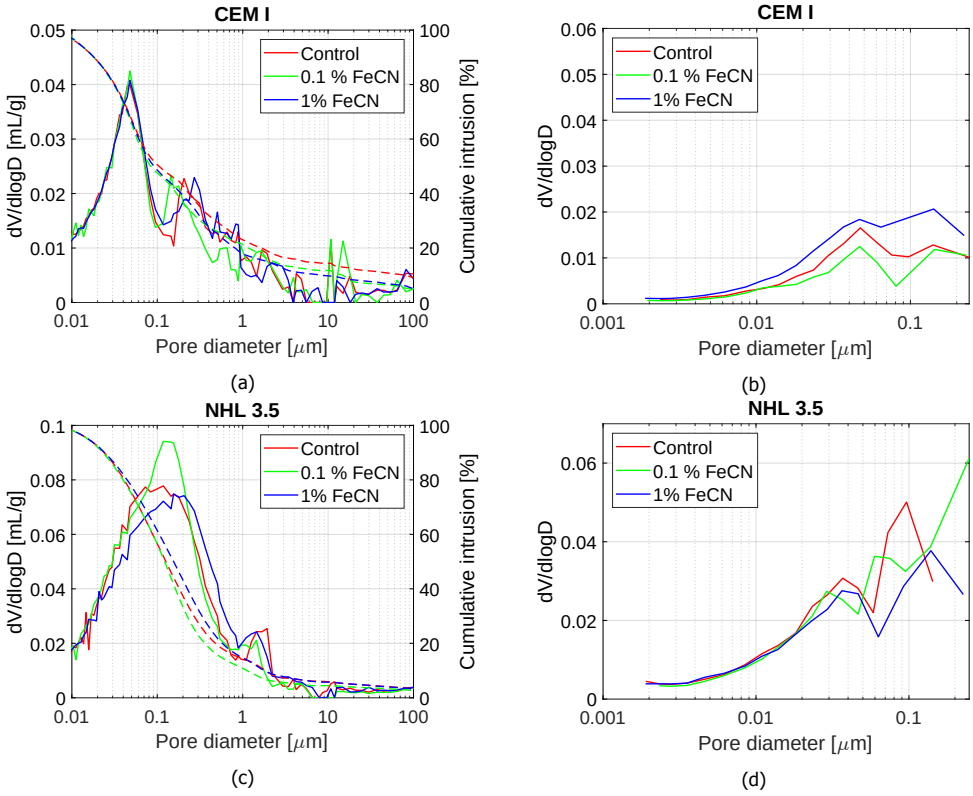

Figure 3.4: Pore size distribution measurements (a) MIP for CEM I (b) N2 adsorption for CEM I (c) MIP for NHL (d) N2 adsorption for NHL

The capillary water absorption curves for CEM I and NHL mortar specimens with and without inhibitor is shown in Figure 3.5. The water absorption is normalised to the dry weight of the specimens to take into account the thickness variation across specimens resulting from hand compaction. The two stages of absorption can be distinctly seen for both CEM I and NHL. Linear regression was performed on two absorption stages and the intersection point was used to calculate the water absorption coefficient (WAC) as per Equation 3.1. The WAC values for different inhibitor contents, as shown in Table 3.2 (CEM I) and Table 3.3 (NHL), are comparable to their respective control specimens. Moreover, the normalised water absorption curves (Figure 3.5) in both the absorption stages show negligible differences between specimens with and without inhibitor.

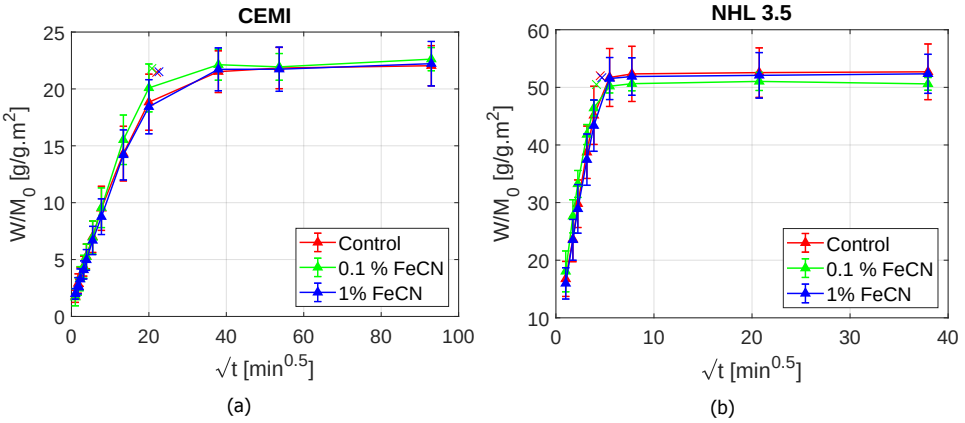

Figure 3.5: Moisture absorption through capillarity for different FeCN concentrations (a) CEMI (b) NHL

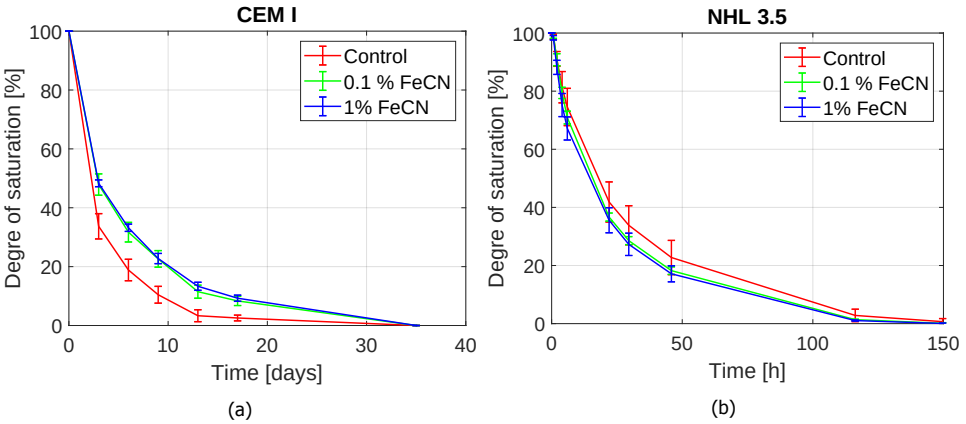

Figure 3.6: Drying behaviour of mortar specimens with different FeCN concentration (a) CEMI (b) NHL

The drying behaviour of CEM I and NHL is shown in Figure 3.6. In case of

CEM I (Figure 3.6a), the specimens with FeCN dry slightly slower than the control specimens. However, considered the high scatter observed in the drying curves of the control specimens, the effect of inhibitor on the drying can be judged to be minor. In the case of NHL specimens the drying curves for specimens with and without FeCN addition are very similar. Based on these results, and taking into account the outcome of the pore size distribution, it can be concluded that the moisture transport properties are not significantly affected by the addition of FeCN.

Table 3.3: Comparison of NHL mortar properties with different inhibitor content

Measured property	Control μ ± σ	0.1% FeCN μ ± σ	1% FeCN μ ± σ
Flow [mm]	143.2 ± 1.8	139 ± 3.7	136.5 ± 2.1
$fc_{28\ days}$ [MPa]	3.22 ± 0.24	3.52 ± 0.06	3.75 ± 0.09
$fc_{90\ days}$ [MPa]	5.64 ± 0.87	5.88 ± 0.2	6.28 ± 0.48
$fb_{28\ days}$ [MPa]	1.30 ± 0.02	1.44 ± 0.13	1.44 ± 0.04
$fb_{90\ days}$ [MPa]	2.23 ± 0.87	2.62 ± 0.07	2.65 ± 0.13
$E\text{-modulus}_{28\ days}$ [MPa]	3441 ± 1025	4324 ± 879	3217 ± 811
WAC [$g/m^2s^{0.5}$]	137.11	123.46	131.97
Open Porosity [%]	23.44	23.51	23.54

μ= mean, σ= standard deviation

3.5. Conclusion

In this paper, the interaction between sodium ferrocyanide, a well-known inhibitor of NaCl crystallisation, and two types of hydraulic binders (NHL and OPC) was studied. Various properties of the binders in fresh paste and of the fresh and hardened mortars were assessed on specimens with different inhibitor concentrations (0%, 0.01%, 0.1% and 1%). The results of all the measurements agree with each other and clearly show that the addition of inhibitor, up to 1%, of the binder weight does not affect the mechanical and moisture transport properties in the studied hydraulic mortars. The hydration of binder paste as well as the setting time is unaffected by the addition of the inhibitor. Therefore, it can be inferred from the results that sodium ferrocyanide remains inert and does not participate in development of the microstructure of the studied mortars. Sodium ferrocyanide thus proves to be a suitable crystallisation inhibitor that can be added during the mixing stage. These results constitute a first step in the development of hydraulic mortars with crystallisation inhibitors, opening new possibilities for the wider use of this inhibitor in different applications, from building renovation to new construction. In future work, the durability of the hydraulic mortars with mixed-in FeCN with respect to salt decay will be assessed, both in laboratory and in situ.

References

[1] G. W. Scherer, *Stress from crystallization of salt,* Cement and Concrete Research **34**, 1613 (2004).

[2] R. P. J. V. Hees, S. Naldini, and J. Delgado, *Plasters and renders for salt laden substrates,* Construction and Building Materials **23**, 1714 (2008).

[3] S. J. Granneman, B. Lubelli, and R. P. van Hees, *Mitigating salt damage in building materials by the use of crystallization modifiers – a review and outlook,* Journal of Cultural Heritage **40**, 183 (2019).

[4] A. A. Bode, V. Vonk, F. J. Van Den Bruele, D. J. Kok, A. M. Kerkenaar, M. F. Mantilla, S. Jiang, J. A. Meijer, W. J. Van Enckevort, and E. Vlieg, *Anticaking activity of ferrocyanide on sodium chloride explained by charge mismatch,* Crystal Growth and Design **12**, 1919 (2012).

[5] E. R. Townsend, W. J. Van Enckevort, J. A. Meijer, and E. Vlieg, *Additive Enhanced Creeping of Sodium Chloride Crystals,* Crystal Growth and Design **17**, 3107 (2017).

[6] C. Rodriguez-Navarro, L. Linares-Fernandez, E. Doehne, and E. Sebastian, *Effects of ferrocyanide ions on NaCl crystallization in porous stone,* Journal of Crystal Growth **243**, 503 (2002).

[7] B. Lubelli and R. P. van Hees, *Effectiveness of crystallization inhibitors in preventing salt damage in building materials,* Journal of Cultural Heritage **8**, 223 (2007).

[8] T. Rivas, E. Alvarez, M. J. Mosquera, L. Alejano, and J. Taboada, *Crystallization modifiers applied in granite desalination: The role of the stone pore structure,* Construction and Building Materials **24**, 766 (2010).

[9] S. Gupta, K. Terheiden, L. Pel, and A. Sawdy, *Influence of Ferrocyanide Inhibitors on the Transport and Crystallization Processes of Sodium Chloride in Porous Building Materials,* Crystal Growth & Design **12**, 3888 (2012).

[10] C. Selwitz and E. Doehne, *The evaluation of crystallization modifiers for controlling salt damage to limestone,* Journal of Cultural Heritage **3**, 205 (2002).

[11] B. Lubelli, T. G. Nijland, R. P. Van Hees, and A. Hacquebord, *Effect of mixed in crystallization inhibitor on resistance of lime-cement mortar against NaCl crystallization,* Construction and Building Materials **24**, 2466 (2010).

[12] S. J. Granneman, B. Lubelli, and R. P. van Hees, *Effect of mixed in crystallization modifiers on the resistance of lime mortar against NaCl and Na2SO4 crystallization,* Construction and Building Materials **194**, 62 (2019).

[13] J. Feijoo, D. Ergenç, R. Fort, and M. A. de Buergo, *Addition of ferrocyanide-based compounds to repairing joint lime mortars as a protective method for porous building materials against sodium chloride damage,* Materials and Structures **54**, 14 (2021).

[14] S. J. Granneman, B. Lubelli, and R. P. Van Hees, *Characterization of lime mortar additivated with crystallization modifiers,* International Journal of Architectural Heritage **12**, 849 (2018).

[15] P. Maravelaki-Kalaitzaki, A. Bakolas, I. Karatasios, and V. Kilikoglou, *Hydraulic lime mortars for the restoration of historic masonry in Crete,* Cement and Concrete Research **35**, 1577 (2005).

[16] B. A. Silva, A. P. Ferreira Pinto, and A. Gomes, *Natural hydraulic lime versus cement for blended lime mortars for restoration works,* Construction and Building Materials **94**, 346 (2015).

[17] B. A. Silva, A. P. Ferreira Pinto, and A. Gomes, *Influence of natural hydraulic lime content on the properties of aerial lime-based mortars,* Construction and Building Materials **72**, 208 (2014).

[18] M. J. Mosquera, B. Silva, B. Prieto, and E. Ruiz-Herrera, *Addition of cement to lime-based mortars: Effect on pore structure and vapor transport,* Cement and Concrete Research **36**, 1635 (2006).

[19] M. Arandigoyen and J. I. Alvarez, *Pore structure and mechanical properties of cement-lime mortars,* Cement and Concrete Research **37**, 767 (2007).

[20] *NEN-EN 196-1: Methods of testing cement - Part 1: Determination of strength*, Tech. Rep. (European committee for standardisation (CEN), 2015).

[21] *NEN-EN 459-2: Building lime-part 2: Test methods*, Tech. Rep. (European committee for standardisation (CEN), 2008).

[22] C. J. Groot, *Effect of water on mortar-brick bond*, Ph.D. thesis, Delft University of Technology (1993).

[23] T. Wijffels and R. van Hees, *The influence of the loss of water of the fresh mortar to the substrate on the hygric characteristics of so-called restoration plaster,* in *International Workshop on Urban Heritage and Building Maintenance VII* (2000) pp. 49–54.

[24] *NEN-EN 196-11: Methods of testing cement-part 11: Heat of hydration-Isothermal Conduction Calorimetry method*, Tech. Rep. (European committee for standardisation (CEN), 2019).

[25] *NEN-EN 196-3 Methods of testing cement-Part3: Determination of setting times and soundess*, Tech. Rep. (European committee for standardisation (CEN), 2016).

[26] *NEN-EN 1015-3: Methods of test for mortar for masonry - Part 3: Determination of consistence of fresh mortar (by flow table)*, Tech. Rep. (European committee for standardisation (CEN), 1999).

[27] *NEN-EN 1015-11: Methods of test for mortar for masnory-Part 11: Determination of flexural and conpressive strength of hardened mortar*, Tech. Rep. (European committee for standardisation (CEN), 2019).

[28] *NEN-EN-1925: Natural stone test methods- Determination of water absorption coefficient by capillarity*, Tech. Rep. (European committee for standardisation (CEN), 1999).

[29] J. Lanas, J. L. Bernal, M. A. Bello, and J. I. Galindo, *Mechanical properties of natural hydraulic lime-based mortars,* Cement and Concrete Research **34**, 2191 (2004).

4

Leaching behaviour of a crystallisation inhibitor in mortars

The results from the previous chapter show that the addition of inhibitor does not have any negative effects on the properties of hydraulic mortars, meaning that it is feasible to mix the inhibitor in hydraulic mortars. However, the high solubility of the inhibitor in water makes it susceptible to leach out of mortar due to mass transport mechanisms, such as advection and diffusion. Leaching and depletion of the inhibitor from mortar might over time, make the inhibitor less effective against salt damage. In this chapter, an experimental leaching test protocol is designed, for the assessment of both diffusion- and advection-driven leaching of the inhibitor in mortar. Natural hydraulic lime (NHL) mortar specimens with mixed-in inhibitor are subjected to the leaching tests and the leaching of the inhibitor is quantified using experimental techniques such as Ultraviolet-visible spectrophotometry (UV-VIS) and inductively coupled plasma-optical emission spectroscopy (ICP-OES).

This chapter is based on the article published in Journal of Building Engineering **9**, 107933 (2023).


$Fe(CN)_6^{4-}$
H_2O
PORE ENT
HELP!
FeCN

4.1. Introduction

Salt crystallisation in pores can result in significant damage to building materials, such as brick, natural stone and mortars. The damage is attributed to the development of crystallisation pressure as salt crystals grow against confined pore walls [1–3]. Soluble salts like sodium sulphate (Na_2SO_4) [4, 5] and sodium chloride (NaCl) [6, 7] are commonly found in buildings and responsible for salt crystallisation damage. NaCl, despite being much less damaging than sodium sulphate in accelerated crystallisation tests is found to cause severe decay in the field, in a wide range of environments [8]. Salt-spray, groundwater and de-icing salts are some of the common sources for NaCl accumulation in buildings [9]. Repeated crystallisation-deliquescence of NaCl crystals have shown to aggravate the damage [10, 11]. Exposed parts of the buildings (e.g., plasters and renders) are particularly susceptible to salt induced weathering, due to repeated crystallisation-deliquescence cycles on account of a continuously changing environment (temperature and humidity changes) [12]. The damage manifests in the form of progressive material loss and is noticeably evident in the built cultural heritage. In fact, ancient mortars, which are mostly based on (hydrated) lime, are particularly vulnerable to salt crystallisation pressures, due to their low mechanical strength [13] and high potential to accumulate salts [14]. However, even in modern concrete, physical salt attack is of concern and cannot be neglected [15]. Current conservation techniques against salt damage, such as desalination, are costly and not always feasible [16]. Repair materials, such as stone-repair mortars and renovation plasters and renders, often have a limited durability and/or compatibility with the existing materials [17]. In the last decades, considerable research has been undertaken to seek alternative, durable solutions. The use of crystallisation inhibitors in porous building materials has shown promising results in numerous studies.

Crystallisation inhibitors are chemical compounds that modify salt crystallisation. Ionic compounds containing ferrocyanide ions ($[Fe(CN)_6]^{4-}$) such as sodium ferrocyanide (NaFeCN) or potassium ferrocyanide (KFeCN), are known to inhibit sodium chloride (NaCl) crystallisation by increasing supersaturation and thereby delaying the onset of crystal nucleation [18]. This favours mass transport of solutes over longer distances before precipitation [19]. Selwitz and Doehne were first to study the potential of alkali ferrocyanides as a treatment for salt damage mitigation in porous building materials [20]. The authors reported an increase in the amount of efflorescence and a decrease in damage in porous limestone contaminated with NaCl in presence of KFeCN, when compared to specimens contaminated with NaCl only. Alkali ferrocyanides are also shown to be habit modifiers, altering NaCl crystal from a regular cubic structure to a dendritic pattern [21]. Changes to the crystal habit are a result of a charge mismatch between $[Fe(CN)_6]^{4-}$ ion and the sodium chloride cluster blocking further crystal growth, by forming weak inter-crystal bridges [22]. This habit modification makes alkali ferrocyanides excellent anticaking agents for table salt, by preventing agglomeration of big crystals [23]. Studies in building materials also confirm NaFeCN's anticaking activity in increasing nucleation density and forming smaller NaCl crystals [24]. This could prevent

pore clogging and reduce crystallisation pressure. Additionally, the dendritic crystal structure has shown to increase the surface area of salt crystals, thereby contributing to faster evaporation and salt transport to the surface [25]. Other studies performed on various porous substrates (stones, bricks, mortars and soil) have reported similar results i.e. increased salt (NaCl) transport out of the substrate (efflorescence), modification of the crystal habit and most importantly, minimal material damage in presence of $[Fe(CN)_6]^{4-}$ ions [21, 26–29].

In recent years, hydrated lime mortars with mixed-in inhibitors have been tested with positive results [30]. A notable difference with the previous studies is the way the inhibitor is introduced to the porous substrate. In these studies, NaFeCN was added directly during the mortar preparation (mixing) stage. Accelerated salt weathering tests showed lower damage on specimens with the inhibitor compared to control specimens [31–33]. This was also evident in a case study, where hydrated lime plaster with mixed-in NaFeCN showed negligible material loss when applied on a salt-contaminated brick wall, after a period of 4 years [34]. Moreover, research has shown that the addition of inhibitor up to 1% of binder weight to lime mortars (hydrated or hydraulic) does not affect the physical and chemical properties of mortar [35, 36]. All these studies point towards NaFeCN/ KFeCN as a suitable crystallisation inhibitor to be mixed in mortars in order to mitigate NaCl-induced decay.

In spite of all the mentioned advantages, one issue could limit the application of NaFeCN in mortar. Sodium ferrocyanide decahydrate, a commonly used source of $[Fe(CN)_6]^{4-}$ ions, has a high water solubility (17 g/100 mL at 25°C)] [37] and might leach out with time, losing its positive effect. Some preliminary observations from past research suggest that this inhibitor might leach out during wet-dry cycles [31] and accumulate at the outer surface due to capillary transport [34]. However, until now no systematic study is done to understand the inhibitor transport and its consequent leaching.

In porous materials, two mechanisms play an important role in transport of the inhibitor: Diffusion and advection. In fact, in all practical situations a competition of advection leading to accumulation (and crystallisation) of solute near the surface and simultaneous levelling of the concentration gradient due to diffusion dictates the transport mechanism [38]. Study of both mechanisms is equally relevant to understand the leaching behaviour. Studying the degree of leaching under both, diffusion and advection, will help in improving the durability of mortars with mixed-in NaFeCN.

This paper investigates transport and leaching of the NaFeCN inhibitor in mortar specimens made with natural hydraulic lime (NHL). In the first part, diffusive transport in mortar specimens containing the inhibitor is studied under controlled conditions using a standard test. The effective diffusion coefficient of $[Fe(CN)_6]^{4-}$ ions from mortar is measured and compared to effective diffusion coefficient of chloride ions from mortar specimens with similar properties. In the second part of the paper, advection driven inhibitor transport under realistic conditions is simulated experimentally. Capillary wetting and drying cycles are used as a driving force for advection. The changes to the spatial distribution of the inhibitor are monitored.

The results from the two tests are discussed and solutions are proposed to minimise leaching.

4.2. Materials and methods

4.2.1. Test materials, specimen preparation and storage

Natural hydraulic lime (NHL) with a strength class of 3.5 was used as the binder. Standard river sand conforming to NEN-EN 196-1 [39] with a particle size distribution between 0.08-2mm was used in mortar preparation. Laboratory grade reagent sodium ferrocyanide decahydrate (chemical formula:$Na_4Fe(CN)_6 \cdot 10\,H_2O$) purchased from Acros organics was used as the crystallisation inhibitor. Laboratory grade sodium chloride (NaCl) was purchased from Sigma Aldrich.

Mortar was cast as cylindrical specimens (Φ=30 mm and H=50 mm) in smooth PVC cylindrical containers. Three types of cylindrical specimens were prepared: (1) Reference samples without any inhibitor [R]. (2) Specimens containing the inhibitor [I]. (3) Specimens containing sodium chloride [S]. All the specimens were cast with NHL and sand in a volumetric proportion (1:3). A water-binder (w/b) ratio of 1.19 was used for all mixes, based on the flow requirements of 165 mm [40] measured on the reference mix [R]. Mixing was carried according to the standards [40].

For specimens containing the inhibitor [I], sodium ferrocyanide decahydrate (abbreviated as NaFeCN), in the amount equivalent to 10% by weight of the binder, was first dissolved in the water used for mixing (0.17 mol kg^{-}1) and then added to NHL and sand. This very high concentration of the inhibitor, much higher than that used in past research (1%) [31], was necessary to stay within detection limits of the used analysis techniques (Section 4.2.3.2).

For specimens containing salt [S], NaCl, in the amount of 0.17 mol kg^{-1} (corresponding to 1.17% of the binder weight) was first dissolved in water and then added to NHL and sand during mixing. This way, [S] and [I] specimens contained the same concentration of Cl^- and $[Fe(CN)_6]^{4-}$ ions respectively, making possible to compare the leaching of these ions across different specimens.

An overview of specimen mix design is shown in Table 4.1.

Table 4.1: Mix design of mortar and different types of specimens used.

Component	Reference [R]	Inhibitor [I]	Salt [S]
Binder: Sand [volume]	1:3	1:3	1:3
w/b	1.19	1.19	1.19
$Na_4Fe(CN)_6 \cdot 10\,H_2O$ [mol kg^{-1}]	-	0.17	-
NaCl [mol kg^{-1}]	-	-	0.17

All specimens were cured in the fog room at > 95% RH and 20°C. Specimens were kept sealed inside PVC cylindrical containers with a screw lid to avoid any leaching during the curing stage and cured for at least 28 days. Additionally, binder paste (without sand) specimens corresponding to [R], [S] and [I] were prepared to

measure fresh properties. For paste specimens, w/b=1 was used. The specimens were tested immediately after mixing.

4.2.2. Materials characterisation

The aim of this section is to evaluate if different types of specimens [R], [I] and [S] used in the leaching tests are comparable to each other. Relevant properties that affect moisture and salt transport are studied in detail.

An overview of characterisation tests is shown in Table 4.2. Their open porosity, bulk density and pore size distribution were measured using mercury intrusion porosimetry (MIP) (Autopore IV by Micromeritics). The test was performed on samples ~ 1 cm^3, freeze dried after the curing period.

Water absorption via capillary suction was performed according to the NEN-EN 1925 standard [41]. The Capillary Moisture Content (CMC) and the time required for reaching CMC was obtained. At the end of the absorption test, the bottom side of the specimens was sealed with a paraffin film and the specimens were dried at 20°C and 50% RH. The specimens were weighed at defined time intervals, to obtain the drying curve.

The heat of hydration was measured on [R], [S] and [I] paste specimens. Measurements were carried out at a constant temperature of 20°C for a period of 7 days, using calorimeter (Tam-AIR).

Table 4.2: Characterisation tests and type of specimens

Material property	Test	Type of specimen	Specimen size	Number of Replicates
Pore size distribution Open porosity Bulk density	MIP	Mortar specimens	1 cm^3	2
Heat of hydration	Isothermal calorimetry	Binder paste	5 g	2
Water absorption and drying	Gravimetry	Mortar specimens	Φ=30 mm H=50 mm	3

4.2.3. Leaching by diffusion

This test aims to study leaching of the inhibitor from mortar specimens under diffusion driven transport. The rate of leaching is obtained by estimating the effective diffusion coefficient of the inhibitor leached from mortar specimens [I] under controlled conditions. This is compared to the effective diffusion of chloride ions, as measured on mortar specimens [S], which are tested independently. In this way, rate of leaching of the inhibitor relative to the rate of leaching of salts (NaCl) is obtained from a similar type of mortar.

4.2.3.1. Test setup for study of leaching

The leaching test is based on ASTM C1308-21 standard [42]. The ASTM procedure was chosen as it enables to estimate the effective diffusion coefficient in a relatively short time (10 days).

The cylindrical mortar specimens (Section 4.2.1) were suspended in a plastic cylindrical tank using a fishing line as shown in Figure 4.1a. A known volume of deionised water was added as the leachant (V_l). V_l was chosen such that the ratio of the surface area of the specimen (S) and the volume of the leachant (V_l) was 0.15 cm^{-1}. The leachate (leachant with dissolved species) was renewed using exactly the same volume (V_l) of deionised water, at the prescribed time intervals as per the standard.Prior to each renewal step, 20 mL of leachate was collected as an eluate analysed for relevant leached ions (section 4.2.3.2). The temperature and humidity in the lab were recorded and found to be around 25°C and 55% RH. The test was conducted in two series, as shown in Figure 4.1b. In the first series, one reference specimen [R] and 3 replicates of specimens containing the inhibitor [I] were tested for leaching of the inhibitor ($[Fe(CN)_6]^{4-}$ ions). In the second series, one reference specimen [R] and 3 replicates of specimens containing sodium chloride [S] were tested for the leaching of chloride ions. For the sake of simplicity, possible binding of chloride (or $[Fe(CN)_6]^{4-}$ ions) to mortar components was not taken into account.

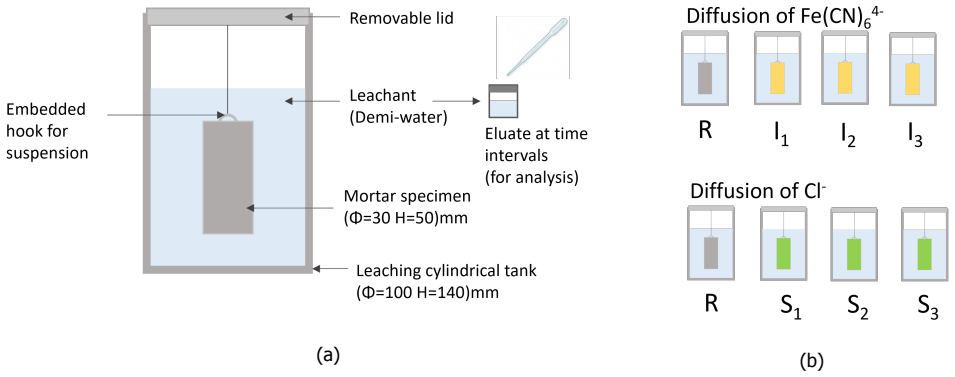

Figure 4.1: : (a) Experimental setup for leaching by diffusion (b) Series of specimens tested in the test.

The cold water extraction (CWE) test based on the work done by Plusquellec et al. [43] was used to estimate amount of inhibitor present in the mortar specimens. The test was conducted on:

- Specimens [I] and [S] that were tested in the tank leaching test, to determine the amount of inhibitor (or chlorides) left within the specimens at the end of the test. The results were then used as an input to calculate the effective diffusion coefficient (Section 4.2.3.3).
- Specimens [I] and [S] not used for the leaching test, to estimate the initial amount of inhibitor and chloride respectively and validate the findings from the tank leaching test.

The specimens were first dried in an oven at 40°C until constant mass. The entire specimens were then crushed to a fine powder in a Retsch ball milling machine. An amount of demineralised water equal to the dry weight of the specimen was added to the finely ground powder. The mixture was stirred at 600 rpm for 5 minutes using a magnetic stirrer at room temperature. The free species were then allowed to dissolve for 24 hours. Subsequently, a sample (5 mL) was passed through a qualitative medium speed filter and analysed for relevant species. Samples from [I] specimens were analysed using ICP-OES to quantify the present Fe ions. Samples from [S] specimens were analysed using ion-chromatography (IC), for measuring the amount of Cl ions (See section 4.2.3.2).

$$A_0 = \sum_{n=1}^{N} a_n + a_f \tag{4.1}$$

The initial amount of species ($[Fe(CN)_6]^{4-}$ or Cl^-) was calculated as per Equation 4.1 where: A_0 [mg] = absolute amount of species present at the start of the test; a_n [mg] = absolute amount of species leached at each n time interval. The absolute value a_n was obtained my multiplying the measured concentration [mg/L] with V_l [mL]. a_f [mg] = absolute amount of species left in the specimen at the end of the leaching test. The absolute value a_f was obtained my multiplying the measured concentration [mg/L] with the volume of water used in CWE [mL].

4.2.3.2. Eluate analysis: Quantification of leached species

Ultraviolet-visible (UV-VIS) spectroscopy

A spectrophotometer (Shimadzu UV2600) was used to quantify the concentration of NaFeCN in eluates. In the presence of $[Fe(CN)_6]^{4-}$ ions, a strong absorption peak is measured at a wavelength of 218 nm [18, 44]. The concentration was measured as per Equation 4.2, following the Beer-Lambert's law [45].

$$Abs = \log_{10}\left(\frac{I_0}{I}\right) = k \cdot C \tag{4.2}$$

Where, Abs is the characteristic wavelength, C is the concentration of NaFeCN, k is the proportionality constant, and I_0 and I correspond to the incident and the transmitted light intensity respectively.

The optical path length of 1 cm was used for all the samples. The value of k was obtained by performing a linear regression with three freshly prepared standard solutions containing 25 mg/L, 12.5 mg/L and 6.25 mg/L of NaFeCN (Figure 4.2b). Samples showing high absorbance (>1.5) were diluted such that the results remained within the linear calibration range.

Inductive Coupled Plasma Optical Emission Spectroscopy (ICP)

ICP was performed as a complimentary technique to cross validate the results obtained using UV-VIS. The eluates from [I] specimens were measured for Fe(II)/Fe(III)

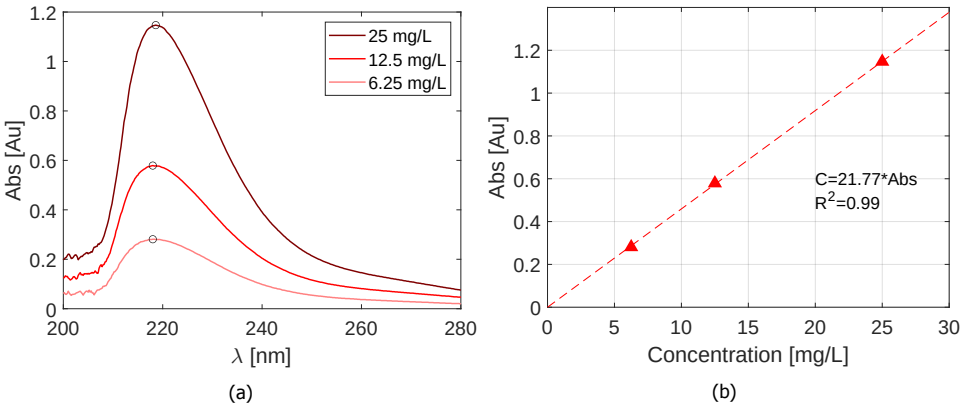

Figure 4.2: : UV-VIS calibration using solutions containing sodium ferrocyanide with known concentrations (a) Presence of $[Fe(CN)_6]^{4-}$ shows a strong peak at 218 nm (b) correlation between measured absorbance and concentration of sodium ferrocyanide obtained using linear regression.

cations. 1 mL of the sample was diluted and acidified with 9 mL of 2% (v/v) HNO_3 and analysed using optical emission spectrometer (Perkin Elmer Optima 5300DV).

Ion Chromatography (IC)

IC was performed on eluates of the sampled leachate from [S] specimens to measure the chloride content. Dionex ICS 90 (by Thermo Fischer) ion chromatographs were used. The anions were separated using AS14A column where a solution of Na_2CO_3 and $NaHCO_3$ was used as an eluent.

4.2.3.3. Model for estimation of the effective diffusion coefficient

The amount of the leached species measured at each time step was used to estimate the effective diffusion coefficient (D_e) of the inhibitor and chloride ions from [I] and [S] specimens respectively, as per finite cylindrical model presented in the standard [46].

As a first step, at each time interval (n), the leached species (i.e., $[Fe(CN)_6]^{4-}$ or Cl^-) are expressed as cumulative fraction leached (CFL), which is a dimensionless quantity. The CFL at nth interval is calculated as per equation 4.3.

$$CFL_n = \sum_{n=1}^{N} \frac{a_n}{A_0} \tag{4.3}$$

The analytical solution is presented in in Equation 4.4 [46],. The test setup and the analytical solution assume the same boundary conditions. A complete mathematical derivation using Fourier-Bessel series can be obtained from the works of Nestor and Pescatore [47, 48]. The CFL obtained from Equation 4.3 is fitted to Equation 4.4 in order to obtain the effective diffusion coefficient D_e .

$$CFL = \left(1 - \frac{32}{\pi^2} S_p(t) S_c(t)\right) \tag{4.4}$$

with the series,

$$S_p(t) = \sum_{j=1}^{\infty} \frac{exp\left[-\left(\frac{(2j-1)\pi}{H}\right)^2 D_e t\right]}{(2j-1)^2} \tag{4.5}$$

$$S_c(t) = \sum_{m=1}^{\infty} \frac{exp\left[-\left(\frac{\beta_m}{R}\right)^2 D_e t\right]}{\beta_m^2} \tag{4.6}$$

Where, R is the radius of the specimen, H is the height of the specimen, t is the time. j represents the number of terms used in the series and m represents the series index that satisfy the zeroth order cylindrical Bessel function β. A tolerance of 10^{-8} was used for the number of terms needed in the series for convergence during the iterative process.

4.2.4. Leaching by advection

The aim of the test is to monitor the advection-driven transport of inhibitor over the specimen height during repeated capillary absorption-drying cycles.

4.2.4.1. Test setup for study of advection

A scheme of the test setup is presented in Figure 4.3. Twelve cylindrical specimens containing the inhibitor [I], prepared as described in Section 4.2.1, were used in this test. Before the start of the test, three specimens were analysed to assess the initial inhibitor distribution (see Section 4.2.4.2). The remaining 9 specimens were oven dried to a constant weight. Later, the sides of the specimens were sealed with a paraffin film to allow only for unidirectional flow. The specimens were subjected to three cycles of capillary suction via their bottom surface followed by drying via the opposite, evaporation surface. This procedure aims to replicate the moisture transport mechanism, which is common in the field, where plaster/renders are subjected to water supply (e.g., due to rising damp) from the wall on which they are applied and allowed to dry only through the exposed surface.

Each cycle consisted of three stages (Figure 4.3c). In the first stage, specimens were saturated with demineralised water via capillary suction (Figure 4.3b). The amount of water used for capillary absorption was equal to the maximum capillary moisture content value obtained from Table 4.3. After absorption was completed, the bottom of the specimens was sealed with a paraffin film. In the second stage, specimens were dried in a climate chamber at 20°C and 50% relative humidity. These conditions reflect common indoor field conditions and were used to facilitate liquid transport to the evaporative surface. In the third stage, at day 10, the specimens were moved to an oven at 40°C /15% RH. This procedure was defined in order to speed-up drying, without significantly affecting the transport of the inhibitor: after 10 days, the moisture content in the specimen is such that liquid transport does

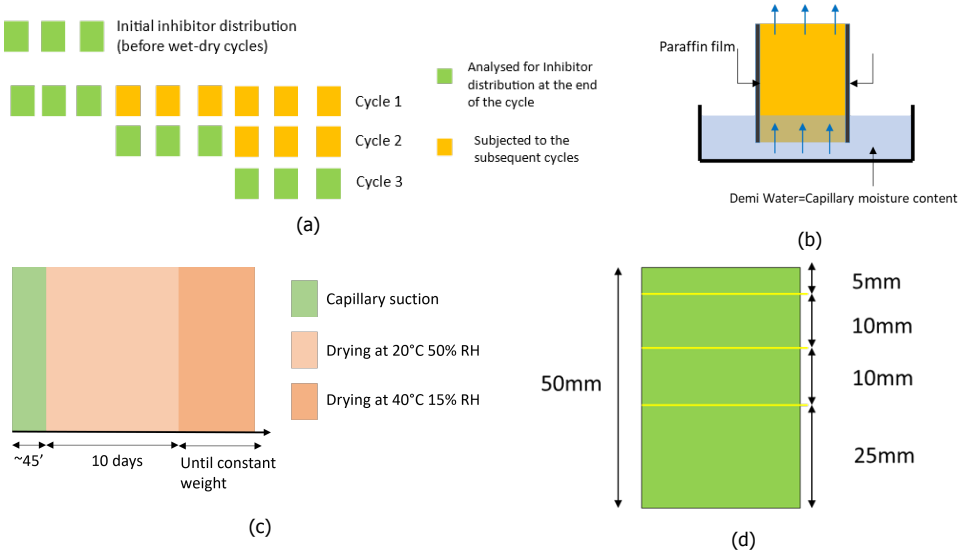

Figure 4.3: (a) Overview of specimens used in each cycle (b) Schematic of capillary suction (c) Composition of the wet-dry cycle (d) schematic for inhibitor distribution.

not play a significant role anymore and thus no further transport of the inhibitor can occur. At the end of each cycle, 3 specimens were used to analyse for the inhibitor distribution (Section 4.2.4.2), and the remaining specimens were subjected to the next cycle. During the test, the weight of the specimens was recorded regularly, and changes to the specimen surface were photographically recorded.

4.2.4.2. Distribution of the inhibitor

At the end of each wet-dry cycle, 3 specimens were brushed to remove any non-adhering efflorescence, which was collected and weighted separately. The specimens were then sliced over the depth (Figure 4.3d) with a dry saw and crushed to a fine powder. 500 mg of the powdered sample passed through 250 micron sieve was dissolved in 30 mL of demineralised water for 24 hours. The concentration of inhibitor in each solution was analysed using UV-VIS (Section 4.2.3.2). Additionally, a small sample from the efflorescence developed on the top surface of the specimen was analysed using UV-VIS to quantify the amount of NaFeCN present in the efflorescent crust.

Environmental scanning electron microscope (ESEM) from FEI Quanta 650 FEG equipped with EDS (Noran EDS system) was used on a polished section of a mortar specimens subjected to one wet-dry cycle, in order to assess the inhibitor distribution in the outer 5 mm layer, by mapping of Fe, Na, N, Ca and Si. The specimen was epoxy impregnated to stabilise the mortar and sawed along the cross-section without using water. The cross-section was again impregnated with epoxy and polished using ethanol to prevent any dissolution of the NaFeCN crystals. The grinding and polishing procedure was followed as per past research [49]. The images were

acquired at a voltage of 15kV.

The crystal morphology of the NaFeCN crystals was studied on both a cross-section of the mortar and the efflorescence crust on the surface. Back-scattered electron (BSE) and secondary electron (SE) detectors were used. The sample for studying morphology was prepared by fracturing the mortar specimen along the height using a tensile splitting test.

4.3. Results

4.3.1. Materials characterisation

The pore size distribution of different types of specimens is presented in Figure 4.4a. It can be seen that the pore size distribution is similar for [R], [I] and [S] specimens. The heat of hydration (Figure 4.4b) also does not show formation of any anomalous hydrates due to the presence of inhibitor or salts. Other relevant microstructure properties (bulk density and open porosity) are shown in Table 4.3 and are comparable across different specimens.

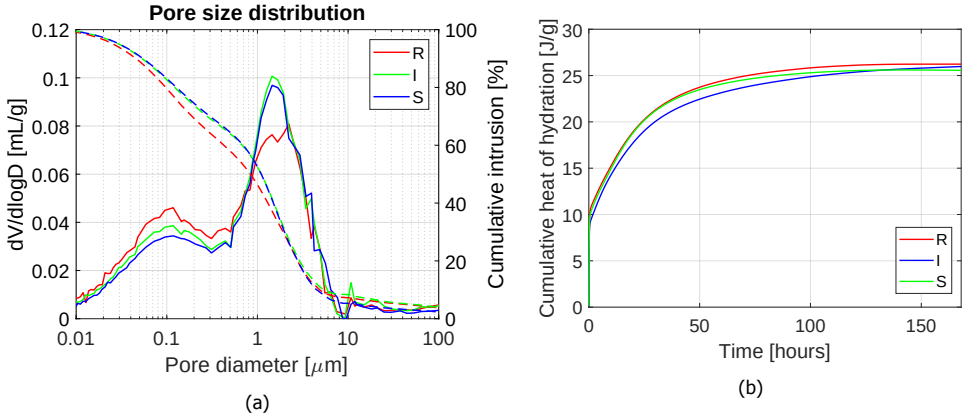

Figure 4.4: (a) Pore size distribution obtained using MIP. (b) Cumulative heat of hydration measured using isothermal calorimetry.

The results of capillary absorption and drying behaviour are presented in Figure 4.5. The rate of capillary absorption and the capillary moisture content across [R], [I] and [S] specimens are similar to each other.The drying of [I] specimens (Figure 4.5a) is significantly slower than the [R] and [S] specimens. A crust of the crystallised inhibitor is formed on the surface as shown in Figure 4.10b due to a high amount of the added inhibitor. This could have resulted in pore clogging and thereby slowing the drying process. Based on these results the drying cycle to be used in the study of advection (section 4.2.4.1) was defined.

4.3.2. Leaching by diffusion

The concentration of leached species measured at each renewal of water step is presented in Figure 4.6. The trend obtained for [I] and [S] specimens, contain-

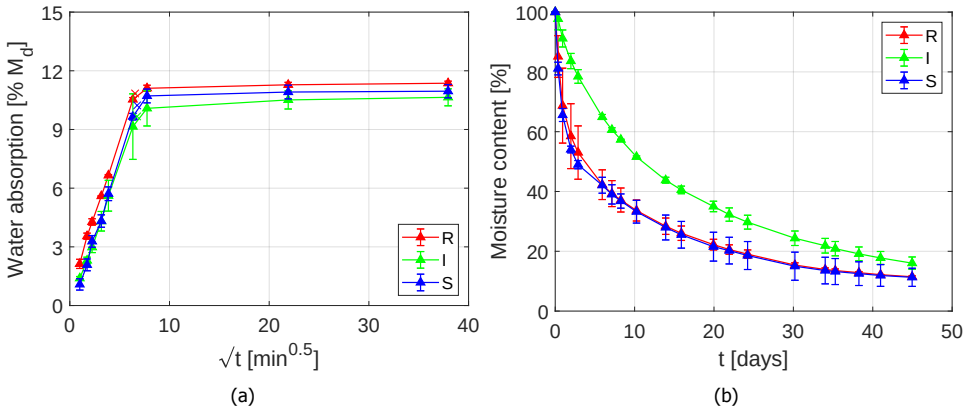

Figure 4.5: (a) Water absorption due to capillary suction (b) drying behaviour.

Table 4.3: Overview of transport related properties

Property	Reference [R]	Inhibitor [I]	Salt [S]
Porosity [%]	26.06±0.92	24.43±0.63	25.55±0.02
Bulk Density [kg/m^3]	1963.5±26.45	1997.3±24.3	1973.5±6.25
Capillary moisture content [% dry wt]	10.84±0.15	9.7±0.9	10.23±0.35
Cumulative heat of hydration [J/g]	26.77±3.25	25.61±1.89	23.25±5.25

ing NaFeCN and NaCl respectively, is similar. The high concentration measured at the first time step (2h) is related to surface washing rather than diffusion. For subsequent time steps, a diffusion controlled leaching process is observed.

No significant scatter is observed between results from replicates samples. The control samples as expected show absence of NaFeCN or NaCl. Therefore, the obtained results can be reliably used to estimate the effective diffusion coefficient, according to the procedure described in section 4.2.3.3.

A comparison of the effective diffusion coefficient (D_e) of $[Fe(CN)_6]^{4-}$ and Cl^- ions obtained by regression analysis is shown in figure 4.7. The model shows a good fit with the measured data and has a high coefficient of determination (R2). It can be seen that the D_e for Cl^- transport is roughly twice that of $[Fe(CN)_6]^{4-}$ transport. This is logical, since a Cl^- ion has a smaller volume than a $[Fe(CN)_6]^{4-}$ ion. However, D_e of $[Fe(CN)_6]^{4-}$ is of the same order of magnitude of Cl^-, meaning the rate of leaching and the subsequent depletion of NaFeCN from the mortar is significant.

The remaining amount of $[Fe(CN)_6]^{4-}$ and Cl^- in the mortar specimens at the end of the leaching test is presented in Figure 4.8, expressed as a percentage of the amount present at the start of the test. At the end of the leaching test, less than 20% inhibitor was still present in the mortar, meaning more than 80% inhibitor had leached out. In case of chloride, less than 10% of the initial amount was left. The

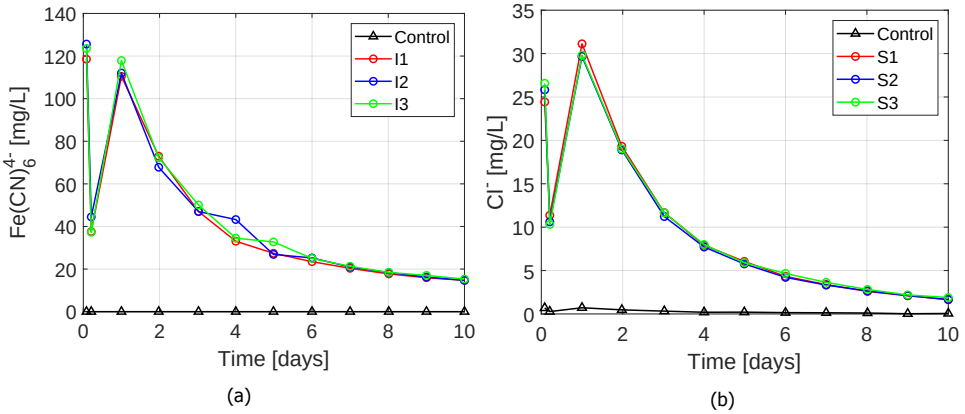

Figure 4.6: Concentration measured at each renewal step (a) Sodium ferrocyanide using UV-VIS from [I] specimens (b) Chloride ions using Ion Chromatography from [S] specimens.

results of the CWE show slightly higher amount of remaining inhibitor, compared to the leaching test. A significant scatter is observed in CWE results; this can be due to the fact the CWE measurements were carried out on other specimens than those used in the leaching test or to the limited stirring (5 min) and dissolution time (24h) used for in the CWE test, which might not be sufficient to fully dissolve NaFeCN, leading to underestimation of the initial inhibitor content. Taking the scatter into account, it can be concluded that the results obtained by CWE confirm and validate the results of the leaching test.

The eluates from [I] specimens were analysed by both UV-VIS for $[Fe(CN)_6]^{4-}$ and ICP for Fe ions. The results are presented in Figure 4.9.The results obtained by these techniques are in good agreement. UV-Vis has the advantages of measuring the concentration of $[Fe(CN)_6]^{4-}$ ions (while ICP can only measure generic Fe ions). Furthermore, UV-VIS is a faster and an inexpensive method compared to ICP. Owing to these reasons, UV-VIS has been preferred to ICP in the following steps of this research.

4.3.3. Leaching by Advection

The drying process and efflorescence development at each wet-dry cycle is presented in Figure 4.10. An increase in the efflorescence, most probably (Na-FeCN crystallisation), is observed in time, indicating a progressive transport of the inhibitor to the surface. After the end of the first cycle, there is a crust adhering to the top surface of the mortar specimens. After rewetting, the crust is seen to lift up. The effect of this is also partially evident in the drying process: the rate of drying is slow during the first cycle, when the well-adhering crust is delaying the evaporation. With subsequent cycles, when the crust was lifted up, the rate of drying increased.

The amount of inhibitor in the efflorescence and in the mortar specimens after each cycle was measured by UV-VIS. The non-adhering efflorescence was collected

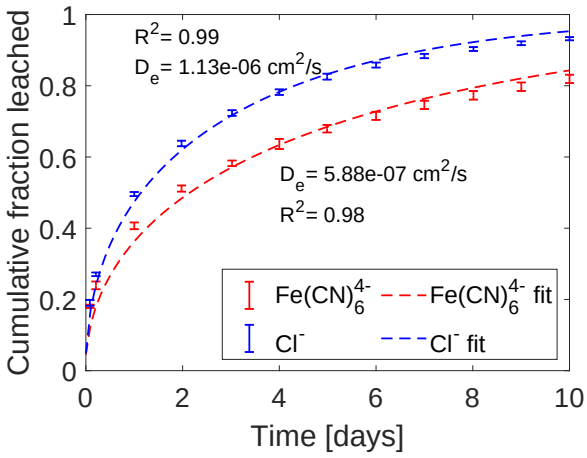

Figure 4.7: Comparison of effective diffusion coefficient (D_e) between specimens containing the inhibitor $[Fe(CN)_6]^{4-}$ and Cl^- obtained from regression analysis

with a dry brush and weighed at the end of each cycle; at the end of the first cycle, no efflorescence could be collected, as they formed a crust very adherent to the surface.

The distribution of the inhibitor over the specimen height as assessed at the end of each cycle is shown in Figure 4.11a. At the start of the test, the inhibitor was homogeneously distributed over the entire height of the sample. At the end of the first cycle, the inhibitor had accumulated in the outer layer of the mortar specimen, at the evaporation surface. With successive cycling there was only a minor increase in the accumulation of the inhibitor in the top layer. Figure 4.11b shows the amount of efflorescence brushed from the surface at the end of the second and third cycle; it is evident that the amount of efflorescence increases with cycling. The composition of the efflorescence, analysed by UV-VIS, shows that these are mainly composed of NaFeCN (89.5% by weight):

The SEM-EDS mapping of the specimen cross-section at the end of first cycle is presented in Figure 4.12. Figure 4.12a shows a lighter colour (indicating the presence of heavier elements) in the outer 200-400 µm: here a high concentration of Na, Fe and even N (low detection accuracy) is measured, confirming the massive presence of sodium ferrocyanide in this layer. The presence of NaFeCN is negligible beyond 400 µm from the evaporation surface. These results are in agreement with those of UV-VIS. Other components of mortar namely Ca and Si are, as expected, homogenously distributed in the mortar matrix. A thin layer of Ca is found at the very surface (figure 4.12d) possibly indicative of a binder-rich layer at the mortar surface.

The morphology of the crystallised inhibitor has been studied by BSE on a cross-section of the mortar and on parts of the detached efflorescence crust (Figure 4.13). In the cross-section crystals of sodium ferrocyanide (NaFeCN) are visible in the mortar matrix. The efflorescence is entirely composed by crystals of NaFeCN,

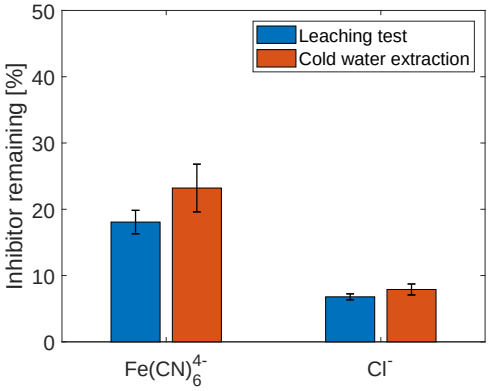

Figure 4.8: Amount of inhibitor or chlorides present in the specimens at the end of the tank leaching test.

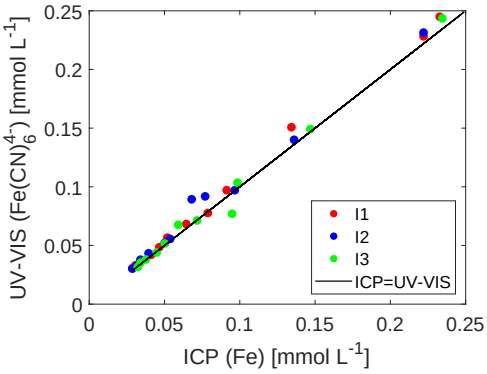

Figure 4.9: Amount of inhibitor or chlorides present in the specimens at the end of the tank leaching test.

larger than those observed in the cross section.

4.4. Discussion and conclusions

In this study, the inhibitor leaching behaviour driven by diffusion and advection, has been experimentally investigated. The diffusion test, based on a combination of ASTM C1308-21 and cold water extraction, was able to reliably measure leaching of $[Fe(CN)_6]^{4-}$ ions from mortar under a concentration gradient. At the end of the diffusion test, more than 80% of the inhibitor had leached out of the specimens, suggesting a strong ability of the inhibitor to transport under a concentration gradient. It should be mentioned that (1) The initial concentration of NaFeCN (10% of binder weight) is higher than the concentration of the inhibitor necessary for obtaining the desired inhibition effect in actual mortars. This high concentration explains the high initial concentration gradient. (2) Replenishing leachant acceler-

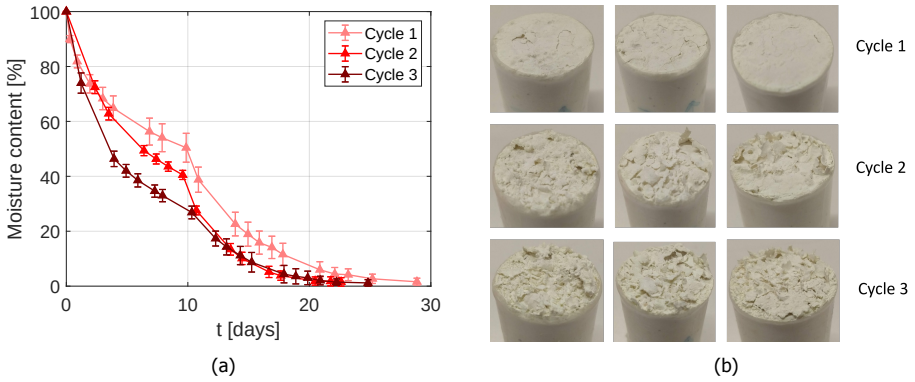

Figure 4.10: (a) Moisture loss during the drying cycles (b) Visual inspection of the NaFeCN efflorescence/crust at the end of each cycle

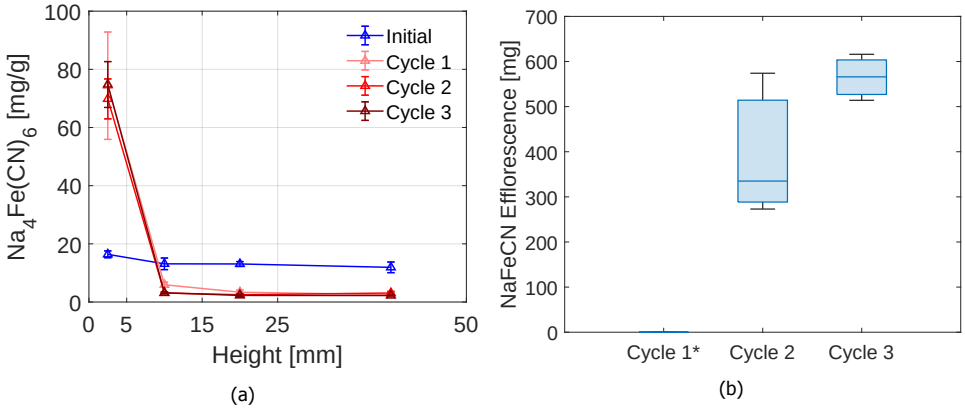

Figure 4.11: (a) Inhibitor distribution over the height of the specimen (b) Weight of Na-FeCN efflorescence measured at the end of each cycle. * Cycle 1 had a tightly adherent efflorescent crust and was not weighed

ates the flux of $[Fe(CN)_6]^{4-}$ ions by maintaining zero surface concentration. Despite the above mentioned points, the effective diffusion coefficient of $[Fe(CN)_6]^{4-}$ and Cl^- can be reliably compared, as the model considers the above parameters and measurements are done at the same experimental conditions. The effective diffusion coefficient of $[Fe(CN)_6]^{4-}$ (5.88 x 10^{-7} cm^2/s) is lower the Cl^- (11.3 x 10^{-7} cm^2/s) thus still in the same order of magnitude. This indicates that the inhibitor is expected to be transported only marginally slower compared to NaCl.

The advection test, consisting of capillary suction-drying cycles, confirmed that significant transport of the inhibitor occurs from depth to the evaporation surface. After one wetting-drying cycle, the inhibitor had accumulated at the surface of the mortar, in the form of a crust of efflorescence. In the outer layer of the mortar, inhibitor concentration increased 4 times to the initial concentration (at the start of

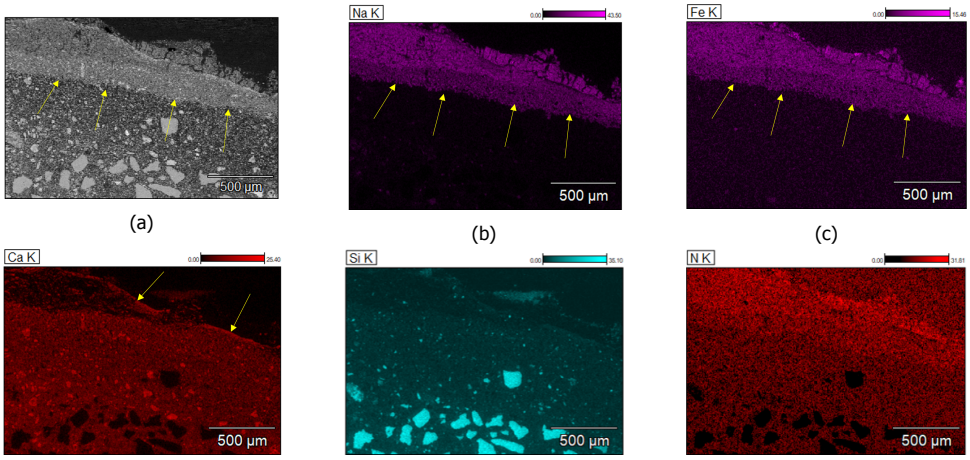

Figure 4.12: (a) SEM-EDS mapping of the outer 1.5 mm of the polished section of a mortar specimen after 1 wet-dry cycle. (a) Grey scaled image (b) sodium (Na) map (c) iron (Fe) map (d) calcium (Ca) map (e) silicon (Si) map and (f) Nitrogen (N) map. The yellow arrows in (a), (b) and (c) indicate accumulation of crystallised sodium ferrocyanide layer and (d) indicates presence of binder rich layer on the mortar surface

the test). SEM-EDS observations confirmed that most of the inhibitor was localised within the first 400 µm from the outer surface. With successive cycling, an increase in the amount of efflorescence was observed at the specimen surface. UV-VIS spectrophotometry showed that 89.5% by mass of the efflorescence was composed of sodium ferrocyanide (inhibitor).

The results from both diffusion and advection studies show high leaching rates of ferrocyanide in presence of water. This suggests that this inhibitor, when mixed in the mortar, will be easily transported towards the surface and eventually leach out of the substrate or accumulate at the evaporative surface. This will lead to depletion of the inhibitor in the inner layers and its positive effect in mitigating salt decay may decline. It is therefore imperative to retard/ slow down inhibitor leaching in order to prolong the durability of such mortars.

Different solutions can be envisaged to limit leaching of the inhibitor and ensure a longer service-life to the mortar. One way would be to reduce the mobility of $[Fe(CN)_6]^{4-}$ ions in the pore solution. This can be possibly done by encapsulating the inhibitor in (polymeric) capsules [50] instead of adding it directly to the mixing water. The polymeric capsule shells would constitute a barrier [51] to transport of the inhibitor into the pore solution. Possibly, capsule shells could be tuned to a smart release under external stimuli such as changes in pH [52, 53] or presence of NaCl [54]. Research is on-going to assess these possibilities.

The methodology adopted in this research was successful in providing a quantitative analysis on the leaching of NaFeCN (crystallisation inhibitor) in mortar. This is the first instance that such a study has been undertaken on crystallisation in-

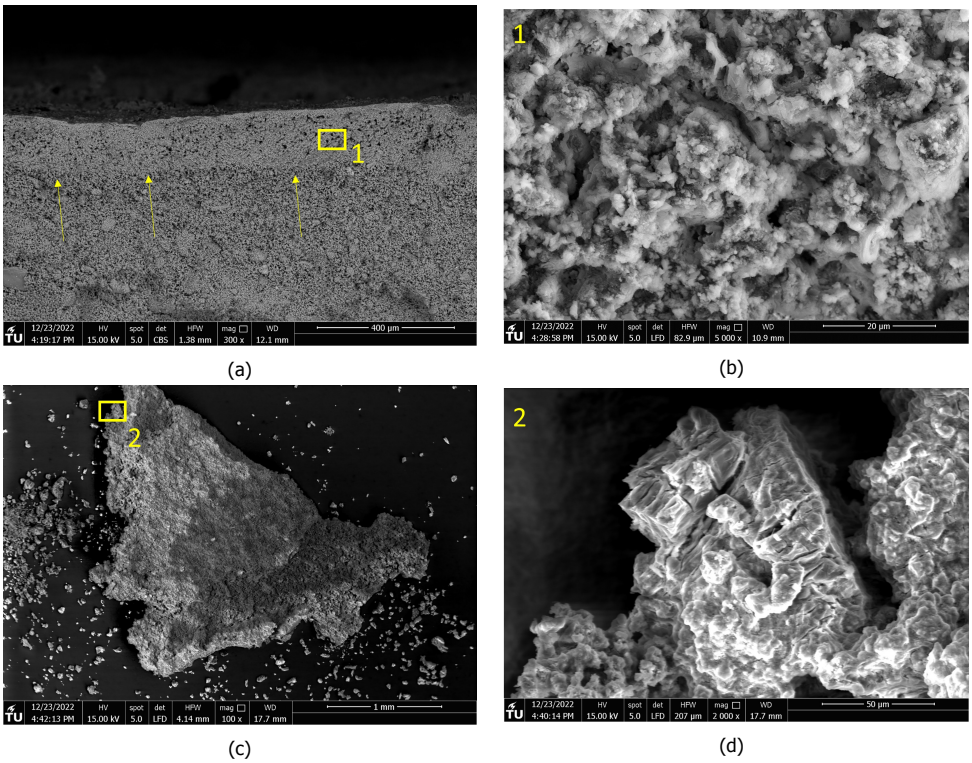

(a) (b)

(c) (d)

Figure 4.13: : SEM images for morphology (a) cross-section (b) magnified image of the cross-section (c) NaFeCN efflorescent crust (d) magnified image of the crust.

hibitors. Studying leaching of NaFeCN in other porous media e.g. natural stone and brine-contaminated salt could provide more relevant insights. Besides NaFeCN, other water soluble additives are vulnerable to leaching. A commonly used corrosion inhibitor in reinforced concrete, sodium nitrite is such an example [55]. The methodology can be further modified and extended to such additives. This can provide a better understanding in improving effectiveness of such additives across building materials.

References

[1] G. W. Scherer, *Stress from crystallization of salt,* Cement and Concrete Research **34**, 1613 (2004).

[2] R. J. Flatt, *Salt damage in porous materials: how high supersaturations are generated,* Journal of Crystal Growth **242**, 435 (2002).

[3] M. Steiger, *Crystal growth in porous materials - I: The crystallization pressure of large crystals,* Journal of Crystal Growth **282**, 455 (2005).

[4] R. J. Flatt, F. Caruso, A. M. A. Sanchez, and G. W. Scherer, *Chemo-mechanics of salt damage in stone,* Nature Communications **5**, 4823 (2014).

[5] M. Schiro, E. Ruiz-Agudo, and C. Rodriguez-Navarro, *Damage Mechanisms of Porous Materials due to In-Pore Salt Crystallization,* Physical Review Letters **109**, 265503 (2012).

[6] B. Lubelli, R. P. Van Hees, and C. J. Groot, *The role of sea salts in the occurrence of different damage mechanisms and decay patterns on brick masonry,* Construction and Building Materials **18**, 119 (2004).

[7] C. Gentilini, E. Franzoni, S. Bandini, and L. Nobile, *Effect of salt crystallisation on the shear behaviour of masonry walls: An experimental study,* Construction and Building Materials **37**, 181 (2012).

[8] B. Lubelli, V. Cnudde, T. Diaz-Goncalves, E. Franzoni, R. van Hees, I. Ioannou, B. Menendez, C. Nunes, H. Siedel, M. Stefanidou, V. Verges-Belmin, and H. Viles, *Towards a more effective and reliable salt crystallization test for porous building materials: state of the art,* Materials and Structures/Materiaux et Constructions **51** (2018), 10.1617/s11527-018-1180-5.

[9] A. E. Charola and C. Bläuer, *Salts in Masonry: An Overview of the Problem,* Restoration of Buildings and Monuments **21**, 119–135 (2015).

[10] B. Lubelli, R. P. Van Hees, H. P. Huinink, and C. J. Groot, *Irreversible dilation of NaCl contaminated lime-cement mortar due to crystallization cycles,* Cement and Concrete Research **36**, 678 (2006).

[11] J. Desarnaud and N. Shahidzadeh-Bonn, *Salt crystal purification by deliquescence/crystallization cycling,* EPL (Europhysics Letters) **95**, 48002 (2011).

[12] H. Derluyn, M. Griffa, D. Mannes, I. Jerjen, J. Dewanckele, A. Sheppard, D. Derome, V. Cnudde, E. Lehmann, I. Jerjen, J. Dewanckele, V. Cnudde, and J. Carmeliet, *Characterizing saline uptake and salt distributions in porous limestone with neutron radiography and X-ray micro-tomography,* Journal of Building Physics http://jen.sagepub.com/ **36**, 353 (2013).

[13] A. Moropoulou, K. Polikreti, A. Bakolas, and P. Michailidis, *Correlation of physicochemical and mechanical properties of historical mortars and classification by multivariate statistics,* Cement and Concrete Research **33**, 891 (2003).

[14] I. Papayianni, M. Stefanidou, V. Pachta, and S. Konopisi, *Content and Topography of Salts in Historic Mortars,* in *Historic Mortars*, edited by J. J. Hughes, J. Válek, and C. J. W. P. Groot (Springer International Publishing, Cham, 2019) pp. 119–126.

[15] H. Haynes, R. O'Neill, M. Neff, and P. Kumar Mehta, *Salt Weathering of Concrete by Sodium Carbonate and Sodium Chloride,* ACI Materials Journal **107**, 258 (2010).

[16] V. Verges-Belmin and H. Siedel, *Desalination of Masonries and Monumental Sculptures by Poulticing: A Review / Entsalzen von Mauerwerk und Steinfiguren mit Hilfe von Kompressen: Ein Überblick,* Restoration of Buildings and Monuments **11**, 391 (2005).

[17] C. Groot, R. van Hees, and T. Wijffels, *Selection of plasters and renders for salt laden masonry substrates,* Construction and Building Materials **23**, 1743 (2009).

[18] A. Glasner and M. Zidon, *The crystallization of NaCl in the presence of [Fe(CN)6]4- ions,* Journal of Crystal Growth **21**, 294 (1974).

[19] R. D. Cody, *Organo-crystalline interactions in evaporite systems; the effects of crystallization inhibition,* Journal of Sedimentary Research **61**, 704 (1991).

[20] C. Selwitz and E. Doehne, *The evaluation of crystallization modifiers for controlling salt damage to limestone,* Journal of Cultural Heritage **3**, 205 (2002).

[21] C. Rodriguez-Navarro, L. Linares-Fernandez, E. Doehne, and E. Sebastian, *Effects of ferrocyanide ions on NaCl crystallization in porous stone,* Journal of Crystal Growth **243**, 503 (2002).

[22] A. A. Bode, V. Vonk, F. J. Van Den Bruele, D. J. Kok, A. M. Kerkenaar, M. F. Mantilla, S. Jiang, J. A. Meijer, W. J. Van Enckevort, and E. Vlieg, *Anticaking activity of ferrocyanide on sodium chloride explained by charge mismatch,* Crystal Growth and Design **12**, 1919 (2012).

[23] S. J. Dorazio and C. Brückner, *Why Is There Cyanide in my Table Salt? Structural Chemistry of the Anticaking Effect of Yellow Prussiate of Soda (Na4[Fe(CN)6]·10H2O),* Journal of Chemical Education **92**, 1121 (2015).

[24] S. Granneman, *Mitigating salt damage in lime-based mortars by built-in crystallization modifiers*, Ph.D. thesis, Delft University of Technology (2019).

[25] S. Gupta, K. Terheiden, L. Pel, and A. Sawdy, *Influence of Ferrocyanide Inhibitors on the Transport and Crystallization Processes of Sodium Chloride in Porous Building Materials,* Crystal Growth & Design **12**, 3888 (2012).

[26] B. Lubelli and R. P. van Hees, *Effectiveness of crystallization inhibitors in preventing salt damage in building materials,* Journal of Cultural Heritage **8**, 223 (2007).

[27] T. Rivas, E. Alvarez, M. J. Mosquera, L. Alejano, and J. Taboada, *Crystallization modifiers applied in granite desalination: The role of the stone pore structure,* Construction and Building Materials **24**, 766 (2010).

[28] K. L. Platt, D. M. Di Toro, R. F. Carbonaro, N. A. Bugher, T. F. Parkerton, L. J. Eastcott, and P. T. Imhoff, *Ferrocyanide enhanced evaporative flux to remediate soils contaminated with produced water brine,* Journal of Hazardous Materials **442**, 130028 (2023).

[29] S. Gupta, H. P. Huinink, L. Pel, and K. Kopinga, *How Ferrocyanide Influences NaCl Crystallization under Different Humidity Conditions,* Crystal Growth & Design **14**, 1591 (2014).

[30] B. Lubelli, T. G. Nijland, R. P. Van Hees, and A. Hacquebord, *Effect of mixed in crystallization inhibitor on resistance of lime-cement mortar against NaCl crystallization,* Construction and Building Materials **24**, 2466 (2010).

[31] S. J. Granneman, B. Lubelli, and R. P. van Hees, *Effect of mixed in crystallization modifiers on the resistance of lime mortar against NaCl and Na2SO4 crystallization,* Construction and Building Materials **194**, 62 (2019).

[32] J. Feijoo, D. Ergenç, R. Fort, and M. A. de Buergo, *Addition of ferrocyanide-based compounds to repairing joint lime mortars as a protective method for porous building materials against sodium chloride damage,* Materials and Structures **54**, 14 (2021).

[33] D. Ergenç, J. Feijoo, R. Fort, and M. Alvarez de Buergo, *Effects of potassium ferrocyanide used for desalination on lime composite performances in different curing regimes,* Construction and Building Materials **259**, 120409 (2020).

[34] B. Lubelli, E. d. Bouvrie, T. G. Nijland, and A. Kamat, *Plasters with mixed-in crystallization inhibitors: Results of a 4-year monitoring of on-site application,* Journal of Cultural Heritage **59**, 10 (2023).

[35] S. J. Granneman, B. Lubelli, and R. P. Van Hees, *Characterization of lime mortar additivated with crystallization modifiers,* International Journal of Architectural Heritage **12**, 849 (2018).

[36] A. Kamat, B. Lubelli, and E. Schlangen, *Effect of a mixed-in crystallization inhibitor on the properties of hydraulic mortars,* AIMS Materials Science **9**, 628 (2022).

[37] J. A. N. Friend, J. E. Townley, and R. H. Vallance, *CCCIII.—The solubility of sodium ferrocyanide in water between 0° and 104°*, J. Chem. Soc. , 2326 (1929).

[38] H. P. Huinink, L. Pel, and M. A. J. Michels, *How ions distribute in a drying porous medium: A simple model,* Physics of Fluids **14**, 1389 (2002).

[39] *NEN-EN 196-1: Methods of testing cement - Part 1: Determination of strength*, Tech. Rep. (European committee for standardisation (CEN), 2015).

[40] *NEN-EN 459-2: Building lime-part 2: Test methods*, Tech. Rep. (European committee for standardisation (CEN), 2008).

[41] *NEN-EN-1925: Natural stone test methods- Determination of water absorption coefficient by capillarity*, Tech. Rep. (European committee for standardisation (CEN), 1999).

[42] *ASTM C1308-21: Standard test method for accelerated leach test for measuring contaminant releases from solidified waste*, Tech. Rep. (ASTM International, 2021).

[43] G. Plusquellec, M. Geiker, J. Lindgård, J. Duchesne, B. Fournier, and K. De Weerdt, *Determination of the pH and the free alkali metal content in the pore solution of concrete: Review and experimental comparison,* Cement and Concrete Research **96**, 13 (2017).

[44] M. Shirom and G. Stein, *The Absorption Spectrum of the Ferrocyanide Ion in Aqueous Solution,* Israel Journal of Chemistry **7**, 405 (1969).

[45] D. F. Swinehart, *The Beer-Lambert Law,* Journal of Chemical Education **39**, 333 (1962).

[46] ASTMC1308-08, *ASTM C1308-95. Standard Test Method for Accelerated Leach Test for Diffusive Releases from Solidified Waste and a Computer Program to Model Diffusive, Fractional Leaching from Cylindrical Waste Forms*, Tech. Rep. April 1996 (ASTM international, 2001).

[47] C. J. Nestor, *Diffusion from solid cylinders*, Tech. Rep. (Oak Ridge National Laboratory (ORNL), Oak Ridge, TN (United States), 1980).

[48] C. Pescatore, *Improved expressions for modeling diffusive, fractional cumulative leaching from finite-size waste forms,* Waste Management **10**, 155 (1990).

[49] C. Nunes, A. Maria Aguilar Sanchez, S. Godts, D. Gulotta, I. Ioannou, B. Lubelli, B. Menendez, N. Shahidzadeh, Z. Slížková, and M. Theodoridou, *Experimental research on salt contamination procedures and methods for assessment of the salt distribution,* Construction and Building Materials **298**, 123862 (2021).

[50] A. P. Esser-Kahn, S. A. Odom, N. R. Sottos, S. R. White, and J. S. Moore, *Triggered release from polymer capsules,* (2011).

[51] J. Li and D. J. Mooney, *Designing hydrogels for controlled drug delivery,* Nature Reviews Materials **1**, 1 (2016).

[52] A. Kamat, D. Palin, B. Lubelli, and E. Schlangen, *Tunable chitosan-alginate capsules for a controlled release of crystallisation inhibitors in mortars,* MATEC Web of Conferences **378**, 02011 (2023).

[53] J. Wang, A. Mignon, G. Trenson, S. Van Vlierberghe, N. Boon, and N. De Belie, *A chitosan based pH-responsive hydrogel for encapsulation of bacteria for self-sealing concrete,* Cement and Concrete Composites **93**, 309 (2018).

[54] W. Xiong, J. Tang, G. Zhu, N. Han, E. Schlangen, B. Dong, X. Wang, and F. Xing, *A novel capsule-based self-recovery system with a chloride ion trigger,* Scientific Reports **5**, 1 (2015).

[55] J. Ress, U. Martin, J. Bosch, and D. M. Bastidas, *pH-Triggered Release of NaNO2 Corrosion Inhibitors from Novel Colophony Microcapsules in Simulated Concrete Pore Solution,* ACS applied materials & interfaces **12**, 46686 (2020).

5

Tunable chitosan-alginate capsules for a controlled release of crystallisation inhibitors in mortars

The previous chapter concluded that the leaching of the inhibitor, when directly mixed-in mortar, is severe. To improve the service life of mortars, the rate of leaching of the inhibitor needs to be reduced. In this chapter, encapsulation of the inhibitor is considered as a potential solution to slow down its leaching. Herein, capsules composed of a polyelectrolyte complex of calcium alginate and chitosan are investigated for the controlled-release of the inhibitor. In the capsule production process, the inhibitor is encapsulated in calcium alginate capsules using extrusion dripping technique and the obtained capsules are complexed with chitosan by varying the chitosan:alginate ratio. The release of the inhibitor from the produced capsules in solutions of various pH values, ranging from 7 to 13 is investigated.

This chapter is based on the article published in MATEC web of conferences, **378**, 02011 (2023).

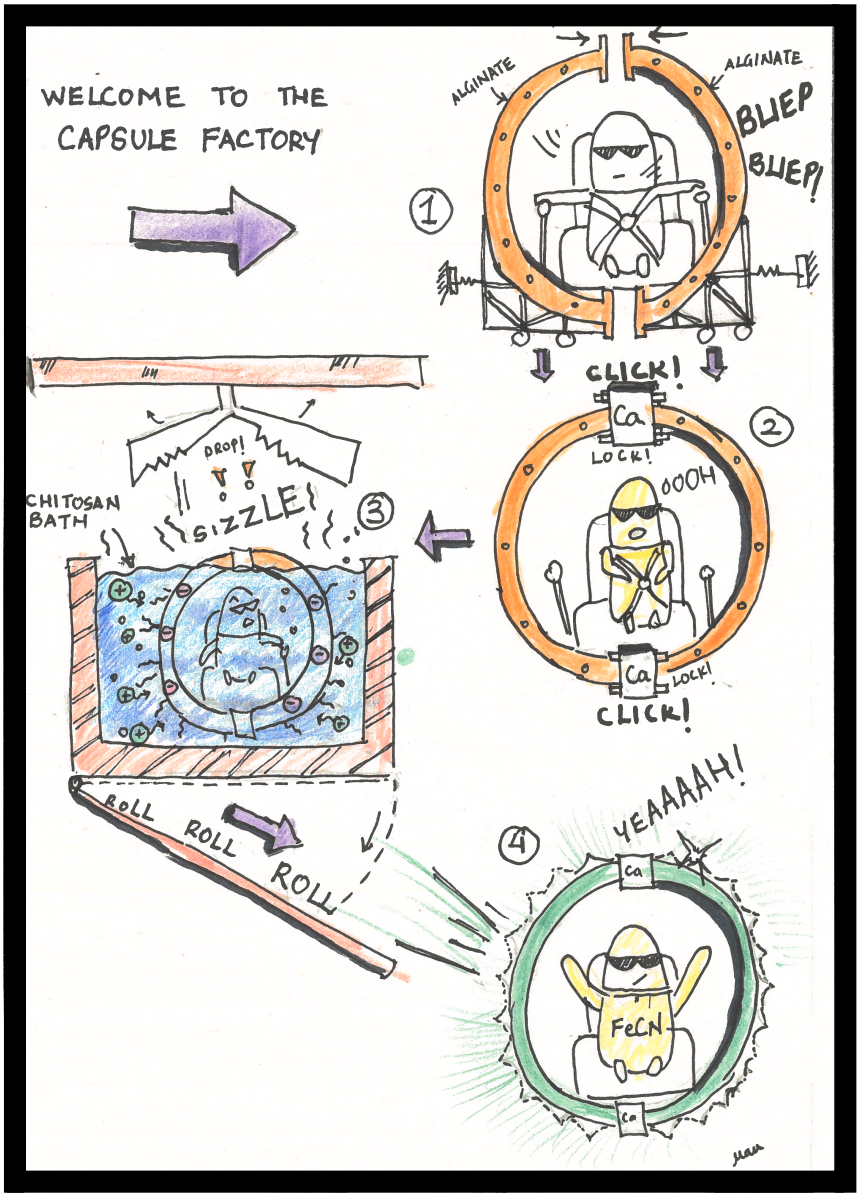
WELCOME TO THE CAPSULE FACTORY
ALGINATE
ALGINATE
BLIEP
BLIEP!
1
CLICK!
Ca
LOCK!
2
OOOH
Ca
LOCK!
CLICK!
DROP!
SIZZLE!
3
CHITOSAN BATH
ROLL ROLL ROLL
4
YEAAAAH!
Ca
FeCN
Ca

5.1. Introduction

Materials used in the built cultural heritage are often susceptible to salt weathering. Salts, like sodium chloride (NaCl), are responsible for crystallisation-induced damage [1]. These salts (as ions) are either originally present in the building materials or find entry into the building materials through capillary transport from various sources (e.g., groundwater, salt spray etc.). Under super-saturated conditions in confined pore networks, salt crystallisation leads to crystallisation pressure in the porous matrix and progressive damage in the form of material loss [2, 3]. Historic buildings are particularly prone to salt damage due to the limited strength of traditional materials they are made of, such as lime mortars, and the accumulation of salts and stresses over time. The costs associated with the repair and maintenance of these buildings are considerable. In particular, plaster and renders are often affected by salt decay and need replacement. The use of salt crystallisation inhibitors mixed in mortar is seen as a potential preventive solution that could reduce costs by improving the durability of repair works. Crystallisation inhibitors are chemical compounds that inhibit salt crystallisation by delaying crystal nucleation and/or modifying crystal habit by adsorbing on specific crystal surfaces, altering crystal growth [4].

Among inhibitors, alkali ferrocyanide (FeCN) is a well-known and an effective inhibitor of NaCl crystallisation, commonly used as an anti-caking agent in table salt [5]. FeCN suppresses NaCl nucleation by increasing the critical supersaturation [6]. Therefore, NaCl in solution in the presence of FeCN remains as ions (Na^+ and Cl^-) at higher supersaturation, allowing transport of the ions towards the evaporation surface. In porous building materials, this property has been exploited to promote harmless efflorescence (free crystallisation at the surface) against more severe subflorescence (confined subsurface crystallisation) [7, 8]. Secondly, the presence of FeCN alters NaCl crystal habit, resulting in the NaCl crystals having disordered dendritic growth forms, as opposed to their equilibrium cubic form. FeCN ions preferentially sorb on the {100} face of NaCl crystals. A charge mismatch between FeCN and the NaCl cluster prevents crystal growth on the {100} faces of the NaCl crystals resulting in dendritic growth forms [9]. Gupta et al., have demonstrated that the increase in the crystal surface area due to the dendritic growth further increases the evaporation rate and promotes the advection of salt to the surface [10]. Crystallisation with high nucleation density (resulting in a high number of small crystals), as observed for NaCl in the presence of FeCN, is also thought to reduce pore clogging and limit crystallisation pressure [11]. Lower damage due to salt crystallisation has been reported in the presence of FeCN on different porous substrates [11–15].

FeCN, when mixed in fresh mortar during preparation, has effectively reduced salt decay [16] without significantly altering the mortar properties [17, 18]. However, Granneman et al. [11], showed that after repeated crystallisation cycles, less than 1% of the initially added inhibitor was left in the mortar specimens; the rest of the inhibitor possibly leached out during moisture transport. Recent results from a case study, where plaster with mixed-in inhibitor was applied on a salt-contaminated wall, showed localised accumulation of FeCN in the outermost layer

of the plaster, suggesting high mobility of FeCN ions and potential leaching [19]. If FeCN is leached out of renovation mortars, it will be depleted, reducing its effectiveness over time. Immobilisation and the controlled release of inhibitors from designer capsules could be an effective solution to this challenge.

Encapsulation and controlled release are common concepts that find many useful applications in drug delivery, fragrance release and corrosion treatments [20]. Even in cementitious materials, the use of capsules to protect and deliver self-healing agents has shown promising results [21–24]. Encapsulated crystallisation inhibitors prevent salt crystallisation and the progressive damage of the mortar. Therefore, a fracture based capsule trigger deployed in various self-healing cementitious materials would be too late to prevent the damage. In order to slow down and sustain the release of the inhibitor, a semi-permeable diffusion-based capsule shell is therefore more suitable than a rupture/dissolution-based trigger [25]. Naturally occurring semi-permeable hydrogels, like alginates, pectin, gelatine and chitosan, show interesting swelling behaviours that can be exploited for controlled release. Alginate-based hydrogels are easy to produce and have shown good survivability in construction materials [26]. However, alginates have one disadvantage in high-alkaline environments typically observed in cementitious systems: alginates are negatively charged (anionic) at pH >5.5 and swell due to electrostatic repulsion creating open structures [27]. These open structures result in high diffusion rates or even burst release of the core [28]. Several studies report improvements to the alginate stability by coating alginate capsules with cationic polymers like chitosan [29]. The positive charged chitosan forms an additional membrane with the negatively charged alginates. Moreover, chitosan shows the opposite swelling behaviour to alginates; chitosan shrinks in high pH solutions, thereby reducing its permeability. Studies with chitosan-coated alginate capsules have reported higher stability, lower leakage and improved controlled release of different encapsulated drugs compared to alginate-only capsules [30, 31]. By using the above concepts, a superior technology with polyelectrolyte hydrogel capsules can be developed to engineer slow inhibitor release in building materials.

This study explores the feasibility of encapsulating FeCN in calcium-alginate (CA) capsules with a chitosan (Cs) coating. In addition, the release of encapsulated FeCN from capsules with different Cs:CA ratios under different pH conditions is investigated.

5.2. Materials and methods

Sodium alginate (SA) and calcium chloride dihydrate were purchased from Sigma Aldrich. Medium molecular weight chitosan (Cs) (190,000-310,000 Da) was obtained from Merck. Cs contained Fe impurities equivalent to ≈0.18% by mass as measured using inductively-coupled plasma (ICP)-optical emission spectroscopy (OES). Acetic acid was bought from J.T.Baker. Lab grade sodium ferrocyanide decahydrate (NaFeCN) used as the crystallisation inhibitor was purchased from Acros organic (Thermo Fischer Scientific).

5.2.1. Preparation of inhibitor loaded capsules

A schematic of the capsule preparation process is presented in Fig. 1

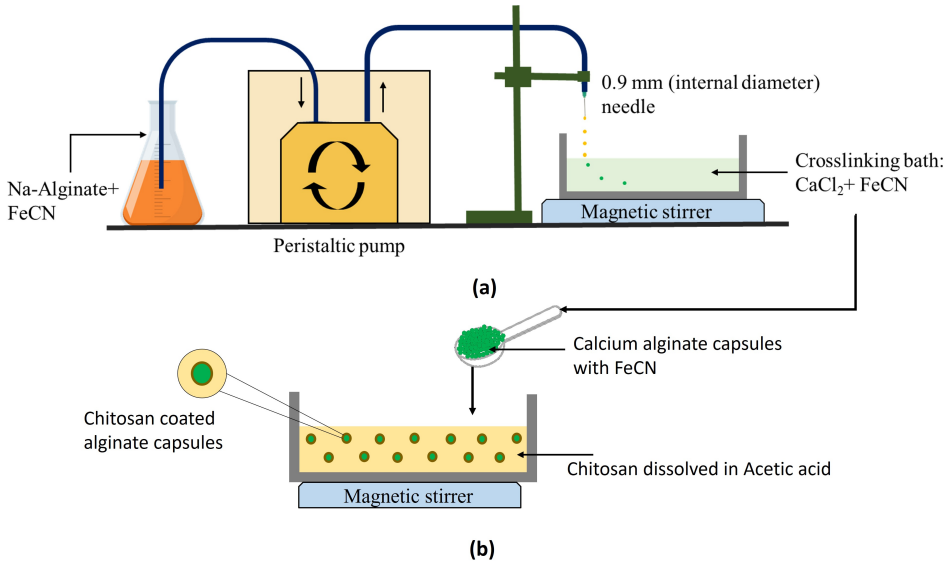

Figure 5.1: Encapsulation of FeCN. (a) Preparation of calcium alginate (CA) capsules with FeCN where the solution containing sodium alginate (2% w/v) and FeCN(2% w/v) is added drop-by-drop into a crosslinking bath containing Ca^{2+} ions (3% w/v $CaCl_2$ + 2% w/v FeCN) at a constant rate using a peristaltic pump (b) Freshly prepared CA-FeCN capsules are coated with chitosan (Cs) by adding them to a gently stirring Cs solution (varying concentration) for a cross-linking time of 15 min.

5.2.1.1. Production of calcium alginate capsules

Capsules were prepared by a simple extrusion dripping technique [32]. SA (2% w/v) was first dissolved in demineralised water using vigorous stirring (1000 rpm) until SA was completely dissolved. Next NaFeCN was mixed in the alginate solution at a concentration of 2% (w/v) and stirred for 30 min. The obtained mixture was extruded drop-by-drop (under gravity) into a 3% (w/v) $CaCl_2$ bath using a peristaltic pump (Masterflex console drive, ColePalmer instruments) connected to a needle with a 0.9 mm internal diameter, forming calcium alginate droplets/capsules with encapsulated FeCN. NaFeCN was added to the $CaCl_2$ bath with the same concentration as in the SA solution to minimise FeCN diffusion from the capsules during production. The bath was continuously stirred using a magnetic stirrer at 300 rpm. The alginate beads were allowed to cross-link with Ca^{2+} ions from the bath overnight to form stable gel capsules. The capsules were filtered out using a Büchner funnel (no paper/vacuum) and washed with demineralised water to remove excess unlinked Ca^{2+} ions. These capsules are denoted CA as they do not have any chitosan coating.

5.2.1.2. Production of calcium alginate capsules with a chitosan coating

Cs solutions were prepared by dissolving chitosan in 0.3 M acetic acid using a magnetic stirrer at 40°C for at least 6 h. Three different Cs baths were prepared containing 1%, 1.5% and 2% of Cs (w/v), respectively. The CA capsules, obtained as described in Section 5.2.1.1 (Figure 5.1(a)), were added to the different Cs baths and cross-linked for 15 minutes. Subsequently, the capsules were filtered and washed with deionised water. At the end, Cs-coated CA capsules with Cs:CA ratios of 0.5, 0.75 and 1 by mass were obtained.

5.2.2. Procedure for testing the inhibitor release at different pH values

The release of FeCN from capsules containing different Cs:CA ratios was tested in bulk solutions with different pHs in the range of 7–13. Demineralised water was used for pH 7. Solutions with a pH of 13, 11 and 9 were prepared by adding potassium hydroxide (KOH) to demineralised water at concentrations of 10^{-1} M, 10^{-3} M, and 10^{-5} M, respectively. The pH of the solutions was measured using a pH meter (Metrohm). 5 g of freshly prepared capsules were added to 40 mL of each solution and placed separately in airtight plastic bottles. At day 7, eluates were sampled using a pipette and analysed using a UV-VIS spectrophotometer (Shimadzu UV2600) at 218 nm. The amount of FeCN released from the capsules was quantified using a calibration curve prepared with three FeCN solutions of known concentrations (6.25, 12.5 and 25 mg/L). When the absorption of the eluates was out of the calibration range, they were diluted 50x to stay within the calibration curve.

5.2.3. Visual observations of the capsules

Capsules with different Cs:CA ratios were imaged and their size measured using a digital light microscope (Keyence VHX-7000). 20 capsules were imaged and measured for each Cs:CA ratio, and the mean measured values with their coefficient of variation are reported.

5.2.4. Measuring Fe impurities in chitosan solutions

The Cs solution used for coating the CA capsules was analysed using ICP-OES for the presence of Fe ions. The samples were first acidified with 1% (v/v) nitric acid (HNO3) and passed through a filter before analysing using ICP. Sample was diluted 10 times.

5.3. Results and Discussion

The capsules were ellipsoids and uniformly sized as shown in Figure 5.2. The mean size along the longer dimension and shorter dimension of the ellipsoid was 2.6 mm and 2.1 mm respectively. The coefficient of variation (C.V) was 0.11 along the longer dimension, higher compared to the shorter dimension (C.V = 0.06). The observed size was irrespective of the Cs:CA ratio.

Increasing the amount of chitosan is shown to alter the colour of the capsules to a bluish-green hue as seen in Fig. 2. The blue colour might be due to formation of

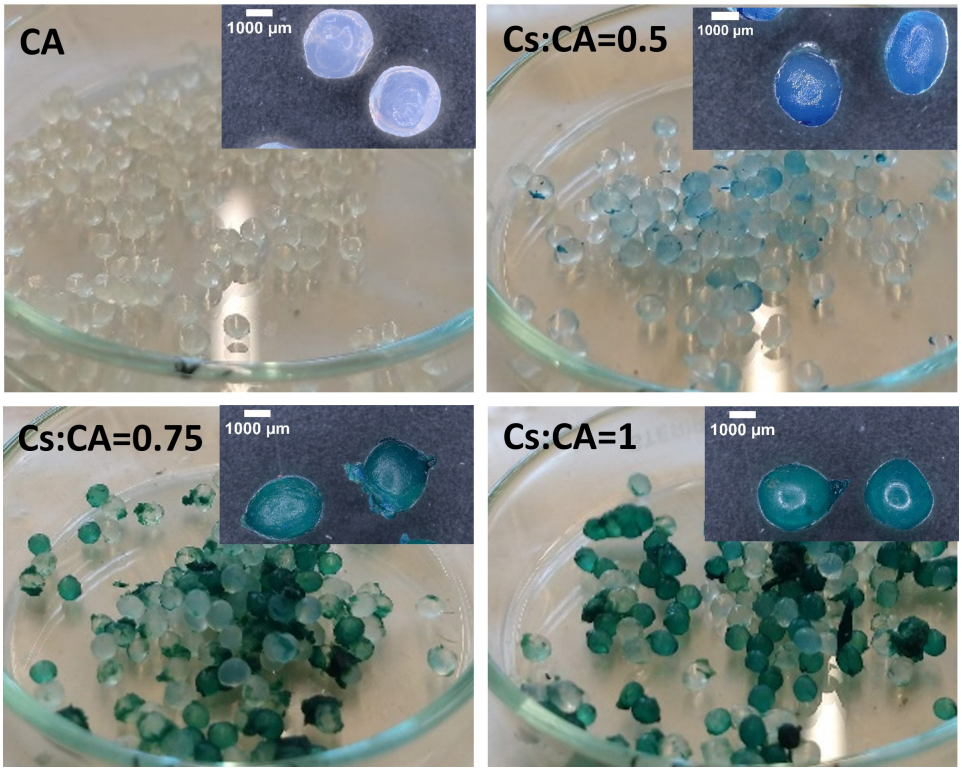

Figure 5.2: FeCN loaded capsules with different chitosan (Cs): calcium alginate (CA) ratios. Inset: microscope image of capsules showing the ellipsoidal shape.

Prussian blue (Iron (III) hexacyanoferrate(II)) as summarised in Equation 1 [32].

$$4\,Fe^{3+} + 3\,[Fe^{III}(CN)_6]^{4-} \longrightarrow Fe_4{}^{III}[Fe^{II}(CN)_6]_3\,(\text{blue}) \tag{5.1}$$

Trace amounts of Fe ion (<0.2%) were detected in the chitosan using ICP (data not shown). This Fe ion in the form of Iron (III) hexacyanoferrate(II) (Equation 5.3) would be sufficient for the blue colouration of the chitosan beads (Figure 5.2). Cs is positively charged at pH <6.5 and could possibly bind with the FeCN ion which has a net negative charge. Cs concentration is indicative of this interaction as we expect that with increased Cs concentration there are more positively charged functional groups on the Cs polymer for the FeCN to react with, thereby increasing the amount of bound or complexed FeCN. This could also contribute to a deeper blue colour (Figure 5.2). However, more research is needed to clarify Cs-FeCN interaction.

The release of FeCN obtained from UV-VIS spectroscopy is presented in Figure 5.3. The CA capsules (without Cs coating) are very permeable and release high amounts of FeCN in the whole pH range (7-13). In general, CA is anionic in nature, under alkaline conditions, the carboxyl group on the alginate ($-COOH$) is

deprotonated to $–COO^-$. As the pH increases, the electrostatic repulsion due to the negative charge increases. The repulsion results in the alginate swelling, increasing the gel's open network structure and permeability. The increased permeability means that the release of encapsulated FeCN is very high.

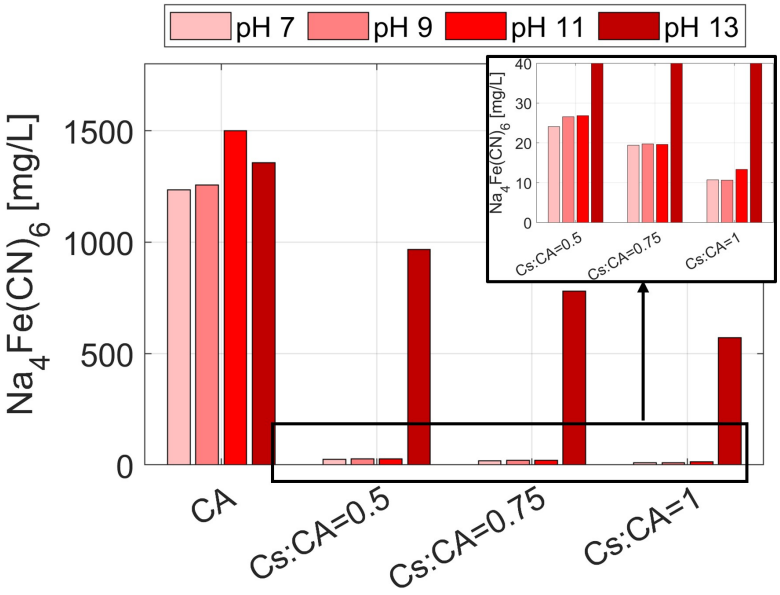

Figure 5.3: Release of FeCN from the capsules in solutions with different pHs as a function of Cs:CA ratio. Inset: zoomed-in image of capsules with Cs:CA ratios for greater clarity.

Increasing the Cs:CA ratio dramatically moderates FeCN release at pH 7-11. Cs:CA capsules release almost 60 times less FeCN compared to CA, making Cs:CA capsules almost impermeable in this pH range. The reduced release is because the Cs coating creates an additional low permeable membrane reducing FeCN transport. In addition, the cationically charged Cs coating shrinks and potentially restricts the alginate from swelling, reducing the release.

At pH 13, the Cs:CA capsules show higher FeCN release compared to release at pH 7-11. However, the Cs coating is still able to reduce the rate of release significantly as compared to CA. It is possible that the Cs is no longer charged at high pH, and the Cs-CA bond is broken, leading to the degradation of the coating. Somewhere between pH 11 and 13, the Cs coating changes its response. Investigating the reason for the abrupt release is relevant for mortar application as the pH of the pore solution in cementitious materials (cement or lime mortar) lies between pH 11-13.

It is expected that the very fast release in high alkaline conditions (pH 13) can be controlled by adjusting the Cs:CA ratio. However, by increasing the Cs amount, complete immobilisation of the inhibitor might arise at lower pH environments, such as those present in carbonated mortar. Therefore, a compromise should be found while designing the capsules.

5.4. Conclusions

In this study, the crystallisation inhibitor FeCN was successfully encapsulated in Cs-coated CA capsules. As expected, pure CA capsules demonstrated significant release in alkaline environments. However, coating of the CA capsules with Cs as a result of the ionic interaction between Cs and CA lowered the release FeCN due to the Cs-coating lowering the permeability of the capsules. In addition, the capsule can be designed to control FeCN release by optimising the Cs:CA ratio.

Furthermore, the presence of chitosan leads to colour alteration of the capsules. The colour change is attributed to the trace iron impurities present in chitosan, that react with the inhibitor. Coloured capsules could lead to unfavourable aesthetic effects like chromatic alteration to mortar. Further research needs to understand this reaction.

5.5. Outlook

This study shows promising results in designing of pH-controlled hydrogel capsules for controlling the release of encapsulated FeCN in bulk solutions. In the future, the effect of capsules will be studied in mortar, focusing on inhibitor leaching, capsule survivability during mixing and the effect of capsules on the performance of mortar against salt damage.

In addition to preventing leaching of FeCN, the application of such capsules can be relevant to other (self-healing, corrosion inhibitors) applications [33, 34], especially those where pH plays an important role.

References

[1] A. E. Charola, *Salts in the Deterioration of Porous Materials : An Overview,* Journal of the American institute for conservation **39**, 327 (2000).

[2] G. W. Scherer, *Crystallization in pores,* Cement and Concrete Research **29**, 1347 (1999).

[3] M. Steiger, *Crystal growth in porous materials - I: The crystallization pressure of large crystals,* Journal of Crystal Growth **282**, 455 (2005).

[4] M. P. Bracciale, S. Sammut, J. Cassar, M. L. Santarelli, and A. Marrocchi, *Molecular Crystallization Inhibitors for Salt Damage Control in Porous Materials : An Overview,* Molecules **25**, 1873 (2020).

[5] A. A. Bode, S. Jiang, J. A. Meijer, W. J. Van Enckevort, and E. Vlieg, *Growth inhibition of sodium chloride crystals by anticaking agents: In situ observation of step pinning,* Crystal Growth and Design **12**, 5889 (2012).

[6] A. Glasner and M. Zidon, *The crystallization of NaCl in the presence of [Fe(CN)6]4- ions,* Journal of Crystal Growth **21**, 294 (1974).

[7] C. Selwitz and E. Doehne, *The evaluation of crystallization modifiers for controlling salt damage to limestone,* Journal of Cultural Heritage **3**, 205 (2002).

[8] C. Rodriguez-Navarro, L. Linares-Fernandez, E. Doehne, and E. Sebastian, *Effects of ferrocyanide ions on NaCl crystallization in porous stone,* Journal of Crystal Growth **243**, 503 (2002).

[9] A. A. Bode, V. Vonk, F. J. Van Den Bruele, D. J. Kok, A. M. Kerkenaar, M. F. Mantilla, S. Jiang, J. A. Meijer, W. J. Van Enckevort, and E. Vlieg, *Anticaking activity of ferrocyanide on sodium chloride explained by charge mismatch,* Crystal Growth and Design **12**, 1919 (2012).

[10] S. Gupta, H. P. Huinink, L. Pel, and K. Kopinga, *How Ferrocyanide Influences NaCl Crystallization under Different Humidity Conditions,* Crystal Growth & Design **14**, 1591 (2014).

[11] S. J. Granneman, B. Lubelli, and R. P. van Hees, *Effect of mixed in crystallization modifiers on the resistance of lime mortar against NaCl and Na2SO4 crystallization,* Construction and Building Materials **194**, 62 (2019).

[12] B. Lubelli and R. P. van Hees, *Effectiveness of crystallization inhibitors in preventing salt damage in building materials,* Journal of Cultural Heritage **8**, 223 (2007).

[13] T. Rivas, J. Feijoo, I. de Rosario, and J. Taboada, *Use of Ferrocyanides on Granite Desalination by Immersion and Poultice-Based Methods,* International Journal of Architectural Heritage **11**, 588 (2017).

[14] T. Rivas, E. Alvarez, M. J. Mosquera, L. Alejano, and J. Taboada, *Crystallization modifiers applied in granite desalination: The role of the stone pore structure,* Construction and Building Materials **24**, 766 (2010).

[15] J. Feijoo, D. Ergenç, R. Fort, and M. A. de Buergo, *Addition of ferrocyanide-based compounds to repairing joint lime mortars as a protective method for porous building materials against sodium chloride damage,* Materials and Structures **54**, 14 (2021).

[16] B. Lubelli, T. G. Nijland, R. P. Van Hees, and A. Hacquebord, *Effect of mixed in crystallization inhibitor on resistance of lime-cement mortar against NaCl crystallization,* Construction and Building Materials **24**, 2466 (2010).

[17] S. J. Granneman, B. Lubelli, and R. P. Van Hees, *Characterization of lime mortar additivated with crystallization modifiers,* International Journal of Architectural Heritage **12**, 849 (2018).

[18] A. Kamat, B. Lubelli, and E. Schlangen, *Effect of a mixed-in crystallization inhibitor on the properties of hydraulic mortars,* AIMS Materials Science **9**, 628 (2022).

[19] B. Lubelli, E. d. Bouvrie, T. G. Nijland, and A. Kamat, *Plasters with mixed-in crystallization inhibitors: Results of a 4-year monitoring of on-site application,* Journal of Cultural Heritage **59**, 10 (2023).

[20] A. P. Esser-Kahn, S. A. Odom, N. R. Sottos, S. R. White, and J. S. Moore, *Triggered release from polymer capsules,* (2011).

[21] B. Dong, Y. Wang, G. Fang, N. Han, F. Xing, and Y. Lu, *Smart releasing behavior of a chemical self-healing microcapsule in the stimulated concrete pore solution,* Cement and Concrete Composites **56**, 46 (2015).

[22] W. Xiong, J. Tang, G. Zhu, N. Han, E. Schlangen, B. Dong, X. Wang, and F. Xing, *A novel capsule-based self-recovery system with a chloride ion trigger,* Scientific Reports **5**, 1 (2015).

[23] A. Al-Tabbaa, C. Litina, P. Giannaros, A. Kanellopoulos, and L. Souza, *First UK field application and performance of microcapsule-based self-healing concrete,* Construction and Building Materials **208**, 669 (2019).

[24] C. Xue, W. Li, J. Li, V. W. Tam, and G. Ye, *A review study on encapsulation-based self-healing for cementitious materials,* Structural Concrete **20**, 198 (2019).

[25] M. Hu, J. Guo, Y. Yu, L. Cao, and Y. Xu, *Research advances of microencapsulation and its prospects in the petroleum industry,* Materials **10**, 369 (2017).

[26] S. Xu, A. Tabaković, X. Liu, and E. Schlangen, *Calcium alginate capsules encapsulating rejuvenator as healing system for asphalt mastic,* Construction and Building Materials **169**, 379 (2018).

[27] W. R. Gombotz and S. F. Wee, *Protein release from alginate matrices,* Advanced Drug Delivery Reviews **31**, 267 (1998).

[28] T. W. Wong, *Alginate graft copolymers and alginate-co-excipient physical mixture in oral drug delivery,* Journal of Pharmacy and Pharmacology **63**, 1497 (2011).

[29] M. George and T. E. Abraham, *Polyionic hydrocolloids for the intestinal delivery of protein drugs: Alginate and chitosan - a review,* Journal of Controlled Release **114**, 1 (2006).

[30] M. L. Huguet and E. Dellacherie, *Calcium alginate beads coated with chitosan: Effect of the structure of encapsulated materials on their release,* Process Biochemistry **31**, 745 (1996).

[31] A. E. Polk, B. Amsden, D. J. Scarratt, A. Gonzal, A. O. Okhamafe, and M. F. Goosen, *Oral delivery in aquaculture: Controlled release of proteins from chitosan-alginate microcapsules,* Aquacultural Engineering **13**, 311 (1994).

[32] E.-S. Chan, B.-B. Lee, P. Ravindra, and D. Poncelet, *Prediction models for shape and size of ca-alginate macrobeads produced through extrusion–dripping method,* Journal of Colloid and Interface Science **338**, 63 (2009).

[33] Y. C. Erşan, H. Verbruggen, I. De Graeve, W. Verstraete, N. De Belie, and N. Boon, *Nitrate reducing CaCO3 precipitating bacteria survive in mortar and inhibit steel corrosion,* Cement and Concrete Research **83**, 19 (2016).

[34] T. A. Söylev and M. G. Richardson, *Corrosion inhibitors for steel in concrete: State-of-the-art report,* Construction and Building Materials **22**, 609 (2008).

6

Capsule controlled release of a crystallisation inhibitor in mortars

The results from the previous chapter suggest that for a specific pH, the release of the inhibitor from chitosan-calcium alginate polyelectrolyte capsules can be tuned by modifying the chitosan:alginate ratio. In this chapter, as a next step in the prototype development, the effect of the capsules on the leaching behaviour of the inhibitor in mortar is investigated. First, the release of the inhibitor from the calcium alginate (CA) and chitosan-calcium alginate (CsCA) capsules is measured in mortar pore solution. Next, CA and CsCA capsules containing the inhibitor are incorporated in hardened mortar and the mortar is subjected to diffusion- and advection-driven leaching tests, as per the protocol developed in Chapter 4. The results are compared with the leaching of the inhibitor from a similar mortar with mixed-in inhibitor. Analytical techniques, such as UV-VIS and ICP-OES, are used to quantify the released (or leached) inhibitor and imaging techniques, such as optical microscopy and scanning electron microscopy, are used to visualise the leached inhibitor.

This chapter is based on the article published in Materials & Design, **244**, 113156 (2024).

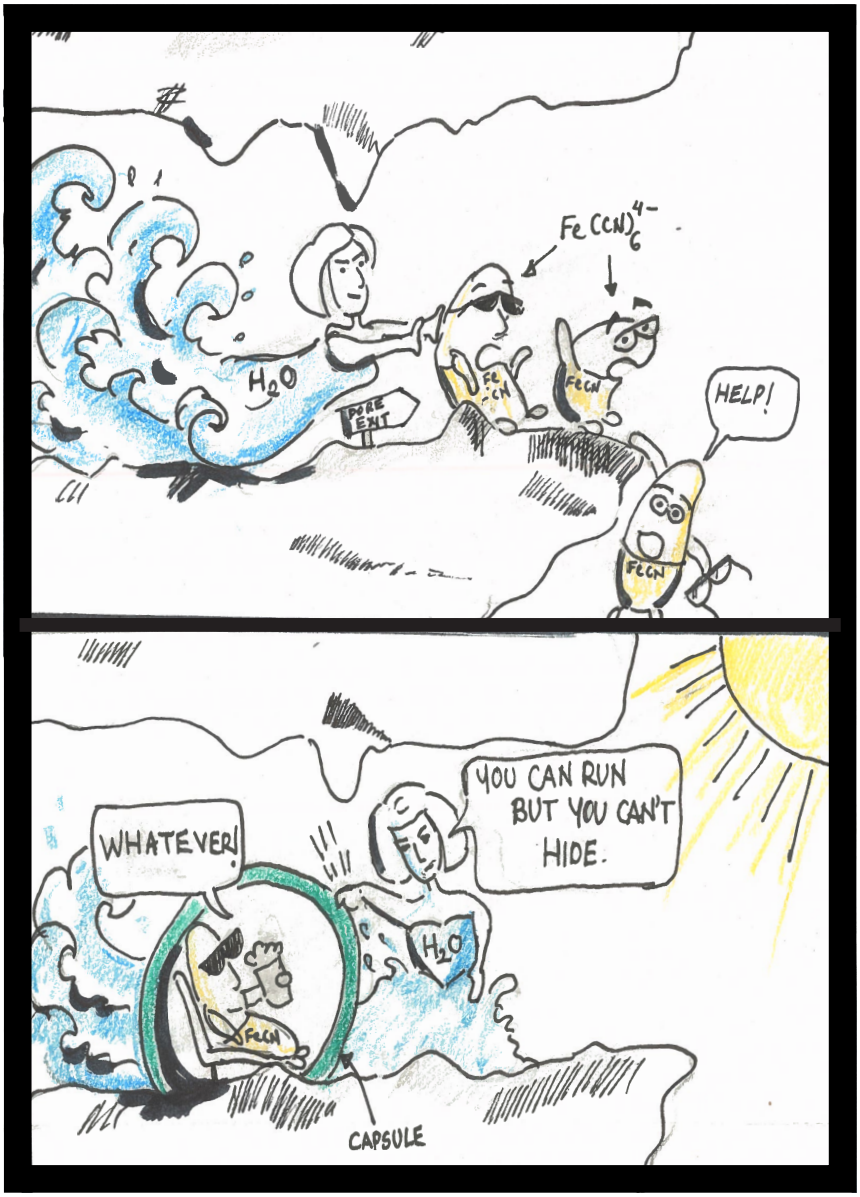
$Fe(CN)_6^{4-}$
H_2O
PORE ENT
HELP!
FeCN
WHATEVER!
YOU CAN RUN BUT YOU CAN'T HIDE.
H_2O
CAPSULE

6.1. Introduction

The crystallisation of salts within porous building materials is a leading cause of building damage [1]. Salts, particularly sodium chloride (NaCl) from various sources like groundwater, salt spray and de-icing, permeate into building materials through capillary transport [2]. Under supersaturated conditions, salts can exert a crystallisation pressure exceeding the mechanical strength of building materials causing damage [3–5]. Exposure to fluctuating environmental conditions, including variations in relative humidity and temperature, can result in repeated cycles of dissolution-recrystallisation [6], exacerbating the damage [7]. Lime-mortar-based plasters and renders, particularly those in exposed locations such as building surfaces, are susceptible to damage, necessitating frequent replacement. Frequent repair and replacement costs can be significant. However, these costs can be minimised by improving the durability of repair mortars. In recent decades, the incorporation of crystallisation inhibitors within mortars has yielded promising results in improving mortar durability by altering the process of salt crystallisation [8].

Crystallisation inhibitors are compounds that inhibit crystal nucleation and modify crystal growth by adsorbing onto specific crystal faces [9]. Sodium ferrocyanide decahydrate ($Na_4Fe(CN)_6 \cdot 10\,H_2O$; hereafter referred to as NaFeCN) is one of the most effective inhibitors of NaCl crystallisation [10]. Hexacyanoferrate(II), $[Fe(CN)_6]^{4-}$ anions from NaFeCN inhibit and/or delay NaCl nucleation by increasing the critical supersaturation [11]. The $[Fe(CN)_6]^{4-}$ anions sorb onto the $\{1\,0\,0\}$ faces of the NaCl crystals, blocking NaCl growth due a difference in the ionic surface charge [12]. This difference results in NaCl crystal growth along the $\langle 1\,1\,1\rangle$ direction, resulting in the formation of dendritic rather than cubic $\{1\,0\,0\}$ crystals [13]. Due to their high surface area, dendritic crystals increase the evaporation rate and promote advection of salt ions away from the solution [14]. When present in NaCl contaminated porous building materials, the delay in NaCl crystal nucleation and the formation of dendritic crystals allows Na^+ and Cl^- ions to be easily transported towards the evaporative surface where NaCl can crystallise as harmless efflorescence (surface crystallisation) without exerting crystallisation pressure within the pore network [13–17]. In recent years, lime-based mortars incorporating NaFeCN have demonstrated reduced salt damage in laboratory settings [8, 18, 19] and in the field [20]. Notably, amongst various NaCl inhibitors, NaFeCN remains stable in the alkaline pH range of mortars [21] and does not alter their physical and chemical properties [22, 23]. This makes NaFeCN a promising additive for mitigating salt damage in mortars. However, NaFeCN's relatively high solubility (17% w/w at 25°C) [24] makes it susceptible to leaching. The depletion of NaFeCN from mortar specimens after repeated wetting-drying cycles has been observed and attributed to the leaching of NaFeCN [18]. A recent systematic study into the leaching behaviour of NaFeCN from mortar specimens incorporating NaFeCN by direct mixing reported severe leaching, concluding that this method of addition may not prevent salt damage in the long run [25]. By slowing down the rate of NaFeCN leaching from mortars it may be possible to prolong their salt damage resistance.

The use of capsules, produced from natural polymer polysaccharides and pro-

teins, for the protection and delivery various cargoes has gained momentum across a wide range of fields [26–28]. These polymers offer rich functional groups, enabling controlled cargo release and distinct advantages over synthetic polymers, including non-toxicity, abundance, commercial availability, and biodegradability [29]. Alginate, a polysaccharide derived from brown algae [30], exhibits pH-responsive behaviour due to the presence of abundant carboxyl functional groups ($-COOH$) on its chains. Calcium alginate (CA) capsules, produced through the ionic gelation of sodium alginate (SA) with calcium ions (Ca^{2+}) [31] have long been exploited for controlled drug release in physiological conditions (up to pH 7.4) [32, 33]. More recently, CA capsules have been used to encapsulate bacterial spores within highly alkaline concrete (pH ≈12) for self-healing concrete applications [34, 35]. However, the employment of CA capsules for controlled release of cargo within alkaline construction materials may pose some challenges as the $-COOH$ deprotonate becoming negatively charged carboxylate ions (COO^-) [36], resulting in capsule swelling and rapid release of cargo [37]. Additionally, CA has been shown to disintegrate in alkaline conditions [38]. Chitosan (Cs), a cationic biopolymer derived from crustaceans such as shrimps and crabs [39] also demonstrates pH responsiveness due to the presence of amine functional groups ($-NH_2$) on its chains [40]. In highly alkaline conditions, the positively charged ammonium ions (NH^{3+}) lose its positive charge resulting in contraction and renders the polymer insoluble [41]. Cs' positive charge attracts net negatively charged ions, such as $[Fe(CN)_6]^{4-}$, allowing Cs capsule's to retain such ions [42]. Furthermore, Cs because of its positive charge can form a polyelectrolyte complex (PEC) with negatively charged alginate [38, 43]. Several studies have used this PEC to produce Cs-CA capsules that demonstrated the sustained release of cargo and increased mechanical stability in the bio-medical field [44–48]. Cs both limits the swelling of the CA capsules providing a tighter physical barrier for slowing down the release of the cargo [49, 50] and reduces the ease of solvation of CA capsules in high pH conditions [38, 51]. In the past, attempts have been made to use synthetic pH-responsive capsules in simulated concrete solutions [52], but so far controlled release of cargo using natural polymers like Cs-CA in construction materials have not been explored.

In a preliminary study, we investigated the release of $[Fe(CN)_6]^{4-}$ from Cs-CA capsules in solutions across a range of alkaline pH values (7–13) for the first time [53]. The results suggest that the ratio between Cs and CA can be used to tune $[Fe(CN)_6]^{4-}$ release in alkaline solutions. This raises an interesting question: Can Cs-CA capsules be used for the controlled release of NaFeCN from within hardened hydraulic lime mortar? To answer this question, we produce Cs-CA capsules containing NaFeCN and incorporate these capsules within natural hydraulic lime mortar and perform series of experiments to assess the controlled release of NaFeCN from the mortar.

6.2. Experimental design

To investigate the controlled release of NaFeCN from mortar-capsule system, an experimental plan was devised consisting of three phases: (1) capsule preparation,

(2) capsule selection, and (3) capsule-controlled release in mortar (Figure 6.1). The results of each phase informing the next phase.

In the initial phase, CA capsules containing NaFeCN were produced through ionic gelation of SA with Ca^{2+}. The subsequent CA capsules were then coated with Cs to obtain Cs-CA capsules. The Cs:SA ratio and the initial concentration of NaFeCN was varied to obtain diverse combinations of capsules.

In the second phase, the morphology of the capsules and encapsulated NaFeCN were characterised. The release of NaFeCN from the capsules was assessed in a synthetic lime mortar pore solution, to mimic conditions within a mortar pore-network. Capsules were selected considering both the rate of release into the pore solution and the total amount of encapsulated NaFeCN.

In the third phase, the selected capsules were incorporated in mortar specimens and the controlled release of NaFeCN was evaluated based on two transport mechanisms: (i) diffusion-driven transport: whereby the effective diffusion coefficient of NaFeCN was measured based on the leaching rate under accelerated conditions; and (ii) advection-driven transport: by subjecting mortar specimens to cycles of capillary absorption-drying and the transport of NaFeCN was monitored. The advection-driven test simulates realistic field conditions. The results were compared with those for mortar specimens made with directly mixed-in NaFeCN.

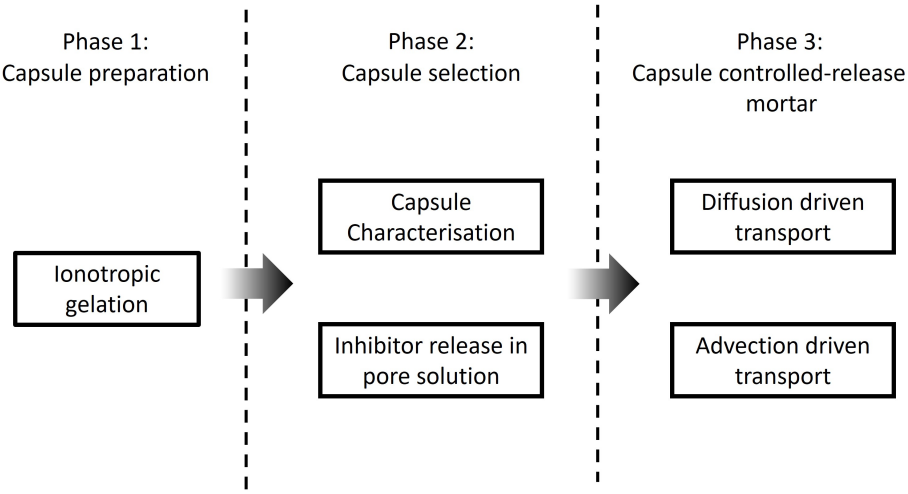

Figure 6.1: The experimental design scheme is divided in three phases. The arrow indicates the workflow where results from the preceding phase informs the experimental design of the subsequent phase.

6.3. Materials and methods

6.3.1. Materials

Sodium alginate (SA, mannuronic/guluronic ratio (M/G) of 1.56), calcium chloride dihydrate ($CaCl_2 \cdot 2\,H_2O$), NaCl and Chitosan (Cs, molecular weight (Mw) ranging from

190–310 kDa) were used to prepare the capsules (all from Sigma-Aldrich). Sodium ferrocyanide decahydrate (NaFeCN; Acros organics) was used as the crystallisation inhibitor. Acetic acid (CH_3COOH; J.T. Baker) and sodium hydroxide (NaOH; Honeywell) were also used in the study. Natural hydraulic lime (NHL) with a strength class of 3.5 MPa (from St. Astier, France) and standard river sand (following NEN-EN 196-1 [54]) were used to prepare of mortar specimens.

6.3.2. Preparation of capsules

6.3.2.1. Calcium alginate capsules

CA capsules containing NaFeCN were prepared with various compositions (Table1) using ionic gelation technique [31]. In brief, SA (2% w/v) and NaFeCN were dissolved in demineralised water. The mixture was then extruded into a continuously stirred (300 rpm) gelation bath of $CaCl_2 \cdot 2\,H_2O$ (3% w/v) using a peristaltic pump (Masterflex console drive, Cole Parmer instruments) connected to a needle (0.9 mm internal diameter). The mixture forming beads crosslinked with Ca^{2+} in the bath to form CA capsules loaded with NaFeCN. To minimise outward diffusion of NaFeCN from the capsules during production, NaFeCN was also added to the gelation bath with the same concentration as the extruded SA mixture. The obtained CA capsules were washed with demineralised water to remove excess unlinked Ca^{2+} and Na^{+} ions and dried at 40°C for 48 hours. Blank CA capsules (CA-blank) were also prepared using the same method but without the inclusion of NaFeCN.

Table 6.1: Overview of the different capsule types and their composition.

Capsule type	Capsule label	SA % (w/v)	Initial F % (w/v)	Cs % (w/v)	Cs:SA
Calcium alginate blank	CA-blank	2	-	-	-
Calcium alginate with sodium ferrocyanide	CA-F_2	2	2	-	-
	CA-F_4	2	4	-	-
Chitosan-calcium alginate with sodium ferrocyanide	Cs-CA 0.25-F_2	2	2	0.5	0.25
	Cs-CA 0.375-F_2	2	2	0.75	0.375
	Cs-CA 0.5-F_2	2	2	1	0.5
	Cs-CA 0.25-F_4	2	4	0.5	0.25
	Cs-CA 0.375-F_4	2	4	0.75	0.375
	Cs-CA 0.5-F_4	2	4	1	0.5

CA=Calcium alginate, F=Sodium ferrocyanide, Cs=Chitosan, SA=Sodium alginate

6.3.2.2. Chitosan-coated calcium alginate capsules

Cs-CA capsule with various compositions were prepared (Table 6.1). A Cs bath was prepared by dissolving Cs in 0.1 M CH_3COOH for 24 hours under stirring at 40°C. Subsequently, wet CA capsules, obtained as described in Section 6.3.2.1,

were added to Cs bath and complexed for 15 minutes under gentle stirring (300 rpm). Different Cs concentrations within the bath were used to obtain Cs-coated-CA (Cs-CA) capsules with different Cs:SA ratios. Following this, the resulting Cs-CA capsules were washed and dried as above (Section 6.3.2.1).

6.3.3. Preparation of mortar specimens

Mortar specimens were prepared by mixing NHL and sand (in a volumetric ratio of 1:3) with a water-to-binder (w/b) ratio of 1.19. Four specimens types were prepared (Table 6.2): (i) Mortar-blank: Mortar specimens containing no NaFeCN or capsules; (ii) Mortar-CA-F: Mortar specimens with incorporated CA-F_2[calcium alginate containing NaFeCN with an initial 2% (w/v)] capsules such that the total mass of NaFeCN was equivalent to 10% of the weight of NHL [25]; (iii) Mortar-Cs-CA-F: mortar specimens with incorporated Cs-CA 0.25-F_4 [chitosan-calcium alginate containing NaFeCN with an initial 4% (w/v)] capsules such that the total mass of NaFeCN was equivalent to 10% of the weight of NHL; and (iv) Mortar-F: plain mortar specimens containing directly added NaFeCN and CA-blank [calcium alginate containing no NaFeCN] capsules. The Mortar-F specimens were prepared by dissolving NaFeCN (10% of the weight of NHL) in the mixing water and adding it to sand and NHL. CA-blank capsules were added to Mortar-F mix to obtain a comparable pore size distribution as Mortar-CA-F and Mortar-Cs-CA-F specimens. Note: The type of capsules mixed into the mortar specimens was based on the results of Phase 2 (Section 6.4.3). All specimens were cylindrical (Φ=30, H=50 mm). The specimens were sealed in polyvinyl chloride containers and cured at 20°C and 95% RH for 28 days before testing.

Table 6.2: Overview of type of mortar specimens and their mix design. The type and dosage of capsules for each mortar type are also stated.

Mortar specimen label	Label of capsule incorporated	F (% NHL weight)	Capsule content (%NHL weight)	NHL:Sand (volumetric)	w/b
Mortar-blank	-	-	-	1:3	1.19
Mortar-CA-F	CA-F_2	10	32.5	1:3	1.19
Mortar-Cs-CA-F	Cs-CA 0.25-F_4	10	37	1:3	1.19
Mortar-F	CA-blank (containing no F)	10 (added directly)	32.5	1:3	1.19

CA=Calcium alginate, Cs=Chitosan, F=Sodium ferrocyanide, NHL=Natural hydraulic lime, w/b=water-to-binder ratio.

6.3.4. Capsules characterisation

The capsules were observed with a digital microscope (Keyence VHX-7000). The dimensions of the capsules were measured using the microscope's in-built software. A minimum of 50 capsules per type were measured along maximum and minimum dimensions. The mean value and the standard deviation were calculated. To quantify the amount of NaFeCN encapsulated within each capsule type, a series

of steps were undertaken. The capsules were first milled to a fine powder using a ball mill (Retsch MM200). The powder was then mixed in 1.5 M NaOH solution and subsequently passed through a 0.45 µm syringe membrane. The filtrate was analysed for Fe(II)/(III) concentration using inductive coupled plasma optical emission spectroscopy (ICP-OES; PerkinElmer Optima 5300DV). The amount of NaFeCN (C_{NaFeCN}) is expressed in mg g^{-1} of capsule mass, calculated as:

$$C_{NaFeCN} = \frac{C_{Fe} * (V_{solution}) * (\frac{Mw_{NaFeCN}}{Aw_{Fe}})}{M_{sample}} \quad (6.1)$$

Where, C_{Fe} is the measured Fe(II)/(III) concentration in mg L^{-1}, $V_{solution}$ is the volume of NaOH solution in L, M_{sample}= Mass of capsule sample in g. Mw_{NaFeCN}/Aw_{Fe} is the ratio of the molecular weight of NaFeCN to the atomic weight of Fe. Based on stoichiometry, Fe and NaFeCN were assumed to contain equal number of moles.

6.3.5. Procedure for assessment of NaFeCN release

6.3.5.1. NaFeCN release in pore solution

Pore solution was prepared as a binder-slurry filtrate based on the method described by [55]. NHL and demineralised water were mixed in a 2:1 ratio, stirred for 24 hours, centrifuged, and the resulting supernatant was vacuum filtered to obtain a clear pore solution. The ionic composition and pH of the solution were analysed by ICP-OES and a pH meter (Metrohm 914), respectively (Table A.1, Appendix A). 100 mg of each type of capsules (Table 6.1) was added to 100 mL of the pore solution and stored within airtight plastic containers. Samples of the pore solutions (500 µL) were collected at various time intervals (10 min–1 hour) over a 6-hour period. The samples were analysed for NaFeCN content using an ultraviolet-visible (UV-VIS) spectrophotometer (Shimadzu UV2600) at a wavelength of 218 nm [11]. To quantify the content of NaFeCN through UV-VIS, a calibration curve was generated (Figure A.1,Appendix A) and the absorbance of the plain pore solution was used as the baseline.

6.3.5.2. NaFeCN leaching from hardened mortar

Diffusion-driven transport

The diffusion-driven transport of NaFeCN from different mortar specimens (Table 6.2) was assessed in accordance with the accelerated leaching test (ASTM C1308-21) [56], a method previously used to assess NaFeCN leaching from mortar [25](Chapter 4). Each mortar specimen was suspended in a separate cylindrical tank filled with demineralised water as the leachant such that the specimen surface area to leachant volume was 0.15 cm^{-1}. Submerging the specimens facilitated the transport of $[Fe(CN)_6]^{4-}$ ions from the mortar matrix into the leachant. Leachate samples (20 mL) were collected at 2 and 5 hours and subsequently every 24 hours until day 10 of the test. The samples were analysed for leached $[Fe(CN)_6]^{4-}$ concentration and their pH by UV-VIS and a pH meter, respectively. After the collection of each leachant sample, the leachant was renewed with fresh demineralised water, effectively resetting the $[Fe(CN)_6]^{4-}$ concentration in the leachant to zero. Leachate

samples from Mortar-blank specimens were used to create a baseline for UV-VIS measurements. The calibration curve (Figure A.1, Appendix A) was used to measure $[Fe(CN)_6]^{4-}$ in the leachate. The concentration of leached $[Fe(CN)_6]^{4-}$ was expressed as cumulative fraction leached (CFL), defined as the ratio of cumulative $[Fe(CN)_6]^{4-}$ amount leached in time to the initial amount of $[Fe(CN)_6]^{4-}$ present in the mortar specimens as stated in ASTM C1308-21 [56]. The effective diffusion coefficient was calculated by fitting CFL data to the analytical solution based on the works of Nestor and Pescatore (Appendix A) [57, 58]. The analytical solution assumes the same boundary conditions as the test setup. Each specimen type was tested in triplicate. To determine the remaining $[Fe(CN)_6]^{4-}$ in the mortar specimens (after the leaching test), a cold water extraction (CWE) was conducted [59]. The test was modified using 1.5 M NaOH as the solvent to release any remaining NaFeCN from the capsules within the specimens. The concentration of Fe ions was measured using ICP-OES and the content of NaFeCN calculated as per Equation 6.1. The initial NaFeCN content in each specimen was calculated based on these results and the leaching results (Appendix A).

Advection-driven transport

The advection-driven transport of three mortar specimen types was tested: Mortar-CA-F, Mortar-Cs-CA-F and Mortar-F (Table 6.2). The specimens were first dried at 40°C until reaching a constant weight. The sides of the specimens were sealed using parafilm® (Bemis Company Inc.). The specimens were subjected to three capillary absorption-drying cycles, each cycle consisting of the following steps: saturating the specimens with demineralised water via capillary absorption from the bottom surface; sealing the bottom surface with paraffin film and placing the specimens in a climate chamber for one week at 20°C, 50% relative humidity (RH). After one week, the specimens were placed in a drying oven at 40°C at 15% RH until reaching a constant weight (typically taking ≈two weeks). Each specimen type was tested in triplicate. At the end of each cycle, images were taken of the drying (top) surface of the specimens using a digital camera. At the end of the three cycles, two methods were employed to assess the distribution of NaFeCN within the specimens. Firstly, two specimens from each mortar specimen type were dry saw cut in slices measuring 0–5 mm (including efflorescent crust), 5–15 mm, 15–25 mm and 25–50 mm measured from the top surface. The slices were ground into a fine powder using a mortar and pestle. 1 g of the powder was subsampled (using the coning and quartering method [60]) from each slice, which was mixed with 30 mL 1.5M NaOH (pH 14). Subsequently, the powders were analysed for Fe(II)/(III) (see above, Section 6.3.4). This procedure was also applied to mortar specimens (two replicates each) that had not been subjected to the leaching test, to assess the initial NaFeCN distribution. For the second method, the third sample from each mortar specimen type was examined using environmental scanning electron microscopy and energy dispersive spectroscopy (ESEM-EDS; FEI quanta 650 FEG, NORAN EDS-Thermo Fischer Scientific) and digital microscopy. For microscopic examination, vertical cross-sections of the specimens (parallel to the direction of the advection-driven transport) were prepared by impregnating the

specimen with epoxy resin, saw-cutting the specimens and polishing the saw- cut surface in ethanol (not with water) in accordance with [61]. ESEM was used to image the cross-sections in back-scattered electron (BSE) acquired at 15 keV and EDS was used to map the distribution of Na and Fe as an indicator for NaFeCN, while digital microscopy under plain polarised light was used to obtain images near the evaporative surface with a large field of view.

6.4. Results

6.4.1. Characterisation of capsules

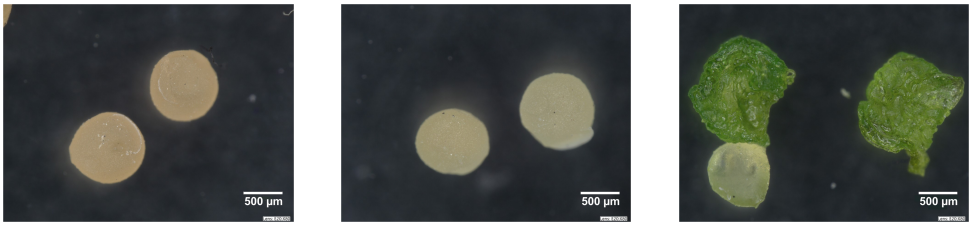

(a) (b) (c)

Figure 6.2: Digital microscope images of three capsule types after drying: (a) CA-blank: a calcium alginate capsule containing no NaFeCN; (b) CA-F_2: a calcium alginate capsule made with an initial concentration of 2% NaFeCN (w/v); and (c) Cs-CA 0.25-F_4: A Chitosan-calcium alginate capsule made with an initial concentration of 4% NaFeCN.

CA capsules have an ellipsoidal shape with a smooth surface (Figure 6.2a, 6.2b). The CA-blank capsules are light brown in colour, typical of alginate hydrogels (Figure 6.2a). The CA-F_2 capsules are pale yellow in colour and are generally bigger size (volume) than the blank CA capsules (Figure 6.2b; Table 6.3). Notably, the Cs-CA-F_2 capsules have an irregular shape and a rough surface and are bright green in colour (Figure 6.2c). The Cs-CA-F 0.25_4 capsules have a similar size as CA-F_2 capsules (Table 6.3). When CA capsules are added to the Cs bath they tend to agglomerate (Figure A.2, Appendix A), with the degree of agglomeration increasing with increasing Cs concentration (Section 6.3.2.2).

Table 6.3: The diameter of capsules along two dimensions, with the mean values and standard deviations reported.

Capsule label	Maximum diameter (µm)	Minimum diameter (µm)
CA-blank	853.7 ± 66.85	709.3 ± 81.99
CA-F_2	1080 ± 90.4	860.27 ± 110.75
Cs-CA 0.25-F_4	1063 ± 124	730 ± 85.5

CA=Calcium alginate, F=sodium ferrocyanide, Cs=Chitosan

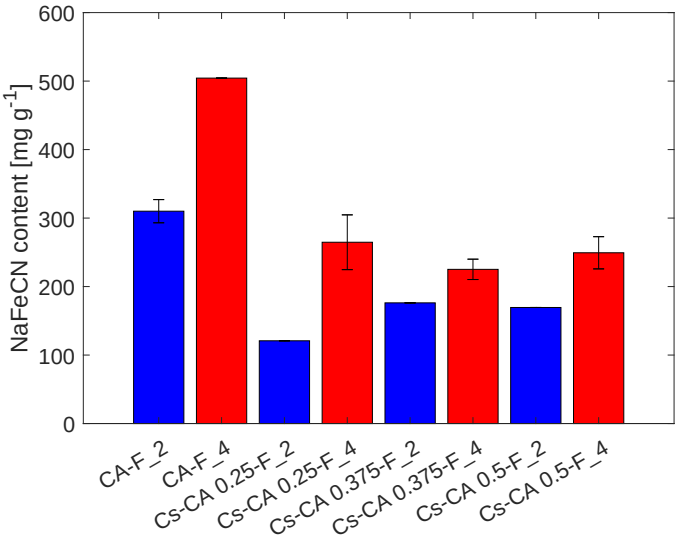

Figure 6.3: Encapsulated NaFeCN content expressed in mg g^{-1} of capsule weight. Higher initial NaFeCN concentration (4%) leads to higher encapsulated NaFeCN content in capsules. The blue bars represent capsules produced with an initial concentration of NaFeCN of 2% (w/v), while the red bars represent capsules produced with an initial NaFeCN concentration of 4% (w/v).

Figure 6.3 shows the amount of encapsulated NaFeCN in the different types of capsules. The graph shows that capsules with a higher initial concentration of NaFeCN (4% w/v, red bars) have a higher ultimate NaFeCN content as compared to capsules with a lower initial concentration (2% w/v, blue bars). Notably, in the case of the Cs-CA 0.25 capsules, increasing the initial concentration of NaFeCN from 2% to 4% (w/v), results in a doubling of the NaFeCN content in the capsules. However, in the case of capsules with higher Cs:SA ratios (i.e., Cs-CA 0.375 and Cs-CA 0.5), this increase in the initial content shows only a marginal rise in the ultimate NaFeCN content. Interestingly, all Cs-CA capsules with initial NaFeCN concentration of 4% (w/v), contain similar ultimate NaFeCN content (i.e. ≈280-300 mg g^{-1} of capsule weight), independent of the Cs:SA ratio.

6.4.2. NaFeCN release in pore solution

Figure 6.4 shows the release of NaFeCN from different capsules. The amount of NaFeCN released from the capsules depends on the initial NaFeCN content of capsules (Figure 6.3). Capsules containing a higher initial NaFeCN concentration of 4% (w/v; Figure 6.4, red lines) released a significantly greater amount of NaFeCN as compared to the capsules containing an initial lower 2% (w/v; Figure 6.4, blue lines). Furthermore, the rate of release (i.e., the slope of the of the linear part of the curve) of NaFeCN also depends on their initial NaFeCN content: a higher initial NaFeCN content leads to a higher (or faster) rate of release. For example, CA-F_4 capsules having the highest NaFeCN content released 90% of their content within the first 10 minutes. In contrast, Cs-CA 0.25-F_2 capsules with the lowest NaFeCN

content took 90 minutes to release 90% of their content.

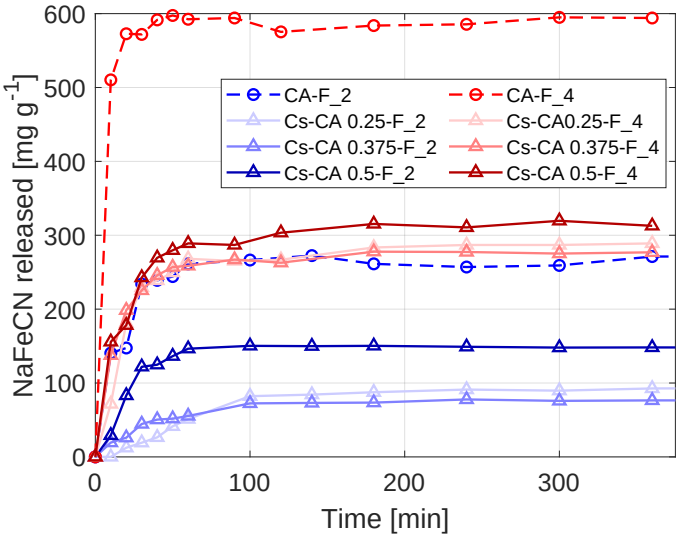

Figure 6.4: Graph showing the release profiles of NaFeCN over time from different capsules into a pore solution, expressed as mg g-1 of capsule. The blue lines represent capsules made with an initial NaFeCN concentration of 2% (w/v), while the red lines represent capsules with an initial NaFeCN concentration of 4% (w/v). CA capsules are represented by dashed lines and Cs-CA capsules with solid lines.

6.4.3. Selection of the type of capsules for mixing in mortar

An ideal mortar with encapsulated salt inhibitor system is the one that contains sufficient salt inhibitor to inhibit salt crystallisation and release it slow enough to prolong its effectiveness over an extended period. The capsule composition plays a key role on its release rate. Different parameters such as the initial concentration of NaFeCN and the Cs content on Cs-CA capsules were tested to obtain the most suitable capsule type. In the NaFeCN release test in pore solution (Section 6.4.2), capsules containing low initial content of NaFeCN (2% w/v) released NaFeCN at a slower rate as compared to capsules containing higher content (4% w/v capsules, Figure 6.4). This difference is due to differences in the concentration gradients between the two capsules and the leachant (pore solution). The higher the gradient the faster the rate of diffusive release from the capsules [62]. However, Cs-CA capsules made with 2% (w/v) NaFeCN (≈100–150 mg g^{-1} of capsule weight) incorporate significantly lower amount of NaFeCN as compared to Cs-CA capsules with 4% (w/v; ≈280-300 mg g^{-1} of capsule weight). Past research suggests that the concentration of NaFeCN in mortar should be equivalent to ≈1% of the binder weight to be effective against salt damage [18]. To achieve sufficient dosage of NaFeCN in mortar, twice as many Cs-CA capsules containing 2% (w/v) NaFeCN would be required as compared to Cs-CA capsules containing 4% (w/v) NaFeCN. Increasing the amount of capsules within the mortar will have a negative effect on its mechanical performance due to additional air voids and weak interface transi-

tion zones between the mortar matrix and the capsules [63]. Based on the above considerations Cs-CA capsules with high initial NaFeCN content (4% capsules) are preferable to capsules with lower content (2% capsules).

Varying the Cs:SA ratio had minimal impact on the encapsulated NaFeCN content as well as its release rate from Cs-CA capsules containing 4% NaFeCN (Figure 6.3 and 6.4). Cs is comparatively more expensive than CA, making capsules with the lowest Cs content more cost-effective to produce while still offering comparable release performance compared to Cs-CA capsules with higher Cs:SA ratios (Figure 6.4). Furthermore, increasing the Cs content in the production of Cs-CA capsules leads to agglomeration (Figure S2) which could be problematic for industrial production. Taking these factors into consideration, Cs-CA capsules with high NaFeCN but low Cs content, i.e. Cs-CA 0.25-F_4, were selected as the most suitable for mixing in mortar. CA-F_2, which have a similar NaFeCN content as Cs-CA 0.25-F_4, were also selected for mixing in mortar to compare NaFeCN leaching from mortar when using Cs-coated versus uncoated capsules (Phase 3, Figure 6.1).

6.4.4. NaFeCN release (leaching) in mortar

6.4.4.1. Diffusion-driven leaching

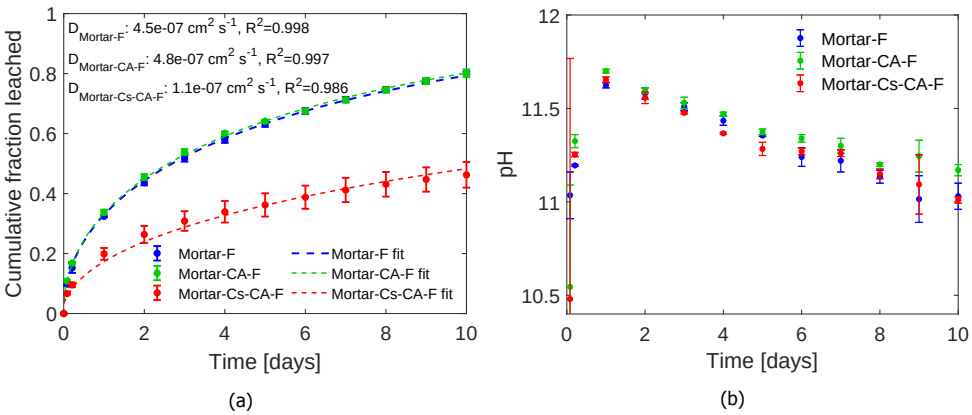

Figure 6.5: (a) A plot showing the cumulative fraction leached of sodium ferrocyanide (NaFeCN) measured from hardened mortar specimens at specific time steps during the diffusion driven-accelerated leaching test. The cumulative fraction leached is the ratio of the total NaFeCN leached with respect to the initial amount at the start of the test. The dotted lines represent the best fit curves obtained from the analytical solution (Appendix A) and their corresponding diffusion coefficients, D, with coefficient of determination (R2), calculated from the best fit are presented in the top left of the plot. (b) pH measurements of the leachate containing NaFeCN measured at ever time step before leachant renewal. The pH shows a decreasing trend over time in a similar range across all mortar specimens. The error bars indicate one standard deviation from the mean measurements.

The diffusion-driven leaching of NaFeCN from mortar specimens over time is presented in Figure 6.5a. The Mortar-CA-F specimens exhibit a comparable leaching rate to the Mortar-F specimens, showing that CA capsules do not reduce leaching from mortar. In contrast, Mortar-Cs-CA-F specimens demonstrate a slower rate

of NaFeCN leaching as compared to Mortar-F specimens. The measured mean effective diffusion coefficient of NaFeCN from Mortar-Cs-CA-F ($1.1x10^{-7}$ $cm^2\,s^{-1}$) is four times lower than that of Mortar-F ($4.5x10^{-7}$ $cm^2\,s^{-1}$). Moreover, at the end of 10-days, the amount of NaFeCN leached from the Mortar-Cs-CA-F specimens drops to just 46.2%, while for the Mortar-Cs-CA-F it is almost 80% (Figure 6.5a and S3). Furthermore, the NaFeCN release from Mortar-Cs-CA-F does not reach a plateau, indicating a sustained release even after 10 days of accelerated testing. The pH measurements on the leachate show an initial increase of pH until first 24 hours, followed by a linear decrease in the pH with every renewal step (Figure 6.5b). The drop in pH is consistent across all types of specimens.

6.4.4.2. Advection-driven leaching

Advection-driven leaching leads to the formation of an efflorescent crust on the drying surface (top surface) of the mortar specimens (Figure 6.6, Figure S4–S6). Mortar-F specimens show crust formation immediately after one absorption-drying cycle, and each cycle leads to a progressive accumulation of the crust. In contrast, the Mortar-CA-F and Mortar-Cs-CA-F specimens display negligible crust formation after the first two absorption-drying cycles. At the end of third cycle, Mortar-CA-F and Mortar-Cs-CA-F show signs of crust formation. In the case of Mortar-Cs-CA-F specimens, the crust is accumulated in localised pockets (Figure 6.6, right column, bottom row; marked with black arrows), while Mortar-F and Mortar-CA-F show homogeneous crust formation over their entire surface. Visually, after three cycles, the total amount of crust formation on the drying surface is highest for Mortar-F and least for Mortar-Cs-CA-F specimens. Examination of the cross-sections of the Mortar-F, Mortar-CA-F and Mortar Cs-CA-F specimens by digital microscopy shows accumulation of white precipitates just below the drying surface (≈0–5 mm depth; Figure 6.7 (a-c)). SEM-EDS maps made in these locations reveal the presence of Fe and Na indicating that these precipitates are likely to be NaFeCN crystals (Figure 6.7 (d–l)).

The initial distribution of NaFeCN across all mortar specimen types, namely Mortar-F, Mortar-CA-F and Mortar-Cs-CA-F fall within a similar concentration range (before cycling; Figure 6.8a). The distribution profile of NaFeCN over the specimen height as measured with ICP-OES on the milled slices of the specimens at the end of the test, underwent a drastic change from a homogenous initial distribution (before cycling; Figure 6.8a) to a skewed distribution near the top drying surface (Figure 6.8b). At the end of the test, a large amount of NaFeCN is transported and accumulated within the first 5 mm below the drying surface and a depletion in the lower depths (5–50 mm). In the first 5 mm, the mean concentration of NaFeCN for Mortar-Cs-CA-F (33.9 $mg\,g^{-1}$) is about half than that of Mortar-F (66.62 $mg\,g^{-1}$) and Mortar-CA-F (71.63 $mg\,g^{-1}$). In the depths, there is a negligible difference in the final concentration of NaFeCN measured across all specimen types (≈8-11 mg $mg\,g^{-1}$).

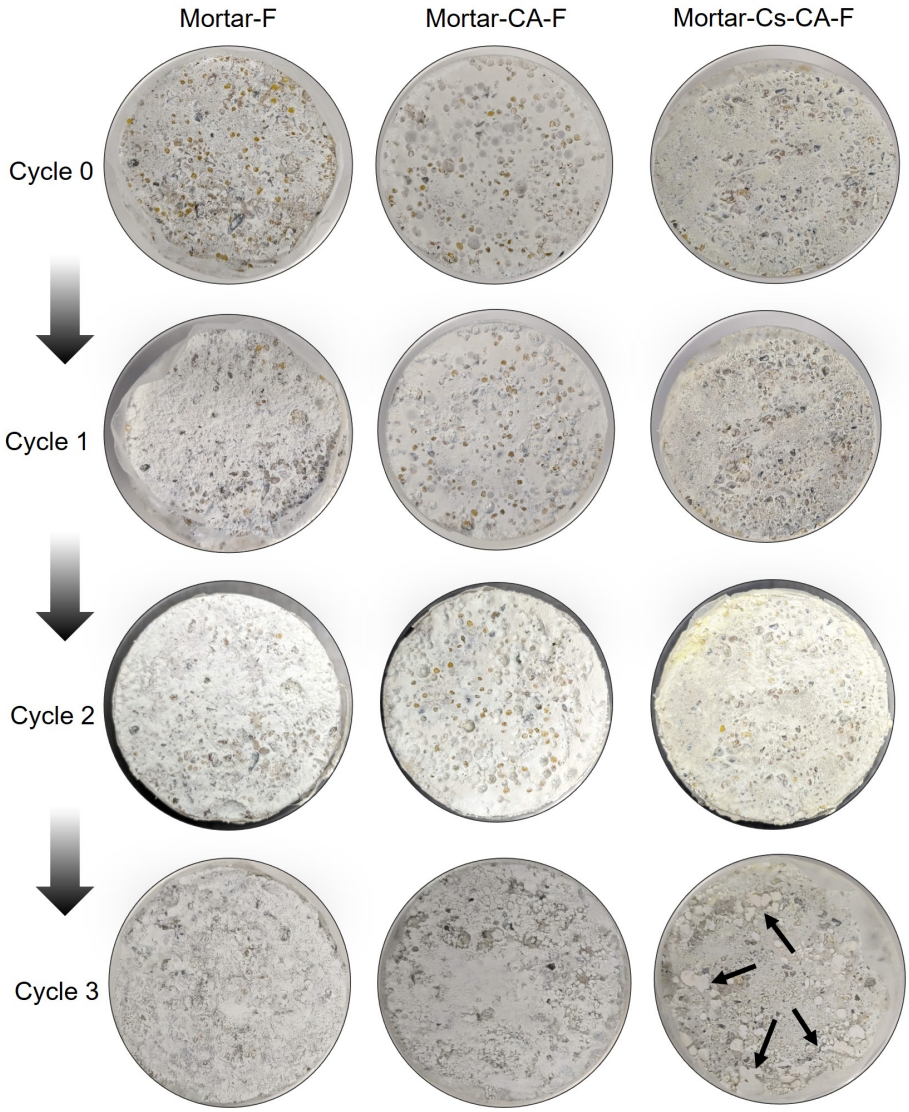

Figure 6.6: Images of Mortar-F, Mortar-CA-F and Mortar-Cs-CA-F showing the progression of a white precipitated crust (efflorescence) on the top surface of the specimens after each absorption-drying cycle. The crust formation increases with each cycle.

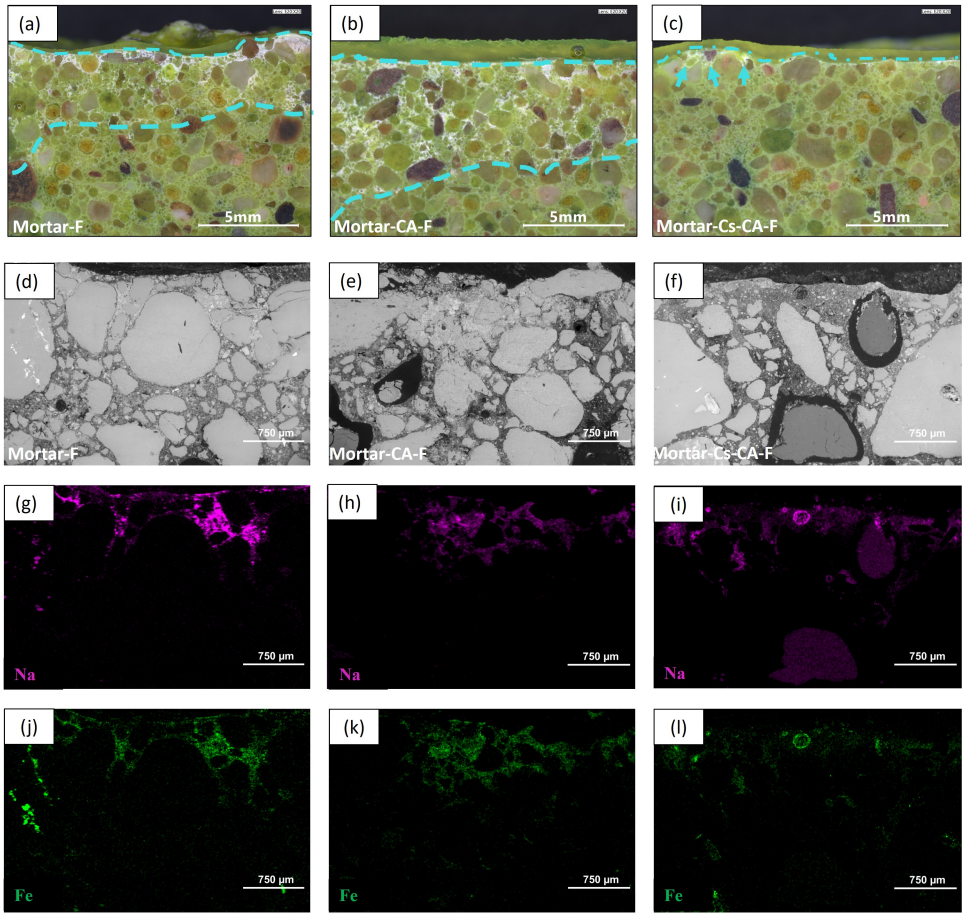

Figure 6.7: (a–c) Digital microscope images showing an epoxy-impregnated polished cross-section of: (a) Mortar-F specimen; (b) Mortar-CA-F specimen; and (c) Mortar-Cs-CA-F specimen, at the end of the adsorption and drying test. The field of view presents the top evaporative surface of these mortar specimens. The extent of precipitation is marked with cyan lines. (d–f) Back scattered electron (BSE) images and (g–l) energy dispersive spectroscopy (EDS) maps of polished cross section of Mortar-F (d,g,j), Mortar-CA-F (e,h,h) and Mortar-Cs-CA-F (f,i,l) specimens respectively are corresponding regions of interest from (a–c). The top of the image is the top edge of the cross-section. The grey scale BSE images show accumulation of light grey precipitates in between the sand aggregates. Na and Fe maps of these BSE images indicate the phase to be NaFeCN. The contrast of Na and Fe maps is exaggerated for better visibility and can be used only qualitatively.

6.5. Discussion

The results from diffusion-driven leaching test on mortar specimens show that Mortar-Cs-CA-F specimens [containing Cs-CA capsules containing NaFeCN], exhibit an effective diffusion coefficient of NaFeCN four times lower than Mortar-F [containing directly added NaFeCN] and Mortar-CA-F specimens [containing CA capsules containing NaFeCN], respectively.(Figure 6.5a). The improved performance

of Cs-CA capsules can be attributed to physico-chemical changes induced by the incorporation of Cs. The addition of Cs to CA is known to reduce permeability of CA [49, 50] and improve mechanical stability of CA network in alkaline conditions [38]. This is achieved by the ability of Cs to restrict the swelling of CA networks in high pH environments [37, 41], possibly due to strong attractive forces between Cs and alginates that prevents repulsion between alginate chains [64], thereby forming tight low porosity networks. A tighter, more stable Cs-CA structure makes it physically more difficult for a small molecule like NaFeCN to escape the capsule matrix [65]. Additionally, Chitosan is also chemically functional due to its positively charged $-NH_2$, which electrostatically interact with negatively charged $[Fe(CN)_6]^{4-}$ ions [66]. Evidence of this interaction can be seen as the green colour of the Cs-CA capsules (Figure 6.2c) related to a formation of an ammonium ferrocyanide bond [67]. The $-NH_2$ of Cs capsules acting as chelating sites for $[Fe(CN)_6]^{4-}$ ions have been shown to retain $[Fe(CN)_6]^{4-}$ ions inside the capsule network [42]. Furthermore, attractive forces due to oppositely charged electrostatic interactions between the matrix and the solute have been shown to hinder diffusion of charged solute species [68]. The electrostatic interaction between $[Fe(CN)_6]^{4-}$ ions to Cs is pH dependent and reversible. At high pH, the binding affinity of Cs for $[Fe(CN)_6]^{4-}$ is low due to Cs's neutral charge; however, this affinity increases as the pH decreases [69]. The mortar leaching experiment with mortar specimens containing Cs-CA capsules aligns with this pH-dependant behaviour. The mortar-Cs-CA-F specimens exhibiting lower cumulative leaching over time (Figre 6.5a) as the pH decreases (Figure 6.5b). Realistically, NHL mortars in the field are also expected to carbonate over time causing a slow drop in pH. This slow drop could contribute towards a slower release of $[FeCN_6]^{4-}$ for longer time periods. It must be noted, however, that very high pH (pH>12), the $-NH_2$ can become negatively charged by losing protons and releasing bound $[FeCN_6]^{4-}$ ions due to repulsion [70].

The results from the advection-driven leaching test show a notable delay in the transport of NaFeCN towards the drying surface of Mortar-Cs-CA-F and Mortar-CA-F as compared to Mortar-F specimens (Figure 6.6). The reason for this delay may be attributed to a limited moisture accessibility. In contrast to the diffusion-driven test setup, where the specimens remain completely saturated, in the advection-driven test, the specimens are only saturated for a short period during the capillary absorption phase and the moisture decreases during the drying phase. In Mortar-F specimens where NaFeCN is already present in the mortar matrix, NaFeCN readily dissolves and is transported to the drying surface even with a limited supply of moisture in the first cycle itself. Conversely, in Mortar-CA-F and Mortar-Cs-CA-F specimens, availability of moisture for a limited time may not be sufficient to swell the hydrogel networks and release enough $[FeCN_6]^{4-}$ ions from the capsules, thereby delaying the $[FeCN_6]^{4-}$ transport. At the end of the test, after three absorption-drying cycles, the effect of slow transport of NaFeCN towards the drying surface (top surface) in Mortar-Cs-CA-F specimens is more evident than Mortar-CA-F specimens (Figure 6.6, 6.7). The distribution profile of NaFeCN at the end of the test confirms this observation as it shows that NaFeCN concentration near the drying

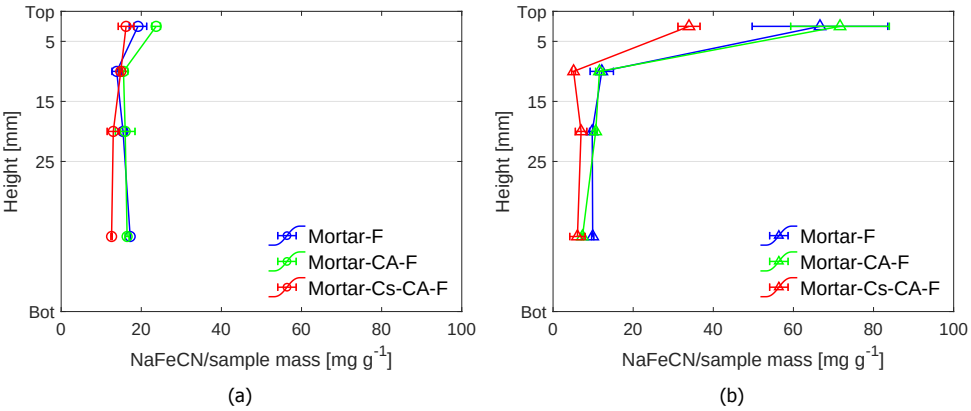

Figure 6.8: Plots showing the distribution profile of NaFeCN over specimen height. (a) before subjecting specimens to the absorption-drying cycles and (b) after subjecting them to three cycles (at the end of the test). Depth is measured as the distance from the top of the specimen surface, as indicated in the Y-axis, Top indicates the top of the specimens (0 mm) and Bot indicates the bottom (50 mm). Measurements were taken at four discrete points using ICP-OES on samples obtained after slicing the specimens using a dry saw between: 0–5 mm, 5–15 mm, 15–25 mm and 25–50 mm. The most significant change in the distribution profile occurs between measurements taken at start and the end of the test in the layer between 0–5 mm.

surface (0–5 mm; Figure 6.8b) in mortar-Cs-CA-F is almost two times lower than that of Mortar-CA-F and Mortar-F. The results show that the presence of Cs is necessary to delay the release of $[FeCN_6]^{4-}$ ions from CA capsules when subjected to successive absorption-drying cycles. However, considering the mass conservation between the NaFeCN distribution profile before cycling (Figure 6.8a) and after the test (Figure 6.8b), one would expect a higher concentration of NaFeCN in the depths of Mortar-Cs-CA-F specimen, but instead a similar depletion of the NaFeCN concentration is observed in Mortar-F and Mortar-CA-F specimens. While the reason for this discrepancy is unclear, one possible reason could be that a portion of NaFeCN remains bound to Cs due to electrostatic interaction and is not fully released, leading to lower measured NaFeCN values. A high degree of immobilisation of NaFeCN to Cs could be a challenge when applying this technology, as it could limit the availability of NaFeCN. However, it can be overcome in the future by making use of ionic cross-linking agents such as sodium tripolyphosphate that can compete with $[FeCN_6]^{4-}$ ions for $-NH_2$ sites on Cs [71].

The results from mortar leaching tests clearly show that Cs-CA capsules reduce the rate of NaFeCN leaching under both diffusion and advection driven transport as compared to directly adding NaFeCN to mortar. When moisture supply is limited, both Cs-CA and CA capsules tend to release NaFeCN slower in mortar matrix as compared to NaFeCN directly mixed in mortar due to the physical barrier presented by the capsule network. However, when a continuous moisture supply is available, CA capsules may swell releasing more NaFeCN and the effect of capsule's physical barrier is diminished. Conversely, Cs-CA capsules, with cationic Cs, swell less pro-

viding a physical barrier for the $[FeCN_6]^{4-}$ anions. Additionally, functional groups on Cs show pH-dependent electrostatic attraction to $[FeCN_6]^{4-}$ ions, hindering their diffusion from the capsule network causing slower release.

The capsules can be further optimised and fine-tuned for specific applications by controlling physical properties of capsules such as porosity and permeability of capsules by varying the molecular weight of chitosan and the M/G ratio of alginates [38]. Use of other cross-linking agents such as sodium tripolyphosphate can also reduce pore diameters and promote better cargo entrapment during production [71]. Modification of Cs such as N-trimethyl chitosan chloride can alter the pH range for protonation to release various charged cargos such as $[FeCN_6]^{4-}$ at specific pH's [41, 72].

The Cs-CA capsules developed in this study offer a range of new possibilities for the controlled release of charged molecules in construction materials. For instance they could be used for the controlled release of corrosion inhibitors [73] that need a slow/delayed release to be effective or as an alternative to existing capsule technologies for delivering chemical retarders such as sucrose in controlling cement hydration [74]. Additionally, the bio-based nature of the capsules makes them a sustainable alternative to synthetic polymers [29]. Furthermore, the immobilisation property of Cs-CA capsules could find application in preventing heavy metal leaching from municipal solid waste incineration fly ash which is a promising supplementary cementitious material, but poses an environmental hazard due to the leaching of toxic heavy metals [75, 76].

6.6. Conclusions and Outlook

This study introduces a proof-of-concept chitosan-calcium alginate capsule designed for the controlled release of a salt crystallisation inhibitor (NaFeCN) with the aim of prolonging the service life of salt-resistant mortars for renovation and construction applications. This study has shown that NaFeCN can be encapsulated in CA capsules and its release can be controlled by complexing CA with Cs. The results from this study demonstrate that incorporation of Cs is necessary for improving the performance of CA capsules in the alkaline conditions of mortar. The Cs coated CA capsules slow leaching of NaFeCN by reducing the effective diffusion coefficient of NaFeCN from the mortar capsule system (Mortar-Cs-CA-F) compared to adding NaFeCN directly to mortar (Mortar-F). Under advection driven transport that is more commonly observed in field conditions, Cs coated CA capsules reduce and/or delay the leaching of NaFeCN with successive absorption-drying cycles.

The controlled release of NaFeCN from the mortar-capsule system offers advantages, including the ability to provide a steady supply of NaFeCN over a prolonged period of time and lower wastage of NaFeCN due to leaching. Consequently, this technology has the potential to improve the durability of mortars against salt-related damage thereby reducing long-term repair costs. The next step of this research will focus on evaluating the performance of mortars containing Cs-CA-F capsules in resisting NaCl damage under accelerated salt weathering conditions. Additionally, the interactions between NaCl and the capsules will be explored, considering past

research indicating that high concentrations of NaCl (Na^+:Ca^{2+}>25:1) may compromise the integrity of CA networks [36, 77] and might affect the release behaviour of NaFeCN.

References

[1] A. Goudie and H. Viles, *Salt weathering hazards* (John Wiley & Sons Ltd, Chichester, 1997) p. 256.

[2] A. E. Charola, *Salts in the Deterioration of Porous Materials : An Overview,* Journal of the American institute for conservation **39**, 327 (2000).

[3] G. W. Scherer, *Crystallization in pores,* Cement and Concrete Research **29**, 1347 (1999).

[4] R. J. Flatt, *Salt damage in porous materials: how high supersaturations are generated,* Journal of Crystal Growth **242**, 435 (2002).

[5] M. Steiger, *Crystal growth in porous materials - I: The crystallization pressure of large crystals,* Journal of Crystal Growth **282**, 455 (2005).

[6] J. Desarnaud and N. Shahidzadeh-Bonn, *Salt crystal purification by deliquescence/crystallization cycling,* EPL (Europhysics Letters) **95**, 48002 (2011).

[7] B. Lubelli, R. P. van Hees, and C. J. Groot, *The effect of environmental conditions on sodium chloride damage: A step in the development of an effective weathering test,* Studies in Conservation **51**, 41 (2006).

[8] B. Lubelli, T. G. Nijland, R. P. Van Hees, and A. Hacquebord, *Effect of mixed in crystallization inhibitor on resistance of lime-cement mortar against NaCl crystallization,* Construction and Building Materials **24**, 2466 (2010).

[9] C. Rodriguez-Navarro and L. G. Benning, *Control of crystal nucleation and growth by additives,* Elements **9**, 203 (2013).

[10] A. A. Bode, S. Jiang, J. A. Meijer, W. J. Van Enckevort, and E. Vlieg, *Growth inhibition of sodium chloride crystals by anticaking agents: In situ observation of step pinning,* Crystal Growth and Design **12**, 5889 (2012).

[11] A. Glasner and M. Zidon, *The crystallization of NaCl in the presence of [Fe(CN)6]4- ions,* Journal of Crystal Growth **21**, 294 (1974).

[12] A. A. Bode, V. Vonk, F. J. Van Den Bruele, D. J. Kok, A. M. Kerkenaar, M. F. Mantilla, S. Jiang, J. A. Meijer, W. J. Van Enckevort, and E. Vlieg, *Anticaking activity of ferrocyanide on sodium chloride explained by charge mismatch,* Crystal Growth and Design **12**, 1919 (2012).

[13] C. Rodriguez-Navarro, L. Linares-Fernandez, E. Doehne, and E. Sebastian, *Effects of ferrocyanide ions on NaCl crystallization in porous stone,* Journal of Crystal Growth **243**, 503 (2002).

[14] S. Gupta, K. Terheiden, L. Pel, and A. Sawdy, *Influence of Ferrocyanide Inhibitors on the Transport and Crystallization Processes of Sodium Chloride in Porous Building Materials,* Crystal Growth & Design **12**, 3888 (2012).

[15] C. Selwitz and E. Doehne, *The evaluation of crystallization modifiers for controlling salt damage to limestone,* Journal of Cultural Heritage **3**, 205 (2002).

[16] B. Lubelli and R. P. van Hees, *Effectiveness of crystallization inhibitors in preventing salt damage in building materials,* Journal of Cultural Heritage **8**, 223 (2007).

[17] T. Rivas, E. Alvarez, M. J. Mosquera, L. Alejano, and J. Taboada, *Crystallization modifiers applied in granite desalination: The role of the stone pore structure,* Construction and Building Materials **24**, 766 (2010).

[18] S. J. Granneman, B. Lubelli, and R. P. van Hees, *Effect of mixed in crystallization modifiers on the resistance of lime mortar against NaCl and Na2SO4 crystallization,* Construction and Building Materials **194**, 62 (2019).

[19] J. Feijoo, D. Ergenç, R. Fort, and M. A. de Buergo, *Addition of ferrocyanide-based compounds to repairing joint lime mortars as a protective method for porous building materials against sodium chloride damage,* Materials and Structures **54**, 14 (2021).

[20] B. Lubelli, E. d. Bouvrie, T. G. Nijland, and A. Kamat, *Plasters with mixed-in crystallization inhibitors: Results of a 4-year monitoring of on-site application,* Journal of Cultural Heritage **59**, 10 (2023).

[21] T. Páez, A. Martínez-Cuezva, J. Palma, and E. Ventosa, *Revisiting the cycling stability of ferrocyanide in alkaline media for redox flow batteries,* Journal of Power Sources **471**, 228453 (2020).

[22] S. J. Granneman, B. Lubelli, and R. P. Van Hees, *Characterization of lime mortar additivated with crystallization modifiers,* International Journal of Architectural Heritage **12**, 849 (2018).

[23] A. Kamat, B. Lubelli, and E. Schlangen, *Effect of a mixed-in crystallization inhibitor on the properties of hydraulic mortars,* AIMS Materials Science **9**, 628 (2022).

[24] J. A. N. Friend, J. E. Townley, and R. H. Vallance, *CCCIII.—The solubility of sodium ferrocyanide in water between 0° and 104°,* J. Chem. Soc. , 2326 (1929).

[25] A. Kamat, B. Lubelli, and E. Schlangen, *Leaching behaviour of a crystallisation inhibitor in mortars,* Journal of Building Engineering **79**, 107933 (2023).

[26] J. Li and D. J. Mooney, *Designing hydrogels for controlled drug delivery,* Nature Reviews Materials **1**, 1 (2016).

[27] A. P. Esser-Kahn, S. A. Odom, N. R. Sottos, S. R. White, and J. S. Moore, *Triggered release from polymer capsules,* (2011).

[28] Y. Yang, Y. Ren, W. Song, B. Yu, and H. Liu, *Rational design in functional hydrogels towards biotherapeutics,* Materials and Design **223**, 111086 (2022).

[29] N. Behabtu and S. Kralj, *Enzymatic Polymerization Routes to Synthetic-Natural Materials: A Review,* ACS Sustainable Chemistry and Engineering **8**, 9947 (2020).

[30] H. H. Tønnesen and J. Karlsen, *Alginate in drug delivery systems,* Drug Development and Industrial Pharmacy **28**, 621 (2002).

[31] E.-S. Chan, B.-B. Lee, P. Ravindra, and D. Poncelet, *Prediction models for shape and size of ca-alginate macrobeads produced through extrusion–dripping method,* Journal of Colloid and Interface Science **338**, 63 (2009).

[32] A. Shilpa, S. S. Agrawal, and A. R. Ray, *Controlled Delivery of Drugs from Alginate Matrix,* Journal of Macromolecular Science, Part C: Polymer Reviews **43**, 187 (2003).

[33] R. Bernasconi, E. Mauri, A. Rossetti, S. Rimondo, R. Suriano, M. Levi, A. Sacchetti, S. Pané, L. Magagnin, and F. Rossi, *3D integration of pH-cleavable drug-hydrogel conjugates on magnetically driven smart microtransporters,* Materials and Design **197** (2021), 10.1016/j.matdes.2020.109212.

[34] D. Palin, V. Wiktor, and H. M. Jonkers, *A bacteria-based bead for possible self-healing marine concrete applications,* Smart Materials and Structures **25**, 084008 (2016).

[35] Y. Wang, G. Fang, W. Ding, N. Han, F. Xing, and B. Dong, *Self-immunity microcapsules for corrosion protection of steel bar in reinforced concrete,* Scientific Reports **5** (2015), 10.1038/srep18484.

[36] W. R. Gombotz and S. F. Wee, *Protein release from alginate matrices,* Advanced Drug Delivery Reviews **31**, 267 (1998).

[37] L. Agüero, D. Zaldivar-Silva, L. Peña, and M. Dias, *Alginate microparticles as oral colon drug delivery device: A review,* Carbohydrate Polymers **168**, 32 (2017).

[38] M. George and T. E. Abraham, *Polyionic hydrocolloids for the intestinal delivery of protein drugs: Alginate and chitosan - a review,* Journal of Controlled Release **114**, 1 (2006).

[39] I. Hamed, F. Özogul, and J. M. Regenstein, *Industrial applications of crustacean by-products (chitin, chitosan, and chitooligosaccharides): A review,* Trends in Food Science and Technology **48**, 40 (2016).

[40] M. Rinaudc, G. Pavlov, and J. Desbrières, *Solubilization of Chitosan in Strong Acid Medium,* International Journal of Polymer Analysis and Characterization **5**, 267 (1999).

[41] T. W. Wong, *Alginate graft copolymers and alginate-co-excipient physical mixture in oral drug delivery,* Journal of Pharmacy and Pharmacology **63**, 1497 (2011).

[42] L. Zemskova, A. Egorin, E. Tokar, and V. Ivanov, *Chitosan-based biosorbents: immobilization of metal hexacyanoferrates and application for removal of cesium radionuclide from aqueous solutions,* Journal of Sol-Gel Science and Technology **92**, 459 (2019).

[43] M. Duran, A. Serrano, A. Nikulin, J. L. Dauvergne, L. Derzsi, and E. Palomo del Barrio, *Microcapsule production by droplet microfluidics: A review from the material science approach,* Materials and Design **223**, 111230 (2022).

[44] G. Pasparakis and N. Bouropoulos, *Swelling studies and in vitro release of verapamil from calcium alginate and calcium alginate-chitosan beads,* International Journal of Pharmaceutics **323**, 34 (2006).

[45] A. K. Anal and W. F. Stevens, *Chitosan-alginate multilayer beads for controlled release of ampicillin,* International Journal of Pharmaceutics **290**, 45 (2005).

[46] I. Hassan and A. Gani, *Alginate-Based pH-Sensitive Hydrogels Encoated with Chitosan as a Bioactive Cargo Carrier with Caffeic Acid as a Model Biomolecule,* ACS Food Science and Technology **2**, 667 (2022).

[47] Y. Murata, T. Maeda, E. Miyamoto, and S. Kawashima, *Preparation of chitosan-reinforced alginate gel beads - effects of chitosan on gel matrix erosion,* International Journal of Pharmaceutics **96**, 139 (1993).

[48] C. Zhang, X. Wang, M. Xiao, J. Ma, Y. Qu, L. Zou, and J. Zhang, *Nano-in-micro alginate/chitosan hydrogel via electrospray technology for orally curcumin delivery to effectively alleviate ulcerative colitis,* Materials and Design **221**, 110894 (2022).

[49] M. A. Santos and M. T. Machado, *Coated alginate–chitosan particles to improve the stability of probiotic yeast,* International Journal of Food Science and Technology **56**, 2122 (2021).

[50] A. D. Sezer and J. . Akbuga, *Release characteristics of chitosan treated alginate beads: I. Sustained release of a macromolecular drug from chitosan treated alginate beads,* Journal of Microencapsulation **16**, 195 (1999).

[51] A. J. Ribeiro, C. Silva, D. Ferreira, and F. Veiga, *Chitosan-reinforced alginate microspheres obtained through the emulsification/internal gelation technique,* European Journal of Pharmaceutical Sciences **25**, 31 (2005).

[52] Y. Zhu, Y. Ma, Q. Yu, J. Wei, and J. Hu, *Preparation of pH-sensitive core-shell organic corrosion inhibitor and its release behavior in simulated concrete pore solutions,* Materials and Design **119**, 254 (2017).

[53] A. Kamat, D. Palin, B. Lubelli, and E. Schlangen, *Tunable chitosan-alginate capsules for a controlled release of crystallisation inhibitors in mortars,* MATEC Web of Conferences **378**, 02011 (2023).

[54] *NEN-EN 196-1: Methods of testing cement - Part 1: Determination of strength*, Tech. Rep. (European committee for standardisation (CEN), 2015).

[55] C. Schröfl, V. Mechtcherine, and M. Gorges, *Relation between the molecular structure and the efficiency of superabsorbent polymers (SAP) as concrete admixture to mitigate autogenous shrinkage,* Cement and Concrete Research **42**, 865 (2012).

[56] *ASTM C1308-21: Standard test method for accelerated leach test for measuring contaminant releases from solidified waste*, Tech. Rep. (ASTM International, 2021).

[57] C. J. Nestor, *Diffusion from solid cylinders*, Tech. Rep. (Oak Ridge National Laboratory (ORNL), Oak Ridge, TN (United States), 1980).

[58] C. Pescatore, *Improved expressions for modeling diffusive, fractional cumulative leaching from finite-size waste forms,* Waste Management **10**, 155 (1990).

[59] G. Plusquellec, M. Geiker, J. Lindgård, J. Duchesne, B. Fournier, and K. De Weerdt, *Determination of the pH and the free alkali metal content in the pore solution of concrete: Review and experimental comparison,* Cement and Concrete Research **96**, 13 (2017).

[60] *ASTM D6323-19: Standard Guide for Laboratory Subsampling of Media Related to Waste Management Activities*, Tech. Rep. (ASTM international, 2019).

[61] C. Nunes, A. Maria Aguilar Sanchez, S. Godts, D. Gulotta, I. Ioannou, B. Lubelli, B. Menendez, N. Shahidzadeh, Z. Slížková, and M. Theodoridou, *Experimental research on salt contamination procedures and methods for assessment of the salt distribution,* Construction and Building Materials **298**, 123862 (2021).

[62] A. Mun, H. Simaan Yameen, G. Edelbaum, and D. Seliktar, *Alginate hydrogel beads embedded with drug-bearing polycaprolactone microspheres for sustained release of paclobutrazol,* Scientific Reports **11**, 1 (2021).

[63] J. Y. Wang, H. Soens, W. Verstraete, and N. De Belie, *Self-healing concrete by use of microencapsulated bacterial spores,* Cement and Concrete Research **56**, 139 (2014).

[64] M. M. Daly and D. Knorr, *Chitosan□Alginate Complex Coacervate Capsules: Effects of Calcium Chloride, Plasticizers, and Polyelectrolytes on Mechanical Stability,* Biotechnology Progress **4**, 76 (1988).

[65] J. A. A. D. Sezer, *Release characteristics of chitosan treated alginate beads: II. Sustained release of a low molecular drug from chitosan treated alginate beads,* Journal of Microencapsulation **16**, 687 (1999).

[66] C. A. Rodrigues, E. Stadler, M. C. M. Laranjeira, and V. Drago, *The preparation and characterization of the hexacyanides immobilized in chitosan,* Journal of the Brazilian Chemical Society **8**, 7 (1997).

[67] J. Luo, B. Hu, C. Debruler, Y. Bi, Y. Zhao, B. Yuan, M. Hu, W. Wu, and T. L. Liu, *Unprecedented Capacity and Stability of Ammonium Ferrocyanide Catholyte in pH Neutral Aqueous Redox Flow Batteries,* Joule **3**, 149 (2019).

[68] O. Lieleg, R. M. Baumgärtel, and A. R. Bausch, *Selective filtering of particles by the extracellular matrix: An electrostatic bandpass,* Biophysical Journal **97**, 1569 (2009).

[69] Y. Zhang, Y. Thomas, E. Kim, and G. F. Payne, *PH- and voltage-responsive chitosan hydrogel through covalent cross-linking with catechol,* Journal of Physical Chemistry B **116**, 1579 (2012).

[70] N. L. Avery and W. Fries, *Selective Removal of Cyanide from Industrial Waste Effluents with Ion-Exchange Resins,* Product R&D **14**, 102 (1975).

[71] M. L. Pita-López, G. Fletes-Vargas, H. Espinosa-Andrews, and R. Rodríguez-Rodríguez, *Physically cross-linked chitosan-based hydrogels for tissue engineering applications: A state-of-the-art review,* European Polymer Journal **145** (2021), 10.1016/j.eurpolymj.2020.110176.

[72] Z. Yaneva, D. Ivanova, N. Nikolova, and M. Tzanova, *The 21st century revival of chitosan in service to bio-organic chemistry,* Biotechnology & Biotechnological Equipment **34**, 221 (2020).

[73] T. A. Söylev and M. G. Richardson, *Corrosion inhibitors for steel in concrete: State-of-the-art report,* Construction and Building Materials **22**, 609 (2008).

[74] L. Dong, Y. Zhang, Y. Guo, X. Shu, X. Shen, Q. Ran, and P. Feng, *Effects of controlled release silica nanocapsules containing sucrose on the heat release of cement hydration,* Colloids and Surfaces A: Physicochemical and Engineering Aspects **670**, 131593 (2023).

[75] H. Luo, Y. Cheng, D. He, and E. H. Yang, *Review of leaching behavior of municipal solid waste incineration (MSWI) ash,* Science of the Total Environment **668**, 90 (2019).

[76] B. Chen, P. Perumal, M. Illikainen, and G. Ye, *A review on the utilization of municipal solid waste incineration (MSWI) bottom ash as a mineral resource for construction materials,* Journal of Building Engineering **71**, 106386 (2023).

[77] R. Vreeker, L. Li, Y. Fang, I. Appelqvist, and E. Mendes, *Drying and rehydration of calcium alginate gels,* Food Biophysics **3**, 361 (2008).

7

Salt weathering resistance of mortars with an encapsulated crystallisation inhibitor

In the previous chapter, the developed mortar prototype i.e. hydraulic mortar with encapsulated inhibitor (CsCA capsules) demonstrated a reduction in the rate of leaching of the inhibitor, thanks to the CsCA capsules. In this chapter, this mortar prototype is tested to validate its performance on three aspects, (a) Fresh and hardened properties (b) resistance to salt-weathering (c) leaching of the inhibitor. Next to the natural hydraulic lime mortar prototype, a commercial two-layer cement-based plaster system, to which capsules have been added, is also tested. For comparative purposes, mortars with mixed-in inhibitor as well as reference mortars (without inhibitor and capsules) are also tested. Various complementary techniques are used to characterise the properties of different types of mortar and an accelerated salt weathering test (based on RILEM 271-ASC recommendations) is carried out to assess the salt weathering resistance of the mortars.

This chapter is based on the article published in Cement and Concrete Composites, **152**, 105682 (2024).

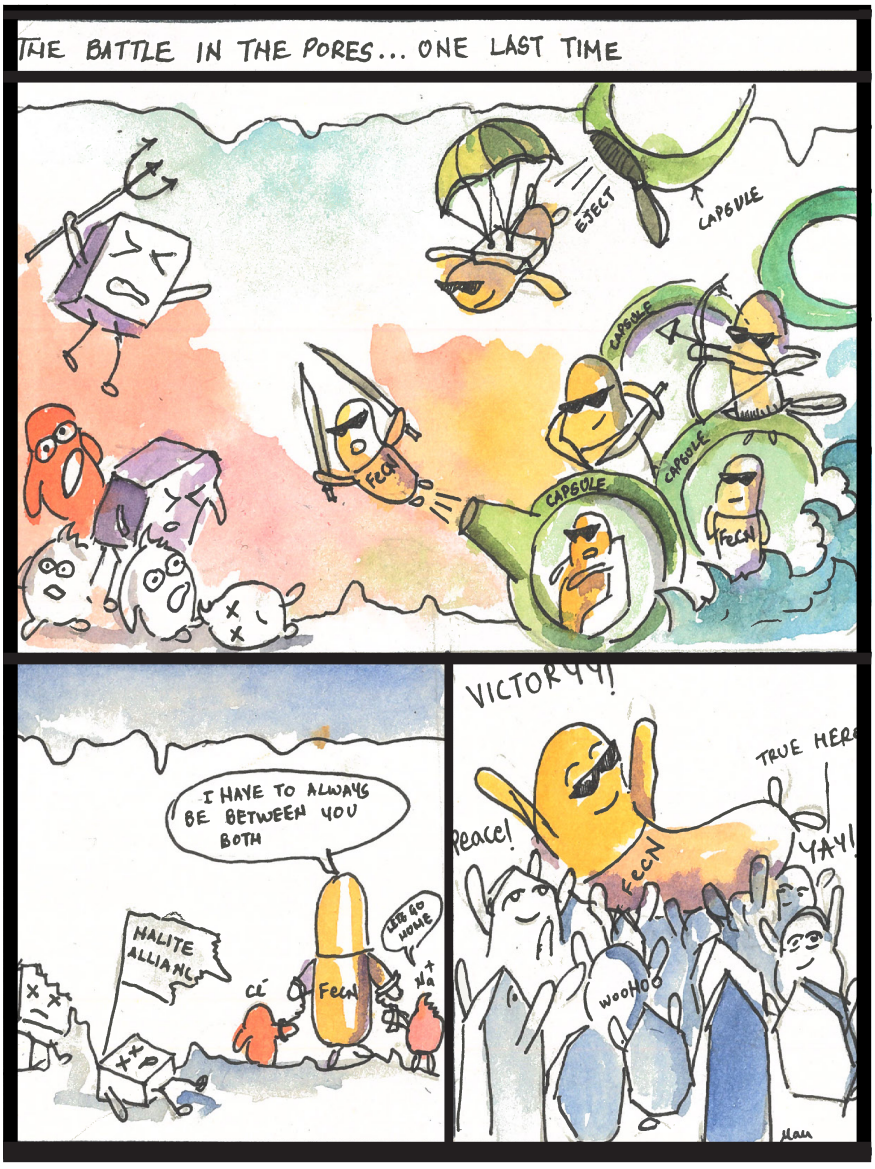
THE BATTLE IN THE PORES... ONE LAST TIME
EJECT
CAPSULE
CAPSULE
CAPSULE
CAPSULE
FECN
FECN
I HAVE TO ALWAYS BE BETWEEN YOU BOTH
HALITE ALLIANCE
LET'S GO HOME
Cl
FECN
VICTORY!!
TRUE HERO
Peace!
FECN
YAY!
WOOHOO

7.1. Introduction

Salt weathering is responsible for severe damage in porous building materials [1]. Commonly occurring soluble salts, such as sodium chloride (NaCl), permeate in building materials from various sources such as ground water, salt spray and de-icing salts [2] and, due to evaporation or temperature changes, crystallise within the pores. Crystallisation of salts under supersaturated conditions can exert crystallisation pressure on the pore walls [3] causing damage when the pressure exceeds materials' mechanical strength [4]. In particular for NaCl, repeated exposure to crystallisation-deliquescence cycles has shown to increase the crystal volume [5] and consequently accelerate the damage propagation [6]. Plasters and renders, also because of their location at the surface of the buildings, are exposed to repeated crystallisation-deliquescence cycles, due to evaporation and exposure to changing climatic conditions. Therefore, plasters and renders need frequent replacements, and entail high maintenance costs. Improving the durability of plasters and renders with respect to salt damage can reduce their replacement frequency and minimise costs. Incorporation of crystallisation inhibitors in mortars has shown encouraging results in improving the durability of plasters/renders by preventing and/or delaying salt damage [7].

Crystallisation inhibitors are chemical additives that inhibit crystal nucleation and growth by adsorbing preferentially on specific crystal faces [8]. Sodium ferrocyanide ($Na_4Fe(CN)_6$, hereafter referred as NaFeCN) is one of the most effective crystallisation inhibitors of alkali halides, and in particular of NaCl [9]. Hexacyanoferrate ions $[Fe(CN_6)]^{4-}$ from NaFeCN preferentially sorb on the $\{1\,0\,0\}$ faces of the NaCl crystals, and block further crystal growth due to a charge mismatch [10]. As a consequence, the rate of crystal growth is suppressed along $\langle 1\,0\,0\rangle$ and the crystal morphology changes from a cubic crystal to a dendritic (skeletal) habit [11, 12]. When introduced to NaCl contaminated porous building materials, NaFeCN has shown to favour crystallisation of harmless efflorescence (surface crystallisation) over harmful subflorescence (confined in-pore crystallisation) and in doing so, has greatly reduced the associated salt damage [12–15]. The reduced damage has been attributed to a delay in NaCl nucleation and crystal growth due to NaFeCN, providing longer time for salt ions to be transported to the evaporation surface [12]. Moreover, the formation of dendritic crystals with a higher surface area has shown to increase the evaporation rate and promote advection of salt ions towards the surface [16]. Recently, a new hypothesis to explain reduced salt damage has been proposed based on the smaller NaCl crystal size observed in presence of NaFeCN. Smaller NaCl crystals, by occupying smaller volume can prevent pore clogging and decrease crystallisation pressure [7]. Incorporating NaFeCN during the production of hydrated lime mortars has been highly effective in reducing salt damage in the laboratory [7, 17, 18]as well as in the field [19]. Early studies show that addition of inhibitor does not affect the properties of hydraulic mortars [20], making the inhibitor also suitable for hydraulic mortar applications. However, the effect of the combination of inhibitor in hydraulic mortars with respect to salt damage is not yet investigated.

Despite the positive results reported on lime-based mortars with mixed-in in-

hibitors, a high depletion of NaFeCN from mortar specimens after successive wetting-drying cycles was observed and attributed to the leaching of NaFeCN [7]. A study specifically focused on the leaching behaviour of NaFeCN from mortar specimens reported severe leaching, and concluded that directly adding NaFeCN to mortar may not prevent salt damage over a long time period [21]. In a recent pilot study, we demonstrated that introducing NaFeCN in chitosan-calcium alginate (CsCA) capsules lead to a controlled release and reduced leaching of the inhibitor from mortar specimens [22]. To develop this technology further, some issues pertaining to the introduction of encapsulated NaFeCN in mortar need to be clarified. A first issue concerns the impact of CsCA capsules on the mortar properties, such as mechanical strength and workability, as past research has shown negative impact of capsules and capsule-like materials on the properties of concrete [23, 24]. Another issue concerns if mortars with encapsulated inhibitor offer similar resistance against salt damage as mortars with mixed-in inhibitor., while slowing down the inhibitor leaching.

To resolve the above issues, two different types of hydraulic mortars- Natural hydraulic lime and commercial two-layer cement-based plasters containing encapsulated inhibitor as well as mixed-in inhibitor are tested. The research is divided in two parts. In the first part, the effect of capsules on the properties of mortars is investigated (Section 7.2.4). In the second part, the salt weathering resistance of mortars and the leaching of inhibitor is assessed (Section 7.2.5).

7.2. Materials and methods

7.2.1. Materials

For the preparation of capsules (Section 7.2.2), lab grade sodium alginate (mannuronic/guluronic (M/G) ratio of 1.56), chitosan (Molecular weight: 190-310 kDa), calcium chloride ($CaCl_2 \cdot 2\,H_2O$) were obtained from Sigma Aldrich. Acetic acid (CH_3COOH) was obtained from J.T.baker and sodium ferrocyanide decahydrate ($Na_4Fe(CN)_6 \cdot 10\,H_2O$) used as the crystallisation inhibitor was obtained from Acros organics.

In the preparation of mortar specimens (Section 7.2.3), Natural hydraulic lime (binder, St. Astier) with a strength class of 3.5 MPa, SP-Levell® (ready-mix mortar, Remmers), SP-Top SR® (ready-mix mortar, Remmers) and standard river sand (0.08-2 mm) as per [25] were used. Maastricht limestone (Netherlands) with a porosity of 50% v/v and a mean pore size of 30 µm [26] was used as a substrate.

7.2.2. Preparation of chitosan-calcium alginate capsules containing NaFeCN

The capsules containing sodium ferrocyanide (NaFeCN) were prepared and characterised according to a procedure developed in a past research [22]. In the first step, calcium alginate containing NaFeCN capsules were prepared using ionic gelation [27], where a mixture of sodium alginate (2% w/v) and NaFeCN (4% w/v) was extruded drop by drop in a cross-linking bath containing a mixture of calcium chloride (3% w/v) and NaFeCN (4% w/v) using a peristaltic pump (Masterflex con-

sole drive, Cole Parmer instruments). In the second step, the obtained capsules were added to a bath of 0.5% w/v chitosan (Cs) in 0.1 M Acetic acid to form a complex of chitosan-calcium alginate capsules containing NaFeCN (CsCA-F). The CsCA-F capsules were dried in an oven at 40±2°C for 48 hours and stored in air-tight containers.

When dry, the CsCA-F capsules had an ellipsoidal form with a maximum diameter of 1063 ± 124 µm, a minimum diameter of 730 ± 85.5 µm. The average encapsulated amount of NaFeCN was 264 mg g^{-1} of dry capsule mass [22].

7.2.3. Preparation of test specimens

7.2.3.1. NHL-based mortar specimens

Different types of natural hydraulic lime (NHL) mortar specimens were prepared (see Table 1) (i) Reference mortar specimens without NaFeCN and capsules **(NHL-R)** were prepared by mixing NHL with river sand in a 1:3 ratio by volume and a water to binder ratio (w/b) of 1.17 to achieve a 165mm flow as per NEN-EN-459-2 [28]. (ii) mortar specimens with mixed-in NaFeCN **(NHL-F)** prepared in the same way as NHL-R, but with addition of NaFeCN at a concentration of 1% weight of the binder. NaFeCN was first dissolved in water to be used for mortar preparation, and then added to NHL and sand. (iii) mortar specimens containing NaFeCN encapsulated in CsCA-F capsules **(NHL-CsCA-F)** were prepared in the same way as NHL-R, but with addition of CsCA-F capsules. The amount of capsule was defined such that the total NaFeCN content was 1% weight of the binder; this resulted in an amount of capsules equal to 3.78% of the binder weight.

The type of specimens/ geometry differed based on characterisation and weathering tests (see Table 7.1). Mortar specimens to be used for mechanical testing were cast as prims (160x40x40) mm as per NEN-EN-1015-11 [29].

Stone-mortar combination specimens to be used for the salt weathering test were casted in the following way. Freshly mixed mortar was cast on pre-wetted, cylindrical (Ø=50 mm, H=30 mm) Maastricht limestone substrate in polyvinyl chloride (PVC) moulds. The mortar thickness was 20 mm, and the total size of the stone-mortar specimen was Ø=50 mm and H=50 mm. The mortar was compacted by hand, using a trowel.

Mortar specimens to be used in the physical characterisation tests were prepared on Maastricht limestone substrate, in the same way as those for the salt weathering test, and then detached after 4 days. A paper towel was placed in between the substrate and the mortar during casting, to allow for easy detachment of the mortar to obtain mortar discs (Ø=50 mm, H=20 mm).

All specimens were covered with a plastic film and cured for one week at 20±2ºC, 95±5 % relative humidity (RH); subsequently, they were demoulded and cured at lab conditions (20 ± 3ºC, 55 ± 5 ºC) for at least three weeks as per NEN-EN-1015-11 before testing [29].

7.2.3.2. Two-layer plaster (cement-based)

A two-layer cement-based plaster system, commercially available and commonly used in renovation for application on salt loaded substrate was selected. The sys-

Table 7.1: : Description of test specimens and explanation of the labels

Binder	Specimen label	Description	Geometry	Size
NHL	NHL-R	NHL reference specimens i.e. without NaFeCN and capsules	Prisms Discs Stone-mortar cylinder	160x40x40 mm Ø=50 mm, H=20 mm Ø=50 mm, H=50 mm (including stone)
	NHL-F	NHL specimens with mixed-in NaFeCN	Prisms Discs Stone-mortar cylinder	160x40x40 mm Ø=50 mm, H=20 mm Ø=50 mm, H=50 mm (including stone)
	NHL-CsCA-F	NHL specimens containing CsCA-F capsules	Prisms Discs Stone-mortar cylinder	160x40x40 mm Ø=50 mm, H=20 mm Ø=50 mm, H=50 mm (including substrate)
2-layer plaster: SP-Levell®(bottom layer) + SP-Top® (top layer)	2L-R	2-layer plaster reference specimens	stone-mortar cylinder	Ø=50 mm, H=50 mm (including substrate)
	2L-CsCA-F	2-layer plaster with CsCA-F capsules in the bottom layer	stone-mortar cylinder	Ø=50 mm, H=50 mm (including stone)
SP-Levell®	SPL	SP-Levell reference specimens	Prisms Discs	160x40x40 mm Ø=50 mm, H=20 mm
	SPL-CsCA-F	SP-Levell specimens with CsCA-F capsules	Prisms Discs	160x40x40 mm Ø=50 mm, H=20 mm
SP-Top®	SPT	SP-Top reference specimens	Prisms Discs	160x40x40 mm Ø=50 mm, H=20 mm

tem is composed of a bottom (base) layer mortar (SP-Levell, Remmers) and a top layer mortar (SP-top SR, Remmers); the top layer is hydrophobic and is meant to stop salt transport to the surface, leading to accumulation of the salts in the inner layer. Characterisation tests were performed on individual cement mortars while the salt weathering test was performed on the composite two-layer plaster system. Different types of specimens were prepared for this study and an overview is presented in Table 7.1. For different characterisation tests (Table 7.2), Cement-based mortar components of the two-layer plaster system were cast separately and labelled as (i) SP-Top **(SPT)** (ii) SP-Levell **(SPL)** and (iii) SP-Levell containing CsCA-F capsules **(SPL-CsCA-F)**. The amount of mixing water was based on the manufacturer's specifications i.e. 325 mL Kg^{-1} for SP-Levell and 250 mL Kg^{-1} for SP-Top. The amount of capsules in SPL-CsCA-F specimens was 0.45% of the dry weight of SP-Levell. Specimens to be used for mechanical testing were cast as prims (160x40x40) mm as per NEN-EN-1015-11 [29]. Specimens used for physical characterisation test (Table 7.2) were cast as discs (Ø=50 mm, H=20 mm) in the same way as NHL specimens (Section 7.2.3.1).

For salt weathering test, stone-mortar specimens were prepared in the same

was as NHL-based mortar specimens (Section 7.2.3.1) where Maastricht limestone was used as the substrate and the mortar made of the two-layer plaster system was cast on top of the substrate. Different types of specimens were prepared as follows (i) Reference two layer plaster without NaFeCN and capsules **(2L-R)** where the bottom layer of the plaster (10 mm thick) was prepared by mixing SP-Levell with water. The top layer of the plaster (10 mm thick) was prepared by mixing SP-Top SR with water and cast on top of the bottom layer after 24 hours. (ii)Two-layer plaster containing capsules containing NaFeCN **(2L-CsCA-F)** where the bottom layer of the plaster (10 mm thick) was prepared by mixing SP-Levell, and CsCA-F capsules equal to 0.45% by the weight of SP-Levell (binder + sand). The top layer of the plaster (10 mm thick) was prepared by mixing SP-Top SR and water and cast on top of the bottom layer after 24 hours. The capsules were not added to the top layer.

All the specimens were demoulded after 4 days and cured at 20±2ºC, 95±5% RH for 28 days before testing.

7.2.4. Characterisation of mortar specimens

The effect of capsules on the fresh and hardened properties of mortar (Table 7.1) was assessed using various experimental techniques (Table 7.2). The workability of freshly mixed mortar was assessed as per NEN-EN-1015-3 [30] using the flow table test. The compressive strength was measured on the mortar prisms after 28 days of curing, per NEN-EN-1015-11 [29] with a loading rate of 0.1 kN s^{-1}

Table 7.2: An overview of the characterisation tests performed on different mortar specimens.

Material property	Method	Standard	Type of mortar	Specimen type	Replicates
Workability	Flow table test	NEN-EN-1015-3		Fresh state	2
Compressive strength	Mechanical testing	NEN-EN-1015-11		Prism	3
Pore size distribution	MIP	-	NHL-R, NHL-F, NHL-CsCA-F, SPL, SPL-CsCA, SPT	Disc (1 cm^3 sample)	2
Open porosity	MIP	-		Disc (1 cm^3 sample)	2
Bulk density	MIP	-		Disc (1 cm^3 sample)	2
Water absorption coefficient	Capillary absorption	NEN-EN-1925		Disc	3
Drying rate	Gravimetry	-		Disc	3
Microscopic examination	PFM SEM	- -	NHL-CsCA-F NHL-CsCA-F	thin section polished section	1 1

The open porosity, bulk density and pore size distribution of all mortars were measured using mercury intrusion porosimetry (MIP, Micromeritics Autopore IV)

on samples of approximately 4 g, collected from the mortar discs. Samples were freeze-dried, before starting the measurements and subjected to a maximum intrusion pressure of 210 MPa.

The water absorption coefficient (WAC) was measured on mortar discs (Table 7.1) as per NEN-EN-1925 [31] through capillary absorption. Mortar discs were dried at 40ºC to a constant weight and their sides sealed with parafilm® (Bemis Company Inc.). The specimens were placed with the bottom surface in water and weighed at prescribed time intervals [31]. The water WAC was calculated as per Equation 7.1.

$$WAC = \frac{m_i - m_0}{A \cdot \sqrt{t_i}} \tag{7.1}$$

Where, m_i [g] is the mass of specimen at time interval t_i[s], where the transition takes place between the first absorption stage and the second absorption stage. m_0 [g] is the dry mass of the specimen and A [m^2] is the surface area of the specimen subjected to capillary absorption.

Following capillary absorption, the specimens were subjected to drying at lab conditions (i.e. 23.1 ± 1.1ºC, RH 51.5 ± 5.1%) and the weight of the specimens was recorded at regular intervals to obtain a drying curve.

In the case of NHL-CsCA-F mortar, one thin-section was prepared to examine the capsule distribution and the mortar porosity. To prepare the thin section, the specimen was first impregnated with an epoxy resin containing a UV-fluorescent dye. The thin-section was prepared following a protocol by [32]. The images were acquired under plane polarised light and UV-light using Keyence VHX-7000 digital microscope.

One polished cross section was prepared to examine the capsule-mortar interface. The polished section was prepared on an epoxy impregnated specimen that was grinded and polished on a lapping table [26]. The images were obtained under back scattered electron (BSE) setting using a scanning electron microscope (FEI Quanta 650 FEG) at an accelerating voltage of 15kV.

7.2.5. Procedure for accelerated salt weathering test

The accelerated salt weathering test is based on the RILEM 271-ASC recommendations [33, 34], and further adapted to allow for testing of stone-mortar combination. As for the RILEM 271-ASC, the procedure used in this research consists of two stages (i) contamination and accumulation with salt and (ii) damage propagation.

7.2.5.1. Contamination and accumulation

The specimens (stone-mortar cylinders, see Table 7.1) were dried in an oven at 40°C to a constant weight and the sides were sealed with parafilm and a textile tape. The specimens were then contaminated from the bottom surface via capillary absorption with 10% w/w NaCl solution; the amount of solution was equivalent to the capillary moisture content of the Maastricht Limestone (31.1% of the dry weight of the stone). After complete absorption of the solution, the bottom of the specimens were sealed with parafilm and the textile tape, and the specimens were placed in a climate chamber at 40±2°C and 15±5% RH until 80% of the water had

evaporated marking the end of the accumulation stage. The specimens were stored in a box inside a climate chamber with a lid made of Japanese paper in order to limit the effect of convection from the ventilator.

7.2.5.2. Damage propagation

After the accumulation stage, specimens were subjected to four 3-week cycles of damage propagation. Each 3-week cycle consisted of temperature and RH cycles, as schematised in Figure 7.1. In between each 3 week-cycle the specimens were rewetted with an amount of demineralised water equivalent to 30% by weight of the solution used for initial contamination. The test was carried out in a programmable climatic cabinet (ClimeEvent, Weiss-Technik). Three replicates were used for each type of specimen.

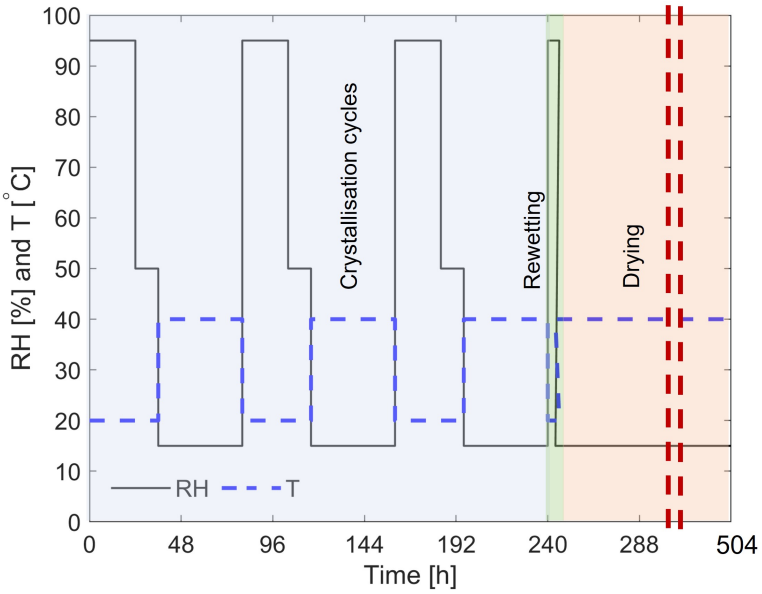

Figure 7.1: Relative humidity (RH) and temperature (T) defined for every three-week propagation cycle as per RILEM 271-ASC [34]. First 240h (light blue area) consists of RH and T cycling, followed by 6h rewetting (light green area) and 258h of drying (light orange area). In total, specimens were subjected to four such cycles.

7.2.5.3. Assessment of damage

Changes to the evaporation surface (top specimen of the mortar) were recorded with a digital camera at the start of the accelerated test, at the end of the accumulation stage and at the end of each 3-week cycle of the propagation stage.

At the end of the test, the material loss, efflorescence and the amount of leached inhibitor from each specimen was measured in the following way. The top surface was brushed with a soft-bristled toothbrush and the collected debris (salt efflorescence plus material loss) was dried to a constant weight at 40°C and its mass was

recorded ($m1$). Demineralised water with a mass at least 10 times of the debris weight or 5g which ever was higher was added to the dry debris and the mixture was stirred to dissolve any salts present in the debris. The volume of the added water was recorded as V [L]. After 24 hours, the mixture was passed through a medium-speed filtration paper to separate material loss (filter paper) and soluble salts (filtrate). The mass of the material loss after separating the salt efflorescence on the filter paper was recorded ($m2$) and the amount of salt efflorescence was calculated as $m1 - m2$. The concentration of Fe(II/III) ions (C_{Fe}) [mgL^{-1}] in the solution was measured by analysing the filtrate using Inductively coupled plasma-optical emission spectroscopy (ICP-OES, Perkin Elmer Optima 5300DV). The amount of NaFeCN in the debris was calculated from the ICP-OES measurements using Equation 7.2.

$$Leached_{NaFeCN} = C_{Fe} * V * (\frac{Mw_{NaFeCN}}{Aw_{Fe}}) \quad (7.2)$$

Where, Mw_{NaFeCN} is the molecular weight of NaFeCN (484.06 g mol-1) and Aw_{Fe} is the atomic weight of Fe (55.85 g mol^{-1}). The number of moles of Fe atoms and NaFeCN molecules are equal. The total amount of NaFeCN leached out in the debris [mg] was reported as the percentage of the initial NaFeCN present in the specimen at the start of the test.

SEM (FEI quanta 650 FEG) was performed on the cross-section of one specimen of each mortar type subjected to the accelerated weathering test to examine the salt crystal morphology. The cross-section was obtained by splitting the mortar specimen vertically using a tensile splitting test. The imaging was acquired just below the evaporation surface.

7

7.3. Results and discussion

7.3.1. Effect of the encapsulated inhibitor on the properties of mortar

In NHL-based mortars, the measured workability (flow) of fresh NHL-CsCA-F is similar to NHL-R specimens (Table 7.3). NHL-F specimens show a slightly higher flow compared to NHL-R with a higher scatter and can be a result of variation in parameters such as mixing speed and mixing time. In cement-based mortars, SPL-CsCA-F specimens show similar workability as the reference mortar SPL (Table 7.3). The above results show that addition of capsules have a negligible effect on workability of both NHL-based and cement-based mortars. Past studies have shown that hydrophilic polymers such as chitosan or alginate can absorb high volume of mixing water and reduce workability [24]. However, in this study, a reduction in workability was not observed and could be due to a relatively low dose of capsules (3.78 % of the binder weight) used during mortar preparation.

The 28-days compressive strength measured on NHL-CsCA-F specimens is higher than NHL-R and NHL-F (Table 7.3), showing that addition of capsules do not negatively affect the mechanical properties of NHL-based mortars. The 28-day compressive strength of NHL-F and NHL-R is also similar showing that addition of inhibitor also has no effect on the compressive strength and is in agreement with a previous

Table 7.3: Overview of measured properties in NHL-based mortars and cement-based mortars. The mean values and one standard deviation away from the mean is reported.

		NHL-based mortars			Cement-based mortars		
Measured property	Test method	NHL-R	NHL-F	NHL-CsCA-F	SPT	SPL	SPL-CsCA-F
Workability [mm]	Flow table	165.67 ± 0.9	172.33 ± 3.1	164.00 ± 1.4	154.3 ± 0.9	144.0 ± 0.8	146 ± 0.14
Compressive strength [MPa]	Mechanical testing	0.42 ± 0.08	0.39 ± 0.07	0.62 ± 0.08	-	1.82 ± 0.14	1.44 ± 0.16
Porosity [%]	MIP	21.83 ± 0.36	22.35 ± 0.27	22.37 ± 0.06	58.99 ± 0.01	58.54 ± 0.48	55.69 ± 0.43
Bulk density [g mL-1]	MIP	2.03 ± 0.01	2 ± 0	1.99 ± 0.02	0.93 ± 0.03	0.97 ± 0.02	1.01 ± 0.01
Water absorption coefficient [g m-2s-0.5]	Capillary absorption	159	147	156	2.33	26.33	25.36

study [20]. Conversely, in cement-based mortars, SPL-CsCA-F specimens have a slightly lower compressive strength as compared to SPL showing that addition of capsules has a minor effect on the compressive strength of cement-based mortars.

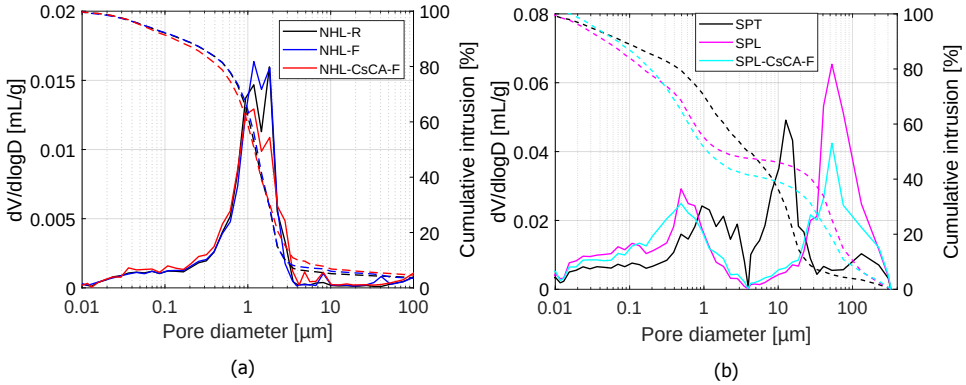

Figure 7.2: The pore size distribution measured using mercury intrusion porosimetry. (a) NHL-based mortars (b) Commercial cement-based mortars.

When considering the physical properties, all types of NHL-based mortar specimens show similar porosity, and unimodal pore size distribution (Figure 7.2a) with a mean pore diameter ranging between 0.5-2 µm. Therefore, it can be concluded that the addition of capsules (NHL-CsCA-F) or mixed-in inhibitor (NHL-F) has a negligible effect on the porosity (Table 7.3) and the pore-size distribution (Figure 7.2a).

The cement-based mortars exhibit a bi-modal pore-size distribution (Figure 7.2b) with the majority of pore diameters in the range of 10-100 µm and 0.1-2 µm. SPT specimens containing the hydrophobic additive has a similar open porosity but a

narrower pores-size distribution than SPL specimens. Different pore-size distribution between SPT and SPL is a result of different mortar composition and water content. To assess the effect of capsules, SPL-CsCA-F and SPL specimens are compared. The porosity measurement is slightly lower in SPL-CsCA-F specimens than SPL specimens (Table 7.3). The reduction in porosity is evident in the range between 10-200 µm (Figure 7.2b). It can be concluded that the effect of capsules on the porosity and pore-size distribution of cement-based mortars is minor.

The water absorption coefficient (WAC) of NHL-based mortars is higher than cement-based mortars (Table 7.3). In NHL-based mortars, the WAC of NHL-CsCA-F and NHL-R is similar. Likewise, In cement-based mortars WAC of SPL-CsCA-F is comparable to its reference (SPL). Presence of capsules, do not have any effect on the capillary absorption as substantiated also by their negligible impact on the pore-size distribution (Figure 7.2). Among cement-based mortars, SPT mortar has 10 times lower WAC than SPL. This is expected and is due to the hydrophobic character of this mortar.

The drying behaviour of both NHL-based and cement-based mortars (Figure 7.3) show that the specimens containing capsules dry slower. The drying rate is significantly slower in NHL-CsCA-F specimens as compared to both NHL-R and NHL-F specimens (Figure 7.3a). Similarly, in cement-based mortars, SPL-CsCA-F specimens show a slower drying rate than the reference SPL specimens (Fig 7.3b); this difference, however, is less prominent as compared to NHL-based mortars. These results clearly show that the slow drying is a consequence of the capsule addition and not NaFeCN.

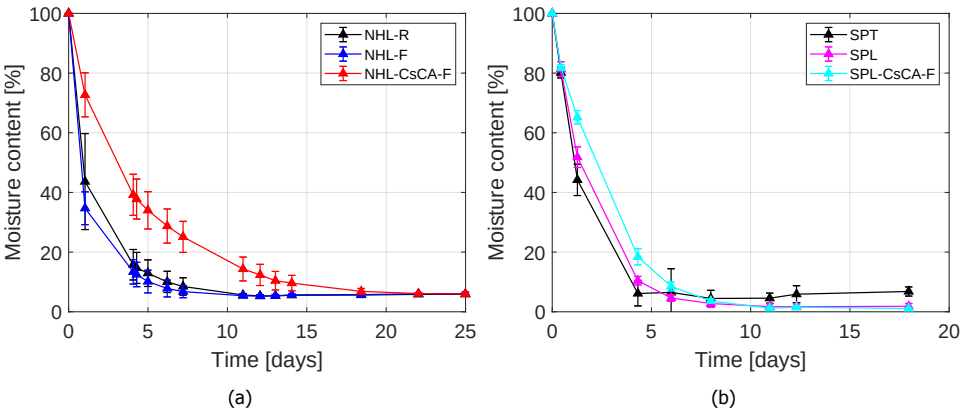

Figure 7.3: : Drying behaviour of mortars (a) NHL-based mortars (b) commercial cement-based mortars

The slow drying rate observed in presence of CsCA-F capsules may be attributed to the hydrophilic nature [35] of chitosan and alginate making them hygroscopic. Slow drying can even be beneficial to prolong mortar hydration and reduce shrinkage, by providing a steady supply of moisture and facilitating internal curing, in a similar manner as superabsorbent polymers [[36]. The higher compressive strength in NHL-based mortar specimens containing the capsules (Table 7.3) can be explained

by the extended hydration provided due to slower drying. NHL mortars were cured for three weeks at laboratory conditions (20 ± 3ºC, 55 ± 5 ºC), meaning that the low degree of hydration in the NHL-R specimens due to faster evaporation of moisture is probably improved in NHL-CsCA-F due to slower loss of moisture. However, an increase in compressive strength is not observed in cement-based mortars (Table 7.3). SPL and SPL-CsCA-F mortars were cured at a high relative humidity (20 ± 2ºC, 95 ± 5 ºC), where possibly the hydration is not hindered. In this situation, the internal curing provided by the capsules is not evident/ relevant. In fact, a slightly lower compressive strength as measured on SPL-CsCA-F specimens can be a result of the introduction of air pockets and weak interfacial transition zones (ITZ) between the capsules and the mortar matrix [37] as evident in Figure 7.4 b-e

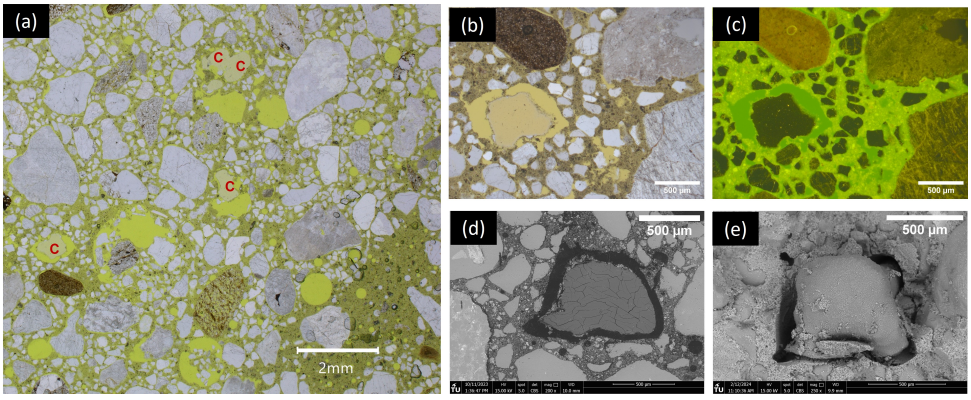

Figure 7.4: Microscopy images of CsCA-F capsules in NHL specimens (a): Low magnification optical micrograph of a thin-section under plane polarised light (PPL) showing pale yellow capsules (marked in red) distributed in the mortar matrix. (b) PPL image showing close up of a capsule. (c) UV-light image of the same capsule as (b). The green fluorescence indicates the locations of epoxy impregnation. The image shows epoxy is unable to impregnate in the capsule pores. (d) Scanning electron microscope (SEM) image on a polished section showing that the capsules have shrunk during drying, leading to the formation of air-pockets around them. Note the capsules do not form a bond with the mortar matrix. (e) SEM-morphology image of a capsule on an unpolished section showing that the capsule remains intact in the hardened mortar and does not bond to the matrix.

Microscopic examination of the capsules in hardened mortar is presented in Figure 7.4. This shows that the capsules are well distributed in the mortar mix (Figure 7.4 a) and are able to survive the mixing process (Figure 7.4 a,e). The capsules have a pale yellow appearance; around the capsules an air-pocket is visible (Figure 7.4 b,c). The formation of air pockets shows that the capsules shrink as they lose moisture. It is possible to observe that the epoxy resin (green fluorescence due to UV excitation) (Figure 7.4 c) which easily penetrates in the mortar matrix, but does not penetrate in the dry capsules; this suggests that the pores of the capsule must be smaller than those of the mortar matrix. The diffusive release of NaFeCN from CsCA capsules is dependent on the pore size of the capsules [22]. Smaller pores of the capsules relative to mortar matrix show that the capsules have a better chance of retaining NaFeCN than the mortar matrix making it less susceptible to

leaching.

The SEM images of the capsule (Figure 7.4 d,e) show that the capsules do not form any bond with the mortar matrix and is thus free to swell/shrink. No cracks were observed in the mortar matrix. This suggests, that capsules can swell and shrink when subjected to wet-dry cycles without imposing expansion stresses due to absence of any constraints.

7.3.2. Assessing mortar damage due to accelerated salt weathering test

The resistance of the mortars against salt crystallisation damage was assessed according to a procedure, adapted from the RILEM 271-ASC accelerated weathering test [34].

7.3.2.1. NHL-based mortar

Figure 7.5 shows the progression of damage, as photographically assessed, on different NHL-based mortar specimens at the start of the test, at the end of the accumulation stage and at the end of the propagation stage (four cycles). At the end of the accumulation stage, all specimens show salt accumulation/ efflorescence at the surface with no material damage (in accordance to the RILEM 271-ASC recommendations [34]). Among specimens containing the inhibitor, NHL-F shows considerably higher efflorescence than NHL-CsCA-F specimens. Damage starts developing during the propagation stage.

In NHL-R specimens (reference), the damage is observed after the first propagation cycle and progressively increases with each cycle (Appendix B); at the end of the test severe material loss is observed (Figure 7.5). The type of damage (i.e. sanding, according to [38]) as seen in these specimens is typically observed on plasters in the field [19], confirming the reliability of the test procedure to reproduce real case scenarios. At the end of the test, after brushing off the debris, a rough surface is observed due to loss of adhesion between the sand grains and the binder (Figure 7.6). Specimens NHL-F and NHL-CsCA-F, containing NaFeCN mixed in and in encapsulated form respectively, show a large amount of salt efflorescence, which increases with each successive cycle (Appendix B). At the end of the test, after brushing off the surface, only negligible surface damage is observed (Figure 7.6).

In order to quantify the damage, the debris brushed off from the surface of the specimen at the end of the test was analysed as described in Section 7.2.5.3. Figure 7.6 shows the total material loss and the amount of salt transported to the surface (as salt efflorescence) measured at the end of the test. NHL-R specimens exhibit severe material loss. Differently, mortars with mixed-in NaFeCN (NHL-F) and encapsulated inhibitor (NHL-CsCA-F) show almost 16 times lower material loss compared to NHL-R specimens and a higher salt efflorescence. When comparing mortars with encapsulated (NHL-CsCA-F) and mixed in NaFeCN (NHL-F), a similar amount of material loss and salt efflorescence is visible. These results confirm that the amount of NaFeCN released from the CsCA capsules is sufficient to prevent damage in mortar.

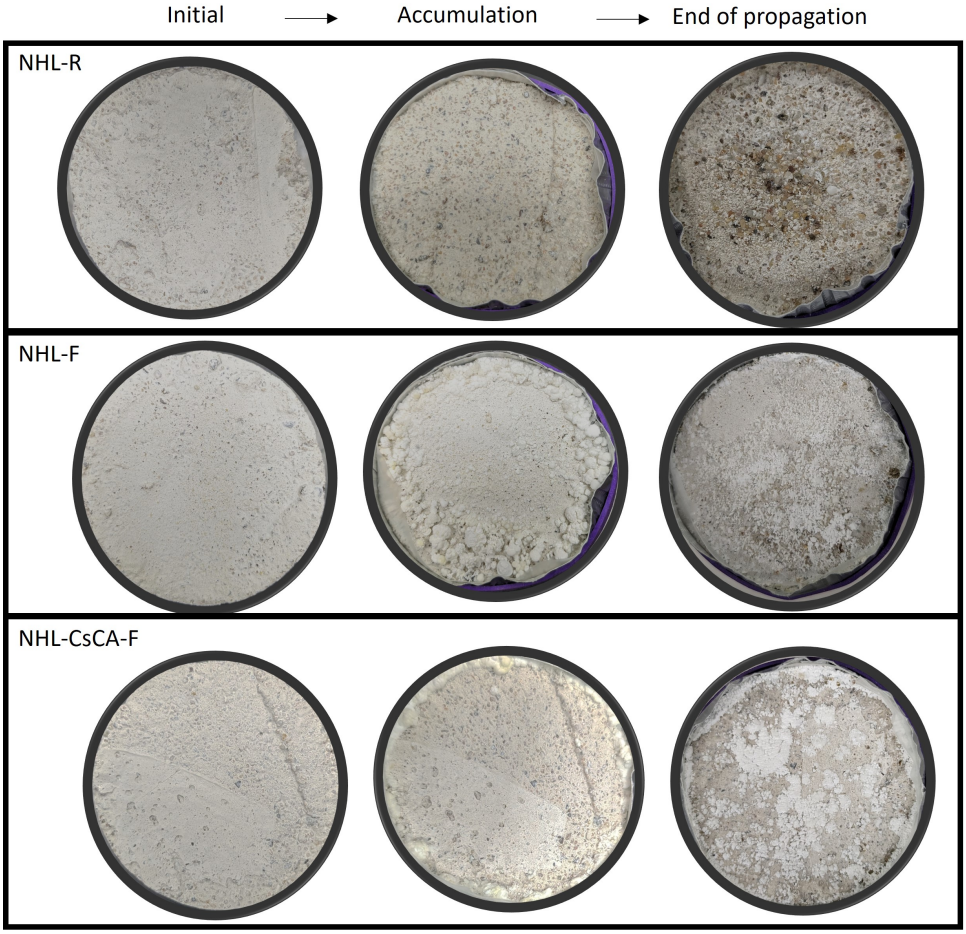

Figure 7.5: Progression of damage in NHL-based mortars due to salt weathering test. The images are taken at the start of the test, at the end of the accumulation stage and the end of the propagation stage (four cycles).

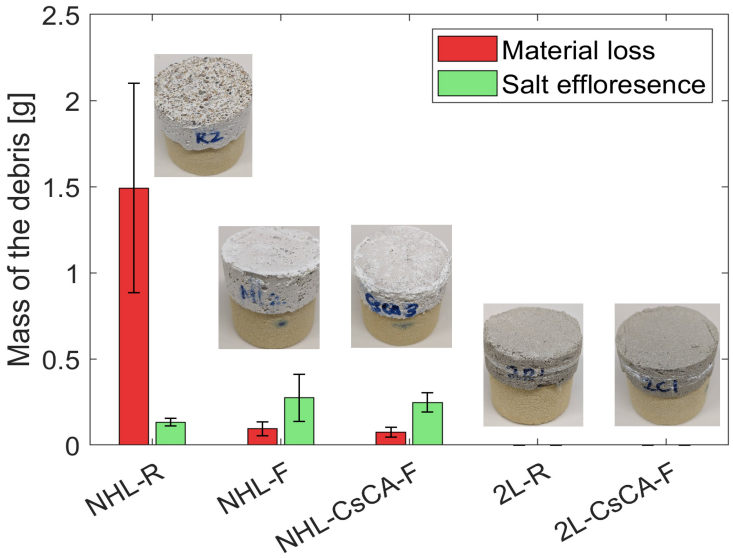

Figure 7.6: The plot showing the material loss (red) and salt efflorescence (green) measured from each type of mortar specimen at the end of the accelerated test. The error bars indicate one standard deviation away from the mean. Inset: images of specimen surface corresponding to each mortar type obtained after brushing the debris.

SEM observations have been performed on the cross-section of NHL-R and NHL-CsCA-F specimens to observe the change in NaCl crystal morphology due to the action of NaFeCN. The SEM images (Figure 7.7) in the cross-section of both NHL-R and NHL-CsCA-F show that not all salt is transported outside the specimen and part of it crystallises within the mortar pores. In NHL-R (Figure 7.7a), it can be observed that NaCl crystals have a cubic habit whereas, in NHL-CsCA-F specimens (Figure 7.7b), NaFeCN leads to a change of crystal morphology, from cubic habit to dendritic growth, and a smaller crystal size as compared to NHL-R. Both changes are in line with the previous studies demonstrating NaFeCN's ability to delay NaCl nucleation and alter NaCl crystal morphology, consequently promoting salt efflorescence over sub-florescence and preventing damage in porous materials [7, 12, 17]. Moreover, the formation of smaller crystals within the pores as evident in Figure 7.7b may have also contributed to lower pore-filling, consequently preventing salt damage in specimens containing NaFeCN, as suggested by [7].

When considering the amount of inhibitor leached out of the mortars, a higher efflorescence observed at the end of the accumulation stage in NHL-F specimens over NHL-CsCA-F specimens (Figure 7.5) is a sign that most of the inhibitor from NHL-F may have already been transported to the surface during the accumulation stage itself. Debris analysis at the end of the test, shows that NHL-CsCA-F has a 30% lower inhibitor leached out of the mortar in comparison to NHL-F, demonstrating that the CsCA capsules used in this study can slow down NaFeCN leaching (Figure 7.8). This implies that encapsulation of the inhibitor can prolong its effectiveness over

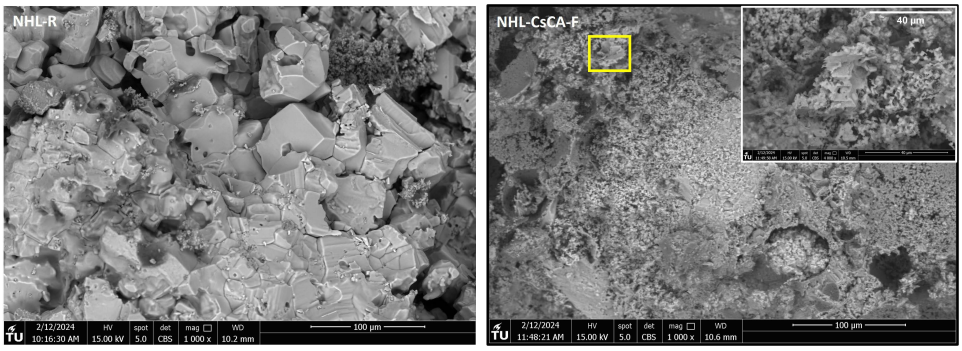

(a) (b)

Figure 7.7: SEM microscopic images of the cross-section of NHL-mortars at the end of the accelerated weathering test. Images are taken at about 1 mm from the evaporation surface (a) cubic NaCl crystals observed in the pores of the reference NHL mortar (NHL-R) which did not contain NaFeCN (b) Dendritic NaCl crystals in mortar NHL-CsCA-F. Note the small size of the crystal in comparison to (a) Inset: magnified image of the area marked in yellow showing the modified dendritic NaCl crystal habit.

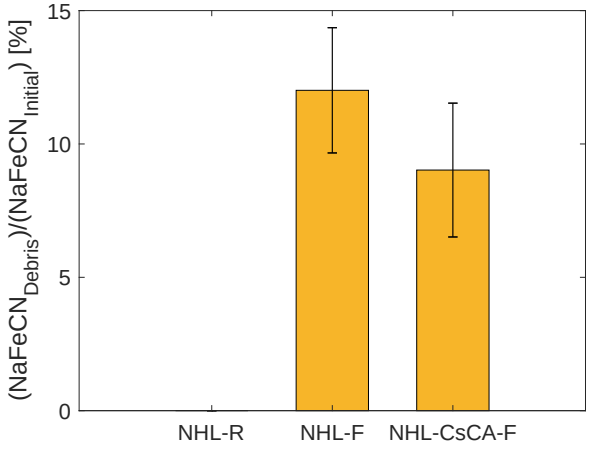

Figure 7.8: NaFeCN measured by means of ICP-OES in the debris collected at the end of the test on NHL -based mortars. The results are expressed as a weight percentage of the initial NaFeCN amount present in each specimen. The error bars indicate one standard deviation away from the mean.

time and improve the service life of the inhibitor.

7.3.2.2. Two-layer cement based plaster system

Both 2-layer cement-based plaster specimens (i.e. 2L-R and 2L-CsCA-F) do not show any visible surface damage at the end of the weathering test (Appendix B). In both cases, independently from the presence of encapsulated inhibitor in the base layer, most of the salt crystallised in between the two mortar layers (Figure 7.9). This behaviour show that the hydrophobic top layer (SPT) is able to stop liquid water and salt transport, as could be deduced based on the measured low WAC (Table 7.3).

Visual observations of the lateral sides of the specimens at the end of the test show the effect of NaFeCN on the crystal habit of NaCl crystallizing in 2L-R specimens (Figure 7.9a) to a dendritic habit (Figure 7.9b). As no damage was observed in both mortars with and without encapsulated inhibitor, no conclusion can be drawn on the positive effect of inhibitors in reducing crystallisation pressure in pores. No observed damage may be associated to a few reasons. The high mechanical strength of both the plaster layers (SPT and SPL) may have resisted the four damage propagation cycles (See Table 7.3). Second, the location of salts in between the two plaster layers, thus further away from the surface may have made it difficult for the small duration of RH cycles to dissolve and recrystallise salts in such depths. Thus, the currently employed crystallisation-deliquescence cycles may not be effective for such type of plaster system.

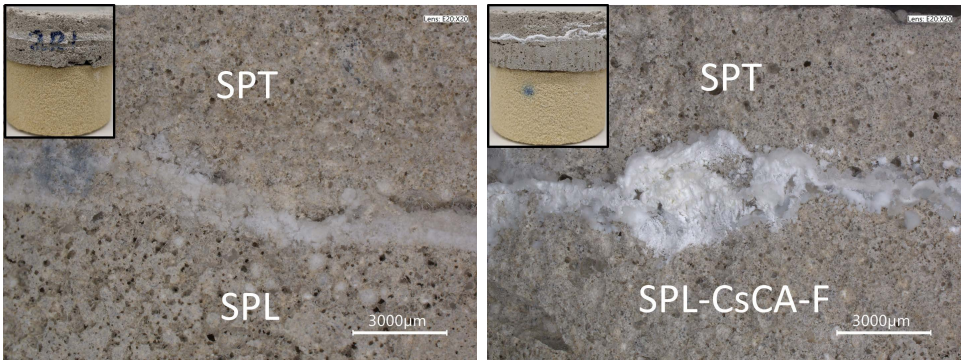

(a) (b)

Figure 7.9: Optical microscopy images showing NaCl accumulation in between the layers of the 2-layer plasters at the end of the accelerated weathering test (a) compact NaCl crystals in reference 2L-R mortar (b) dendritic NaCl crystals in 2L-CsCA-F mortar. Inset: high field of view images (digital camera) of both the specimens showing the extent of salt accumulation in between the layers.

7.4. Conclusions and outlook

In this research, the effect of NaFeCN, inhibitor of NaCl crystallisation on the properties and durability with respect to salt crystallisation of hydraulic (NHL- and cement-based) mortars was investigated. The inhibitor was either mixed-in directly (in an

aqueous solution) in the mortar or encapsulated in chitosan-calcium alginate capsules, which were added to the mortar during mixing. Various experimental techniques were used to assess the mechanical (compressive strength) and physical properties (porosity, pore size distribution, water absorption and drying behaviour) of the mortar. The durability of the mortar to NaCl-induced crystallisation damage was assessed using accelerated salt weathering test as per the RILEM- 271 recommendations. The results show that the addition of the inhibitor, both directly mixed-in and encapsulated, improve the durability of the studied hydraulic mortars with respect to salt damage, without negatively affecting their properties. Moreover, encapsulation of the inhibitor was successful in reducing leaching of the inhibitor out of mortar, while still guaranteeing the same durability performance as mortars with mixed-in inhibitor. These observations suggest that encapsulation of the inhibitor is able to prolong the service life of the inhibitor without compromising on the salt weathering resistance of the mortar.

For the future, some questions are left to be investigated. From the fundamental point of view, the supposed positive effect of NaFeCN on NaCl crystallisation pressure still needs to be experimentally assessed. Moreover, the possibility of fine-tuning the composition of the capsules to adapt to the rate of inhibitor release based on the severity of the conditions (i.e. salt and moisture load) could be considered.

References

[1] A. Goudie and H. Viles, *Salt weathering hazards* (John Wiley & Sons Ltd, Chichester, 1997) p. 256.

[2] A. E. Charola, *Salts in the Deterioration of Porous Materials : An Overview,* Journal of the American institute for conservation **39**, 327 (2000).

[3] M. Steiger, *Crystal growth in porous materials - I: The crystallization pressure of large crystals,* Journal of Crystal Growth **282**, 455 (2005).

[4] G. W. Scherer, *Stress from crystallization of salt,* Cement and Concrete Research **34**, 1613 (2004).

[5] J. Desarnaud and N. Shahidzadeh-Bonn, *Salt crystal purification by deliquescence/crystallization cycling,* EPL (Europhysics Letters) **95**, 48002 (2011).

[6] B. Lubelli, R. P. van Hees, and C. J. Groot, *The effect of environmental conditions on sodium chloride damage: A step in the development of an effective weathering test,* Studies in Conservation **51**, 41 (2006).

[7] S. J. Granneman, B. Lubelli, and R. P. van Hees, *Effect of mixed in crystallization modifiers on the resistance of lime mortar against NaCl and Na2SO4 crystallization,* Construction and Building Materials **194**, 62 (2019).

[8] C. Rodriguez-Navarro and L. G. Benning, *Control of crystal nucleation and growth by additives,* Elements **9**, 203 (2013).

[9] M. A. R. Blijlevens, E. R. Townsend, P. Tinnemans, W. J. P. van Enckevort, and E. Vlieg, *Effect of the Anticaking Agent FeCN on the Creeping Properties of Alkali Halide Crystals,* Crystal Growth & Design **22**, 6575 (2022).

[10] A. A. Bode, V. Vonk, F. J. Van Den Bruele, D. J. Kok, A. M. Kerkenaar, M. F. Mantilla, S. Jiang, J. A. Meijer, W. J. Van Enckevort, and E. Vlieg, *Anticaking activity of ferrocyanide on sodium chloride explained by charge mismatch,* Crystal Growth and Design **12**, 1919 (2012).

[11] A. Glasner and M. Zidon, *The crystallization of NaCl in the presence of [Fe(CN)6]4- ions,* Journal of Crystal Growth **21**, 294 (1974).

[12] C. Rodriguez-Navarro, L. Linares-Fernandez, E. Doehne, and E. Sebastian, *Effects of ferrocyanide ions on NaCl crystallization in porous stone,* Journal of Crystal Growth **243**, 503 (2002).

[13] C. Selwitz and E. Doehne, *The evaluation of crystallization modifiers for controlling salt damage to limestone,* Journal of Cultural Heritage **3**, 205 (2002).

[14] B. Lubelli and R. P. van Hees, *Effectiveness of crystallization inhibitors in preventing salt damage in building materials,* Journal of Cultural Heritage **8**, 223 (2007).

[15] T. Rivas, J. Feijoo, I. de Rosario, and J. Taboada, *Use of Ferrocyanides on Granite Desalination by Immersion and Poultice-Based Methods,* International Journal of Architectural Heritage **11**, 588 (2017).

[16] S. Gupta, K. Terheiden, L. Pel, and A. Sawdy, *Influence of Ferrocyanide Inhibitors on the Transport and Crystallization Processes of Sodium Chloride in Porous Building Materials,* Crystal Growth & Design **12**, 3888 (2012).

[17] B. Lubelli, T. G. Nijland, R. P. Van Hees, and A. Hacquebord, *Effect of mixed in crystallization inhibitor on resistance of lime-cement mortar against NaCl crystallization,* Construction and Building Materials **24**, 2466 (2010).

[18] J. Feijoo, D. Ergenç, R. Fort, and M. A. de Buergo, *Addition of ferrocyanide-based compounds to repairing joint lime mortars as a protective method for porous building materials against sodium chloride damage,* Materials and Structures **54**, 14 (2021).

[19] B. Lubelli, E. d. Bouvrie, T. G. Nijland, and A. Kamat, *Plasters with mixed-in crystallization inhibitors: Results of a 4-year monitoring of on-site application,* Journal of Cultural Heritage **59**, 10 (2023).

[20] A. Kamat, B. Lubelli, and E. Schlangen, *Effect of a mixed-in crystallization inhibitor on the properties of hydraulic mortars,* AIMS Materials Science **9**, 628 (2022).

[21] A. Kamat, B. Lubelli, and E. Schlangen, *Leaching behaviour of a crystallisation inhibitor in mortars,* Journal of Building Engineering **79**, 107933 (2023).

[22] A. Kamat, D. Palin, B. Lubelli, and E. Schlangen, *Capsule controlled release of crystallisation inhibitors in mortars [Under review],* (2024).

[23] J. Y. Wang, H. Soens, W. Verstraete, and N. De Belie, *Self-healing concrete by use of microencapsulated bacterial spores,* Cement and Concrete Research **56**, 139 (2014).

[24] C. Schröfl, K. A. Erk, W. Siriwatwechakul, M. Wyrzykowski, and D. Snoeck, *Recent progress in superabsorbent polymers for concrete,* Cement and Concrete Research **151**, 106648 (2022).

[25] *NEN-EN 196-1: Methods of testing cement - Part 1: Determination of strength*, Tech. Rep. (European committee for standardisation (CEN), 2015).

[26] C. Nunes, A. Maria Aguilar Sanchez, S. Godts, D. Gulotta, I. Ioannou, B. Lubelli, B. Menendez, N. Shahidzadeh, Z. Slížková, and M. Theodoridou, *Experimental research on salt contamination procedures and methods for assessment of the salt distribution,* Construction and Building Materials **298**, 123862 (2021).

[27] E.-S. Chan, B.-B. Lee, P. Ravindra, and D. Poncelet, *Prediction models for shape and size of ca-alginate macrobeads produced through extrusion–dripping method,* Journal of Colloid and Interface Science **338**, 63 (2009).

[28] *NEN-EN 459-2: Building lime-part 2: Test methods*, Tech. Rep. (European committee for standardisation (CEN), 2008).

[29] *NEN-EN 1015-11: Methods of test for mortar for masnory-Part 11: Determination of flexural and conpressive strength of hardened mortar*, Tech. Rep. (European committee for standardisation (CEN), 2019).

[30] *NEN-EN 1015-3: Methods of test for mortar for masonry - Part 3: Determination of consistence of fresh mortar (by flow table)*, Tech. Rep. (European committee for standardisation (CEN), 1999).

[31] *NEN-EN-1925: Natural stone test methods- Determination of water absorption coefficient by capillarity*, Tech. Rep. (European committee for standardisation (CEN), 1999).

[32] T. Nijland and J. Larbi, *Microscopic examination of deteriorated concrete,* in *Non-Destructive Evaluation of Reinforced Concrete Structures* (Elsevier, 2010) pp. 137–179.

[33] B. Lubelli, A. M. Aguilar, K. Beck, T. De Kock, J. Desarnaud, E. Franzoni, D. Gulotta, I. Ioannou, A. Kamat, B. Menendez, I. Rörig-Dalgaard, and E. Sassoni, *A new accelerated salt weathering test by RILEM TC 271-ASC: preliminary round robin validation,* Materials and Structures **55**, 238 (2022).

[34] B. Lubelli, I. Rörig-Daalgard, A. M. Aguilar, M. Aškrabić, K. Beck, C. Bläuer, V. Cnudde, A. M. D'Altri, H. Derluyn, J. Desarnaud, T. Diaz Gonçalves,

R. Flatt, E. Franzoni, S. Godts, D. Gulotta, R. van Hees, I. Ioannou, A. Kamat, T. De Kock, B. Menendez, S. de Miranda, C. Nunes, E. Sassoni, N. Shahidzadeh, H. Siedel, Z. Slížková, M. Stefanidou, M. Theodoridou, R. Veiga, and V. Vergès-Belmin, *Recommendation of RILEM TC 271-ASC: New accelerated test procedure for the assessment of resistance of natural stone and fired-clay brick units against salt crystallization,* Materials and Structures **56**, 101 (2023).

[35] A. Mignon, G.-J. Graulus, D. Snoeck, J. Martins, N. De Belie, P. Dubruel, and S. Van Vlierberghe, *pH-sensitive superabsorbent polymers: a potential candidate material for self-healing concrete,* Journal of Materials Science **50**, 970 (2015).

[36] J. Liu, N. Farzadnia, and C. Shi, *Microstructural and micromechanical characteristics of ultra-high performance concrete with superabsorbent polymer (SAP),* Cement and Concrete Research **149**, 106560 (2021).

[37] Y. Li, H. Luo, B. Zhang, X. Wei, F. Wang, W. Wang, P. Liu, and J. Zhu, *Internal curing of natural hydraulic lime with superabsorbent polymers,* Materials Today Communications **34**, 105064 (2023).

[38] *Monument Diagnosis and Conservation System,* .

8

Conclusions and outlook


IN A PARALLEL UNIVERSE... IRON MAN, FeCN & THE SO-CALLED INDEPENDENT RESEARCHER GO OUT FOR A DRINK...
FeCN, ARE YOU FEELING BLUE TODAY?
EVERY TIME I MEET YOU, IRON MAN (Eq. 5.1)
AND MR. RESEARCHER, WHAT DO YOU PLAN TO DO AFTER THIS?
NOW EVEN I START TO FEEL BLUE, FeCN!

8.1. Key findings and conclusions

The main aim of this research was to improve the salt resistance and service life of hydraulic mortars using crystallisation inhibitors. For this reason, a literature review (Chapter 2) was carried out and two performance related issues were identified. The first issue concerned the possibility of mixing crystallisation inhibitors in hydraulic mortars and the second issue concerned slowing down leaching of the inhibitor to improve the service life of mortars. These two issues were addressed by developing an experimental research plan as described in Figure 1.2 (Chapter 1) and executing it. A summary of key findings and conclusions of this thesis are given below:

Possibility of mixing crystallisation inhibitor in hydraulic mortars

- At first, the possible interactions between the crystallisation inhibitor (sodium ferrocyanide) and hydraulic binders (NHL and OPC) were studied indirectly, by experimentally investigating the effect of the inhibitor on the properties of binder paste and mortar specimens (See Chapter 3). At the scale of the binder paste, it was shown that addition of the inhibitor in a concentration up to 1% of the binder weight does not have any effect on the setting time and the heat of hydration. Similarly, at the scale of the mortar, the presence of the inhibitor in an amount up to 1% of the binder weight does not have any negative effect on the fresh properties (workability, setting time), mechanical properties (compressive strength, flexural strength and E-modulus), physical properties (porosity, bulk density and pore-size distribution) and moisture transport properties (water absorption coefficient and drying rate). These results show that it is practically feasible to mix-in sodium ferrocyanide with hydraulic binders without having any negative impact on the properties of the studied hydraulic mortars.

- In the next step, the resistance of hydraulic mortars with mixed-in inhibitors to salt damage was assessed and compared with hydraulic mortars without the inhibitor, using an accelerated salt weathering test (Chapter 7). While the reference hydraulic (NHL) mortars without the inhibitor showed a severe progression of damage in terms of material loss, hydraulic (NHL) mortars with the crystallisation inhibitor showed negligible damage. Moreover, in mortars containing the crystallisation inhibitor, a higher amount of salt was transported to the mortar surface as efflorescence as compared to mortars without the inhibitor. The scanning electron microscope images of the cross section of mortar specimens, acquired at the end of the weathering test showed precipitation of smaller NaCl crystals and a modification of NaCl crystal habit from cubic to dendritic in presence of the inhibitor. A higher surface area on account of a dendritic crystal habit, is a likely reason to promote higher advection of salt to the surface as efflorescence, thereby preventing confined in-pore crystallisation and the consequent damage. The results from this thesis are consistent with the observations from previously conducted studies on different porous media and unequivocally demonstrate the positive effect of

the crystallisation inhibitor in preventing salt damage when mixed-in hydraulic mortars.

Reducing leaching of the inhibitor to prolong the service life of mortars with mixed-in inhibitor

- As reported in the previous section, directly mixing the inhibitor in hydraulic mortar was shown to be effective in preventing salt damage. However, the high solubility of the inhibitor in aqueous conditions makes it susceptible to leaching out of the mortar. Due to a lack of quantitative data on the leaching behaviour of the inhibitor, a test protocol was developed in Chapter 4 to assess the risk of the inhibitor leaching out of mortar, under diffusion and advection. In the diffusion-driven leaching test, a high diffusion coefficient of the leached out inhibitor was measured. The advection driven leaching test showed that most of the inhibitor leached out after just one wetting-drying cycle, causing depletion of the inhibitor in the depth of the mortar. This rapid loss of the inhibitor due to leaching would diminish the positive effect of the mixed-in inhibitor over time and thereby, reduce the service life of the mortar. Therefore, a solution was sought to reduce the rate of leaching of the inhibitor.

- Encapsulating the inhibitor and controlling its release was considered as a potential solution to slow down leaching of the inhibitor. Two hydrogels made of bio-polymers, alginate and chitosan, were selected based on their pH-responsive swelling and consequent release characteristics. In Chapter 5, the inhibitor was successfully encapsulated in calcium alginate (CA) capsules using ionic gelation and the CA capsules were further complexed with varying concentration of chitosan to obtain chitosan-calcium alginate (CsCA) capsules containing the inhibitor. The release of the inhibitor from different capsule compositions was tested in bulk solutions over a pH range of 7 to 13. It was shown that CA capsules (i.e. without chitosan) released high amount of inhibitor in the tested pH range. Conversely, CsCA capsules showed a lower release of the inhibitor, which decreased as a function of the chitosan concentration. These results show that the CsCA capsules have a potential to be tuned towards obtaining a desired release of the inhibitor at a certain pH by modifying the chitosan:alginate ratio.

- On the outlook of these positive results, in Chapter 6, the release rate of the inhibitor from CsCA capsules was measured in mortar pore solution and the capsules were characterised to measure their encapsulation capacity. Based on these results, CsCA capsules with the most suitable release, were incorporated in hydraulic mortars and subjected to the leaching test developed in Chapter 4. The results of both diffusion and advection driven tests clearly show that the mortar containing CsCA capsules leaches (i.e. releases) the inhibitor significantly slower compared to the mortar with mixed-in inhibitor. Chitosan role's in counteracting the swelling of calcium alginate capsules as well as the electrostatic interaction between the ferrocyanide anions and the

positively charged chitosan are likely to be responsible for the observed slower release of the inhibitor.

- In the final phase of the research, the performance of the prototype mortar (i.e. hydraulic mortar with encapsulated inhibitor) was assessed (Chapter 7). First, the effect of the capsules on the fresh and hardened properties of the mortar was investigated. It was shown that incorporation of capsules up to 3.78 % weight of binder (equivalent to 1% inhibitor as weight of binder) in mortar does not have any negative effect on the fresh (workability), mechanical (compressive strength), physical (porosity and pore-size distribution) and transport (water absorption coefficient and drying rate) properties of mortar. Next, the salt resistance of the prototype mortar was assessed by performing an accelerated salt weathering test (Chapter 7). Mortars with mixed-in and encapsulated inhibitor showed a significant and a similar reduction in salt damage as compared to reference mortar (without inhibitor). In addition to that, the amount of inhibitor leached at the end of the test from mortar with encapsulated inhibitor was lower than in mortar with mixed-in inhibitor.

Summarising the above results, it can be definitively concluded that the prototype hydraulic mortars with encapsulated inhibitor and mixed-in inhibitor have a considerably improved salt weathering resistance as compared to hydraulic mortars without the inhibitor. Moreover, the mortars with encapsulated inhibitor, thanks to the controlled release of the inhibitor, are expected to have a longer service life than mortars with directly mixed-in inhibitor. And finally, since neither the inhibitor nor the capsules affect the properties of hydraulic mortar in a negative way, the application of the developed mortar prototypes is feasible in practice.

8.2. Contribution to science

This research introduces a novel application of hydrogels within building materials. For the first time, chitosan-alginate hydrogels have been explored for controlled-release applications within the field of building materials. The conclusions of this research can spark interest of researchers working in a similar domain and expand the possibilities of using hydrogels in the field of construction.

This research provides insights in the pH-responsive release behaviour of chitosan and alginate hydrogels in an alkaline range. Existing research has mostly investigated chitosan-alginate hydrogels limited to physiological conditions (i.e. pH up to 7.4), due to their relevance in the field of medicine. The results from this PhD research extends the knowledge of these hydrogels, opening new possibilities for their application and better understanding their behaviour fundamentally.

A pH reversible electrostatic interaction between ferrocyanide and chitosan, as observed in this research, is not widely reported in the literature. Exploring these interactions further may have implications in understating the chelation capability of chitosan, cross-linking ability of charged metal complexes and thereby contribute towards development of novel materials.

The salt crystallisation test results in this PhD research confirms the reliability of the RILEM 271-ASC procedure (accelerated salt weathering) [1] and demon-

strates the possibility to adapt the test to consider composite materials, such as as substrate-plaster systems. In the past, accelerated weathering tests have often struggled due to a lack of repeatability and/or reliability. The conclusions from this PhD research improve the credibility of the test and can hopefully, contribute towards a wider acceptance of this test procedure. A credible standardised procedure will help in providing a benchmark for comparison of results across various laboratories and validating novel solutions against salt damage.

8.3. Impact on the society

The main contribution of this work is a plaster/render prototype with additives that can mitigate salt damage over a long time period, reducing the need for frequent repairs. Frequent repair/ replacement interventions lead to considerable maintenance costs, not only due to materials but also due to labour wages and scaffolding. High costs are also one of the reasons for reluctance on the part of the owner/ responsible agencies to undertake timely interventions. This often leads to a dilapidated state of buildings, including the built cultural heritage. Therefore, the work done in this research will directly impact the owners/responsible agencies in reducing the repair costs over time and enable them to take timely interventions. Secondly, durable plasters and renders would lead to a lower material usage and hence, reduce the impact on the environment.

The practical feasibility in extending crystallisation inhibitors to hydraulic mortars as demonstrated by this research, is also expected to broaden the field of application of the inhibitors to a wider range of buildings and objects. This technology will contribute towards improving the renovation of existing buildings as well as preventing salt damage in new constructions. The prototype may also offer a compatible solution in the restoration of built cultural heritage and is therefore, a step closer towards preservation of the built cultural heritage for future generations.

8.4. Outlook

The findings from this thesis create some interesting opportunities for future work. These are presented as follows:

- The inhibitor, sodium ferrocyanide, has proven its effectiveness in preventing NaCl induced damage. In reality, porous building materials are likely to be contaminated with a mixture of salts. The effect of sodium ferrocyanide on NaCl crystallisation in presence of other salts still needs to be investigated.
- At a fundamental level, the effect of crystallisation inhibitor on the development of the crystallisation pressure (rather disjoining pressure) still needs exploration. This thesis along with previous studies have shown that in the presence of the inhibitor, a single NaCl crystal has a smaller size. Precipitation of smaller crystals (much smaller than a pore diameter) spread across the pore (e.g. as observed in [2]) may prevent the disjoining pressure to be imposed on the pore-walls. Currently, difficulties pertain to developing a controlled experimental setup that can accurately measure the disjoining pressure. This

hypothesis, if proven can be beneficial in preventing salt damage in situations where salt extraction/ efflorescence is not possible, for e.g. glazed tiles, plasters with a water-repellent surface and low porosity substrates.

- The proof-of-concept of the capsules with inhibitor developed in this research showcases the potential of the capsule technology in reducing leaching of the inhibitor from mortar. However, the capsule composition still requires optimisation to gain a better control over the release rate of the inhibitor. Various parameters such as the method of encapsulation, concentration of sodium alginate, polymer structure of alginate (e.g. mannuronic:guluronic acid ratio), type of cross-linking agents, molecular weight of chitosan etc. affect the release performance of the capsules. It is necessary to understand influence of each parameter at a more fundamental level to be able to tune a case specific response. A multi-disciplinary collaboration between experts from different fields is necessary to improve the efficiency of this capsule technology.
- One of the by-products of the calcium alginate capsule production is the formation of sodium chloride (NaCl) (See Figure C.4, Appendix C). This occurs during the gelation process, as the Na^{+} ions from sodium alginate combine with Cl^{-} from the calcium chloride ($CaCl_2$) bath. This production method introduces some NaCl in the capsules and may increase the overall salt load in the mortar. In future work, a different water soluble source of Ca^{2+} ions such as calcium acetate or calcium lactate can be considered instead of $CaCl_2$ to eliminate the risk of additional NaCl formation.
- The chitosan-calcium alginate capsules for controlled release can find applications in other cementitious materials, when a slow sustained release of additives is necessary. For instance, the technology can be used for a pH dependent release of corrosion inhibitors in reinforced concrete or for delaying the release of chemical retarders to control cement hydration. The biological origin and the abundant availability of these polymers may also prove to be a sustainable alternative to synthetic polymers. Looking beyond encapsulation applications, the immobilisation potential of chitosan (such as its attraction/binding to anions) can be exploited as a treatment to mitigate damage caused by sodium sulfate (Na_2SO_4), as chitosan can immobilise sulfate (SO_4^{2-}) anions and prevent Na_2SO_4 crystallisation. In the field of concrete, chitosan-calcium alginate matrices can be used as sorbents to prevent leaching of heavy metals from municipal solid waste incineration (MSWI) fly ash. MSWI fly ash is a promising supplementary cementitious material but its use is currently marred by an environmental risk due to presence of soluble toxic heavy metals in its composition.

References

[1] B. Lubelli, I. Rörig-Daalgard, A. M. Aguilar, M. Aškrabić, K. Beck, C. Bläuer, V. Cnudde, A. M. D'Altri, H. Derluyn, J. Desarnaud, T. Diaz Gonçalves, R. Flatt,

E. Franzoni, S. Godts, D. Gulotta, R. van Hees, I. Ioannou, A. Kamat, T. De Kock, B. Menendez, S. de Miranda, C. Nunes, E. Sassoni, N. Shahidzadeh, H. Siedel, Z. Slížková, M. Stefanidou, M. Theodoridou, R. Veiga, and V. Vergès-Belmin, *Recommendation of RILEM TC 271-ASC: New accelerated test procedure for the assessment of resistance of natural stone and fired-clay brick units against salt crystallization,* Materials and Structures **56**, 101 (2023).

[2] A. Kamat, B. Lubelli, and E. Schlangen, *Effect Of Alkali Ferrocyanides On Crystallisation Of Sodium Chloride,* in *Proceedings of the SWBSS: Fifth International Conference on Salt Weathering of Buildings and Stone Sculptures*, edited by B. Lubelli, A. Kamat, and W. Quist (TU Delft OPEN Publishing, Delft, 2021) pp. 109–118.

A

Supplementary information to Chapter 6

Supplementary materials and methods

UV-VIS Spectrophotometry calibration curve

A calibration curve for quantification of NaFeCN was prepared by measuring absorbance of three solutions with known concentrations of NaFeCN in ultra-pure water. The three solutions were prepared by dissolving NaFeCN in ultrapure water such that the concentration of NaFeCN was 5 mg L^{-1}, 10 mg L^{-1} and 20 mg L^{-1}. The absorbance of each solution was measured at a wavelength of 218 nm using the ultraviolet-visible (UV-VIS) spectrophotometer (Shimadzu UV2600). The calibration curve was obtained by performing linear regression on the absorbance-concentration data (Figure A.1). The equation from the calibration curve was used to calculate NaFeCN concentration of samples used in the experiments. Every sample to be tested was always diluted to be within the calibration range (i.e. 0–20 mg L^{-1}).

Analytical solution for accelerated testing (diffusion)

The analytical solution provided by ASTM-C1308-08 using Fourier-Bessel series is based on diffusion through a finite cylinder of height H and radius R as shown in Equation A.1.

$$CFL_n = \left(1 - \frac{32}{\pi^2} S_p(t) S_c(t)\right) \tag{A.1}$$

with the series,

$$S_p(t) = \sum_{j=1}^{\infty} \frac{exp\left[-\left(\frac{(2j-1)\pi}{H}\right)^2 D_e t\right]}{(2j-1)^2} \tag{A.2}$$

A

$$S_c(t) = \sum_{m=1}^{\infty} \frac{exp\left[-\left(\frac{\beta_m}{R}\right)^2 D_e t\right]}{\beta_m^2} \quad (A.3)$$

Where, a_n is the amount of NaFeCN leached [mg] at nth interval, A_0 is the amount of NaFeCN present in the tested mortar specimen at the start of the test [mg] and is estimated using Equation A.4. CFL_n is the cumulative fraction leached defined as the ratio between cumulative a_n to A_0. t is time, j represents the number of terms used in the series and m represents the series index that satisfy the zeroth order cylindrical Bessel function (β). D_e is the effective diffusion coefficient that needs to be determined by fitting the experimentally measured CFL values to the above equation.

$$A_0 = \sum_{n=1}^{N} a_n + a_f \quad (A.4)$$

Where, a_f corresponds to the amount of NaFeCN left [mg] at the end of the leaching test (Figure A.3).

Supplementary tables and figures

Table A.1: Chemical composition and pH of the pore solution prepared using binder-slurry filtrate. The pore solution was used to study release of NaFeCN from capsules

[mg L^{-1}]	Ca	K	Al	Si	Mg	Na	pH
μ±σ	914 ±58	132±1.73	0.37±0.21	0.29±0.1	<0.001	21.33±1.27	12.32±0.21

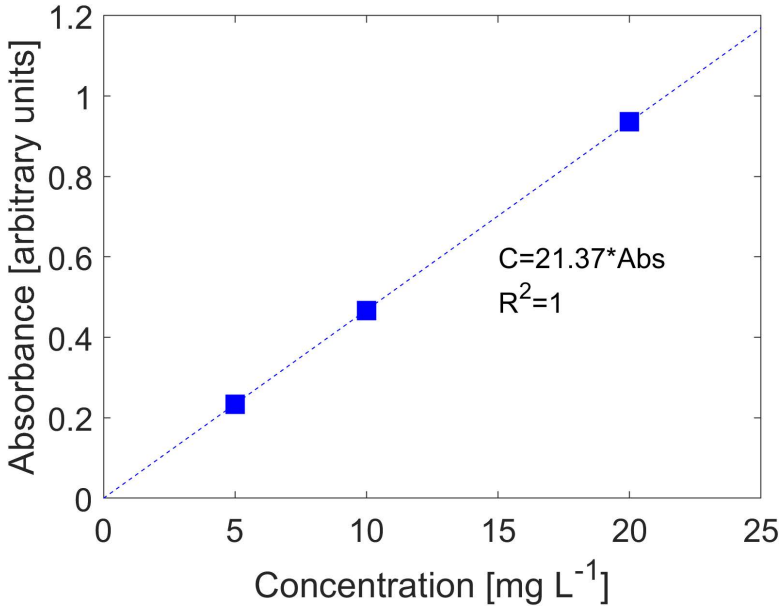

Figure A.1: Plot showing the ultraviolet-visible absorption calibration curve for NaFeCN in ultrapure water. The linear fit is presented and inset C stands for concentration of NaFeCN (mg L^{-1}) and Abs stands for the absorption of light (ultraviolet regime) at a wavelength of 218 nm. R2 stands for the coefficient of determination. The range of the calibration curve is between 0–20 mg L^{-1}.

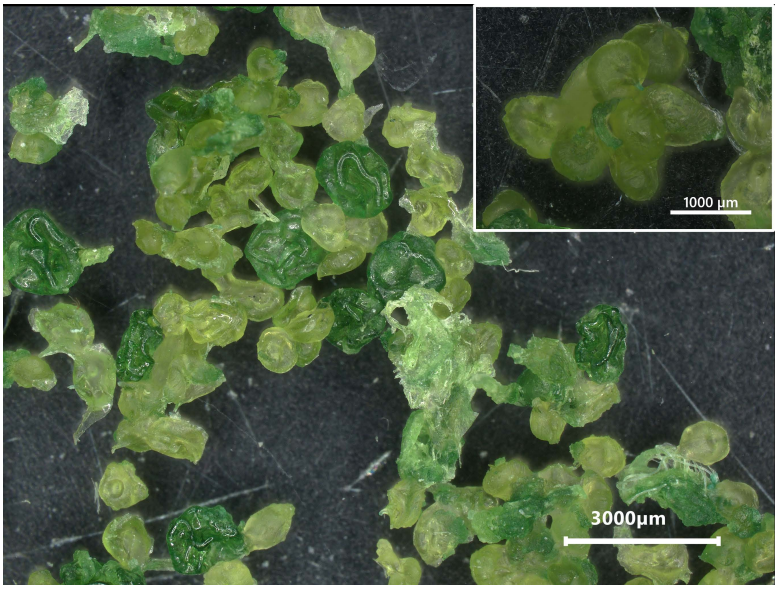

Figure A.2: Digital microscope image of capsule agglomeration that occurs with an increasing Cs content. The capsules in this example are Cs-CA 0.5_F_4. The inset image shows a closeup of an agglomeration consisting of at least eight capsules.

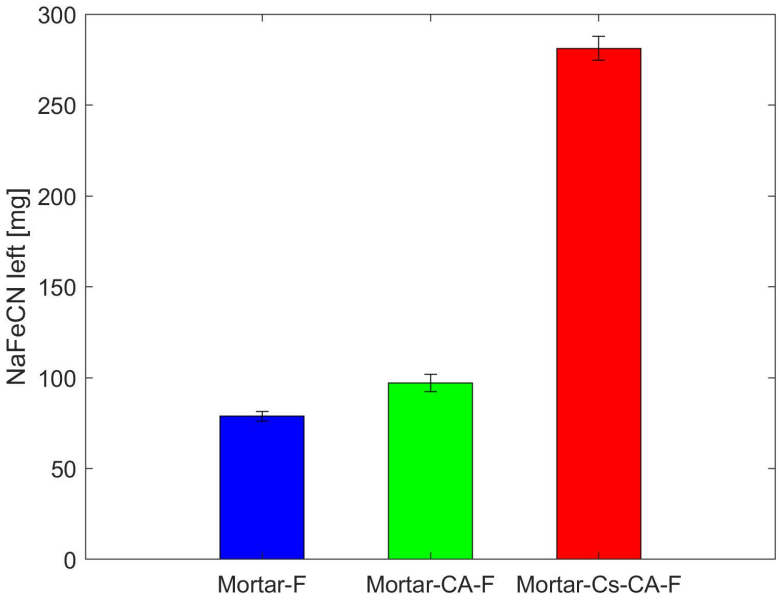

Figure A.3: A bar graph showing the absolute amount of NaFeCN left inside the Mortar-F, Mortar-CA-F and Mortar-Cs-CA-F specimens at the end of accelerated leaching test (diffusion) measured using the cold-water extraction method (Section 6.3.5.2). Mortar-Cs-CA-F specimens retain the highest amount of NaFeCN indicating the lowest leaching.

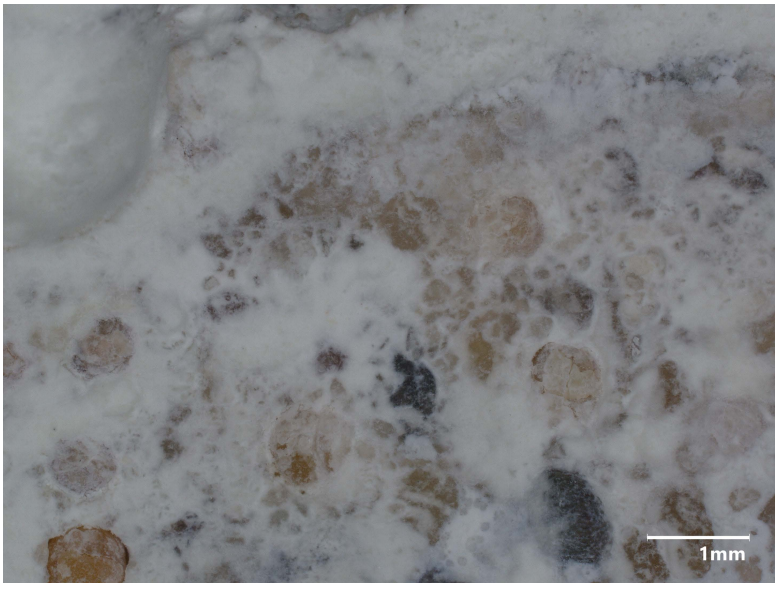

Figure A.4: A magnified image of the efflorescent crust on the surface of an Mortar-F specimen (corresponding to Figure 6.6, left column). The image was acquired at the end of the third absorption-drying cycle.

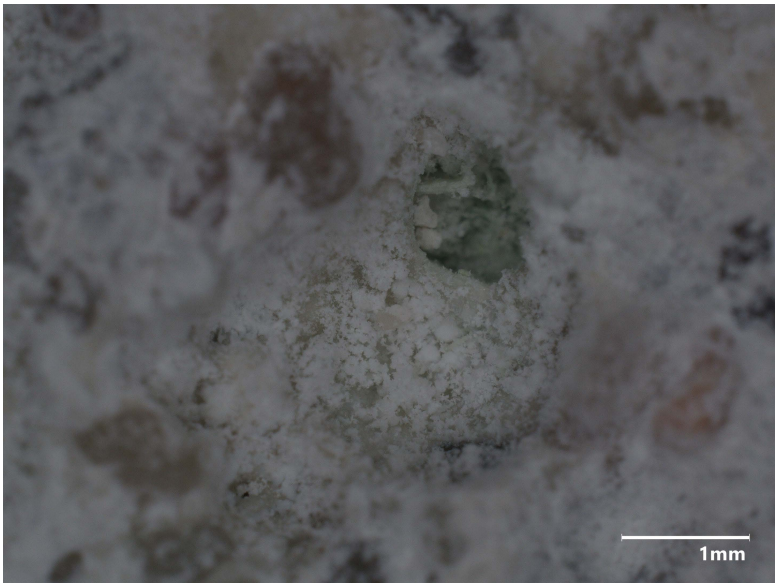

Figure A.5: A magnified image of efflorescent crust on the surface of a Mortar-CA-F specimens (corresponding to Figure 6.6, central column). The image was acquired at the end of the third absorption-drying cycle.

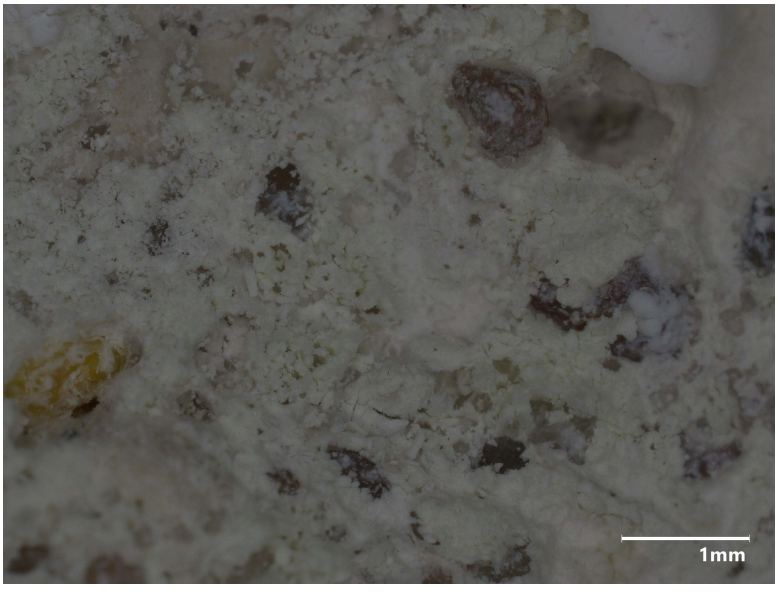

Figure A.6: A magnified image of efflorescent crust in Mortar-Cs-CA-F specimens (corresponding to Figure 6.6, right column). The image was acquired at the end of the third absorption-drying cycle.

B

Supplementary information to Chapter 7

B

Damage progression after each propagation cycle

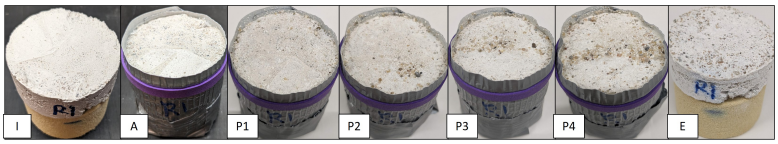

(a) NHL-R-1

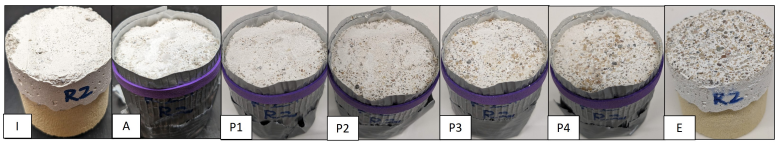

(b) NHL-R-2

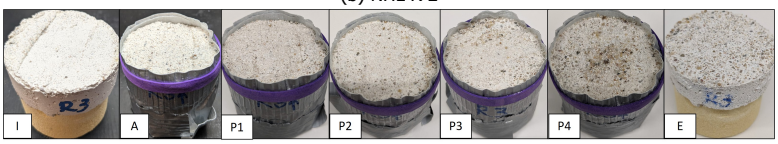

(c) NHL-R-3

Figure B.1: Damage propagation of NHL-R specimens

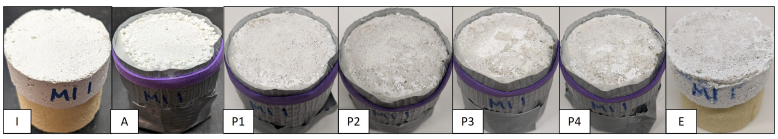

(a) NHL-F-1

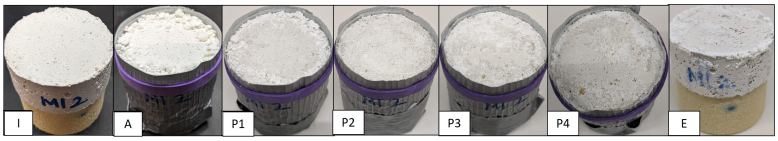

(b) NHL-F-2

(c) NHL-F-3

Figure B.2: Damage propagation of NHL-F specimens

I=Initial before testing, A=Accumulation, P1=Propagation cycle 1, P2=Propagation cycle 2, P3=Propagation cycle 3, P4=Propagation cycle 4, E=End of the test after brushing the debris

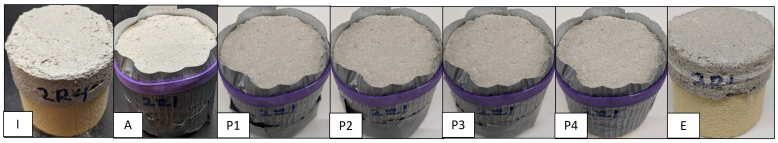

(a) 2L-R-1

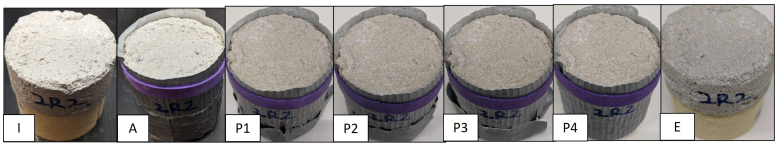

(b) 2L-R-2

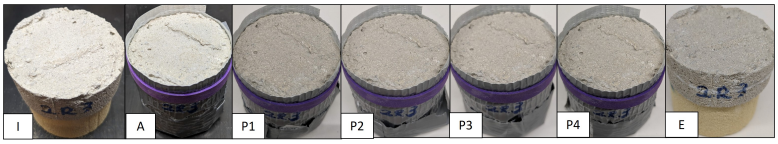

(c) 2L-R-3

Figure B.3: Damage propagation of 2L-R specimens

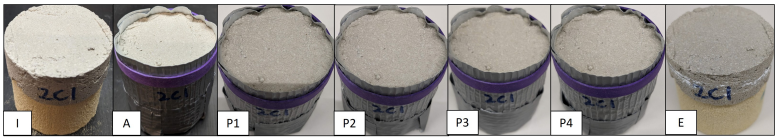

(a) 2L-CsCA-F-1

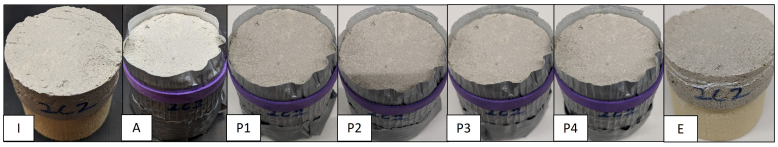

(b) 2L-CsCA-F-2

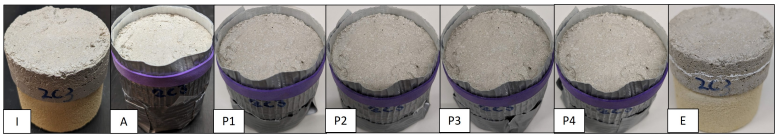

(c) 2L-CsCA-F-3

Figure B.4: Damage propagation of 2L-CsCA-F specimens

I=Initial before testing, A=Accumulation, P1=Propagation cycle 1, P2=Propagation cycle 2, P3=Propagation cycle 3, P4=Propagation cycle 4, E=End of the test after brushing the debris

C

Additional characterisation of capsules

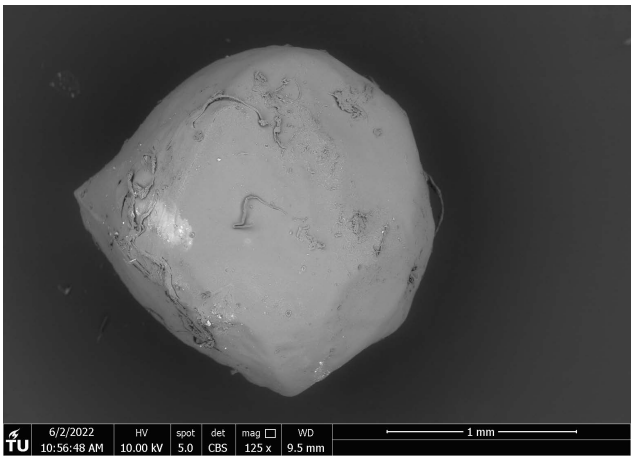

Figure C.1: SEM image of a chitosan-coated calcium alginate capsule in its fresh swollen state

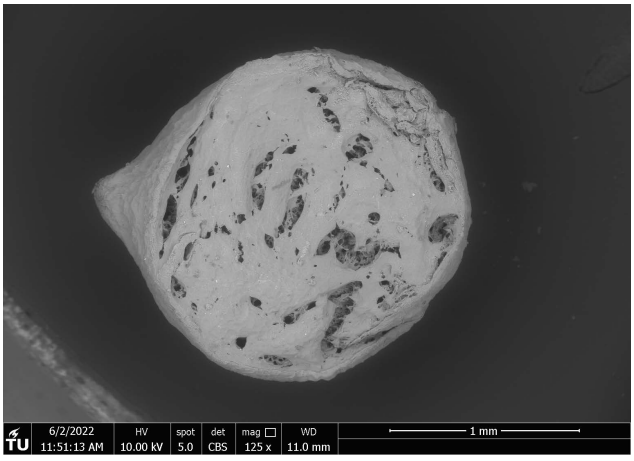

Figure C.2: SEM image on a cross-section a chitosan-coated calcium alginate capsule in its fresh swollen state. The inner structure resembles three-dimensional intertwined polymeric networks

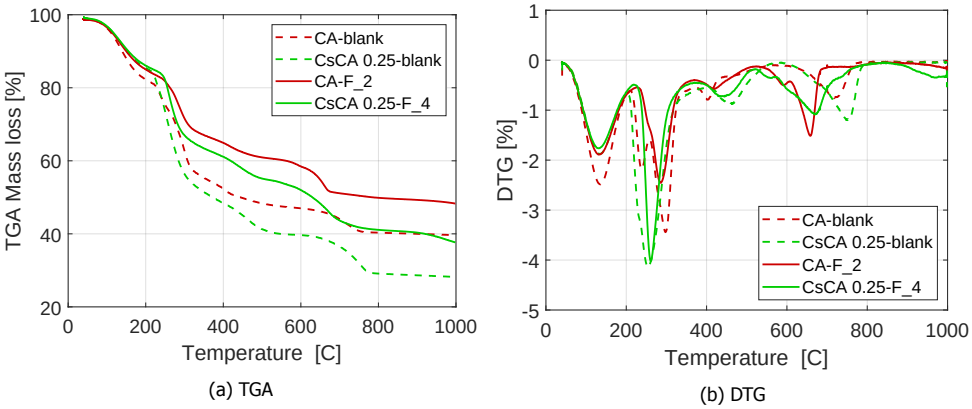

(a) TGA (b) DTG

Figure C.3: Thermogravimetric (TGA) analysis of capsules. (a) TGA (b) First derivative of TGA. The main decomposition of the polymer phases takes place between 200°C to 400 °C. Lower mass loss in capsules containing NaFeCN compared to their corresponding blank capsules is an indication of the encapsulated inhibitor. Presence of chitosan leads to a higher mass loss as the mass proportion of the polymer content increases

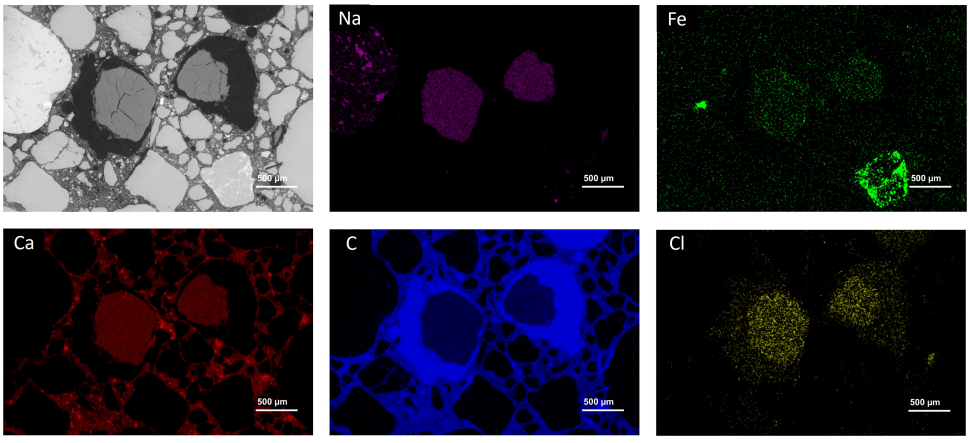

Figure C.4: SEM-EDS elemental mapping on a polished mortar cross-section showing two embedded chitosan-calcium alginate capsules. The capsules shows presence of Ca, C elements from hydrogels, Na, Fe from the inhibitor and Na, Cl which is a bi-product of the encapsulation process.

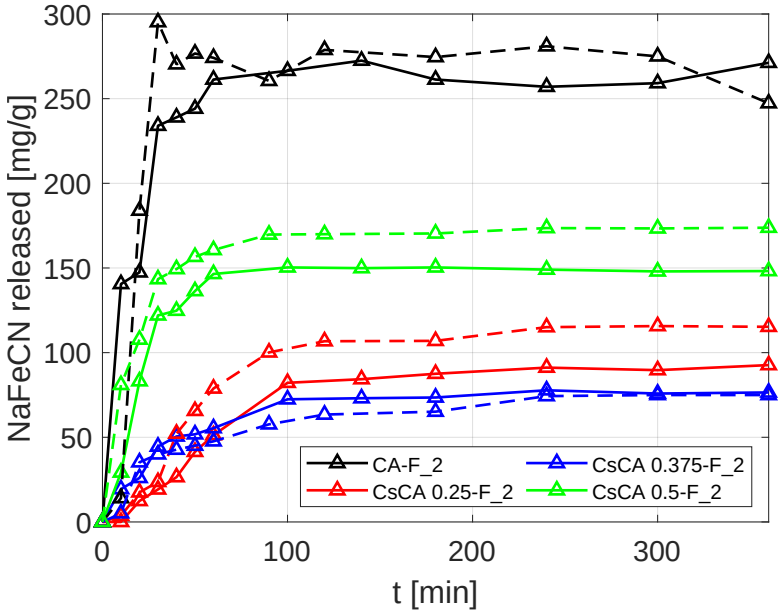

Figure C.5: Graph shows a comparison between the release of inhibitor from CsCA and CA capsules in mortar pore solution (solid lines) and mortar pore solution containing 5% w/v NaCl (dotted lines). A higher and a faster of the inhibitor release is observed in presence of NaCl, possibly related to the degradation of calcium alginate hydrogel networks

Summary

Repeated crystallisation of salts in the pores of building materials is a common cause of damage in buildings. Sodium chloride (NaCl) is one of the most common salts, responsible for weathering in the built environment. Mortars, especially when used as plasters and renders on the surface of walls, experience fast degradation as they are exposed to conditions perfectly conducive to salt weathering. As a consequence, their service life is often compromised, requiring frequent replacements. Costs associated with replacement interventions have a high economic and a social impact. Over the last two decades, the use of crystallisation inhibitors as an additive to prevent/mitigate salt crystallisation damage in building materials has shown promising results. Sodium ferrocyanide (NaFeCN), a crystallisation inhibitor of NaCl is particularly effective in preventing damage by inhibiting/delaying NaCl nucleation and altering NaCl's crystal habit. When mixed-in air lime-based mortars, NaFeCN has been shown to considerably improve the salt weathering resistance.

The present work aims to extend the application of NaFeCN to hydraulic mortars with a final goal to improve the durability of renovation mortars with respect to salt damage. As a first step, the state of the art was reviewed, focusing on the applications of the crystallisation inhibitor as an additive for mitigation of salt damage in porous building materials, including mortar. Based on the outcome of the literature review, two issues were identified that needed to be addressed in order to improve the performance of mortars with mixed-in inhibitors. The first issue concerned with the possible interactions that could arise on mixing the inhibitor and the hydraulic binders. These interactions could negatively affect the properties of mortar. The second issue was related to the loss of the inhibitor due to its susceptibility to leach out of mortar. A high rate of leaching can reduce the effectiveness of the inhibitor in the long run, and shorten the service life of mortars. An experiment-based research plan was formulated to investigate and address these issues.

The experimental campaign was initiated by assessing the effect of the inhibitor on the fresh and hardened properties of hydraulic mortars. Two commonly used hydraulic binders, natural hydraulic lime (NHL) and Ordinary Portland Cement (OPC) were investigated at the level of binder-paste and mortar. It was experimentally demonstrated that the addition of the inhibitor up to a concentration of 1% of the binder weight does not have any negative effects on the fresh and hardened properties of the studied hydraulic mortars. These conclusions meant that the inhibitor can be added to the hydraulic mortars without compromising on the latter's functionality.

In the next step, an experimental leaching test protocol was developed to quantify the rate of leaching of the inhibitor in mortar. This step was essential as the literature lacked data on the leaching behaviour of the inhibitor. Specimens made of NHL mortar with mixed-in inhibitor were prepared and subjected to leaching

tests taking into account diffusion- and advection-driven transport. In the diffusion-driven test, a high diffusion coefficient of the leached NaFeCN ($[Fe(CN)_6]^{4-}$) ions was measured, marginally lower than the diffusion coefficient of salt ions (Cl^-). In the advection-driven test, most of the inhibitor leached out of the mortar as efflorescence after a single wetting-drying cycle. The experiments concluded that the rapid depletion of the inhibitor in the mortar due to leaching will decrease the long-term effectiveness of the inhibitor against future salt load.

To ensure a long-term positive effect of the inhibitor, its rate of leaching in mortar had to be slowed down. Hence in the next phase, encapsulation of the inhibitor to control its release and consequently, reduce its leaching in mortar was explored. On the outcome of the literature review encompassing fields such as medicine and polymer chemistry, two bio-based hydrogels, chitosan and alginate were selected as potential capsule materials. The selection was based on the hydrogel's diffusion-based release and a pH-tunable response. The capsules were produced in a two-step process. First, the inhibitor was encapsulated in calcium alginate capsules (CA) using extrusion dripping and ionic gelation. Next, the obtained capsules were complexed with chitosan to obtain chitosan-calcium alginate polyelectrolyte capsules containing the inhibitor (CsCA). Since the release behaviour of CsCA capsules in an alkaline environment, was not known in the literature, the release of the inhibitor from capsules was investigated in solutions over a pH range of 7-13. In the studied pH range, the CsCA capsules released lower amount of inhibitor compared to CA capsules. Moreover, the magnitude of release was found to be dependent on the capsules' chitosan to alginate ratio. The results suggested that at a certain pH, the release of the inhibitor from CsCA capsules can be controlled by modifying the chitosan: alginate ratio. On the outcome of these positive results, the release of the inhibitor from CsCA capsules was tested in mortar pore solution and in hardened mortar. The outcome of these experiments showed a slower leaching (release) of the inhibitor from mortars containing CsCA capsules as compared to mortars with CA capsules and mortars with mixed-in inhibitor. The slower release of the inhibitor was attributed to chitosan's role in reducing the permeability of CsCA capsules and its electrostatic attraction to the negatively charged $[Fe(CN)_6]^{4-}$ ions, thereby hindering outward transport of the inhibitor.

The final phase of this research involved the assessment of the performance of the hydraulic mortars with inhibitor in both encapsulated and mixed-in form. The performance was assessed on three aspects (a) impact on fresh and hardened properties of mortar (b) salt-weathering resistance and (c) leaching of the inhibitor. Two types of hydraulic mortars, NHL-based and cement-based two-layer plaster system, were investigated. For comparison, reference mortars without inhibitor (and capsules) were also assessed. The impact on the fresh and hardened properties of mortar was studied using various characterisation and complementary experimental techniques. The addition of the capsules (equivalent to 1% inhibitor by binder weight) did not have any negative effects on the properties of hydraulic mortars. The salt-weathering resistance of the mortars was assessed by performing an accelerated salt-weathering test (RILEM 271-ASC). At the end of the test, the reference NHL mortars suffered severe damage in terms of material loss. Differently, NHL

mortars with inhibitors, both in encapsulated and mixed-in form showed negligible material loss, strongly demonstrating the role of the inhibitors in reducing the damage. In case of cement-based two-layer plaster system, no damage was observed in any of the specimens including the reference specimens. Therefore, no concrete conclusions on the inhibitor's effect could be drawn in the two layer-cement based plasters. Finally, at the end of the weathering test, the leached inhibitor from each type of mortar was quantified using ICP-OES. The mortars with encapsulated inhibitor showed lower leaching than the mortars with mixed-in inhibitor. These results confirm that encapsulating the inhibitor is beneficial in reducing leaching of the inhibitor. A lower leaching is expected to extend the effectiveness of the inhibitor over long time and thereby, increase the service life of mortars.

The results from the above experimental studies definitively conclude that incorporation of the crystallisation inhibitor (sodium ferrocyanide) improves the salt-weathering resistance of hydraulic mortars without any negative effects on the properties of mortar. Moreover, mortars containing encapsulated inhibitor, thanks to controlled-release are expected to have a longer service-life than mortars with mixed-in inhibitor. In addition to that, incorporating capsules in mortar do not have a negative impact on the fresh and hardened properties of mortars, making their application feasible in practice.

This research marks the first-ever application of using CsCA capsules towards controlled-release of additives in the field of building materials. The results suggest new opportunities in expanding the use of bio-based hydrogels in the field of building and construction. In future, additional research is needed to optimise the capsule composition to tune a case-specific release response. Additionally, research addressing some fundamental issues, such as the effect of the inhibitor on crystallisation pressure and salt mixtures, will help in developing this technology further.

Samenvatting

Herhaaldelijke kristallisatie van zouten in de poriën van bouwmaterialen is een veel voorkomende oorzaak van schade aan gebouwen. Natriumchloride (NaCl) is een van de meest voorkomende zouten die verantwoordelijk is voor verwering in de gebouwde omgeving. Mortels, vooral gebruikt als pleister op de buitenzijde van de muren, worden snel aangetast omdat ze worden blootgesteld aan omstandigheden die perfect geschikt zijn voor zoutverwering. als gevolg daarvan wordt hun levensduur verminderd, en moeten ze vaak worden vervangen. De kosten van vervangingsinterventies hebben een grote sociale en economische impact. De afgelopen twintig jaar heeft het gebruik van kristallisatieinhibitoren als additief om schade door zoutkristallisatie in bouwmaterialen te voorkomen/verminderen veelbelovende resultaten laten zien. Natriumhexacyanoferraat (NaFeCN), een kristallisatieinhbitor van NaCl, is bijzonder effectief in het voorkomen van schade door het remmen/uitstellen van NaCl-nucleatie en het veranderen van de kristalgewoonte van NaCl. Als NaFeCN in mortels op kalkbasis wordt gemengd, blijkt het dit weerstand tegen zoutverwering aanzienlijk te verbeteren.

Het huidige werk is erop gericht om de toepassing van NaFeCN uit te breiden naar hydraulische mortels met als uiteindelijk doel om de weerstand van renovatiemortels tegen zoutschade te verbeteren. Als eerste stap werd de stand van de techniek bekeken, gericht op de toepassingen van de kristallisatie-inhibitor als additief om zoutschade in poreuze bouwmaterialen, waaronder mortel, te beperken. Op basis van de resultaten van het literatuuronderzoek zijn twee problemen geïdentificeerd die aangepakt moesten worden om de prestaties van mortels met ingemengde inhibitoren te verbeteren. Het eerste probleem betrof de mogelijke interacties die zouden kunnen ontstaan bij het mengen van de inhibitor en de hydraulische bindmiddelen. Deze interacties kunnen de eigenschappen van mortel negatief beïnvloeden. Het tweede probleem had te maken met het verlies van de inhibitor door zijn gevoeligheid voor uitloging uit mortel. Een hoge mate van uitloging kan de effectiviteit van de inhibitor op de lange termijn verminderen en de levensduur van mortels verkorten. Er werd een experimenteel onderzoeksplan opgesteld om deze problemen te onderzoeken en aan te pakken.

De experimentele campagne werd gestart door eerst het effect van de inhibitor op de verse en verharde eigenschappen van hydraulische mortels te bepalen. Twee veelgebruikte hydraulische bindmiddelen, namelijk natuurlijke hydraulische kalk (NHL) en Ordinary portland cement (OPC) werden onderzocht op het niveau van bindmiddel-pasta en mortel. Experimenteel werd aangetoond dat de toevoeging van de inhibitor tot een concentratie van 1 % van het bindmiddelgewicht geen negatieve effecten had op de verse en verharde eigenschappen van de bestudeerde hydraulische mortels. Deze conclusies betekenen dat de inhibitor kan worden toegevoegd aan de hydraulische mortels zonder de functionaliteit ervan aan te tasten.

In de volgende stap werd een experimenteel testprotocol voor uitloging ontwikkeld om de uitloging van de inhibitor in mortel te kwantificeren. Deze stap was essentieel omdat de literatuur geen gegevens bevatte over het uitlooggedrag van de inhibitor. Proefstukken gemaakt van NHL mortel met ingemengde inhibitor werden voorbereid en onderworpen aan uitloogtesten waarbij rekening werd gehouden met diffusie- en advectiegedreven transport. In de diffusiegedreven test werd een hoge diffusiecoëfficiënt van de uitgeloogde NaFeCN ($[Fe(CN)_6]^{4-}$) ionen gemeten, marginaal lager dan de diffusiecoëfficiënt van zoutionen (Cl^-). In de advectiegedreven test lekte het grootste deel van het inhibitor uit de mortel als uitbloeiingen na één enkele bevochtigingsdroogcyclus. Uit de experimenten werd geconcludeerd dat de snelle uitputting van de inhibitor in de mortel door uitloging de langetermijneffectiviteit van de inhibitor tegen toekomstige zoutbelasting zal verminderen.

Om een langdurig positief effect van de inhibitor te garanderen, moest de uitloging ervan in mortel worden vertraagd. Daarom werd in de volgende fase gekeken naar het inkapselen van de inhibitor om het vrijkomen ervan te controleren en dus het uitlogen ervan in mortel te verminderen. Op basis van het literatuuronderzoek op gebieden zoals geneeskunde en polymeerchemie werden twee biogebaseerde hydrogels, chitosan en alginaat, geselecteerd als potentiële capsulematerialen. De selectie werd toegeschreven aan de diffusiegebaseerde afgifte van de capsules en de pH-regelbare respons. De capsules werden in twee stappen geproduceerd. Eerst werd de inhibitor ingekapseld in calciumalginaatcapsules (CA) door middel van extrusiedruppelen en ionische gelering. Vervolgens werden de verkregen capsules gecomplexeerd met chitosan om chitosan-calciumalginaat polyelektrolytcapsules te verkrijgen die de inhibitor (CsCA) bevatten. Aangezien het afgiftegedrag van CsCA-capsules in een alkalisch milieu, een bereik dat relevant is in mortels, niet bekend was in de literatuur, werd het vrijkomen van de inhibitor uit capsules onderzocht in oplossingen over een pH-bereik van 7-13. In het bestudeerde pH-bereik bleek de CsCA-inhibitor niet vrij te komen van de capsules. In het bestudeerde pH-bereik gaven de CsCA-capsules een lagere hoeveelheid inhibitor vrij in vergelijking met CA-capsules. Bovendien bleek de mate van afgifte afhankelijk te zijn van de verhouding tussen chitosan en alginaat in de capsules. De resultaten suggereren dat bij een bepaalde pH de afgifte van het inhibitor uit CsCA-capsules kan worden geregeld door de verhouding chitosan/alginaat te wijzigen. Op basis van deze positieve resultaten werd het vrijkomen van de inhibitor uit CsCA-capsules getest in een poriënoplossing in mortel en in uitgeharde mortel. Het resultaat van deze experimenten toonde een langzamere uitloging (afgifte) van de inhibitor uit mortels met CsCA-capsules in vergelijking met mortels met zowel ingemengde inhibitor als CA-capsules. De langzamere afgifte van de inhibitor werd toegeschreven aan de rol van chitosan in het verminderen van de permeabiliteit van CsCA-capsules en de elektrostatische aantrekkingskracht op de negatief geladen $[Fe(CN)_6]^{4-}$ ionen, waardoor het naar buiten gerichte transport van de inhibitor werd belemmerd.

De laatste fase van dit onderzoek bestond uit het beoordelen van de prestaties van de hydraulische mortels met inhibitor in zowel ingekapselde als ingemengde vorm. De prestaties werden beoordeeld op drie aspecten (a) invloed op de verse en verharde eigenschappen van mortel (b) weerstand tegen zout weer en (c) uit-

loging van de inhibitor. Er werden twee soorten hydraulische mortels onderzocht, een op NHL gebaseerd en een cementgebaseerd pleistersysteem met twee lagen. Ter vergelijking werden ook referentiemortels zonder inhibitor (en capsules) beoordeeld. De invloed op de verse en verharde eigenschappen van mortel werd bestudeerd met behulp van verschillende karakterisatietechnieken en aanvullende experimentele technieken. De toevoeging van de capsules (gelijk aan 1 % inhibitor per bindmiddelgewicht) had geen negatieve effecten op de eigenschappen van hydraulische mortels. De zout-weersbestendigheid van de mortels werd beoordeeld door het uitvoeren van een versnelde zout-weersproef (RILEM 271-ASC). Aan het einde van de test liepen de referentie NHL mortels ernstige schade op in termen van materiaalverlies. NHL mortels met inhibitoren, zowel in ingekapselde als ingemengde vorm, vertoonden daarentegen verwaarloosbaar materiaalverlies, wat de rol van de inhibitoren in het beperken van de schade sterk aantoonde. In het geval van het cementgebaseerde pleistersysteem met twee lagen werd geen schade waargenomen in de monsters, inclusief de referentiemonsters. Daarom konden er geen concrete conclusies worden getrokken over het effect van de inhibitoren in de pleisters op basis van cement met twee lagen. Tot slot werd aan het einde van de test de uitloging van de inhibitor uit elk type mortel gekwantificeerd met behulp van ICP-OES. De mortels met ingekapselde inhibitor vertoonden een lagere uitloging dan de mortels met ingemengde inhibitor. Deze resultaten suggereren dat het inkapselen van de inhbitor gunstig is voor het verminderen van de uitloging van de inhbitor. Een lagere uitloging zal naar verwachting de levensduur van mortels verlengen.

De resultaten van de bovengenoemde experimentele studies concluderen definitief dat de toevoeging van de kristallisatie-inhibitor (natriumhexacyanoferraat) de zout-weersbestendigheid van hydraulische mortels verbetert zonder negatieve effecten op de eigenschappen van de mortel. Bovendien wordt verwacht dat mortels met ingekapselde inhibitor dankzij de gecontroleerde afgifte een langere levensduur hebben dan mortels met ingemengde inhibitor. Bovendien heeft de opname van capsules in mortel geen negatieve invloed op de verse en verharde eigenschappen van mortel, waardoor de toepassing ervan in de praktijk haalbaar is.

Dit onderzoek markeert de allereerste toepassing van het gebruik van CsCA-capsules voor de gecontroleerde afgifte van additieven op het gebied van bouwmaterialen. De resultaten hopen nieuwe mogelijkheden te creëren voor de uitbreiding van het gebruik van biogebaseerde hydrogels in de bouw. In de toekomst is aanvullend onderzoek nodig om de capsulesamenstelling te optimaliseren om een gevalspecifieke afgiftereactie af te stemmen. Daarnaast zal onderzoek naar enkele fundamentele, nog niet opgeloste problemen, zoals het effect van de inhibitor op de kristallisatiedruk en zoutmengsels, helpen bij de verdere ontwikkeling van de technologie.

Acknowledgements

My PhD journey has been long and winding, even surviving a global pandemic. I never thought I could write so much text in my life, and yet here I am with this long dissertation. This dissertation would not have been possible without the support and contributions of many, whom I met along this journey.

Foremost I want to thank my promotors, Barbara and Erik for giving me an opportunity to work on this project and supporting me throughout the process. Your different styles of supervision played a key part in ensuring my progress always remained on track.

Thank you Barbara, you are every PhD candidate's dream supervisor. You have been extremely passionate, accessible, proactive and impressively lightning fast with your feedback. It is only because of you that I could manage to finish my work within a reasonable time without any compromise. Having said that, you were not easily convinced with my ideas (and probably never will be with my writing) but you always encouraged me to push my own boundaries, while always having my back. All your critical remarks have helped me become a better researcher. I truly enjoyed working with you, be it working in the lab or attending conferences, discussing food, culture or the architectural style of Jože Plečnik!

Thank you Erik for being calm and super patient. You always played the good cop, giving an enthusiastic yes to my somewhat feasible ideas and your trademark 'yeaaauw' to the more ridiculous ones, but never a no! Every meeting with you always instilled a sense of calmness in me and allowed me to take two steps back, breathe and look at the big picture. Observing you has taught me that in life it is important to be a good listener, a message that I hope I can apply in future as effortlessly as you do.

Thank you Damian for becoming my 'unofficial' supervisor. I am so glad that you came out of the blue with a box of ideas at a time when I was struggling with all my experiments. I always looked forward to our online meetings. You also showed me that academic writing can be less boring, taught me how to write polite rebuttals and demonstrated how to use the word 'odd' in hundred different ways. I hope to meet you in person one day!

Next, I would like to thank NWO and therefore extend my gratitude to the tax-payers in the Netherlands for financing this research project. I am also thankful to Prof. Rodriguez-Navarro, Prof. Steiger, Prof. Picken, Prof. Keutzer and Oguzhan for being part of my thesis committee and taking time to read and assess my dis-sertation. I am also grateful to my NWO users committee and research partners-Marije (NWO), Rob (WTA), Timo (TNO), Anton (Delstuc), Patrick (Remmers), Michiel (RCE), Leo (Tu/e), Elias (RU), Hugo (RU) and Nia (RU) for all the lively discussions. Your feedback has definitely helped me to improve my research and presentation.

Leo, thank you especially for introducing me to the lab facilities in TU Eindhoven, where I obtained some of my most important results.

I was really lucky to have all the help from all the skilled laboratory staff around me. John, you have done most of the heavy lifting for me and I really admire your professionalism. I am truly indebted for the countless ICP measurements you did for me and really enjoyed working with you. You were always precise about two things- quantifying iron concentration and predicting the next Dean's drinks! Thank you, Patricia, Jane and Armand from the water-lab for quickly helping me out with your ICP, when our own ICP was getting repaired. Hans (Tu/e) for explaining me so many concepts in analytical chemistry and training me with UV-VIS. Every time I spoke with you, I learnt something new. Arjan thanks for your help with MIP, ESEM and persisting with me in Dutch (though all your tongue twisters were not my favourite). Maiko, thanks for your help in designing setups for some of my experiments and finding clever simple solutions in the lab. You were always the glue that kept all the PhD's together, be it going up the stairs or down :). Thank you Ton for your help and patience in the casting room, sawing and drilling hundreds of cores and Kees for all your time and effort in designing our crystallisation pressure setup (I hope one day we will succeed!).

A big thank you to the entire Microlab for accepting me as one of your own and creating so many memories that I will cherish. Wherever I go, I will miss all of you. Thank you Oguzhan, it was your classes and masters thesis supervision back in 2017 that compelled me to switch to the the world of materials. Thanks for encouraging me to apply for this position. A big hug to the entire 'concrete nest 6.15 gang', it was such a privilege to share the office with you- Thank you Marija for always lending an ear to all my worries and being super optimistic even on the gloomiest days. You are the kindest person I have ever met. Farnaz, for always making sure that every small achievement must be celebrated with a cake, Laura for your positive enthusiasm and caving in to Farnaz's cake demands, Yading for making sure that I was never locked out of my office during late hours and Claudia for emphasising from day 1 on making a plan to connect different research sections in to a coherent story. Your advice was very valuable. Thank you Luiz for your sense of humour and your help with TGA, calorimetry and FTIR. I forgive you despite all your evil attempts to sabotage cyanide detection. Yu zhang, for all your help in brainstorming about capsule preparation, preparing polished sections and accompanying me to the lab on Sundays. Shan for your quick help with EDS mapping and Guilherme for arranging memorable parties with unforgettable hangovers. Guilherme, you were also my only lime-mortar friend, suffering together through the painful demoulding process. Anne linde and Branko, thanks a lot for always saying yes to a cup of coffee and discussing everything other than research. Anne linde, your annual help in tackling the stressful Sinterklaas poems will always be remembered. Thank you Yask, I always enjoyed talking with you over the historical figures of the microlab. A big thank you to Mayank, Wen, Qiu, Jinbao, Burcu, Rowin, Ali, Minfei, Xuhui, Zhi, Ze, Yun, Mohammed, Chen Liu, Yu, Theodora (sublime), Gabriel (Smartincs) and Xu Shi for all the lunches and 'Ganbeis' in PSOR.

I thank all the AE+T PhD's in the PhD room for my time spent in BK. Thank

you Hedieh for all the laughs, dinners and venting about the lengthy publication process! and Emeline for reminding me what day it was, every time I met you. I also appreciate your help in making my cover page more beautiful. Thanks Komal, Prateek(s), Hamza, Nima, Aga, Mahda, Guiseppe, Pablo, Pedro and Agnese for organising bowling, beach volleyball and cooking sessions. Thank you Wido for your help in organising SWBSS conference and the fun HA outings. Thanks Carla (AE+T) for helping me navigate the administrative stuff and Jacqueline (3MD) for including me in all the fun events in 3MD. I would like to thank all the kindhearted people working at the logistic point who also happened to be my lab neighbours in BK. Especially Mark and Ageeth, you were always super helpful in solving my lab issues even when it was not your job.

During my PhD, I am really glad to have met Shikha, Cedric, Bharat, Priyanshu, Ajay and Anusha who made the whole Covid-19 pandemic liveable. Thanks for all the dinners, baking, walks, barbecues and your friendship! Thank you Lidia for providing me with accommodation on some days when I had to go to Eindhoven for my experiments. Thank you Fungi, Abhilash, Saurabh and Garima for helping me forget my worries and Rasika for the long phone calls over the Atlantic.

I am very happy to have Patrick and Apte on my side as my Paranymphs. Patrick, you were the person I always relied on in the lab and discussions with you were always comforting. You always went out of your way to help me and your simple inventions like the metal ruler and the mosquito nets form a strong foundation of my experimental design. Apte, I have always relied on you for most of my life and consider it to be almost my right to do so. This time is going to be no different! Thank you Ruchira for all your love and for sharing 'your invention' of controlled-release with me. I wish you could make it to my defence, but I am sure you will make up for it. Mum and dad for all the sacrifices you made to support my education and for always being my superheroes. Thank you Marleen, for always checking on me like a mom and finally, thank you Sophie, the love of my life for being the way you are. You were dragged into this PhD with no fault of your own, going through all my mood swings and yet you carried me over the line on your strong shoulders. You are better than the best!

Curriculum Vitæ

Ameya Anand KAMAT

21-05-1991 Born in Mumbai, India.

Education

2009–2013 Bachelor of Engineering (civil engineering)
University of Mumbai, India

2015–2017 Master of Science (civil engineering)
Delft University of Technology, The Netherlands

2020–2024 PhD. Materials Science (building and construction)
Delft University of Technology, The Netherlands
Thesis: Improving salt weathering resistance of hydraulic mortars with an encapsulated crystallisation inhibitor
Promotor: Dr. B. Lubelli
Promotor: Prof. dr. ir. E. Schlangen

Work experience

2013–2015 Junior Structural Engineer
Toyo Engineering India Ltd. (Mumbai, India)

2017 Student researcher
Delft University of Technology (Delft, the Netherlands)

2017–2020 Researcher
Concrefy B.V. (Venlo, the Netherlands)

List of Publications

PhD related Journal publications

4. **A. Kamat**, E. Schlangen & B. Lubelli, *Encapsulated crystallisation inhibitor as a long-term solution to mitigate salt damage in hydraulic mortars*, Cement and Concrete Composites, **152**, 105682 (2024).

3. **A. Kamat**, D. Palin, B. Lubelli & E. Schlangen, *Capsule controlled release of crystallisation inhibitors in mortars*, Materials & Design, **244**, 113156 (2024).

2. **A. Kamat**, B. Lubelli & E. Schlangen, *Leaching behaviour of a crystallisation inhibitor in mortars*, Journal of Building Engineering **9**, 107933 (2023).

1. **A. Kamat**, B. Lubelli & E. Schlangen, *Effect of a mixed-in crystallization inhibitor on the properties of hydraulic mortars*, AIMS Materials Science **9**, 4 (2022).

Other Journal publications

4. M. Nedeljković, **A. Kamat**, P. Holthuizen, N. Tošić, E. Schlangen & S. Fennis, *Energy consumption of a laboratory jaw crusher during normal and high strength concrete recycling*, Minerals Engineering **204**, 108421 (2023).

3. B. Lubelli, I. Rörig-Daalgard, A.M. Aguilar, M. Aškrabić, K. Beck, C. Bläuer, V. Cnudde, A.M. D'Altri, H. Derluyn, J. Desarnaud, T. Diaz Gonçalves, R. Flatt, E. Franzoni, S. Godts, D. Gulotta, R. van Hees, I. Ioannou, **A. Kamat**, T. De Kock, B. Menendez, S. de Miranda, C. Nunes, E. Sassoni, N. Shahidzadeh, H. Siedel, Z. Slížková, M. Stefanidou, M. Theodoridou, R. Veiga, V. Vergès-Belmin, *Recommendation of RILEM TC 271-ASC: New accelerated test procedure for the assessment of resistance of natural stone and fired-clay brick units against salt crystallization*, Materials and Structures **56**, 5 (2023).

2. B. Lubelli, E. Bouvrie, T. Nijland, **A. Kamat**, *Plasters with mixed-in crystallization inhibitors: Results of a 4-year monitoring of on-site application*, Journal of Cultural Heritage **59** (2023).

1. B. Lubelli, A.M. Aguilar, K. Beck, T. De Kock, J. Desarnaud, E. Franzoni, D. Gulotta, I. Ioannou, **A. Kamat**, B. Menendez, I. Rörig-Dalgaard, E. Sassoni, *A new accelerated salt weathering test by RILEM TC 271-ASC: preliminary round robin validation*, Materials and Structures **55**, 9 (2022).

Conference publications

4. **A. Kamat**, B. Lubelli & E. Schlangen, *A study on leaching of crystallisation inhibitor in mortars*, In 3-3. Abstract from CRYSPOM VIII: 8th International Crystallization in Porous Media Workshop, Ghent, Belgium (2023).

3. **A. Kamat**, D. Palin, B. Lubelli & E. Schlangen, *Tunable chitosan-alginate capsules for a controlled release of crystallisation inhibitors in mortars*, In T. Van Mullem, N. De Belie, L. Ferrara, E. Gruyaert, & K. van Tittelboom (Eds.), SMARTINCS'23 Conference on Self-Healing, Multifunctional and Advanced Repair Technologies in Cementitious Systems, Ghent, MATEC web of conferences, EDP Sciences **378**, 02011 (2023).

2. **A. Kamat**, B. Lubelli & E. Schlangen, *Experimental Study on Properties of Hydraulic Mortars with Mixed in Crystallisation Inhibitors*, In V. B. Bosiljkov (Ed.), HMC 2022: Conservation and Restoration of Historic Mortars and Masonry Structures, Ljubljana, RILEM Bookseries **42**, (2023).

1. **A. Kamat**, B. Lubelli, E. Schlangen, *Effect Of Alkali Ferrocyanides On Crystallisation Of Sodium Chloride: Preliminary results*, In B. Lubelli, **A. Kamat**, W. Quist (Eds.), Proceedings of the Fifth International Conference on Salt Weathering of Buildings and Stone Sculptures, Delft, pp. 109-118 (2021).